Return To C. Vining

GE Astro Space

Development of Improved Thermoelectric Materials for Space Nuclear Power Systems

TECHNICAL PROGRESS REPORT
CONTRACT DE-AC01-84NE-32123

PERIOD FROM 28 SEPTEMBER 1984 THROUGH 17 APRIL 1989

FINAL REPORT

GE Astro Space

Astro-Space Division
General Electric Company
P.O. Box 8555, Philadelphia, PA 19101
215 354-1000

In reply refer to:
CDB-PL1-152

17 April 1989

Department of Energy
Office of Procurement Operations
1000 Independence Avenue, S.W.
Washington, DC 20585

Attention: Dr. William J. Barnett, Project Manager
NE-53

Subject: **Contract No. DEAC01-84NE-32123,**
Submission of Final Report

Enclosure: "Final Report - Development of Improved Thermoelectric Materials for Space Nuclear Power Systems, September, 1984 - April, 1989,
3 copies

Gentlemen:

General Electric Company, Astro-Space Division, is pleased to submit the approved final report in accordance with paragraph B.003, Item 2, of the subject contract. Distribution of this report is made as indicated on the attached distribution list.

All contract effort is completed with this submission.

Please call me at (215) 354-2140 if you have any questions.

Very truly yours,

GENERAL ELECTRIC COMPANY

Constance D. Beversdorf

GE Astro Space

Astro-Space Division
General Electric Company
P.O. Box 8555 Philadelphia PA 19101
215 354-2140

In reply refer to:
GDB-PLI-152

17 April 1989

Department of Energy
Office of Procurement Operations
1000 Independence Avenue, S.W.
Washington, DC 20585

Attention: Dr. William J. Barnett, Project Manager
NE-55

Subject: **Contract No. DEAC01-84NE-32123, Submission of Final Report**

Enclosure: "Final Report - Development of Improved Thermoelectric Materials for Space Nuclear Power Systems, September, 1984 - April, 1989." 3 copies

Gentlemen:

General Electric Company, Astro-Space Division, is pleased to submit the approved final report in accordance with paragraph 8.003, item 2, of the subject contract. Distribution of this report is made as indicated on the attached distribution list.

All contract effort is completed with this submission.

Please call me at (215) 354-2140 if you have any questions.

Very truly yours,

GENERAL ELECTRIC COMPANY

Cynthia D. Beveredorf
Contract Manager

jmv

cc: Mr. R. Lewis, DOE, MA-453.2 (l/o)

Development of Improved Thermoelectric Materials for Space Nuclear Power Systems

by

P.D. Gorsuch, J. Nakahara, G.A. Slack*, E. Feingold, C. Vining**

FINAL REPORT

Prepared for
U.S DEPARTMENT OF ENERGY
COVERING THE PERIOD
28 SEPTEMBER 1984 THROUGH 17 APRIL 1989

Prepared by
General Electric Company
Astro-Space Division
P.O. Box 8555
Philadelphia, PA 19101

In Response to
Contract No. DE-AC01-84NE-32123

* GENERAL ELECTRIC CORPORATE RESEARCH AND DEVELOPMENT CENTER, SCHENECTADY, NY
** CURRENTLY LOCATED AT THE NASA-JET PROPULSION LABORATORY, PASADENA, CA, - A MAJOR CONTRIBUTOR TO SECTION 4.0

CONTRACT DE-AC01-84NE32123
DEVELOPMENT OF IMPROVED THERMOELECTRIC MATERIALS
FOR
SPACE NUCLEAR POWER SYSTEMS

TECHNICAL PROGRESS REPORT DISTRIBUTION LIST

Address	Attention	# of Copies
U.S. Department of Energy Office of Special Applications Mail Stop NE-53 Washington, DC 20545	J. Turi W. Barnett E. Mastel T. Clark	1 2 1 1
U.S. Department of Energy Office of Procurement Operations MA453.5 1000 Independence Ave., S.W. Washington, DC 20585	R. Lewis R.J. Woytko	1 1
U.S. Department of Energy DOE Patent Office 1000 Independence Ave., S.W. Washington, DC 20585	ATTN: General Counsel for Patents	1
Oak Ridge National Laboratory P.O. Box X, Building 4508 Oak Ridge, TN 37831-6083	M.M. Martin	1
Technical Information Center Special Assistant for Reproduction and Processing P.O. Box 62 Oak Ridge, TN 37838		2
Oak Ridge National Laboratory Building 4500 South Mail Stop D61 Oak Ridge, TN 37831	W. Foster	1
Jet Propulsion Laboratory California Institute of Technology Mail Stop 277-102 4800 Oak Grove Drive Pasadena, CA 91109	J. Vandersande G. Stapfer L. Putnam C. Vining	1 1 1 1
Thermo Electron Corp. 101 First Avenue Waltham, MA 02254	V. Raag	1

Address	Attention	# of Copies
ERADCOM USA Electronics Technology and Devices Laboratory Fort Monmouth, NJ 07703	Dr. Guido Guazzoni	1
Fairchild Space and Electronics Co. Energy Systems Department 20301 Century Building Germantown, MD 20767	R. Carpenter E. Skrabek	1 1
Battelle Columbus Laboratory 505 King Avenue Columbus, OH 43201	C. Alexander	1
Ames Laboratory Iowa Sate University Ames, Iowa 50011	B.J. Beaudry	1
General Electric Company Corporate Research and Development P.O. Box F Schenectady, NY 12301	Dr. J.H. Rosolowski Dr. G.A. Slack	1 1

TABLE OF CONTENTS

TABLE OF CONTENTS (Cont'd)

TABLE OF CONTENTS (Cont'd)

LIST OF ILLUSTRATIONS

LIST OF ILLUSTRATIONS (Cont'd)

LIST OF ILLUSTRATIONS (Cont'd)

LIST OF ILLUSTRATIONS (Cont'd)

LIST OF ILLUSTRATIONS (Cont'd)

LIST OF ILLUSTRATIONS (Cont'd)

LIST OF TABLES

LIST OF TABLES (Cont'd)

ABSTRACT

Reliable, reproducible fabrication of n-type SiGe-GaP alloys with improvements in average high temperature figures-of-merit (Z) in the 30 to 40 percent range has been demonstrated. This corresponds to an average value of Z in the temperature range from 300° to 1000°C of about 1.0 to 1.2 x 10^{-3}/K. Some alloys exhibited power factors (S^2/ρ) approaching 40 $\mu W/cmK^2$, but much of the improvement resulted from large reductions in lattice thermal conductivities.

The highly successful vacuum melting/chill casting/grinding/hot pressing approach developed here uses powder blends of (1) Ge rich Si-Ge (50/50) alloys with high concentrations of soluble GaP and (2) highly doped Si material. This combination of hot pressed powders appears to have produced the improvement by at least four effects; namely, (1) reduction in the magnitude of energy barriers at grain boundaries, (2) enhanced phonon scattering by the fine grain size (approximately 5 micron median diameter), (3) enhanced phonon scattering by small diameter GaP precipitates, and (4) increased charge carrier concentrations. Effects (1) and (4) appear to improve the power factors and effects (2) and (3) provide the reduced lattice thermal conductivities.

Detailed review of the high temperature thermoelectric property test results at GE-ASD and Ames and Battelle-Columbus Laboratories suggest that the level of improvements may be as much as 5 to 20 percent higher when the characteristics of the test procedures are taken into account. Also, the data suggest that additional improvements up to as much as 20 percent can be achieved when the tests are conducted under in-gradient conditions and/or through heat treatments in specific temperature ranges. Thermoelectric device tests will probably be required to eventually establish the upper limits of performance capabilities of these improved materials.

SECTION 1
INTRODUCTION

1.1 GENERAL BACKGROUND

Thermoelectricity involves the diffusion of electrons and phonons along a temperature gradient in electrically conducting solids. These diffusion currents are controlled by the concentration of the particles, and by their interaction with each other and with impurities or additives and defects in the crystal structure. Using simple physical arguments, expressions can be derived for the critical thermoelectric transport parameters; namely, electrical and thermal conductivities and Seebeck coefficients. For thermoelectric power generation, it is extremely important to maximize the diffusion of electrons and minimize the phonon diffusion. Approaches that have been demonstrated to have great potential in this respect are: (1) the achievement of a heavily doped, degenerate condition in semiconductors; (2) solid solution alloying to promote phonon scattering by mass fluctuations; and (3) the introduction of disorder in the structure such as grain boundaries and point defects (vacancies).

A parameter of great importance in assessing the potential of thermoelectric materials is the figure-of-merit, Z, which is defined as:

$$Z = \frac{S^2\sigma}{K}$$

where S is the Seebeck coefficient (sometimes called the thermopower), σ is the electrical conductivity and K is the thermal conductivity. Z has the units of inverse temperature (K^{-1} or $^{\circ}C^{-1}$). Since the conversion efficiency is directly related to Z, the highest possible figure-of-merit, averaged over the operating temperature range, is a highly desirable goal. Also, since the figure-of-merit is a function of temperature and material properties only, an understanding of the impact of variations in material behavior and characteristics on this property can provide much of the technical guidance needed for developing and/or improving the materials.

Material properties that are critically important to optimizing thermoelectric power generation include:

1. The lattice thermal conductivity should be as low as possible since heat conducted by the lattice is lost to the conversion process.

2. The charge carrier mobilities should be maintained as high as possible.

3. The semiconductors used must be extrinsic conductors at the highest operating temperatures so that the ratio of electron conductance to hole conductance in the n-type leg, and the ratio of hole conductance to electron conductance in the p-type leg, are both high.

4. The materials used must be chemically, thermally, and mechanically stable at the operating temperatures.

5. The materials used must permit good electrical and thermal connections at their hot and cold junctions or interfaces.

6. The materials used must be capable of synthesis by reproducible techniques or processes which are adaptable to scaling to production requirements.

Thus, it follows that the problem of developing new or improved materials with superior thermoelectric properties or predicting the potential of any system resolves itself into selecting and/or identifying materials (1) with maximum ratios of carrier mobility to lattice thermal conductivity and (2) the means for increasing the value of this ratio in a given material, the most notable of which is by solid solution alloying and control of carrier concentration, n. Provided the adjustment of n by controlled impurity additions is possible, the concentration giving maximum value of Z can be readily determined; and this value usually corresponds to degeneracy.

The theory of heavily doped semiconductors with respect to thermoelectric applications was developed during major efforts motivated by the U.S. Navy and by space programs in this Country and the Soviet Union. The results of those efforts to improve the conversion efficiency of thermoelectric devices in the 1950's and 1960's have remained largely unchanged for the last twenty years. During this early period, the framework was laid for our present understanding of the physics of thermoelectric devices. The early searches for potentially useful materials were quite exhaustive and still, today, the most useful

thermoelectric materials are the time tested Bi or Pb based tellurides and Si-Ge based alloys developed during this period.

The promise of Si-Ge alloys as useful thermoelectric materials was recognized in the early sixties and successfully developed through the sixties and early seventies. For over a decade, the Si-Ge unicouple has been the workhorse thermoelectric device for space RTG power systems being employed in the MHW and GPHS-RTG Programs. Very little further optimization of these materials was attempted for many years and, in fact, most currently available Si-Ge alloys are virtually identical in performance to alloys studied by RCA in the mid-sixties. This is no accident since these Si-Ge alloys were very successfully applied, often exceeding program goals in terms of reliability and lifetime characteristics.

Further optimization or development of these Si-Ge alloy thermoelectric materials was efficiently and expeditiously accomplished in the Program summarized here by conducting systematic iterative experimental/theoretical studies of the effects of variations in the parameters which control their thermoelectric properties. Based on these trends, it was possible to select compositions and processing procedures for producing significantly improved materials. This sort of program was carried out at RCA 20 years ago which resulted in the selection of a high performance Si-Ge alloy composition near 80 a/o Si with the charge carrier doping levels currently in use.

1.2 PROGRAM GOALS

This two-phase program had, as goals, emphasis on two types of material as outlined below.

1. Optimization of Si-Ge Alloy Thermoelectric Materials

   Si-Ge n- and p-type thermoelectric materials were to be developed, characterized and demonstrated as to performance capability under in-gradient test conditions which simulated flight temperature regimes. The materials were expected to have an average figure-of-merit, Z, of 1.0×10^{-3}/K over the temperature range of T_{HJ} equal to 1000°C and T_{CJ} of 300°C. Other characteristics were to be equal to or superior to the standard MHW/GPHS-RTG Si-Ge alloys.

2. New Technology n- and p-Type Thermoelectric Materials

In addition to the optimization of Si-Ge alloys, new n- and p-type thermoelectric materials were to be identified with the potential of achieving an average figure-of-merit over the temperature range of 300 to 1000°C of at least 1.3×10^{-3}/K. These materials were to be stable for at least 40,000 hours of operation, have low vapor pressures (less than 10^{-6} torr at 1100°C) and have appropriate mechanical and physical properties.

A very comprehensive summary of the candidate advanced technology materials reviewed is given in Appendix B, with a short summary given in Section 2 of this Report. Because of the Department of Energy's technical direction, during conduct of this Program, to place emphasis on improving Si-Ge alloys, not enough significant experimental/theoretical progress was made to justify including the advanced alloy studies in this Report.

1.3 OPTIMIZATION OF FIGURE-OF-MERIT OF Si-Ge ALLOY THERMOELECTRIC MATERIALS

Si-Ge alloy systems have been found to be very effective for a number of practical thermoelectric energy conversion applications for more than a decade, including several space applications. The best known of these applications are the Radioisotope Thermoelectric Generators (RTGs) used on the two Voyager spacecraft, and LES 8/9 satellites.

The requirements of a large energy band-gap to minimize intrinsic conduction at higher temperatures and that of a high melting point have placed emphasis on the silicon rich alloys. The addition of Ge also promotes a reduction in lattice conductivity by mass fluctuation scattering, and alloys of compositions near 80 a/o Si and 20 a/o Ge have produced the highest figures-of-merit. Typical values of figure-of-merit at the start of the program for Voyager, MHW and GPHS-RTG, Si-Ge and SiGe-GaP alloys were 0.7×10^{-3} and 0.85×10^{-3}/°C, respectively.

The figures-of-merit for Si-Ge alloys are usually optimized at carrier concentrations which exceed the solid solubility limits at the chosen operating temperature range for the n-type and p-type dopants; namely, phosphorus and boron, respectively. Under these temperature conditions, the dopants precipitate with time and the material thermoelectric properties

change a few percent resulting in a reduction in Si-Ge thermopile converter performance. Since these precipitation effects are predictable they can be accounted for in the RTG design.

The general approach used here for increasing the figure-of-merit of the alloys consisted of iterative experimental and theoretical studies designed to provide an understanding of the effects of GaP additions to Si-Ge in lowering the thermal conductivity supplemented with experiments to determine the effects of (1) grain size down to about 0.2 micron, (2) improved homogeneity in the one to two percent variation range, (3) variations in GaP addition levels and method of addition, (4) n- and p-type alloy compensation, and (5) level of doping supersaturation. In addition, factorial type experimentation was used to establish the interaction of the major material behavior variables, and the effectiveness of the material(s) developed was demonstrated through tests both at GE and at DOE sponsored laboratories, including Ames Laboratory of Iowa State University and Battelle-Columbus Laboratory.

Strong experimental and theoretical support for the Program was initially based on the studies of Rowe and Bandhari[1] and Pisharody and Garvey[2]. The former studies showed the strong dependence of K on grain or particle size, and the latter results indicated major modification in thermoelectric property characteristics by alloying with GaP.

1.4 REFERENCES*

(1) C.M. Bandhari and D.M. Rowe, J. of Phys. C2, 147 (1969).

(2) R.K. Pisharody and L.P. Garvey, in Proc. 13th Intersociety Energy Conversion Engineering Conference, (Society of Automotive Engineers, 1978), p. 1963.

* Each Section in this Report is self-contained and the References are listed at the end.

SECTION 2
FIGURE-OF-MERIT OPTIMIZATION

2.1 Si-Ge ALLOYS

2.1.1 BACKGROUND

Silicon germanium mixed crystals* (or alloys) have been used in high temperature thermoelectric generators for many years. The efficiency of a thermoelectric generator operating over a prescribed temperature range made from these materials can be calculated from the temperature dependent material parameter Z, the thermoelectric figure-of-merit. The value of Z is given by:

$$Z = \frac{S^2\sigma}{K}$$

where S is the Seebeck coefficient, σ is the electrical conductivity and K is the thermal conductivity. The larger Z is, the greater the efficiency. In other words, a good thermoelectric material would be characterized by high values of S and σ and a low thermal conductivity. It has been shown that the total thermal conductivity K can be written as the sum of two contributions, one of which represents the electronic part K_e and the other represents the lattice contribution K_g. The electronic part is proportional to the electrical conductivity which means that in order to increase the figure-of-merit of a thermoelectric, one should look into minimizing its lattice thermal conductivity. A calculation of the minimum thermal conductivity was made in order to better understand the variables that affect the value of the thermal conductivity. Then, the values of K_{min} for $CdGeAs_2$, Si, Ge and Si-Ge alloys were estimated so as to establish a theoretical lower limit for this class of materials. A comparison with literature data on amorphous Si, Ge and $CdGeAs_2$ reveals that the method of calculation of K_{min} gives values within 8% of those actually observed. Thus, it can be concluded with some certainty that for 80% Si-20% Ge, K_{min} is 9.0×10^{-3} W/cmK.

* A homogenous, single-phase, solid solution of two elements.

The discussion in this section expands these considerations and suggests the upper limit of Z for Si-Ge alloys.

Derivation of the Minimum Thermal Conductivity for Si-Ge Alloys

These analyses start with Callaway and Von Baeyer[1], who derived an expression for the thermal conductivity in the Debye approximation. Their Equation 6 for the thermal conductivity, K, can be written as:

$$K = \frac{4\pi k^4 T^3}{h^3 v} \int_0^{\Theta/T} \frac{\tau x^4 e^x dx}{(e^x-1)^2} \qquad (1.1)$$

where:

- k = Boltzmann's constant
- h = Planck's constant
- T = absolute temperature
- Θ = Debye temperature
- v = sound velocity
- τ = phonon relaxation time
- $x = h\upsilon/kT$
- υ = phonon frequency

For the case when the phonon mean-free-path, ℓ, defined by:

$$\ell = v\tau \qquad (1.2)$$

is assumed to be independent of the phonon frequency, and equal to the average interatomic distance, δ, Equation 1.1 becomes

$$K = \frac{4\pi k^4 T^3 \ell}{h^3 v^2} \int_0^{\Theta/T} \frac{x^4 e^x dx}{(e^x-1)^2} \qquad (1.3)$$

At high temperatures where $T \geq \Theta$, Equation 1.3 reduces to:

$$K = \frac{4\pi k v \delta}{3} \left(\frac{k\Theta}{hv}\right)^3 \qquad (1.4)$$

In the Debye approximation for the specific heat capacity of a solid we have

$$\frac{4\pi}{3} \left(\frac{k\Theta}{hv}\right)^3 = \frac{1}{\delta^3} \qquad (1.5)$$

Then Equation 1.4 reduces to:

$$K = \frac{kv}{\delta^2}, \qquad (1.6)$$

Equation 1.6 can also be derived from the simple Debye expression for K, which is:

$$K = \frac{1}{3} \ell \, v \, C \qquad (1.7)$$

where C = heat capacity per unit volume by substituting:

$$\ell = \delta$$

$$C = \frac{3k}{\delta^3}$$

In the discussion by Slack[2] of the minimum thermal conductivity of crystals, the shortest possible mean-free-path for acoustic phonons is taken to be one wavelength. In this approximation

$$\ell = \frac{2\pi v}{\omega} = \frac{hv}{kTx} \qquad (1.8)$$

where ω = angular phonon frequency in radians/sec.

Equations 1.2 and 1.8 yield:

$$\tau = \frac{h}{kTx} \tag{1.9}$$

When Equation 1.9 is substituted into Equation 1.1 and the temperature is restricted to $T \geq \Theta$, one obtains:

$$K = \frac{kv}{\delta^2}\left[\frac{3}{2}\left(\frac{4\pi}{3}\right)^{1/3}\right] \tag{1.10}$$

Note that Equation 1.10 is just a factor of 2.418 times larger than Equation 1.6. Equation 1.10 is also identical to Equation 19.3 of Reference 2 if we use the substitution of Equation 1.5. Thus, we see that Equation 1.10 is the calculated minimum thermal conductivity of the acoustic phonons in the high temperature limit when $T >> \Theta$, denoted in Reference 2 as $K^{1}_{SMINA\infty}$.

For crystals of Si and Ge there are both acoustic and optic phonon branches. Hence, the minimum thermal conductivity is a sum of the contributions from both sets of branches. The calculated minimum K values from Reference 2 using such a sum are given in Table 2-1. We note that these calculated values are appreciably larger than the measured ones.

Table 2-1. Minimum Thermal Conductivity Values of Some Adamantine Structures at Temperatures Above Θ

Material	Observed		Calculated	
	10^{-3} W/cm K	Reference	10^{-3} W/cm K	Reference
Silicon	10.6	3	28.9	2
			9.76	Eq. (1.11)
			12	5
Germanium	5.15	4	15.1	2
			5.37	Eq. (1.11)
CuCl	2.9 ± 0.4	6	3.89	Eq. (1.11)
			3.13	6
$CdGeAs_2$	3.9	4	3.80	Eq. (1.11)
SiC	---	---	22.1	Eq. (1.11)

A second type of simple calculation can be made for Si or Ge in which the acoustic phonon mean-free-path, ℓ, is taken to be equal to δ. This yields 1/2 the value from Equation 1.6 for the acoustic phonon contribution. The 1/2 arises because there are 2 atoms in the unit cell. The total is:

$$K_{min} = \frac{k}{2\delta}\left[\frac{v}{\delta} + \upsilon_o\right] \qquad (1.11)$$

where

υ_o = the average optical phonon frequency[2]

The numerical values in Equation 1.11 for Si and Ge are taken from Reference 2. For CuCl we have used:

$v = 2.37 \times 10^5$ cm/sec.
$\upsilon_o = 6.45$ THz
$\delta = 2.703 \times 10^{-8}$ cm.

These average values have been computed from the data in Reference 6. For $CdGeAs_2$ single crystals we used the measured elastic constants[7] and a density of 5.600 gm/cm^3 to calculate an average acoustic phonon velocity of:

$$v = 2.504 \times 10^5 \text{ cm/sec}$$

The value of $\delta = 2.922 \times 10^{-8}$ cm, while υ_o has been taken to be 7.53 THz, an average of those of GaAs and InAs. It is realized that $CdGeAs_2$ has the tetragonal chalcopyrite structure, and has 4 atoms/unit cell. However, it can be treated as though the Cd and Ge were randomly mixed and that its phonon spectrum is like that of $Ga_{0.5}In_{0.5}As$. From Equation 1.11 we calculate for $CdGeAs_2$:

$$K_{min} = 3.80 \times 10^{-3} \text{ W/cmK}$$

In order to provide a comparison for the data on Si and Ge we have also calculated K_{min} for cubic SiC using:

$v = 9.57 \times 10^5$ cm/sec

$\upsilon_o = 25.6$ THz

$\delta = 2.174 \times 10^{-8}$ cm

The result is K_{min} (SiC) = 22.1×10^{-3} W/cmK. Someday it may be appropriate to consider SiC as a high temperature thermoelectric generator material.

A much more sophisticated theoretical calculation of K_{min} for Si has been carried out by Allen and Feldman[5]. The results have not yet been published. However, the agreement of their calculation both with the observed value for Si and with Equation 1.11 is quite good (see Table 2-1).

It is concluded that Equation 1.11 gives a good approximation to the measured value, and that the measured values really are for amorphous materials. Any residual crystallinity in the samples is too small to give erroneously high thermal conductivity values. Thus, we can be confident that no further reduction in K can be made below the measured values in Table 2-1.

The minimum thermal conductivity of a $Si_{0.7}Ge_{0.3}$ mixed crystal (or alloy) will be almost equal to a weighted arithmetic average of those of Si and Ge. Thus, at high temperatures:

$$K_{min}(Si_{0.7}Ge_{0.3}) = 8.97 \times 10^{-3} \text{ W/cmK}$$

The Debye temperature of this mixed crystal is 577 K. Thus we expect that this value of K_{min} is accurate for all temperatures above 600 K, the range where the thermoelectric generators are used.

Calculation of the Maximum Figure-of-Merit of Si-Ge Alloys

The best possible performance of a Si-Ge thermoelectric generator, i.e., the nighest Z, will be obtained when the electrical properties, S and σ, of the Si-Ge alloy are those of a single crystal while the thermal conductivity, K, is that of an amorphous sample. It is realized that this exact combination is unobtainable, but one can make progress in this direction starting from "standard", zone-leveled Si-Ge alloys.

For this purpose, it is assumed that the electrical conductivity, σ, and the Seebeck coefficient, S, are given as a function of doping level by the results of Dismukes et al[8]. Using these values, Z is calculated from:

$$Z = \frac{S^2\sigma}{K_g + L_o\sigma T}$$

where:

L_o = the Lorenz number

K_g = the lattice thermal conductivity (assumed to be essentially independent of temperature for $T \geq 300$ K)

We then have taken values of K_g varying from 25×10^{-3} W/cmK to 8×10^{-3} W/cmK, and calculated at each temperature the maximum Z that could be obtained if the carrier concentration were allowed to vary. This "local" value of Z for n-type 70 atom% Si plus 30 atom% Ge is shown plotted in Figure 2-1 for various values of K_g*. The dashed curve in the upper right-hand corner of Figure 2-1 is the calculated behavior for $K_g = 8 \times 10^{-3}$ W/cmK if the bipolar thermal conductivity is artificially set equal to zero. In any real sample it will not be zero. Thus, the other curves all contain a bipolar contribution to K_{TOTAL}. Thus,

$$K_{TOTAL} = K_g + L_o\sigma T + K_{BIPOLAR}$$

The $L_o\sigma T$ is the monopolar electric thermal conductivity.

For the temperature range of 500°C to 1000°C the curves in Figure 2-1 allow one to calculate an average value of Z over this (or any other) temperature interval. Such a temperature average value is termed $\overline{Z}(n)$. This $\overline{Z}(n)$ value for n-type is arithmetically averaged with a similar temperature range average for p-type called $\overline{Z}(p)$. The result is:

* Calculations were made for 70-30 a/o Si-Ge alloys because of extensive background and data from RCA[8].

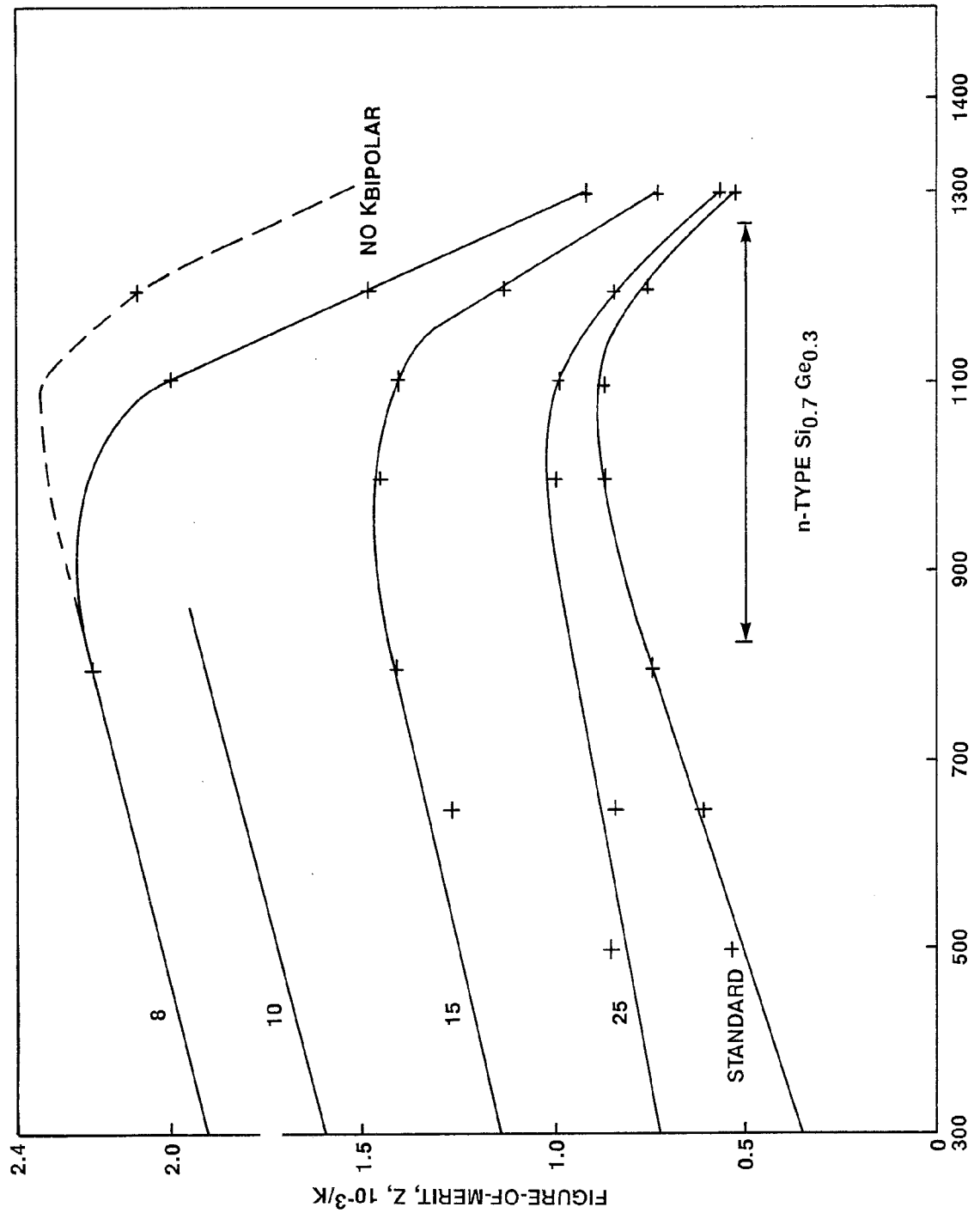

Figure 2-1. Figure-of-Merit Versus Temperature for n-type $Si_{0.7}Ge_{0.3}$
Different curves correspond to different K_g values.

$$\bar{\bar{Z}} = 1/2(\bar{Z}(n) + \bar{Z}(p)).$$

The results in Figure 2-2 show $\bar{\bar{Z}}$ versus K_g for the 500°C to 1000°C temperature range for 70 atom% Si plus 30 atom% Ge alloys. The result is that the maximum is $\bar{\bar{Z}} = 1.8 \times 10^{-3}/K$ if $K_g = 9 \times 10^{-3}$ W/cmK. The standard material has an effective K_g of 33×10^{-3} W/cmK and a $\bar{\bar{Z}}$ of $0.8 \times 10^{-3}/K$. Thus, if one can successfully reduce K_g to its minimum value of 9×10^{-3} W/cmK, the $\bar{\bar{Z}}$ can, in theory, be increased a factor of 2.25.

In all probability such a large reduction in K_g cannot be achieved. However, more modest reductions could yield Z values significantly greater than $1 \times 10^{-3}/K$ in suitably manufactured Si-Ge alloys.

It is believed that the incorporation of second-phase inclusions of sizes in the 50 Å to 100 Å diameter range at concentrations of a few volume percent is a highly promising approach for reducing K_g.

Summary

Theoretical analyses conducted on this Program suggest strongly that there is much potential for further major improvement in the thermoelectric properties of Si-Ge alloys.

2.2 ALTERNATE MATERIALS

2.2.1 BACKGROUND

All of the known materials that might make useful thermoelectrics were extensively reviewed. Figure 2-3 shows the temperature dependence of the figure-of-merit for a number of compounds relative to Si-Ge alloys. Emphasis was directed toward selecting those materials which had higher temperature capability than Si-Ge alloys. The total review is summarized and attached to this report as Appendix B, and only a very short summary of the results is presented here.

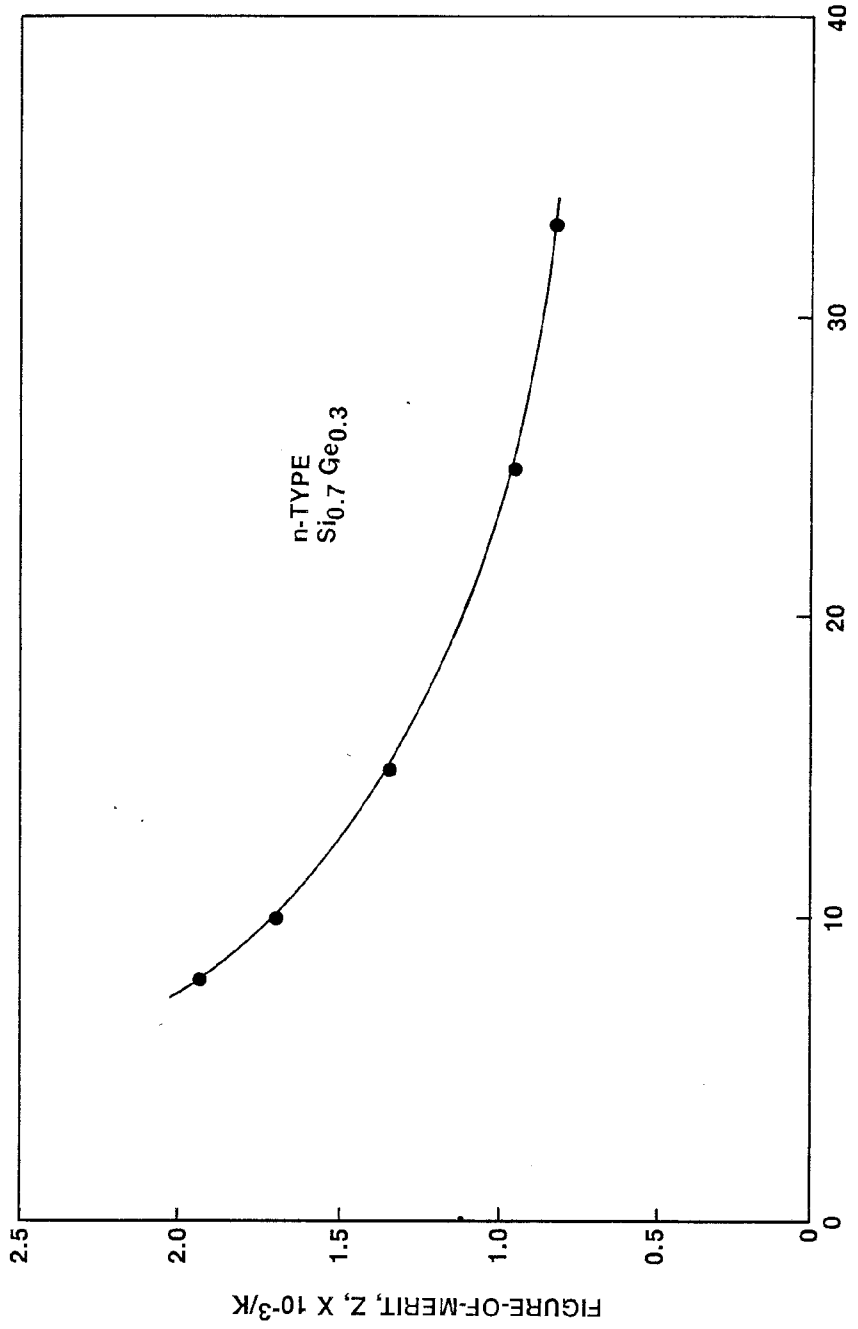

Figure 2-2. $\bar{Z}$ versus K_g for n-type $Si_{0.7}Ge_{0.3}$

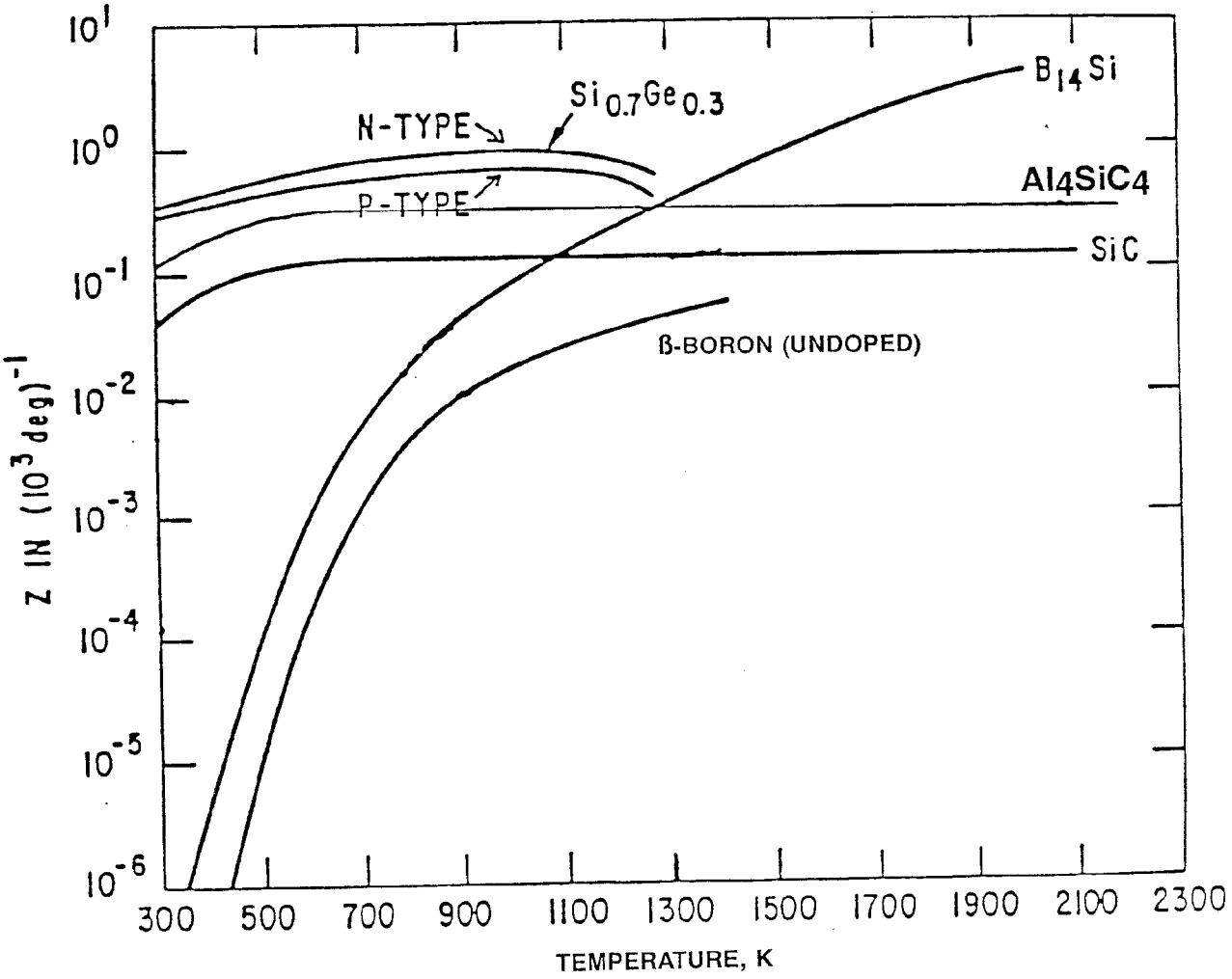

Figure 2-3. The Estimated Thermoelectric Figure-of-Merit (Z) as a Function of Temperature for a Number of Compounds

Shortly after initiation of the Program, direction was given by the Department of Energy to emphasize only Si-Ge alloys. None of the activities on these alternate materials advanced to a point that was significant, so no data on them are included in this Report. Initial activities were, however, presented in some of the monthly reports.

Alternate Materials

- SiC and Al_4SiC_4. Two semiconductors that have larger band-gaps and higher melting points than Si-Ge alloys are SiC and Al_4SiC_4. The estimates of their minimum thermal conductivities are:

$$K_{min}(SiC) = 22 \times 10^{-3} \text{ W/cmK}$$

$$K_{min}(Al_4SiC_4) = 7 \times 10^{-3} \text{ W/cmK}$$

  Thus Al_4SiC_4 might be as good as Si-Ge alloys if its thermal conductivity can be reduced to somewhere near its minimum value. The result depends on its doping and mobility characteristics which are unknown. Its band-gap is about 2.5eV, which is quite suitable.

- Other Carbides. There are other binary and ternary semiconducting carbides such as Be_2C, B_4C, Al_4C_3, $Al_8B_4C_7$, and $Ce_4B_2C_6$. Some studies on B_4C have shown at least limited promise for this material; the other are virtually unstudied to date.

- Silicides. A number of silicides are known to be semiconducting. Some of these are $BaSi_2$, $CrSi_2$, $MnSi_2$, $FeSi_2$, $ReSi_2$, $OsSi_2$, and Ir_3Si_5. Of these the best known one is $OsSi_2$ with a band-gap of 1.8eV and a probable carrier mobility of about 10 cm^2/volt sec. It should be dopable with Al, B, or Re for p-type and P, As, or Ir for n-type. Additions of the isoelectric impurities Fe, Ru, or Ge should enable one to reduce the lattice thermal conductivity to values around 20×10^{-3} W/cmK. The other silicides appear to have band-gaps too small to be useful high temperature thermoelectric materials.

- Nitrides. Two possible nitride thermoelectrics are ScN and $Sm_3Si_6N_{11}$. Other nitrides appear to have either much too large band-gaps or are unstable in moisture, or both. However, the present electrical data are meager, and no useful predictions can be made.

- Boron and Borides. Boron and most of the light-metal borides are semiconductors with very high melting points (>2300 K). They are mechanically rugged, have low vapor pressures, low thermal expansion coefficients, and band-gaps of 1 to 3eV. Their Seebeck coefficients are acceptably large, at least for p-type materials. The most severe limitations are the low carrier mobilities. The most promising ones are α-boron, β-boron, B_6P, B_6As, B_4C, α-AlB_{12}, $B_{48}Al_3C_2$, and $B_{12}Be$.

Some estimated carrier mobilities at room temperature in pure material are:

α-boron : 100 cm^2/volt-sec.

β-boron : 0.1 cm^2/volt-sec.

B_6P : 20 cm^2/volt-sec.

B_4C : 60 cm^2/volt-sec.

$B_{12}Be$: ~20 cm^2/volt-sec.

Thus the carrier mobilities are comparable to those in Si-Ge alloys, except for β-boron, which has a very low mobility. More data are needed to assess their potentials as thermoelectrics.

A second group of borides with potential are metallic borides such as YB_{12} or LuB_{12}. These possess one too many electrons per formula unit to be semiconductors. We suggest here that ternary compounds such as $YBeB_{11}$ or $LuBeB_{11}$ will be semiconductors with mobilities of the order of 50 cm^2/volt-sec and reasonable other thermoelectric properties.

- Oxides. There are a large number of oxide semiconductors, but none appear to have high enough mobilities to be interesting. Many of them are ionic or partially ionic conductors which causes severe troubles at long operating times and large current throughput.

- Sulfides, Selenides, Tellurides. These materials tend to have high vapor pressures at high temperatures, large thermal expansion coefficients, and to be mechanically weak. The sulfides, which are more thermally stable than the selenides or tellurides, tend to lose sulfur by evaporation and turn metallic. Data on Sc_2S_3, Y_2S_3, and La_2S_3 are sufficient to make these materials seem rather unattractive by comparison with Si-Ge, or the borides, carbides, or silicides.

Summary

A review of all of the possible alternative materials led us to rank the prospective materials in the following order of promise to replace Si-Ge alloys.

1. $OsSi_2$
2. $B_{12}Be$
3. $YB_{11}Be$
4. Al_4SiC_4

Thus we recommended some initial efforts on the first of these materials, $OsSi_2$ to study its doping and electrical properties.

2.3 REFERENCES

(1) J. Callaway and H.C. vonBaeyer, Phys. Rev. 120, 1149 (1960).

(2) G.A. Slack, Solid State Phys. 34, 1 (1979).

(3) D.G. Cahill, H.E. Fischer, T. Klitsner, E.T. Swartz, and R.O. Pohl, J. Vac. Sci. Tech., to be published (1989).

(4) D.G. Cahill and R.O. Pohl, Phys. Rev. B37, 8773 (1988).

(5) P.B. Allen and J.F. Feldman, Private communication (1988).

(6) G.A. Slack and P. Andersson, Phys. Rev. B26, 1873 (1982).

(7) T. Hailing, G.A. Saunders, W.A. Lambson and R.S. Feigelson, J. Phys. C15, 1399 (1982).

(8) J.P. Dismukes et al., J. Appl. Phys. 35, 2899 (1964).

SECTION 3
HIGH TEMPERATURE THERMOELECTRIC PROPERTY MEASUREMENTS

3.1 BACKGROUND

The measurement of the thermophysical properties which enter the calculation of the material figure-of-merit is a demanding task. Five distinct measurements are needed with only the density measurements contributing negligible errors to its calculation. Each of the remaining measurements, namely, heat capacity, thermal diffusivity, electrical resistivity and Seebeck coefficient, as a function of temperature, have some accuracy uncertainties. While reasonably precise (5-10%) comparisons of the figures-of-merit are possible if all of the measurements involved are taken on the same instruments, interlaboratory comparisons of the figure-of-merit are subject to quite large discrepancies. As an example, the figure-of-merit of Si-Ge alloy ITM 63 calculated using the Ames Laboratory electrical properties and the Purdue University thermal properties is about 15% higher than calculated using the GE data. While some of these deviations may be attributed to the differences between samples taken from within a single compact, most of this is attributable to measurement technique differences.

Thermoelectric applications place great demands on making high temperature thermophysical property measurements with high accuracy. Currently available techniques have not been able to provide figure-of-merit data unambiguously accurate to a few percent, even though improvements in thermoelectric properties as small as 10% are technologically quite important. Continuing and ongoing efforts must, therefore, emphasize the development of improved thermophysical measurement techniques as well as suitable materials for standards in the range of properties and test temperatures encountered in thermoelectric materials investigations.

Because of the importance of thermoelectric property measurements, a detailed summary of the techniques used in assessing the property improvements achieved on the Program is presented.

3.2 THERMOELECTRIC PROPERTY ASSESSMENT APPROACH AT GE-ASD

The technique used at GE-ASD has the capability of determining the Seebeck coefficient and electrical resistivity simultaneously from room temperature to 1000°C on bar samples, 1/4" x 1/4" x 2". The tests were made on a modified Dynatech TCFCM-N20 thermal conductivity apparatus with the bar samples being instrumented with four chromel-alumel thermocouples (0.005" diameter). The thermocouples were anchored into 0.065" diameter by 0.150" deep holes with Aremco Graphibond adhesive. In addition, the thermocouple beads were coated with Graphibond to form a diffusion barrier between the thermocouple and silicon-germanium alloy sample. The instrumented bar is transferred to the Dynatech station and placed between two graphite plates. The bar is sandwiched between the plates by hand tightening a screw mechanism. Proper electrical contact between the bar and graphite plates is critical since this contact will provide a path for the current input for the determination of the electrical resistivity. A stack heater is adjacent to each graphite plate to provide the thermal gradient necessary for the determination of the Seebeck coefficient. The working temperature is provided by a guard furnace while the static thermal gradient is established by setting the temperature of the upper heater stack 30°C higher than the lower heater stack.

The cavity consisting of the sample, graphite plates, heater stacks, guard furnace and thermal insulation is evacuated by a mechanical pump and a vacuum of 10^{-2} torr is maintained throughout the experiment.

Computer software controls the temperature and acquires, processes, and stores the data. A Hewlett Packard 86B computer is interfaced to a Keithley 181 nanovoltmeter, a Keithley 220 programmable current source, a Hewlett Packard 3497A data acquisition/control unit and three Eurotherm heater controllers. Figure 3-1 shows a schematic diagram of the experimental setup.

The Seebeck coefficient is determined by establishing a static temperature drop between 1° and 30°C across the length of the bar. The voltage output of all four thermocouples is first measured to determine the temperature difference. The induced thermal voltage is then measured between the negative (alumel) leads of the first and second, first and third, and first and fourth thermocouples. This is repeated for the positive (chromel) leads. The

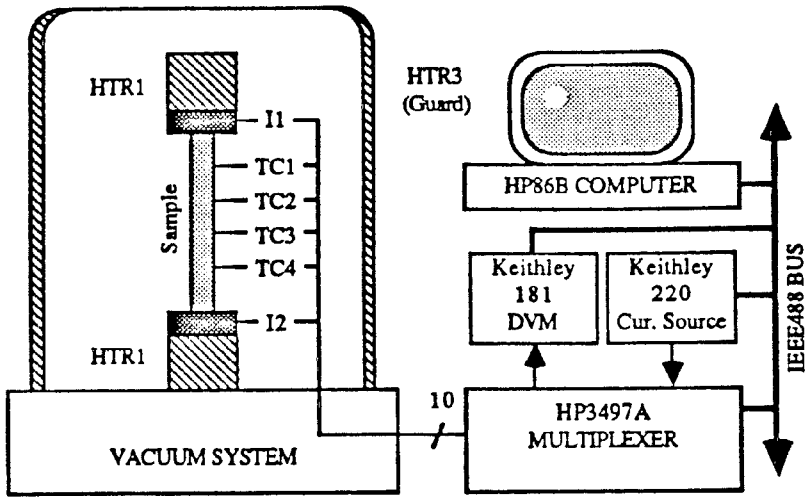

Figure 3-1. Schematic Diagram of Experimental Setup for the Determination of Seebeck Coefficient and Electrical Resistivity for Bar Samples

voltage output of all four thermocouples is measured again to determine the average working temperature and thermal gradients. The Seebeck coefficient, with respect to each thermocouple lead, is the slope of a least squares fit of three Seebeck voltage versus thermal gradient points. The absolute Seebeck coefficient is determined by adjusting for the contribution from the lead wires followed by arithmetic averaging. The errors associated with how well the line goes through the origin and the scatter from the best fit line are also calculated. An example of such a plot is shown in Figure 3-2.

The four point DC method is used to determine the electrical resistivity. The voltage output of all four thermocouples is first measured to determine the average temperature and thermal gradient. A known current (100 mA) in the forward bias is passed from the Keithley 220 programmable current source to the graphite plates through the sample. The steady state voltage produced by this current is measured between the negative (alumel) leads of the first and second thermocouples. The current is then set to zero milliamps and the instantaneous Seebeck voltage drop is measured. A negative bias current is passed through the sample and the steady state voltage thus produced is measured. The zero current instantaneous and steady state Seebeck voltages are measured between the alumel leads. This procedure is then repeated for the alumel leads between the first and third and first and fourth thermocouples. The same procedure is used for measuring the resistances with

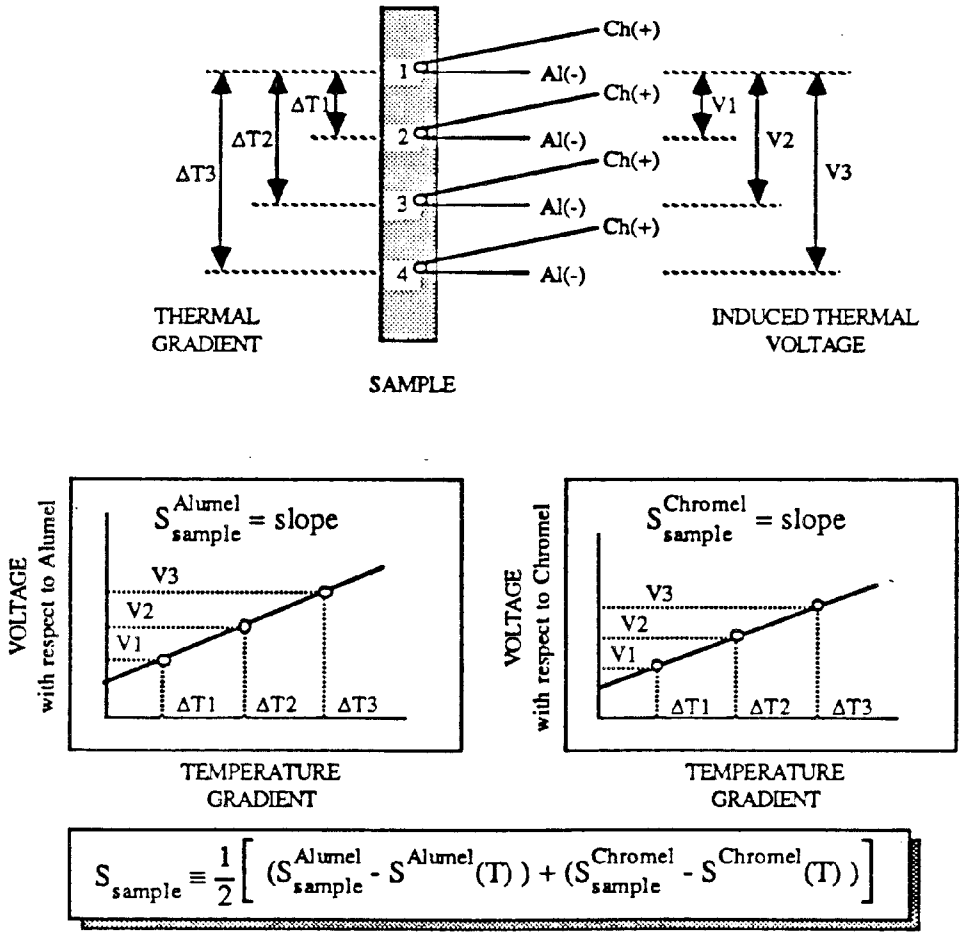

Figure 3-2. Seebeck Coefficient Determination for Bar Samples

respect to the positive (chromel) leads. The electrical resistivity at the working temperature is the slope of a linear least squares fit of the average resistances with respect to the negative and positive leads versus the ratio of the distance between measuring thermocouples to the cross sectional area. The average resistance is the sum of the forward and reverse bias resistances divided by 2. The errors associated with how well the line goes through the origin and the scatter from the best fit line are also calculated. An example plot is shown in Figure 3-3.

A flow diagram indicating the measurement sequence is presented in Figure 3-4.

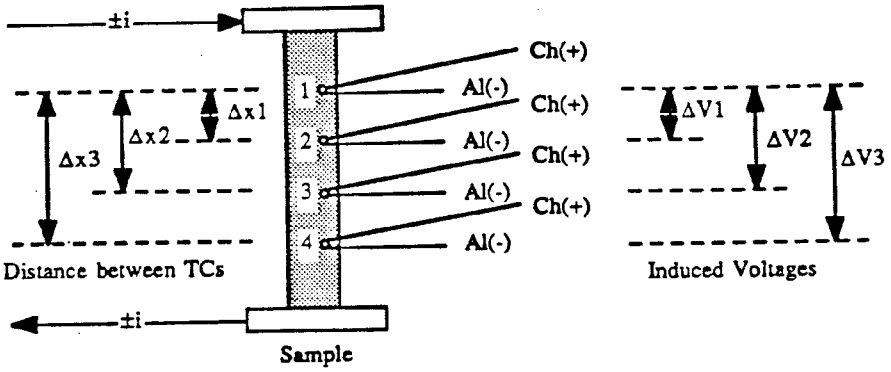

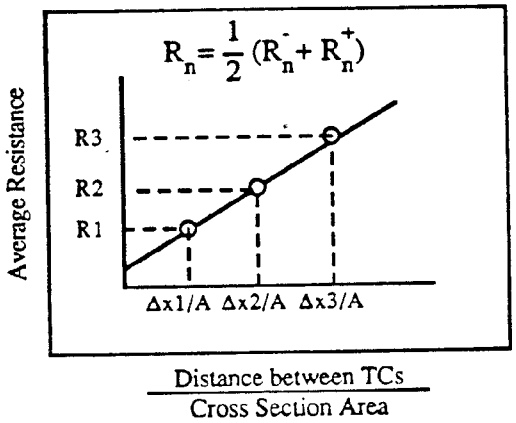

Slope = resistivit

Reverse(-) & Forward(+) Bias Resistances:

$$R_n^- = \frac{(V_n^- - V_0)}{i^-} \qquad R_n^+ = \frac{(V_n^+ - V_0)}{i^+}$$

n=1,2,3

V_0 = open circuit voltage (zero current)

Figure 3-3. Electrical Resistivity Determination for Bar Samples

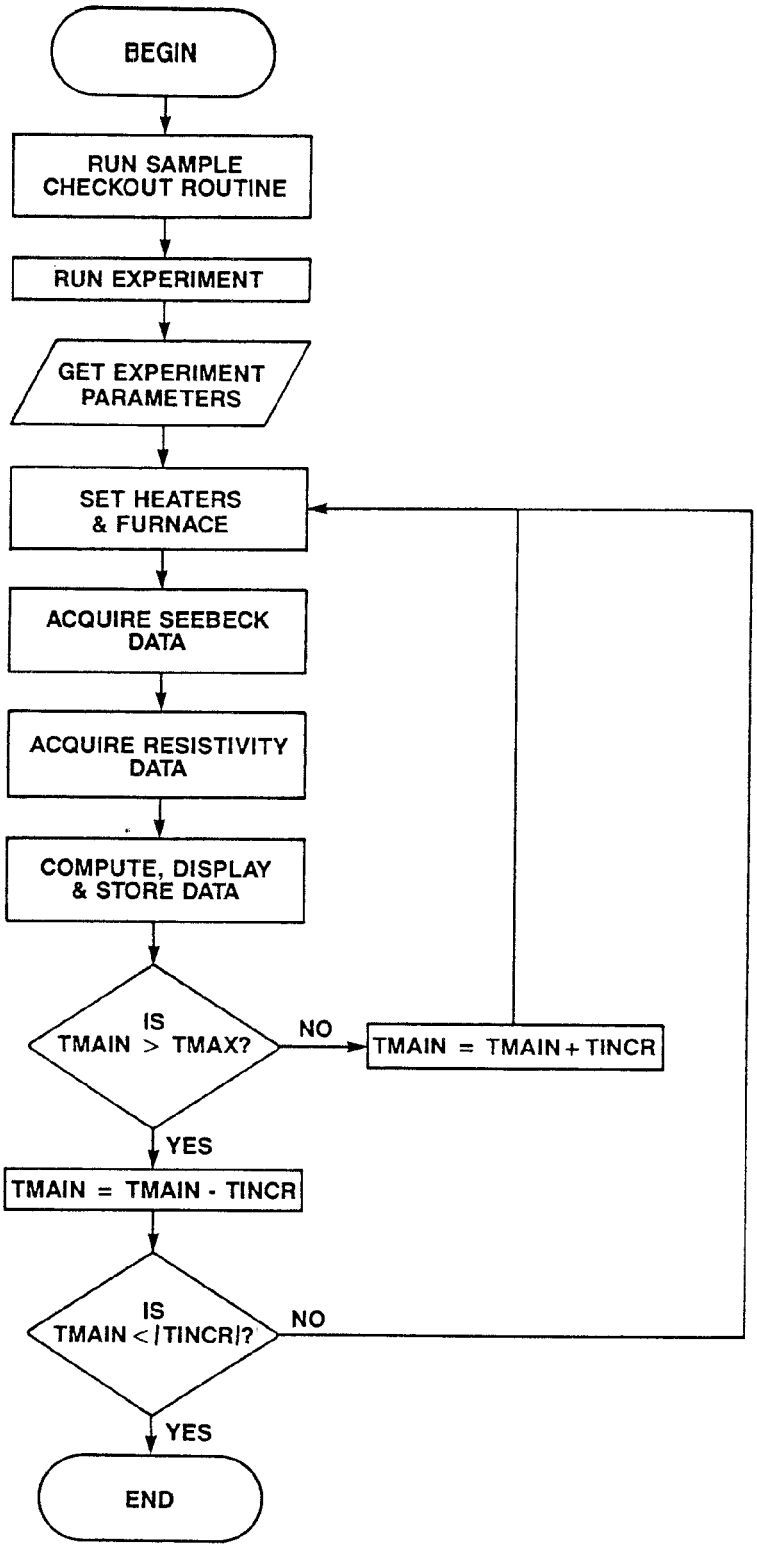

Figure 3-4. Main Routine Chart for Determining the Seebeck Coefficient and Electrical Resistivity of Bar Samples

The laser flash technique is employed to determine the temperature dependent thermal diffusivity. The state-of-the-art facility at GE-ASD combines a Laser Applications 1.06 micron neodymium laser, a Theta high vacuum system and an indium antimonide infrared detector for monitoring the temperature rise of the back face of the disk specimen (Figure 3-5). The thermal conductivity is then calculated from the measured thermal diffusivity, heat capacity and density.

3.3 TEST APPROACHES OF AMES AND BATTELLE-COLUMBUS LABORATORIES

Materials developed on this Program were also tested at the Ames Laboratory of Iowa State University and Battelle-Columbus Laboratory for independent confirmation of results. Both laboratories are also capable of measuring the Seebeck coefficients and electrical resistivities simultaneously. A description of their test setups and procedures are described below.

Ames Laboratory instruments a thin bar sample, 0.25" x 0.1" x 0.6", with a pair of voltage probes. These probes are tapered molybdenum pins which are pushed firmly into holes previously drilled into the sample.

The working temperature and thermal gradient are produced by two tantalum-wound boron nitride heaters placed above and below the sample. A 1000 watt DC power supply is used for each heater. A thermocouple sandwich consisting of Pt and Pt13Rh thermocouple wires (spot welded) between two 15 mil thick Mo disks, is placed between the sample and each heater. This arrangement minimizes the interaction between the sample and TC wires. However, the measured temperature difference is larger and hence the resultant Seebeck coefficient will be smaller. The sample, thermocouple sandwiches and heaters are held in place by a spring loaded device.

The test apparatus is equipped with a mechanical and diffusion pump to maintain a vacuum level of 10^{-6} torr throughout the run. Control of temperature and thermal gradient, data acquisition, and data reduction are computer assisted. Figure 3-6 is a schematic diagram of the Ames Laboratory experimental setup.

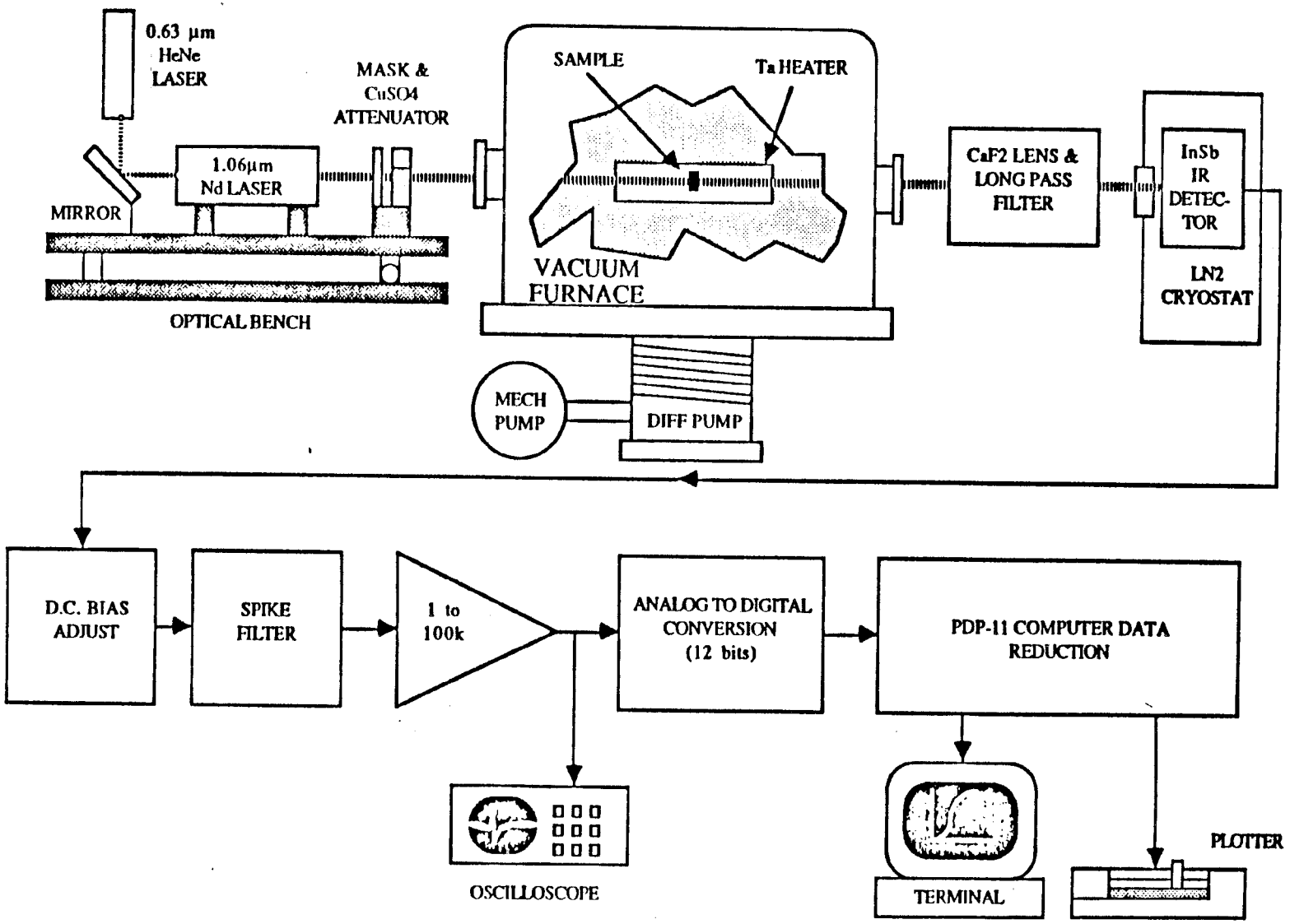

Figure 3-5. GE Laser Flash Thermal Diffusivity Apparatus

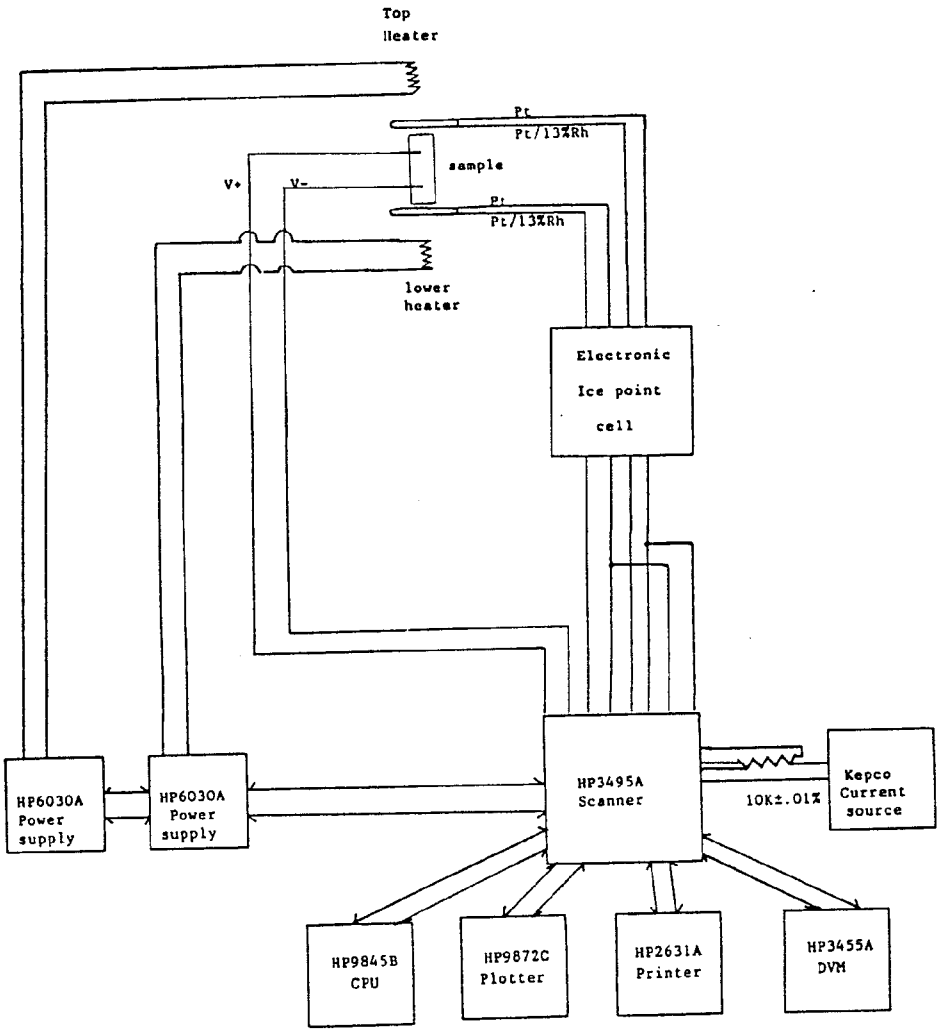

Figure 3-6. Seebeck and Electrical Resistivity Test Setup at Ames Laboratory

For the determination of the Seebeck coefficient, the thermal gradient is allowed to continuously change from zero to 10° or 20°C. The Seebeck voltage (measured between the Pt legs of the thermocouples) and temperatures are measured at ten second intervals. The Seebeck coefficient is obtained from the slope of a linear least squares fit of a series of 25 pairs of Seebeck voltage and thermal gradient measurements. The absolute Seebeck coefficient is derived by adjusting the resultant slope for the contribution from the Pt lead wires.

A four point DC method with current reversal is used to determine the electrical resistivity. A 25 mA current is sent through the Pt leg of the thermocouple in one direction and the voltage is measured between the Mo probes in the sample. The direction of the current is reversed instantaneously and the voltage is measured again. The resistance is calculated from the equation:

$$R = -(V_+ - V_-)/2i$$

where V_+ and V_- are the forward and reverse voltages, respectively, and i is the current. The resulting electrical resistivity is the product of the resistance and the ratio of the cross sectional area to the distance between voltage probes. The resistivity is determined each time the Seebeck voltage and thermal gradient are measured, but the reported value is at, or near zero thermal gradient.

The laser flash technique is also employed by Ames for determining the thermal diffusivity. The unit was designed in-house and uses an indium antimonide infrared detector for monitoring the temperature rise of the back face of the disk specimen.

Battelle-Columbus instruments a bar sample, 1/4" x 1/4" x 0.8", with three W5Re-W26Re thermocouples mechanically embedded into holes previously drill'd. A little W spring is wrapped around one thermocouple leg and is allowed to unwind when placed in a hole to make a snug coupling.

The instrumented bar is placed between molybdenum foil electrodes and heaters, as shown in Figure 3-7. Boron nitride insulators are placed between the current electrodes and heaters. A vacuum of 3×10^{-6} torr is maintained by evacuating the chamber with a mechanical and diffusion pump.

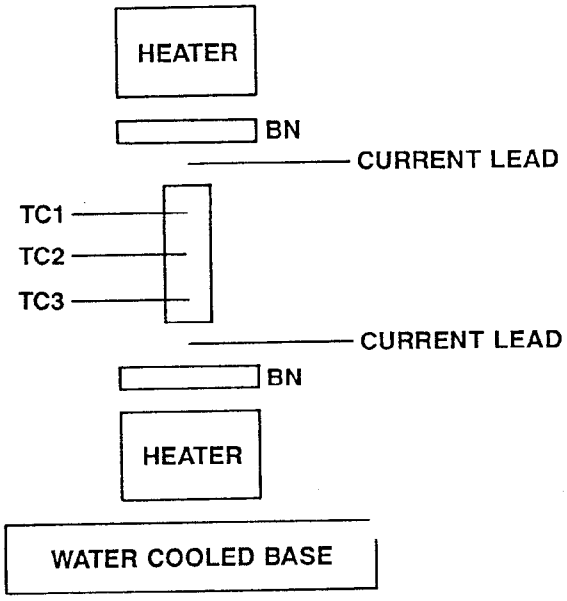

Figure 3-7. Seebeck and Electrical Resistivity Test Setup at Battelle-Columbus

Temperature control and data acquisition are all performed manually. At each working temperature, a static temperature drop ranging from 0 to 20°C is established by adjusting the power to the heaters. The thermal gradient and induced Seebeck voltages are measured between the top and middle positions (TC1-TC2) and the middle and bottom positions (TC2-TC3). The Seebeck coefficient is determined from the slope of a linear least squares fit of the Seebeck voltage versus thermal gradient and is corrected for the Seebeck coefficient of the W5Re thermocouple leg.

The electrical resistivity is determined by the 4 point AC method. At zero thermal gradient, a 40 Hz 10mA current is passed through the molybdenum current leads and the voltage is measured between TC1-TC2 and TC2-TC3 using the W5Re thermocouple legs. The electrical resistivity is the slope of a linear least squares fit of the resistance versus the ratio of the distance between voltage probes to the cross sectional area.

Battelle-Columbus is also capable of measuring thermal diffusivity of disk specimens by the laser flash technique. Battelle uses a mercury cadmium telluride (MCT) detector below 300°C and an indium antimonide infrared detector above 300°C. The MCT detector gives a much higher (but noisier) signal output than the InSb detector at the lower temperatures.

Table 3-1 lists the features of the GE-ASD, Ames and Battelle test arrangements and measurement techniques for the determination of the Seebeck coefficient and electrical resistivity. Several differences can be noted with respect to:

- Thermocouple type
- Method of thermocouple attachment
- Vacuum level
- Design of voltage probes
- Current level

The overall effects of these differences cannot be assessed.

3.4 ROUND ROBIN TEST RESULTS

GE-ASD, Ames Laboratory and Battelle-Columbus participated in round robin testing of a p-SiGe compact fabricated to the MOD-RTG Program specification by the ITM Program. Jet Propulsion Laboratory and Thermo Electron also participated, although they did not perform measurements on the other materials developed on this Program. The measurements taken by GE were authorized by the SP-100 Program.

Table 3-1. Comparison of Test Setup and Procedure for Determining the Seebeck Coefficient and Electrical Resistivity

LAB: / INSTRUMENT:	GE/ASD Old Dynatech	AMES	BATTELLE
MEASUREMENT:			
Simultaneous Seebeck & Resist	Yes	Yes	Yes
Run Time			
Room Temp -> 1000°C (hrs)	25	7	6
1000°C -> Room Temp (hrs)	25	10	6
Temperature Increment (°C)	25	100	100
Computer Controlled	Yes	Yes	No
Calibration Standards Used			
Seebeck	No	No	No
Resistivity	No	Std Resistors	No
Optimal Sample Size (in.)	.25x.25x2"	.25x.1x.6"	.25x.25x.8"
Thermocouple Type	.005" Chromel Alumel	.01" Platinum Pt13%Rh	.005" W5%Re W26%Re
Thermocouple Attachment	Embedded with Graphite Paste	Spring Loaded with 500 psi Pressure	W Springs unwind in drilled holes secure TC
Vacuum	Mechanical	Mech & Diff	Mech & Diff
Typical Pressure (torr)	1.00E-02	1.00E-06	3.00E-06
SEEBECK COEFFICIENT:			
Thermal Gradient	Static	Transient	Static
Temp. Drop Range (°C)	1 to 30	5 to 25	0 to 30
How Determined	slope ΔV vs ΔT	slope ΔV vs ΔT	ΔV/ΔT (2TCs) slope ΔV vs ΔT (3TCs)
ELECTRICAL RESISTIVITY:			
Method Used	4 pt DC with Current Reversal	4 pt DC with Current Reversal	4 pt AC at 40 Hz
Voltage Probes	Chromel-Alumel TCs	Mo pins	W5%Re-W26%Re TCs
Size of Current (mA)	100	25	10
Current Density (A/cm^2)	0.25	0.21	0.025

As shown in Figure 3-8, the Ames and Battelle Seebeck coefficients are lower (by 5-10%) than the GE data. The lower Ames values can be explained by the larger temperature drops measured since the thermocouples are not instrumented into the sample. Ames' electrical resistivities were consistently lower by approximately 5%, while Battelle's were approximately 2% higher than GE values, as shown in Figure 3-9. These discrepancies may be due to the differences noted above relative to sample instrumentation.

The round robin thermal diffusivity data are shown in Figure 3-10. The GE, Ames and Battelle curves are significantly higher than data obtained by NASA-JPL and Thermo Electron. The spread between the lowest (Ames) and the highest (GE) ranges from 5-10%. The Ames and Battelle data were not corrected for heat loss while the GE data were. When the Ames and Battelle data are corrected for heat loss, using the algorithm developed jointly by JPL and Thermo Electron, the data drop down to values approaching JPL and Thermo Electron. The same algorithm doesn't seem to apply to GE data and an explanation is not available at this time.

3.5 CARRIER CONCENTRATION AND MOBILITY

The charge carrier concentration and mobility in the alloys developed on this Program were monitored with a Hall effect apparatus. The equipment is capable of room temperature measurements of both Hall effect and electrical resistivity. In addition, equipment at GE-CR&D was used to supplement the tests. The GE-CR&D equipment can operate in the range of temperatures from -100° to +100°C and can measure the Hall coefficients of samples in which the Hall mobility is about 1 cm^2/volt sec or greater.

3.6 SUMMARY

Extensive property measurements were made on this Program, and it is believed that the trends reported in the following sections of this Report are statistically valid. Also, the data suggest that the improvements reported may be even greater if the accuracy could be improved.

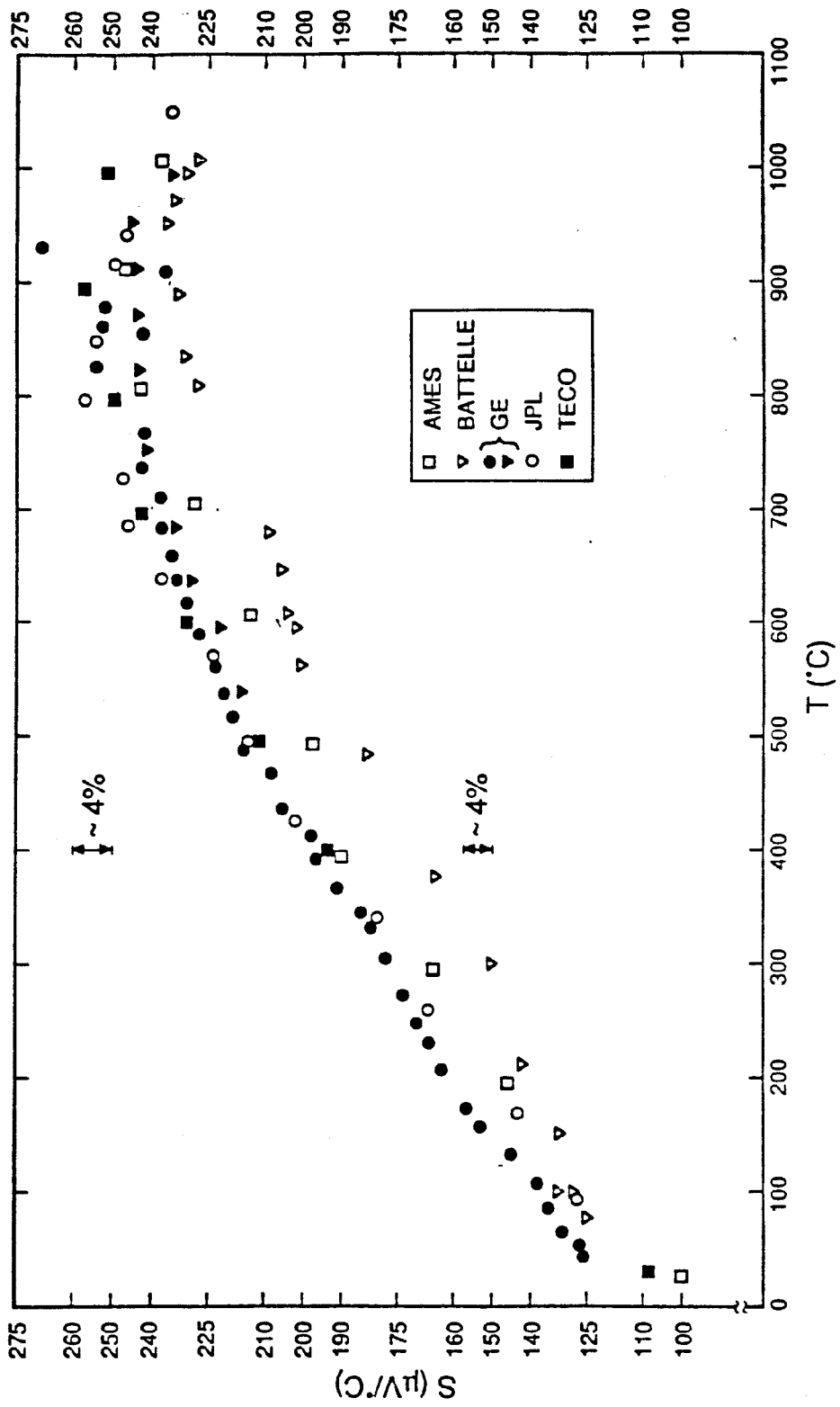

Figure 3-8. Seebeck Coefficient Round Robin Results of a p-SiGe Compact, MHPS-8008-P, Fabricated to MOD-RTG Specification on the ITM Program

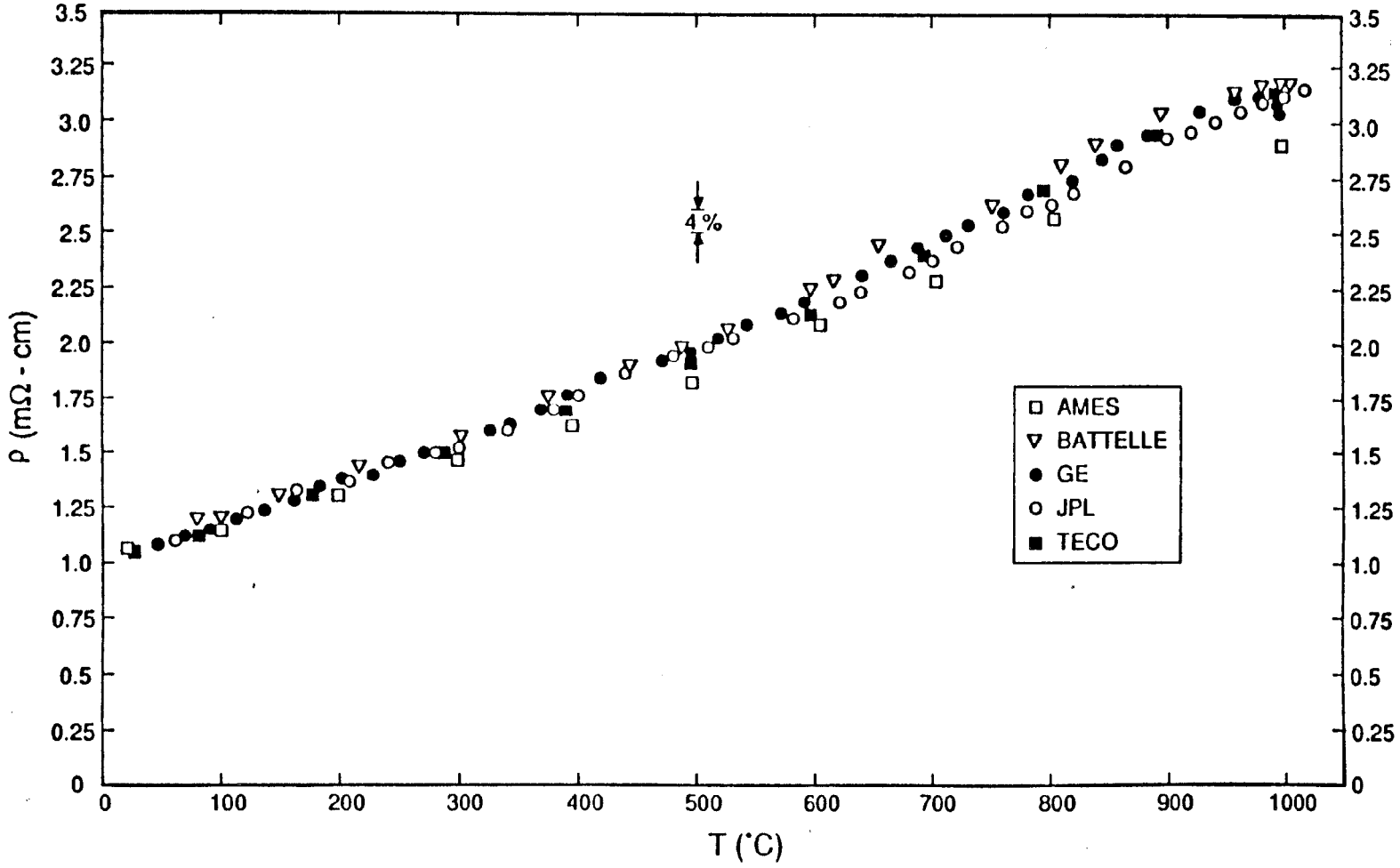

Figure 3-9. Electrical Resistivity Round Robin Results of a p-SiGe Compact, MHPS-8008-P, Fabricated to MOD-RTG Specification on the ITM Program

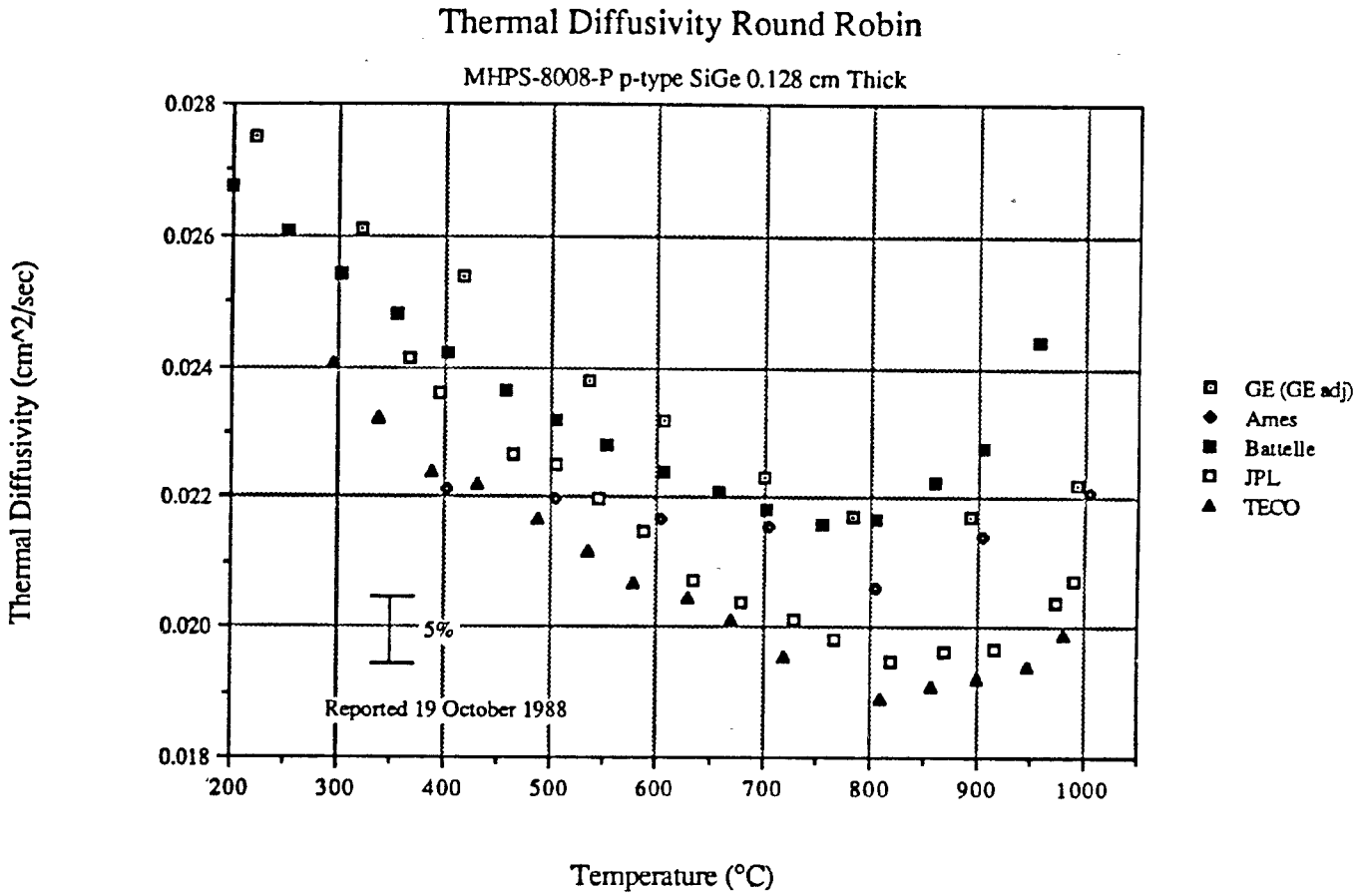

Figure 3-10. Thermal Diffusivity Round Robin Results of a p-SiGe Compact, MHPS-8008-P, Fabricated to MOD-RTG Specification on the ITM Program

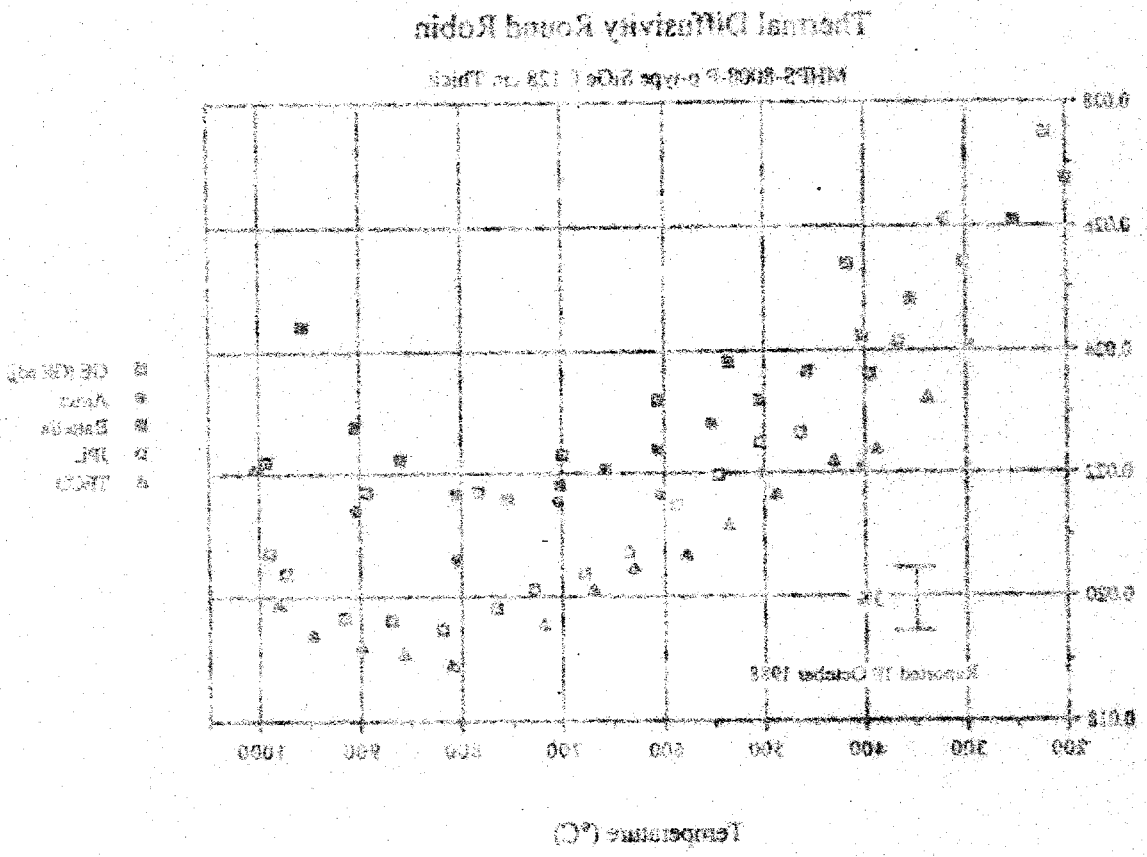

Figure 3-10. Thermal Diffusivity Round Robin Results of a p-SiGe Compact, MHPS-8008-P, Fabricated to MOD-RTG Specification on the ITM Program

SECTION 4

PHASE I - Si-Ge ALLOY THERMOELECTRIC PROPERTY IMPROVEMENT BY PARTICLE/GRAIN SIZE CONTROL

4.1 BACKGROUND

This phase of the Program evaluated the hypothesis of Rowe and others[1-5] that sintered* silicon-germanium alloys may be superior to single crystal materials for use in thermoelectric energy conversion applications. Apart from practical advantages such as ease of preparation and superior mechanical strength afforded by the use of sintered materials, previous theoretical[2,6-12] and experimental[2-4,13,14] evidence had suggested that phonon scattering at grain boundaries could reduce the thermal conductivity, K, compared to single crystal alloys of the same composition. Since the conversion efficiency of a thermoelectric heat engine depends on the temperature range of operation and the material properties through the dimensionless figure-of-merit $ZT = S^2\sigma T/K$, where S is the Seebeck coefficient, σ is the electrical conductivity and T is the temperature, a reduction in K should result in an increased figure-of-merit, and therefore conversion efficiency, if the other properties remain unchanged. This effort reflected results of recent reviews on thermoelectricity in general[15] and heavily doped silicon germanium in particular[5].

Goldsmid and Penn[6] first pointed out that boundary scattering may significantly reduce the thermal conductivity in solid solutions, even for characteristic boundary scattering length scales much larger than a typical phonon mean free path, because a relatively large proportion of the heat is carried by long wavelength phonons. Further theoretical calculations based on the Klemens-Callaway formalism[16,17] have allowed estimates of the magnitude of the reduction in K for undoped[6,7] and heavily doped[2,8-12] silicon germanium of as large as 50% for particle sizes of 1 μm. As carrier mean free path lengths are much smaller than 1 μm, several authors have suggested pressure sintered materials might exhibit electrical properties essentially identical to single crystal materials,[2,8,12,14] with proper

* In this section, sintering is used interchangeably with the actual method of fabrication, namely high temperature pressure sintering or hot pressing.

preparation. Some reports of electrical resistivity measurements[2,18-21] on hot pressed materials support this view in the best cases, but more often the electrical resistivity of the sintered materials are higher than zone leveled materials.[1] In no instance had the anticipated improvement in figure-of-merit due to grain boundary scattering been realized experimentally in silicon germanium alloys, with the possible exception of one report in which GaP was combined with silicon germanium.[22]

This section summarizes experimental results which confirm the reported reduction of the thermal conductivity of sintered materials compared to similar zone leveled materials. It is accompanied, however, by a highly correlated, compensating degradation in the electrical properties. Thus, only limited improvement in the figure-of-merit with reduction in grain size was obtained. The temperature dependence of the observed reduction in the thermal conductivity appears to be inconsistent with the Klemens-Callaway formalism calculations, suggesting that the reduction in thermal conductivity may be due to an altogether different mechanism, one which affects the electrical conductivity in a similar manner.

4.2 EXPERIMENTAL DETAILS

Fifty-five (55) compacts of silicon germanium alloys were prepared by vacuum hot pressing of powders made by a variety of techniques. The starting point for 50 of these compacts was the induction melting of silicon and germanium in a 4 to 1 atomic ratio in fused silica crucibles under high vacuum. N-type materials were prepared by adding 0.55 weight % phosphorus to the melt while p-type samples were prepared with 0.08 weight % boron in the crucible. Some exceptions are indicated in Table 4-1. The melt was cast into a water cooled copper mold to produce a 400 gram ingot which was mechanically pulverized to -80 mesh powder. The resulting powders were then subjected to a variety of different comminution techniques in order to achieve various median particle sizes. Table 4-1 summarizes the comminution techniques employed and the median particle sizes achieved.

Three compacts were prepared from alloy powders produced by a gas atomization technique,[23] and two compacts were prepared by direct pressure sintering of mixed powders of elemental silicon, germanium and boron.

Table 4-1. Summary of Preparation Method and Properties for Hot Pressed $Si_{0.8}Ge_{0.2}$ Alloy Compacts

Hot pressing soak time of 30 minutes at pressing temperature of 1513 K unless otherwise noted.

Sample Preparation Conditions and Compact Number		esd[1] μm	K W/m-K	S μV/K	σ Ω-m 10^{-5}	μ $m^2/V-s$ 10^{-4}	n m^{-3} 10^{26}	Density g/m^{-3} 10^7	ZT** maximum	Oxygen[m] wt%
n-type samples: nominal phosphorus content = 0.59 a/o (unless otherwise noted)										
3332	SB*	>174	4.66	-108.9	0.87	55.8	1.29	3.05	0.917	0.14
68	SB	124	5.03	-121.6	1.06	55.1	1.07	2.87	0.832	0.17
110	GA	15.0	4.51	-97.7	0.73	51.1	1.68	3.01	0.972	
111	GA	16.0	4.47	-102.3	0.78	51.9	1.54	2.99		
69	SB	13.5	4.82	-116.4	0.93	52.7	1.28	3.04	0.762	0.24
130	SB+WM	5.0	5.09	-104.2	0.85	53.2	1.39	2.92	0.942	
70	SB+DM	3.9	4.17	-114.3	1.07	46.4	1.26	3.02	0.967	0.91
79	SB+WM	2.4	3.81	-119.5	1.30	41.4	1.16	2.98		
63	SB+WM	3.3	4.11	-112.3	1.09	44.8	1.28	2.99	0.969	1.00
81	SB+AM	3.3	3.54	-121.4	1.30	43.0	1.12	3.01	0.971	1.31
116	SB+AJP	2.8	4.43	-119.2	0.98	53.7	1.19	2.94		
93	SB+WM,a	1.8	3.97	-115.9	1.15	43.8	1.25	2.96	1.040	0.92
84	SB+HM	1.3	3.74	-117.2	1.14	46.5	1.18	2.96	0.952	2.93
152	WM, b	2.1	3.81	-110.8	1.03	47.2	1.29	3.02	0.943	
151	WM, c	2.4	3.83	-110.6	1.04	46.3	1.30	2.99	0.918	
153	WM, d	1.9	3.90	-105.0	0.91	49.4	1.39	3.01	0.920	

* Refer to notes at end of Table 4-1 for key to abbreviations.

** Estimated from high temperature thermoelectric property data for 26 of the compacts. Typical data from which the estimates are made are summarized for 12 of the compacts in Appendix C.

Table 4-1. Summary of Preparation Method and Properties for Hot Pressed $Si_{0.8}Ge_{0.2}$ Alloy Compacts (Cont'd)

Sample Preparation Conditions and Compact Number		esd[1] μm	K W/m-K	S μV/K	σ Ω-m 10^{-5}	μ m^2/V-s 10^{-4}	n m^{-3} 10^{26}	Density g/m^{-3} 10^{7}	ZT** maximum	Oxygen[m] wt%
p-type samples: nominal boron content = 0.23 a/o (unless otherwise noted)										
3334	SB	>174	5.00	112.5	1.07	34.2	1.72	3.01	0.522	0.21
73	SB	124	5.02	114.6	1.16	32.5	1.66	2.87	0.568	0.15
112	GA	15.0	4.96	117.8	1.07	33.7	1.73	2.98		
74	SB	11.0	5.25	117.0	1.14	32.8	1.67	2.94	0.501	0.28
131	SB+WM	6.1	4.75	117.7	1.11	34.2	1.64	2.99	0.506	
78	SB	4.5	4.37	119.5	1.28	31.5	1.55	2.98	0.619	0.99
62	SB+WM	4.1	4.26	124.2	1.34	31.1	1.50	2.99	0.564	1.00
72	SB+AM	3.0	3.32	131.3	2.06	25.1	1.21	2.98	0.537	2.20
117	SB+AJP	2.8	4.86	123.5	1.25	34.6	1.46	2.96		
99	SB+SM	2.7	3.99	133.5	1.68	29.8	1.25	2.99		1.49
75	SB	2.6	3.88	120.9	1.39	29.2	1.54	2.96	0.619	1.53
60	SB+WM	2.3	4.30	123.3	1.36	31.1	1.48	3.00		
82	SB+AM	2.3	3.22	132.3	1.78	27.9	1.26	2.97	0.564	1.73
103	SB+WM	2.2	3.93	131.4	1.86	29.7	1.13	3.00		0.91
104	SB+WM, e	2.2	3.24	133.4	2.24	26.8	1.04	3.00		4.68
101	SB+SM	1.6	4.10	131.7	1.62	31.3	1.23	3.02		0.37
102	SB+SM, f	1.5	3.90	139.0	2.11	30.2	0.98	3.03	0.519	0.23
83	SB+HM	1.3	3.63	124.2	1.70	27.6	1.33	2.95	0.535	2.84
124	SB, g	8.1	5.73	278.4				2.98	0.184	
11	SB, h	>44	5.32	79.2	0.55	33.2	3.45	3.00		
12	SB, i	>44	5.31	80.2	0.55	33.2	3.45	3.00		
13	SB, j	>44	5.44	78.8	0.54	32.1	3.61	2.99		
14	SB, k	>44	5.42	80.2				2.98		
66	DR	4.2	4.18	149.5	2.39	29.3	0.89	2.97		
66A	DR	4.6	3.77	150.6	2.65	28.7	0.82	2.96	0.523	

Table 4-1. Summary of Preparation Method and Properties for Hot Pressed $Si_{0.8}Ge_{0.2}$ Alloy Compacts (Cont'd)

Sample Preparation Conditions and Compact Number	esd[l] μm	K W/m-K	S μV/K	σ Ω-m 10^{-5}	μ $m^2/V-s$ 10^{-4}	n m^{-3} 10^{26}	Density g/m^{-3} 10^{7}	ZT** maximum	Oxygen[m] wt%
The following 3 samples were prepared from a single lot of SB + WM powder with varying hot pressing soak time:									
86 15 min.	2.0	3.62	127.4	1.67	28.4	1.32	2.93		1.52
88 30 min.	2.0	3.78	127.5	1.63	28.2	1.36	2.96		
87 60 min.	2.0	4.03	127.1	1.50	29.1	1.43	2.98		
The following 4 samples were prepared from a single lot of SB + WM powder with varying hot pressing soak temperatures (Series A):									
89 1513 K	2.2	3.68	129.6	1.69	27.0	1.37	2.94		
90 1528 K	2.2	3.91	126.5	1.54	29.3	1.38	2.96		
91 1543 K	2.2	4.05	124.2	1.40	30.9	1.44	2.99		
92 1558 K	2.2	4.49	124.7	1.39	30.8	1.46	3.00		1.50
The following 4 samples were prepared from a single lot of SB + WM powder with varying hot pressing soak temperatures (Series B):									
97 1513 K	1.9	3.90	129.7	1.31	32.6	1.46	2.98	0.565	1.60
94 1573 K	1.9	4.18	122.7	1.30	33.0	1.45	3.00		
95 1588 K	1.9	4.35	123.4	1.20	31.9	1.64	2.96		
96 1603 K	1.9	4.54	123.1	1.22	28.2	1.82	2.94		
The following three samples were not intentionally doped									
2		124	7.03				2.88		
8		16	6.65		2240		3.00		
1 SB+AJP	2.5	3.75					2.88		

Table 4-1. Summary of Preparation Method and Properties for Hot Pressed $Si_{0.8}Ge_{0.2}$ Alloy Compacts (Cont'd)

Key to Abbreviations

SB - Pulverization in a shatter box

GA - Gas atomization from the melt[23]

DR - Hot pressed mixture of elemental silicon, germanium and boron

AJP - Air jet pulverization

DM - Planetary ball milling in agate using dry agate balls

WM - Planetary ball milling in agate using agate balls, in a hydrocarbon

AM - Attrition milled[24]

HM - Planetary ball milling in agate using agate balls, in water

SM - Planetary ball milling in steel using steel balls, in a hydrocarbon

a - Limited exposure of the powder to air before hot pressing

b - 0.77 atomic % Phosphorus

c - 0.9 atomic % Phosphorus

d - 2.0 atomic % Phosphorus

e - Same powder lot as 103, but roasted in air at 773 K before hot pressing

f - Powder was handled under an inert atmosphere during hot pressing

g - 0.025 atomic % Boron

h - 1.0 atomic % Boron

i - 2.0 atomic % Boron

j - 4.0 atomic % Boron

k - 8.0 atomic % Boron

l - Equivalent spherical diameter

m - Oxygen content determined by neutron activation analysis

The particle sizes listed in Table 4-1 were determined on the powders with a Micromeritics Sedigraph 5000D. The particle sizes were also determined by optical metallography on most of the hot pressed compacts. A good correlation was observed between the particle sizes determined by the two techniques. However, the microstructure of these alloys may be somewhat more complex as the University of Virginia has shown that grains smaller than those revealed by either the Micromeritics or optical methods can be seen in transmission electron microscopy tests (see discussion in Section 6).

Pressure sintering was performed in a double action vacuum hot press with a vacuum level of about 8×10^{-5} torr. TZM dies and molds with a light graphite coating to reduce friction during compact ejection were used. The pressing pressure was 180 MPa and was applied after achieving the soak temperatures. The heating rate to the soak temperature was about 25 K/min. After soaking at temperature (see Table 4-1 for soak times and temperatures), the pressure was released and the compact ejected from the die. Furnace power was then turned off and the furnace allowed to cool. The resulting compacts were 5.08 cm diameter by 1.27 cm thick, dense, crack free and dull gray in appearance.

The thermoelectric properties summarized below on these alloys were obtained using the procedures described in Section 3.

4.3 EXPERIMENTAL RESULTS

Table 4-1 summarizes the results of room temperature measurements of the median particle size of the feed powder, thermal conductivity, Seebeck coefficient, electrical resistivity, Hall mobility, carrier concentration, density and oxygen content for each of the alloys, as well as the hot pressing conditions used. The maximum figure-of-merit calculated from high temperature measurements are also summarized.* As an aid in analyzing the results of Table 4-1, previous room temperature results[1] on zone leveled $Si_{0.8}Ge_{0.2}$ have been parameterized using a purely empirical interpolation scheme as follows:

* The maximum ZT was calculated from the high temperature thermoelectric property measurements on 26 of the alloys. The typical data obtained are summarized for 12 of the alloys in Appendix C.

p-type

$$\ln(S_{zl}) = -0.451 \ln(n) + 5.02,$$
$$\ln(\mu_{zl}) = -0.116 \ln(n) + 3.75,$$
$$\ln(K_{zl}) = -0.089 \ln(n) + 1.78,$$

n-type

$$\ln(-S_{zl}) = -0.502 \ln(n) + 4.82,$$
$$\ln(\mu_{zl}) = -0.300 \ln(n) + 4.19,$$
$$\ln(K_{zl}) = -0.085 \ln(n) + 1.67$$

with S_{zl} in $\mu V/K$, μ_{zl} in 10^{-4} $m^2/V\text{-}s$, K_{zl} in $W/m\text{-}K$ and n in 10^{26} m^{-3}.

The measured thermal conductivity of a hot pressed sample has been normalized by calculating the thermal conductivity of a corresponding zone leveled sample using the Hall carrier concentration of the pressure sintered sample and the zone leveled data above. The resulting ratio of measured to calculated thermal conductivities is shown as a function of the feed particle size in Figure 4-1 for 20 p-type samples of sintered $Si_{0.8}Ge_{0.2}$. Samples prepared using similar comminution techniques and hot pressed under similar conditions (Compact Numbers 62, 74, 75, 78, 83, 99, 131, indicated by the open circles) show a systematic decrease in thermal conductivity as the particle size decreases.

For constant particle size, the thermal conductivity increases systematically with increasing hot pressing times (indicated by TIME: Compact Numbers 86, 87 and 88) or increasing pressure sintering temperatures (TEMPERATURE: Compact Numbers 89, 90, 91 and 92), as indicated by the two sets of data connected by vertical lines in Figure 4-1. Variations in preparation technique also significantly affect the thermal conductivity as indicated by the samples produced by gas atomization (GA: Compact Number 112) and alternate comminution techniques such as air jet pulverization (AJP: Compact Number 117) and attrition milling (AM: Compact Numbers 72 and 82). Intentionally increasing the oxygen content (HO: Compact Number 104) by roasting the powder in air resulted in a significant further reduction in the thermal conductivity, while a decrease in the oxygen content produced by handling the powder under an inert atmosphere (LO: Compact Number 102) may have resulted in a slight increase.

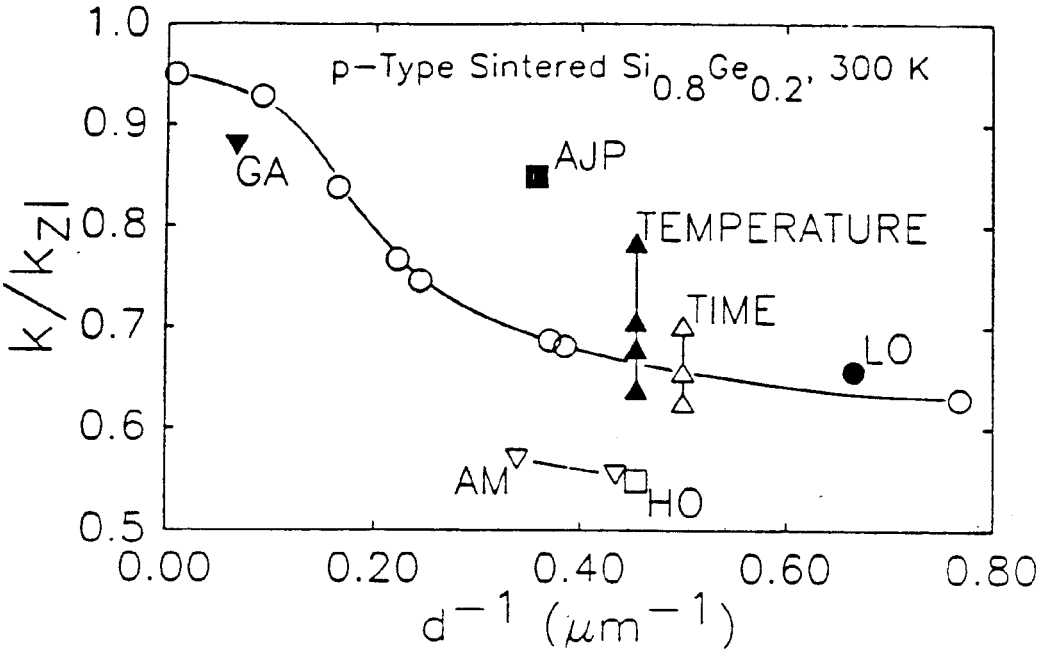

Figure 4–1. The thermal conductivity of hot pressed, heavily doped, p-type $Si_{0.8}Ge_{0.2}$ alloys, normalized to the thermal conductivity of zone leveled material with the same carrier concentration, as a function of feed particle size. The labels indicate variations in preparation procedures as defined in Table 4–1.

A normalization procedure similar to that described above for the thermal conductivity results has also been applied to the Hall mobility results. Figure 4–2 shows the Hall mobility values, normalized to the Hall mobility of zone leveled[1] alloys of the same carrier concentration, obtained on the same 20 samples described above. The mobility trends are seen to be qualitatively similar to the thermal conductivity, with a few exceptions, and a strong correlation between thermal conductivity and Hall mobility is observed.

To demonstrate this effect the quantity $S^2\sigma$, the electrical power factor, has been normalized to similarly doped zone leveled material in the same way as described above for the thermal conductivity. Since the Seebeck coefficient is expected to be a function of the carrier concentration alone, the normalized power factor is expected to be identical to the normalized Hall

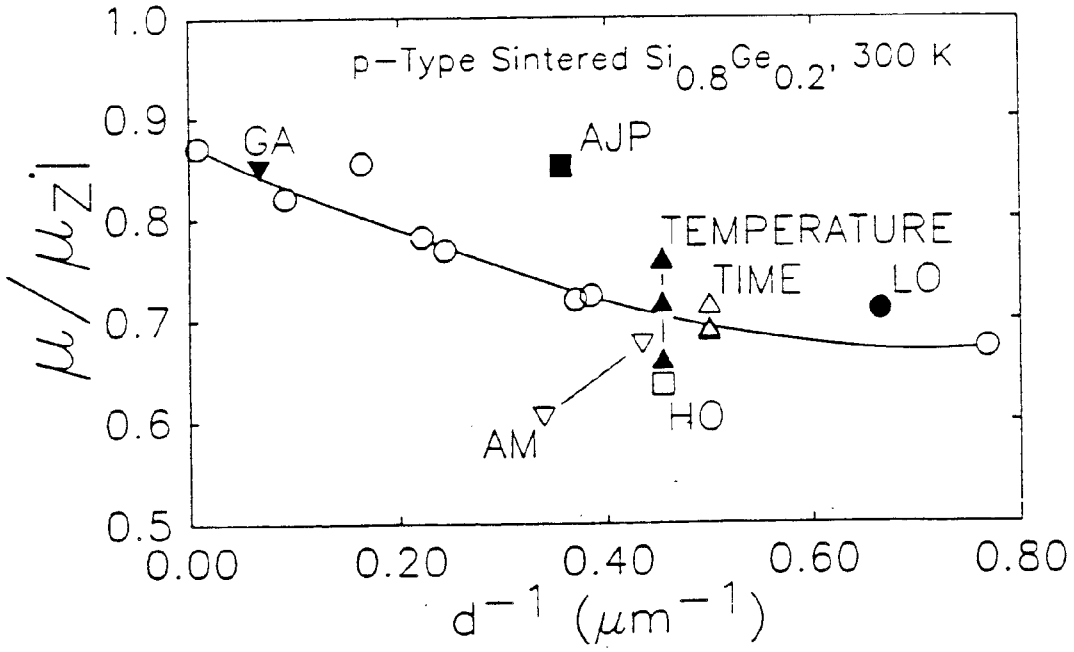

Figure 4-2. The Hall mobility of hot pressed, heavily doped, p-type $Si_{0.8}Ge_{0.2}$ alloys, normalized to the Hall mobility of zone leveled material with the same carrier concentration, as a function of feed particle size. The labels indicate variations in preparation procedures as defined in Table 4-1.

mobility. Figure 4-3 shows the normalized electrical power factor plotted against the normalized thermal conductivity for the samples listed in Table 4-1. The point (1,1) in Figure 4-3, indicated by the end of the solid line, represents zone leveled material and the solid line connects the origin with this point. A data point above this line represents a figure-of-merit higher than zone leveled material and a point below the line represents a lower figure-of-merit compared to zone leveled material. While there is considerable scatter in the data shown in Figure 4-3, the general correlation between electrical and thermal properties is quite strong. Since the thermal conductivity data in Figure 4-1 is determined on the full 5.08 cm compacts, while the electrical mobility and electrical conductivity in Figures 4-2 and 4-3 are determined on a thin sample cut from the compact, some of the scatter in Figure 4-3 may be attributed to inhomogeneities within the compacts.

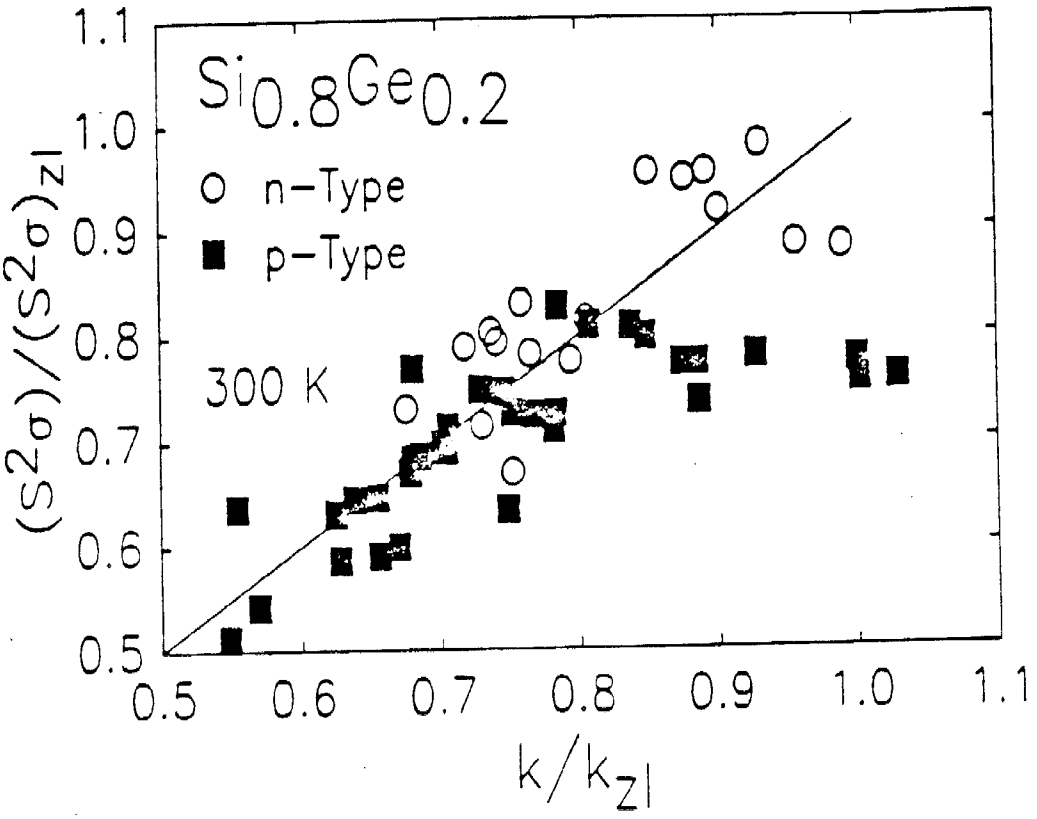

Figure 4-3. The electrical power factor as a function of thermal conductivity of hot pressed $Si_{0.8}Ge_{0.2}$ alloys, normalized to the electrical power factor of zone leveled material with the same carrier concentration. The solid line represents a figure-of-merit equivalent to zone leveled material.

Figure 4-4 shows the Seebeck coefficient, electrical resistivity, thermal conductivity and figures-of-merit for hot pressed n-type (93) and p-type (75) compacts and sample 1834 from Dismukes,[1] the only zone leveled $Si_{0.8}Ge_{0.2}$ sample characterized at high temperatures in that study. The agreement between the figure-of-merit of the pressure sintered and zone leveled materials is quite good and probably within experimental error. While the data in Figure 4-4 are typical of the quality of the high temperature data collected, the two samples selected as examples represent the highest figures of merit observed in this series of tests.

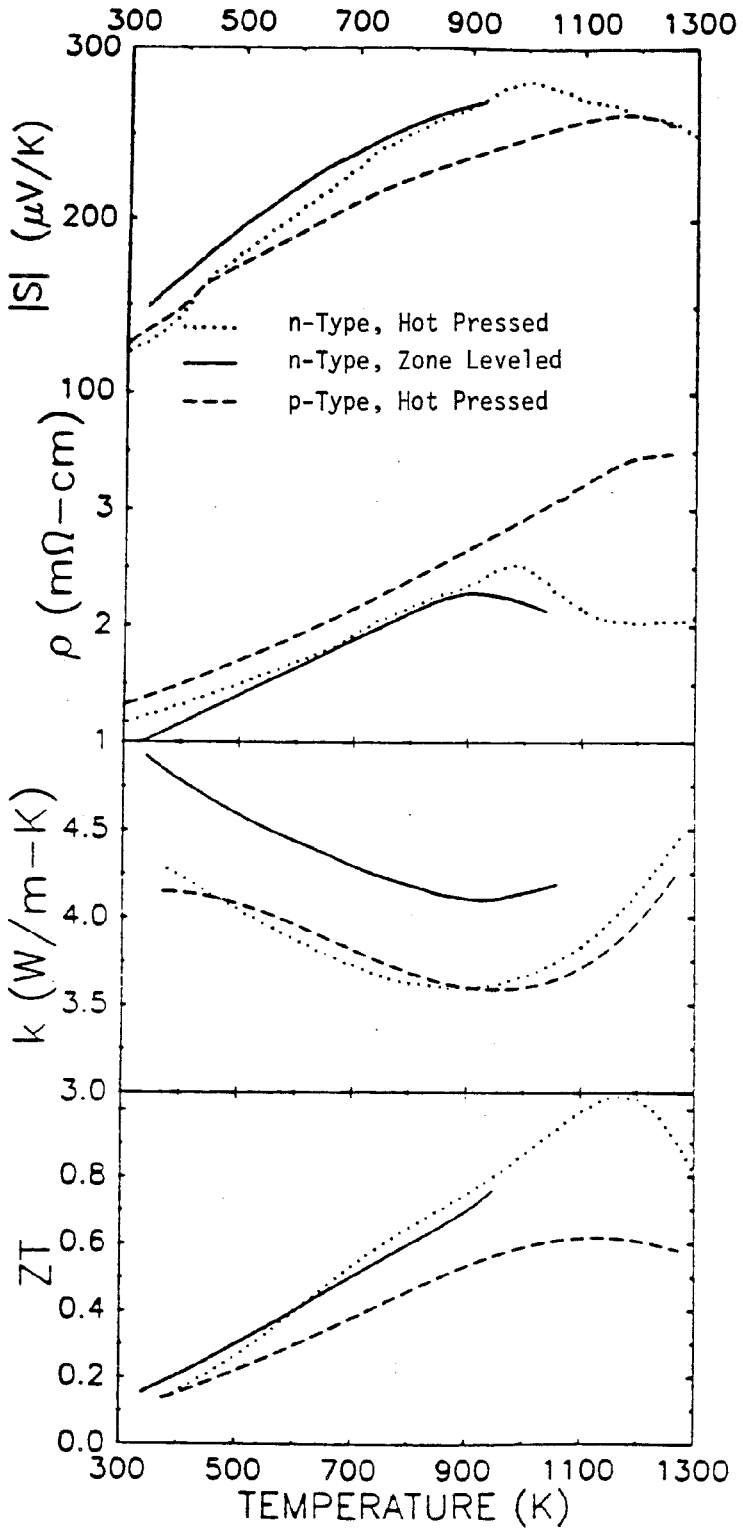

Figure 4-4. The Seebeck coefficient, electrical resistivity, thermal conductivity and figure-of-merit as a function of temperature for n- and p-type sintered $Si_{0.8}Ge_{0.2}$ and n-type zone leveled $Si_{0.8}Ge_{0.2}$ [1] alloys.

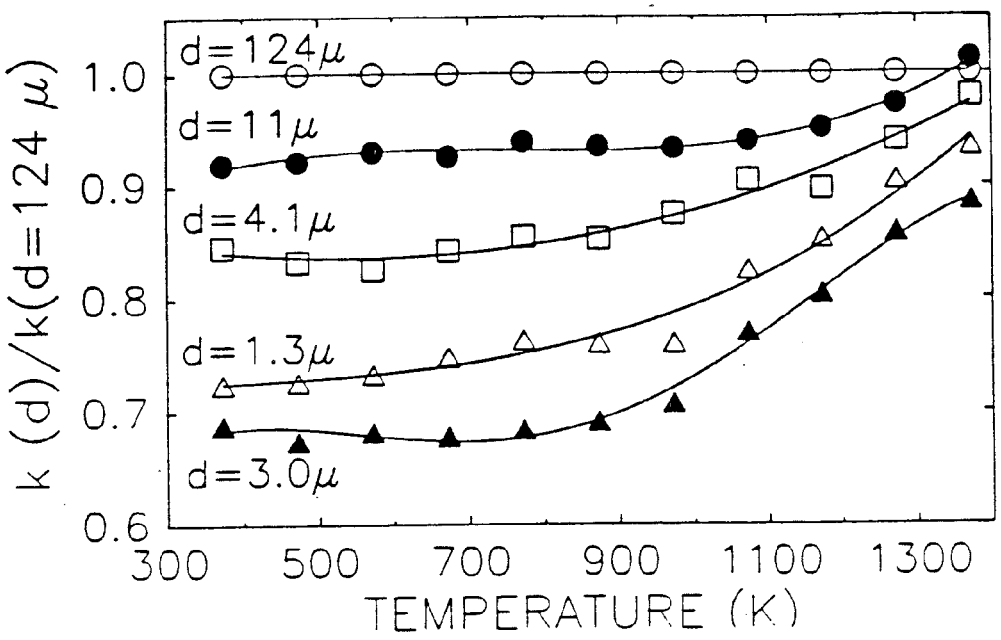

Figure 4-5. The thermal conductivity of five samples of hot pressed p-type $Si_{0.8}Ge_{0.2}$ (Compacts 73, 74, 83, 62 and 72), normalized to the thermal conductivity of the largest particle size sample (Compact 73), as a function of temperature.

decreases with decreasing particle size, with the exception of Compact 72 (3.0 μm) which was prepared by attrition milling, consistent with the low temperature, steady state thermal conductivity data shown in Figure 4-1. The normalized thermal conductivity appears to be nearly independent of temperature between 300 K and about 1000 K. Above 1000 K the conductivity of the smaller particle size samples approaches the conductivity of the larger particle size samples.

Figure 4-6 shows a combined plot of the Seebeck coefficient and the electrical conductivity. Following Jonker[29] a S-σ plot can be described by:

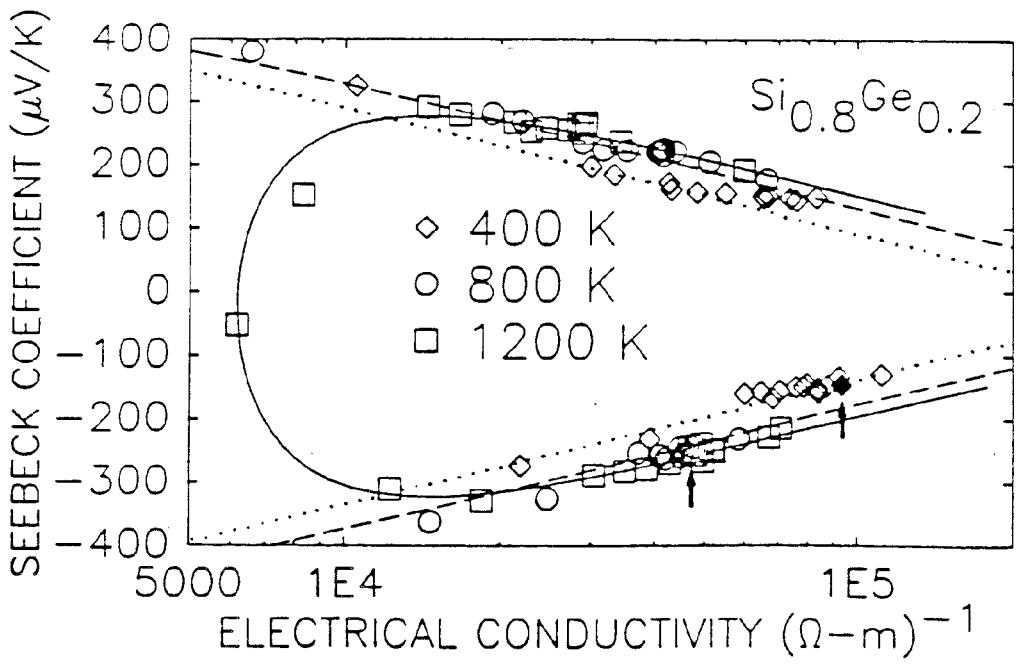

Figure 4-6. The Seebeck coefficient of $Si_{0.8}Ge_{0.2}$ alloy as a function of electrical conductivity. The solid line is a theoretical fit to the data at 1200 K. The dashed and dotted lines indicate a theoretical extrapolation to 800 K and 400 K, respectively, based upon the fit at 1200 K. The arrows and solid circles indicate previous data on zone leveled material[1].

$$S = \pm\frac{k}{2e}\left(\frac{E_g}{kT} + A_+ + A_-\right)\left(1 - \frac{\sigma_{min}}{\sigma^2}\right)^{1/2} - \frac{k}{e}\ln\left[\frac{\sigma}{\sigma_{min}}\left\{1 \pm \left(1 - \frac{\sigma_{min}}{\sigma^2}\right)^{1/2}\right\}\right] + \frac{k}{2e}\ln\left(\frac{N_- e^{A+}\mu_-}{N_+ e^{A-}\mu_+}\right) \quad (1)$$

where $N_{\pm}$, $\mu_{\pm}$ and $A_{\pm}$ are the density of states, mobilities and transport coefficients, respectively, of holes (+) and electrons (-). The solid line in Figure 4-6 represents a fit of the data at 1200 K to Equation (1) with

$(E_g/k_BT + A_+ + A_-) = 11.01 \pm 0.08$,

$\sigma_{min} = 6170 \pm 40$ ohm^{-1}-m^{-1} and

$N_+e^{A+}\mu_+/N_-e^{A-}\mu_- = 0.59 \pm 0.05$.

Much of the scatter in Figure 4-6 is attributed to variations in electrical mobility resulting from the pressure sintering processing. The systematic variations in electrical properties, which correlate with the thermal conductivity (Figure 4-1) and not with carrier concentration, are too small in magnitude to mask the much larger doping effects and hence appear as scatter in Figure 4-6.

The dashed and dotted lines in Figure 4-6 represent calculated Seebeck coefficient at 800 K and 400 K, respectively, based upon Equation (1), the coefficients resulting from the fit to the data at 1200 K and taking into account the temperature variation of σ_{min}, but with no additional adjustable parameters. The agreement between the experimental data and the theoretical curves is quite reasonable, although the p-type Si-Ge alloy data at 400 K deviate somewhat from the predicted curve based upon the 1200 K data. The curvature of the p-type data at 400 K may be indicative of degenerate statistics and the close agreement between the data and the calculated curves at 800 K and 1200 K indicate degeneracy of the carriers has been lifted by 800 K.

Literature estimates of the temperature variation of the energy gap of Si vary from $dE_g/dT = 2.3$[30] to 4.3[31] $\times 10^{-4}$ eV/K. Using E_g (0 K) = 1.07 eV and assuming the same scattering mechanism for electrons and holes gives $A_- = A_+ = 1.7$ to 2.8, indicating either acoustic (A=2) or optical (A=3) phonon scattering of carriers as the dominant scattering mechanism. Insufficient data are available in the low conductivity region of Figure 4-6 to allow a more definitive, independent estimate of dE_g/dT, and hence the scattering mechanism remains somewhat uncertain.

Figures 4-7 and 4-8 show the electrical power factor ($S^2\sigma T$), in thermal conductivity units, as a function of thermal conductivity for n-type and p-type $Si_{0.8}Ge_{0.2}$, respectively. The correlation of electrical and thermal properties shown in Figure 4-3 at room temperature is also evident in

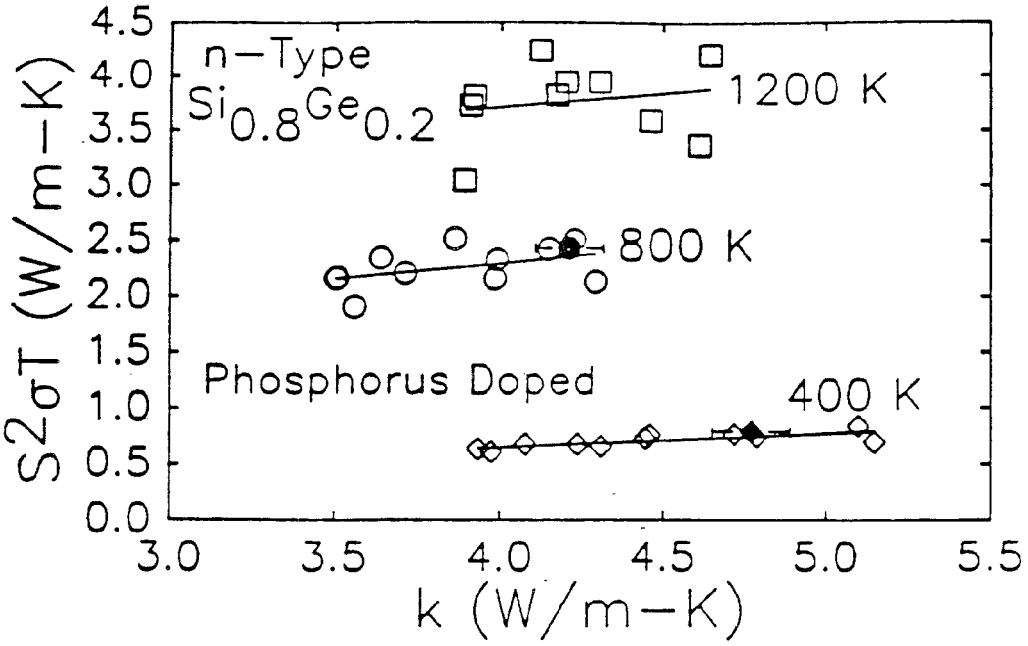

Figure 4-7. Correlation between electrical power factor ($S^2\sigma T$) and thermal conductivity in sintered n-type $Si_{0.8}Ge_{0.2}$ alloys. Error bars indicate $\pm$2.5% and are not actual estimates of the error. Solid lines are least squares fits to the data.

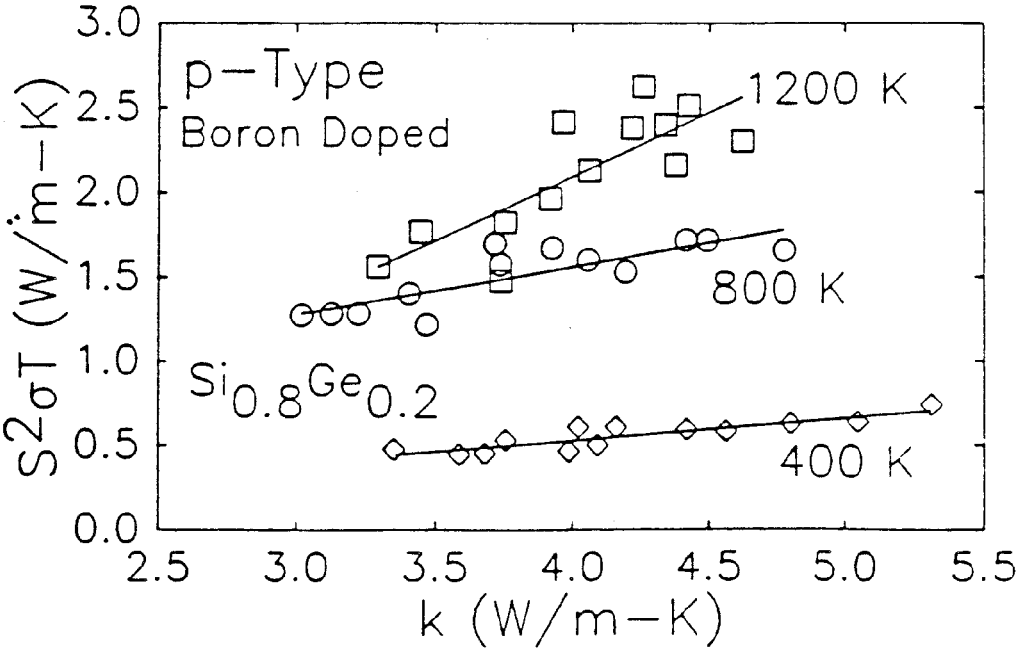

Figure 4-8. Correlation between electrical power factor ($S^2\sigma T$) and thermal conductivity in sintered p-type $Si_{0.8}Ge_{0.2}$ alloys. Solid lines are least squares fits to the data.

the high temperature data, although somewhat less clearly due to carrier concentration variations. The electrical and thermal properties of sintered n-type $Si_{0.8}Ge_{0.2}$ shown in Figures 4-6 and 4-7 are as good as the results of Dismukes[1] on zone leveled material of the same composition; however many samples exhibit lower K and lower $S^2\sigma T$ values.

4.4 DISCUSSION

While the reduction in the thermal conductivity due to reduced particle size (Figure 4-1) has been ascribed to grain boundary scattering of phonons, the correlation between both the Hall mobility and electrical power factor and the thermal conductivity, indicated by the normalized room temperature results shown in Figures 4-2 and 4-3 and supported by the high temperature results of Figures 4-7 and 4-8, is somewhat surprising. Numerous authors have discussed the effect of grain boundary scattering on thermal conductivity,[2-13] but the effect on the electrical conductivity of heavily doped silicon germanium is often neglected because the electron mean free path is estimated to be several orders of magnitude smaller than the expected grain boundary scattering length.

In polycrystalline Si, however, significant reduction in carrier mobility, due to potential scattering at grain boundaries, is well documented and can amount to several orders of magnitude at low doping levels.[32] While discussing 0.2 μm grain size, heavily doped ($\geq 10^{25}$ carriers/m^3) polycrystalline Si, Seager comments that "the mobility will approach (within, say factors of two or three) single crystal values" (Ref. 32, p. 296). As pressure sintered materials can be expected to have more disordered grain boundaries than typical of polycrystalline Si, mobility reductions on the order of 10% to 50% seem quite plausible for 1 μm particle size hot pressed materials due to grain boundary effects alone.

The highly correlated reduction in the electrical and thermal properties observed here may be the result of these two physically different scattering mechanisms for carriers and phonons, both of which may happen to be about the same order of magnitude and correlate well with particle size. The different nature of the scattering mechanisms, however, suggests rather different temperature dependencies would be expected. While there is considerable

scatter in the data, Figures 4-6 and 4-7 suggest the correlation observed at room temperature in Figure 4-3 persists in approximately the same form for tests at high temperatures.

Perhaps more significant is the temperature independence of the reduction in the thermal conductivity due to particle size effects up to about 1000 K and the pronounced change in the temperature dependence at about 1000 K (Figure 4-4). All of the contributions to the thermal conductivity are presumably similar for the samples shown, with the exception of pressure sintering-related effects. As the average phonon mean free path decreases with increasing temperature, the effect of grain boundaries is expected to become less important with increasing temperature. Neither the observed temperature independence below 1000 K nor the more rapid temperature dependence above this temperature seem consistent with the usual Klemens-Callaway formalism, although detailed calculations are required to confirm this assertion.

Assuming a single mechanism is acting similarly on both properties, the following picture is suggested. Consider currents between two particles in a sintered body as flowing essentially unimpeded where the particles are well fused to each other and not at all where the particles are not well fused, regardless of the reason for the lack of fusion.* Estimation of the effective conductivities (thermal or electrical) of the body reduces to the topological problem of calculating the effective path-length of the tortuously connected medium. In such a case, both electrical and thermal current flow would be similarly affected, except at very high temperatures where radiation can contribute to heat transport.

If such defects are responsible for the observed reductions in K and σ, then only limited improvement in the figure-of-merit of hot pressed alloys as currently fabricated is feasible and other approaches must be used. The optimum doping level estimated from the data in Figure 4-6 offers some modest room for growth. The optimum electrical power factors ($S^2\sigma$) for n- and

* Includes SiO_2 particles or inclusions or films as boundary scattering mechanisms.

p-type sintered $Si_{0.8}Ge_{0.2}$ alloys are 3.93×10^{-3} and 2.31×10^{-3} $W/m\text{-}K^2$, which occur at $S = -171\ \mu V/K$, $\sigma = 135{,}000\ ohm^{-1}\text{-}m^{-1}$ and $S = 168\ \mu V/K$, $\sigma = 82{,}000\ ohm^{-1}\text{-}m^{-1}$, respectively, as given by the theoretical fit at 1200 K. These values are close to those predicted for zone leveled materials. Achieving the optimum carrier concentration may require doping beyond the solubility limits, particularly in n-type materials, which will possibly limit the temperature capability of the materials. Due to the logarithmic dependence of S on σ, however, even a factor of 2 deviation from optimum doping results in only about a 10% loss in electrical power factor.

4.5 SUMMARY AND CONCLUSIONS

The empirical values of ZT = 1 previously found in zone leveled $Si_{0.7}Ge_{0.3}$ was achieved, but not significantly surpassed in hot pressed $Si_{0.8}Ge_{0.2}$ alloys. In spite of reductions in the thermal conductivity approaching 50% in fine particle size material, the maximum increase in ZT values was limited to about 10% due to associated reductions in electrical conductivity.

The apparent failure of phonon grain boundary scattering theory to account for the qualitative temperature dependence of the thermal conductivity prompts the suggestion that transport in hot pressed silicon germanium differs from zone leveled materials primarily due to the tortuous connectivity of the former compared to the latter and the possible presence of oxygen films at the particle boundaries. This suggestion also seems consistent with the observed effects of processing and the correlated nature of the variations in electrical and thermal conductivities. Finally, analysis indicates either acoustic or optical phonon scattering of the charge carriers dominates the temperature dependence of the high temperature electrical properties.

These results provided much information as to changes in composition and processing procedures that were needed to more closely achieve the program goal for Si-Ge alloys. The use of GaP as an addition to offset grain boundary effects and/or increase charge carrier levels and mobilities was evaluated and these data and results are summarized in Section 5.

4.6 REFERENCES

(1) J.P. Dismukes, L. Ekstrom, E.F. Steigmeier, I. Kudman, and D.S. Beers, J. Appl. Phys. 10, 2899 (1964).

(2) H.R. Meddins and J.E. Parrott, J. Phys. C: Solid State Phys. 9, 1263 (1976).

(3) D.M. Rowe, V.S. Shukla, and N. Savvides, Nature 290, 765 (1981).

(4) D.M. Rowe and V.S. Shukla, J. Appl. Phys. 52, 7421 (1981).

(5) C.M. Bhandari and D.M. Rowe, Contemp. Phys. 21, 219 (1980).

(6) H.J. Goldsmid and A.W. Penn, Phys. Lett. 27A, 523 (1968).

(7) J.E. Parrott, J. Phys. C: Solid State Phys. 2, 147 (1969).

(8) D.M. Rowe, J. Phys. D: Appl. Phys. 7, 1843 (1974).

(9) C.M. Bhandari and D.M. Rowe, J. Phys. D: Appl. Phys. 10, L10 (1977).

(10) C.M. Bhandari and D.M. Rowe, J. Phys. C: Solid State Phys. 11, 1787 (1978).

(11) N. Savvides and J.J. Goldsmid, J. Phys. C: Solid State Phys. 13, 4671 (1980).

(12) C.M. Bhandari and D.M. Rowe, in Proceedings of the Second International Conference on Thermoelectric Energy Conversion, Edited by K.R. Rao, (IEEE Publishing Services, New York, 1978), p. 32.

(13) D.M. Rowe and R.W. Bunce, J. Phys. D: Appl. Phys. 2, 1497 (1969).

(14) N. Savvides and H.J. Goldsmid, J. of Mat. Sci. 15, 594 (1980).

(15) D.M. Rowe and C.M. Bhandari, Modern Thermoelectrics, (Reston Publishing Co., Reston, Virginia, 1983).

(16) P.G. Klemens, Proc. Phys. Soc. A68, 1113 (1955).

(17) J. Callaway, Phys. Rev. 113, 1046 (1959).

(18) R.W. Bunce and D.M. Rowe, Mater. Sci. Engng. 2, 278 (1967).

(19) P.R. Sahm and L.H. Gnau, Z. f. Metalkunde 59, 137 (1968).

(20) D.M. Rowe, J. Phys. D: Appl. Phys. 4, 1816 (1971).

(21) R.D. Nasby and E.L. Burgess, in Proceedings of the 7th Intersociety Energy Conversion Engineer Conference, (IEEE Publishing Services, New York, 1972), p. 130.

(22) R.K. Pisharody and L.P. Garvey, in Proceedings of 13th Intersociety Energy Conversion Engineer Conference, (IEEE Publishing Services, New York, 1978), p. 1963.

(23) S.A. Miller, in Amorphous Metallic Alloys, edited by F.E. Luborsky (Butterworth and Co., Ltd., London, 1983).

(24) D.H. Stutz, S. Prochazka, and J. Lorenz, J. Am. Ceram. Soc. 68, 479 (1985).

(25) L.J. van der Pauw, Philips Res. Repts. 13, 1 (1958).

(26) R.E. Taylor and K.D. Maglic, in Compendium of Thermophysical Property Measurement Methods, Vol. 1, edited by K.D. Maglic, A. Cezairliyan and V.E. Peletsky (Plenum Press, New York, 1984), p. 305.

(27) T. Amano, B.J. Beaudry, K.A. Gschneidner, Jr., R. Hartman, C.B. Vining and C. Alexander, J. Appl. Phys. 62, 819 (1987).

(28) N. Cusack and P. Kendall, Proc. Phys. Soc. Lond. 72, 898 (1958).

(29) G.H. Jonker, Philips Res. Repts. 23, 131 (1958).

(30) B.R. Pamplin, in Handbook of Chemistry and Physics, 54th Edition, edited by R.C. Weast, (CRC Press, Cleveland, Ohio, 1983), p. E98.

(31) F.J. Morin and J.P. Maita, Phys. Rev. 96, 28 (1954).

(32) C.H. Seager, Ann. Rev. Mater. Sci. 15, 271 (1985).

(32) D.H. Sargent, Annu. Rev. Mater. Sci.

SECTION 5

PHASE II - Si-Ge ALLOY THERMOELECTRIC PROPERTY IMPROVEMENT BY SOLUTION OF GaP

5.1 BACKGROUND

As early as 1976, GaP was suggested as a promising additive for improving the performance of silicon germanium alloys under a Jet Propulsion Laboratory (JPL) sponsored program at the SYNCAL Corporation.[1] GaP was postulated to lower the lattice component of the thermal conductivity by increasing the "complexity" or mass fluctuation scattering of the lattice in a manner similar to the thermal conductivity lowering mechanism which results from the additions of germanium to silicon.[2] Since that time, measurements in several laboratories, including Purdue University, Battelle-Columbus and General Electric, as well as at SYNCAL, have confirmed the low thermal conductivities of samples containing GaP. Direct comparison with samples not containing GaP but prepared in similar ways has been quite difficult, due to the large differences in the behaviors of the various materials, the sensitivity to processing parameters and the complex processing procedures used for SiGe-GaP alloy fabrication.

While some degradation of the electrical properties of GaP containing materials has been consistently observed, data supporting an overall improved thermoelectric performance due to the reductions in thermal conductivity resulted in the selection of SiGe-GaP alloys for use in multicouple device evaluation in the DOE MOD-RTG Program in 1983. The procedure used for the preparation of SiGe-GaP is exceedingly complex and one of the major thrusts of the ITM Program was an attempt to separate the contributions of the various manufacturing processes to the performance of the material and, hence, optimization of the processes.

This section of the report summarizes the results of iterative experimental/theoretical tasks to develop techniques for maximizing the properties of n-type SiGe-GaP alloys. The chemistry of GaP additions is quite complex and this was considered to be the origin of the poor reproducibility of electrical property improvements on the alloys. To overcome these difficulties, a number of approaches were evaluated for increasing and/or controlling the nature of

the solution of GaP in the alloys. Included were zone leveling, composition/heat treatment control and charge carrier compensation. Major emphasis was directed at maximizing GaP solubility by controlling Si/Ge ratios in the alloys.

5.2 FIGURE-OF-MERIT DETERMINATION AT MAXIMUM GaP SOLUBILITY

5.2.1 THE EFFECT OF GaP DOPING ON 50/50 Si-Ge ALLOYS

The solubility of gallium phosphide in 80% silicon-20% germanium appears to be fairly low, probably less than 1/2 Mol percent. Figure 5-1 shows the trends in GaP concentrations associated with grains of various Si-Ge ratios in a polycrystalline sample prepared by GE-CR&D with a bulk composition of 2 Mol percent gallium phosphide after a one week anneal at 840°C. The dashed line approximates the GaP concentrations observed in the same sample after melting but before annealing. From these data, a single phase region in the GaP-SiGe system is expected. The data also suggested that gallium phosphide solubility was expected to increase sharply with increased Ge contents up to at least the 50/50 Si-Ge alloy compositions.

Based upon these data, an experiment was designed to produce samples of 50/50 Si-Ge alloys to which 2, 4, 8 and 16 Mol percent GaP were added. Table 5-1 shows the nominal compositions of the samples fabricated. (The similarity between the atomic and weight fractions is purely a coincidence resulting from the atomic masses of the elements involved.)

Table 5-1. 50% Si-50% Ge Samples with High Gallium Phosphide Content

Sample Number	Atomic Fraction				Weight %	Formula
	Si	Ge	Ga	P	GaP	
190	0.42	0.42	0.08	0.08	16	(SiGe) 0.84 (GaP) 0.16
191	0.46	0.46	0.04	0.04	8	(SiGe) 0.92 (GaP) 0.08
192	0.48	0.48	0.02	0.02	4	(SiGe) 0.96 (GaP) 0.04
193	0.49	0.49	0.01	0.01	2	(SiGe) 0.98 (GaP) 0.02

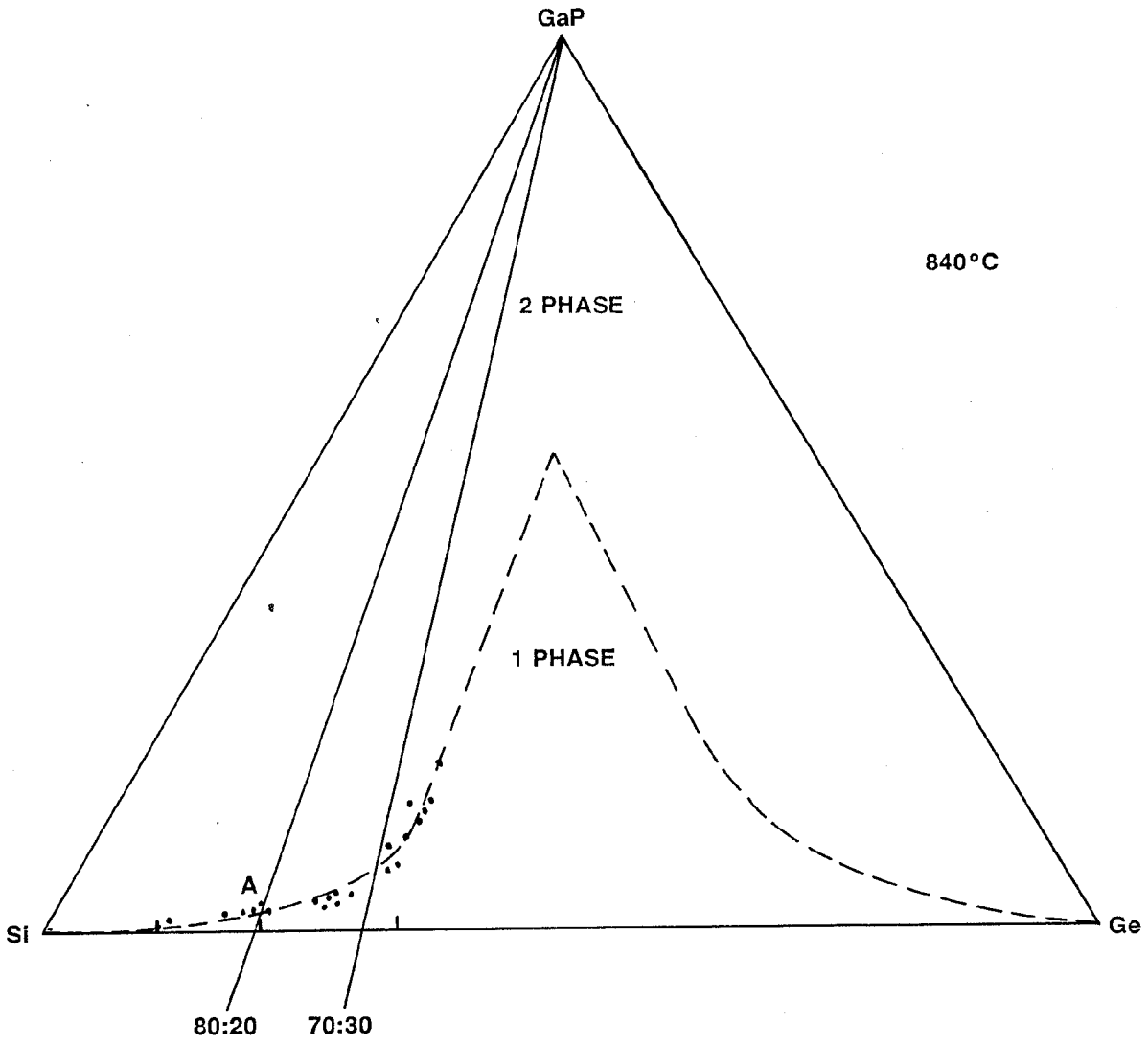

Figure 5-1. Isothermal SiGe-GaP Ternary Phase Diagram

The isothermal SiGe-GaP ternary phase diagram as indicated by electron beam microprobe analysis of a heterogeneous sample prepared by melting under 40 atmospheres of overpressure followed by annealing for one week at 840°C.

5.2.1.1 Fabrication

The procedure used to prepare these samples is referred to as the vacuum melting/chill casting/grinding/hot pressing technique. It involves the melting of GaP, Ge and Si in a fused silica crucible and subsequently vacuum hot pressing the resultant crushed powder. The fused silica crucible was filled in the following order: first, GaP; second, Ge; and third, Si. The crucible was placed in a graphite susceptor and inductively heated under 0.5 atmosphere of argon. The layering of the constituent materials enabled the germanium to melt first and combine with the GaP before the vapor pressure of the GaP became too large.

Once a completely molten state was attained, the liquid was poured into a water cooled, copper mold. The resulting ingot was then mechanically pulverized to about 5 micron median particle size and hot pressed at a temperature near the estimated solidus.

This process was used successfully to prepare 14 compacts in the early phases of the ITM Program (Compacts 5, 6, 7, 9, 10, 21, 22, 23, 24, 25, 38, 39, 40 and 41). While considerable clouding of the casting chamber occurred during the melting process, indicating some material loss and complicating the temperature determination just prior to casting, the actual amount of material loss, as determined by weighing the resulting casting, was shown to be a small fraction of the GaP added.

The schematic process flow for fabricating the four alloys in Table 5-1 are shown in Figures 5-2 through 5-5. Figure 5-6 summarizes the typical hot pressing conditions for the compacts. Three of the alloys (2, 4 and 8 Mol % GaP) were satisfactorily produced as three inch (3") diameter by approximately three-quarter inch (3/4") thick compacts, and were annealed at temperatures as high as 1100°C without significant melting (a temperature consistent with expected phase equilibrium). The 16 Mol percent alloy exhibited some tendency to melt in the 1000° to 1100°C range and no significant tests were made on it. The additional annealing was done in order to promote homogenization and further solution of the GaP.

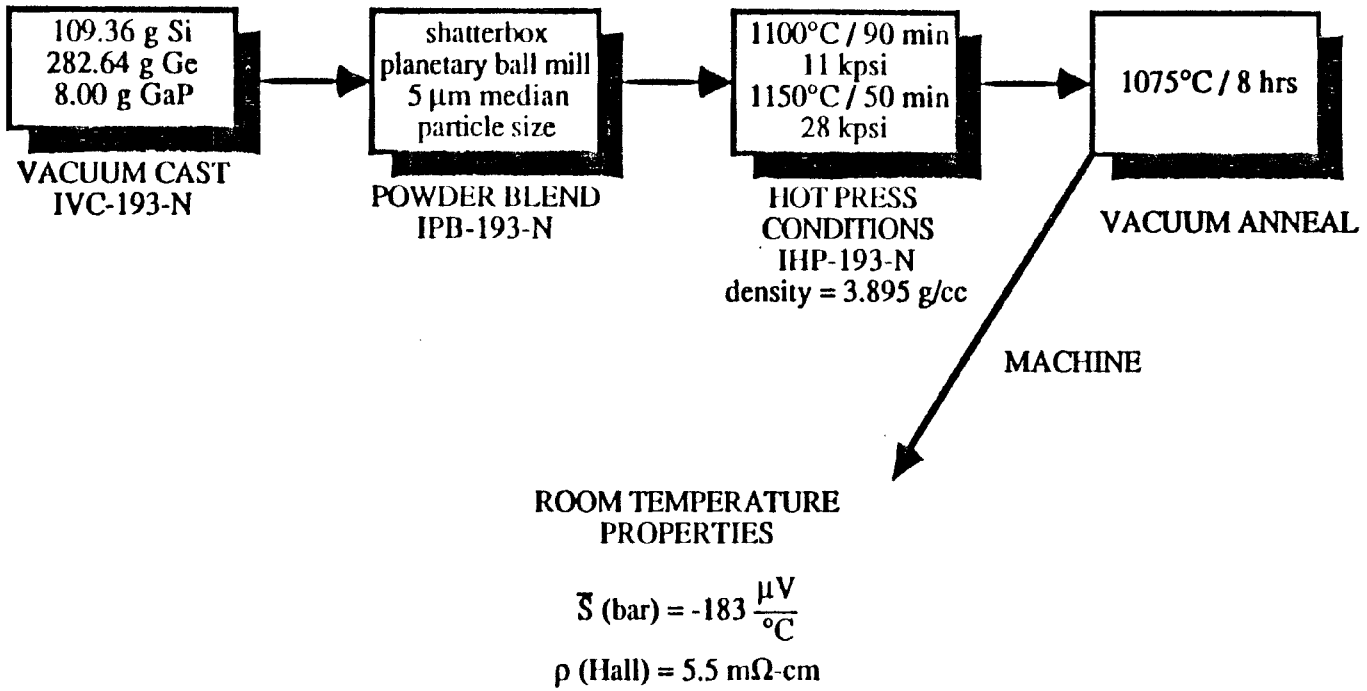

Figure 5-2. ITM-193 2 Mol Percent GaP in 50/50 Si-Ge

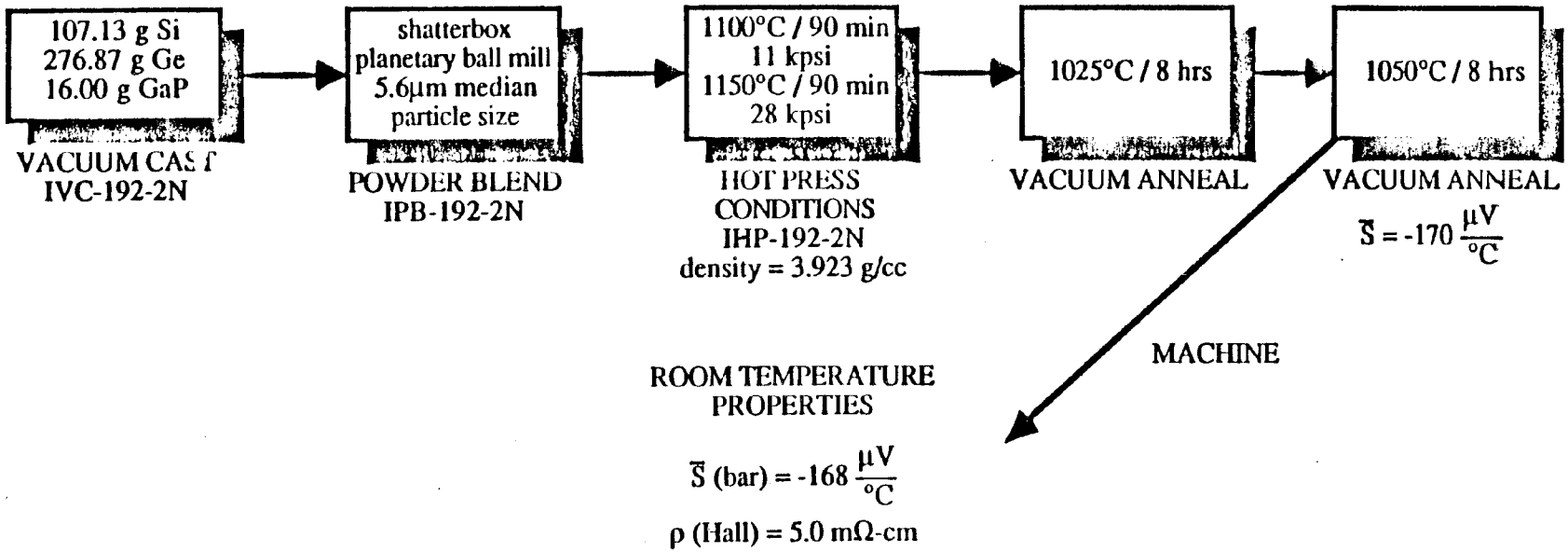

Figure 5-3. ITM-192 4 Mol Percent GaP in 50/50 Si-Ge

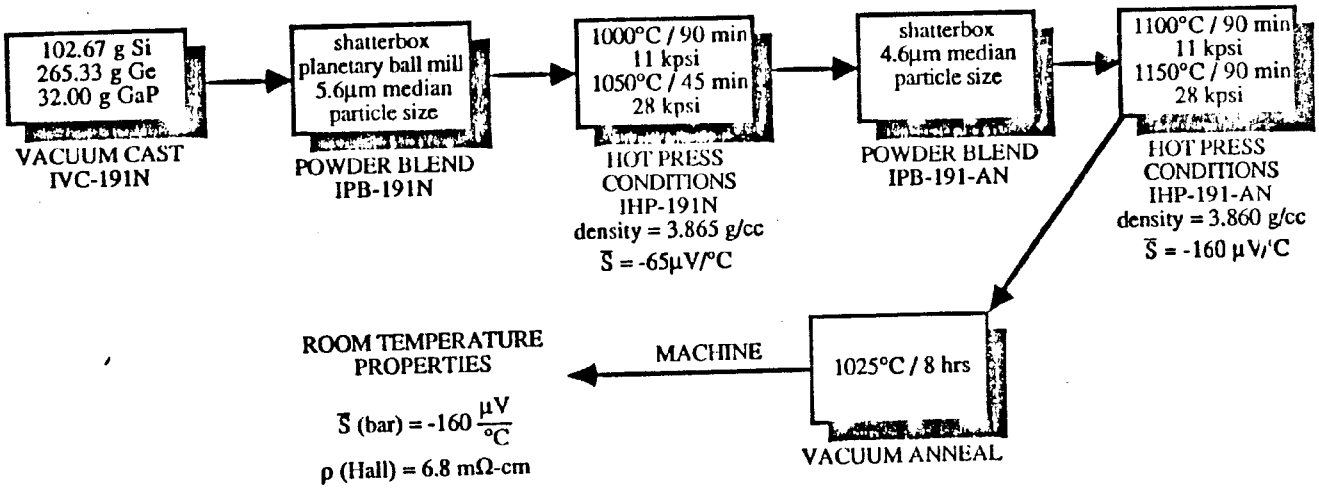

Figure 5-4. ITM-191 8 Mol Percent GaP in 50/50 Si-Ge

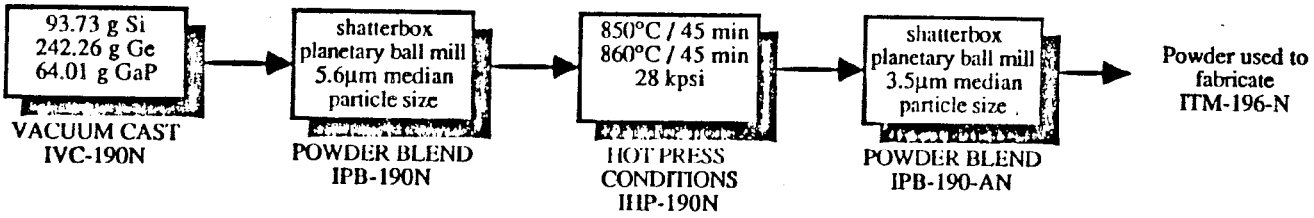

No property data obtained because material is brittle and subject to incipient melting during vacuum annealing.

Figure 5-5. ITM-190 16 Mol Percent GaP in 50/50 Si-Ge

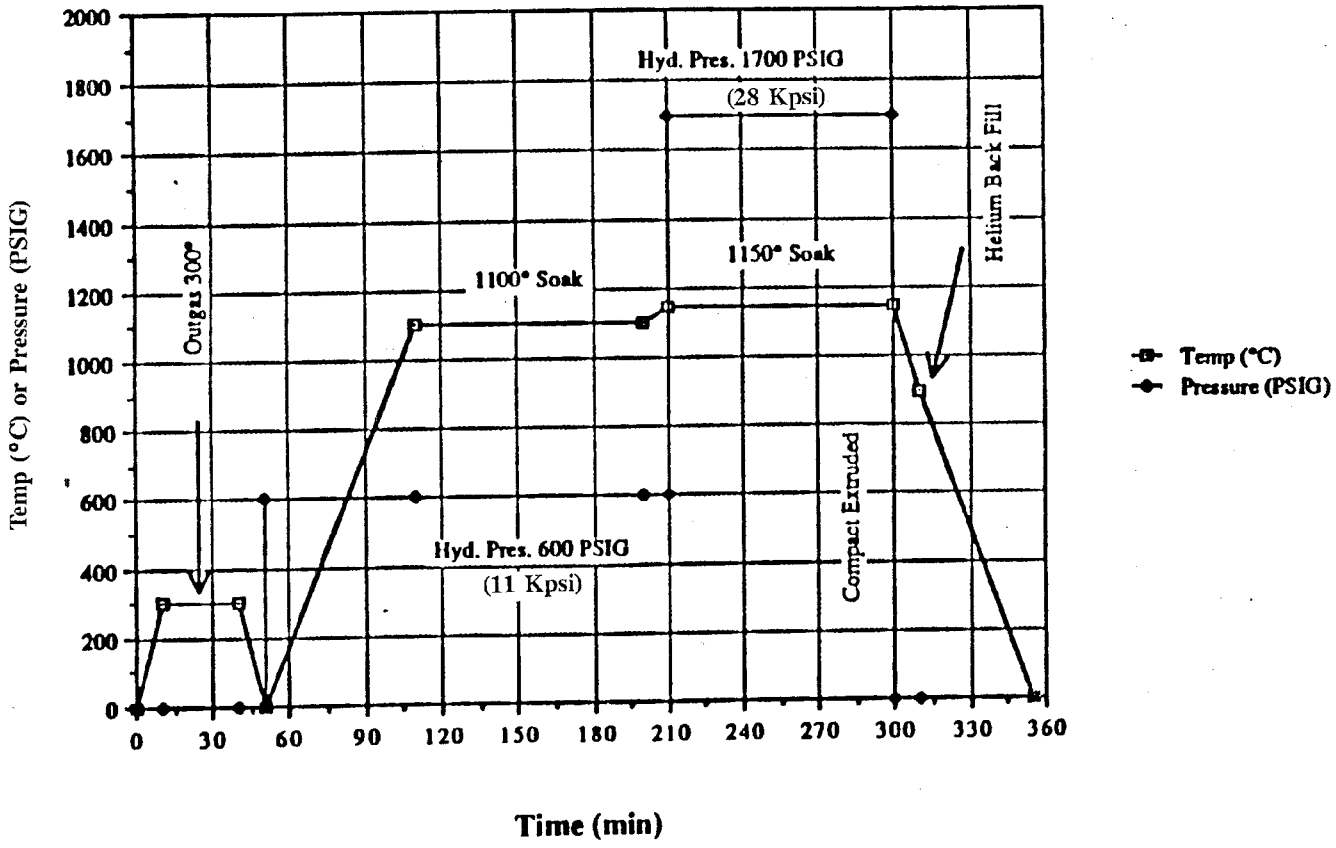

Figure 5-6. Hot Press Cycle for ITM-192-2N

5.2.1.2 Material Characterization

X-ray diffraction and scanning electron microscopy/energy dispersive x-ray spectroscopy were performed on three of these alloys in order to determine the compositional homogeneity and degree of GaP solubility. X-ray diffraction patterns were obtained from each of the specimens before and after heat treatment using a computer controlled Siemens D500 automatic diffractometer. The diffraction patterns produced from these materials each contained nine diffraction lines between 2-theta = 10 degrees and 2-theta = 115 degrees using monochromatic copper radiation. The (311) x-ray diffraction profiles were selected for careful study. These profiles were linearized, stripped of their copper k-alpha-2 components, smoothed, and deconvoluted into Lorentz functions. These analytical procedures were accomplished with computer software obtained from Siemens. The compositions corresponding to the centroid positions of each of the Lorentz functions were determined using RCA data[3] which relates the composition of Si-Ge to the lattice parameter 'a' where:

$$a = d_{(311)} \cdot \sqrt{11} \; ; \; d_{(311)} = \frac{\lambda}{2} \operatorname{Sin} \Theta_{(311)}$$

A plot of the RCA data is shown in Figure 5-7.

A typical (311) diffraction profile is described here for ITM-193 which contained 2 Mol percent GaP. Figure 5-8 is the (311) diffraction profile in the as-pressed condition and Figure 5-9 is after vacuum heat treatment at 1075°C. The top half of each figure is an expanded view of the diffraction profile and their constituent Lorentz functions. The bottom half of each figure is a plot of the compositions (atom percent silicon) and the relative volumes (volume percent) of the Si-Ge phases present in the material. The compositions were determined from the lattice parameters 'a', obtained from the 2-theta positions of the centroids of the Lorentz functions, using the RCA relations between lattice parameters and composition. The relative volumes (volume percent) of these compositions were determined from the relative areas of the Lorentz functions adjusted for atomic structure factors.

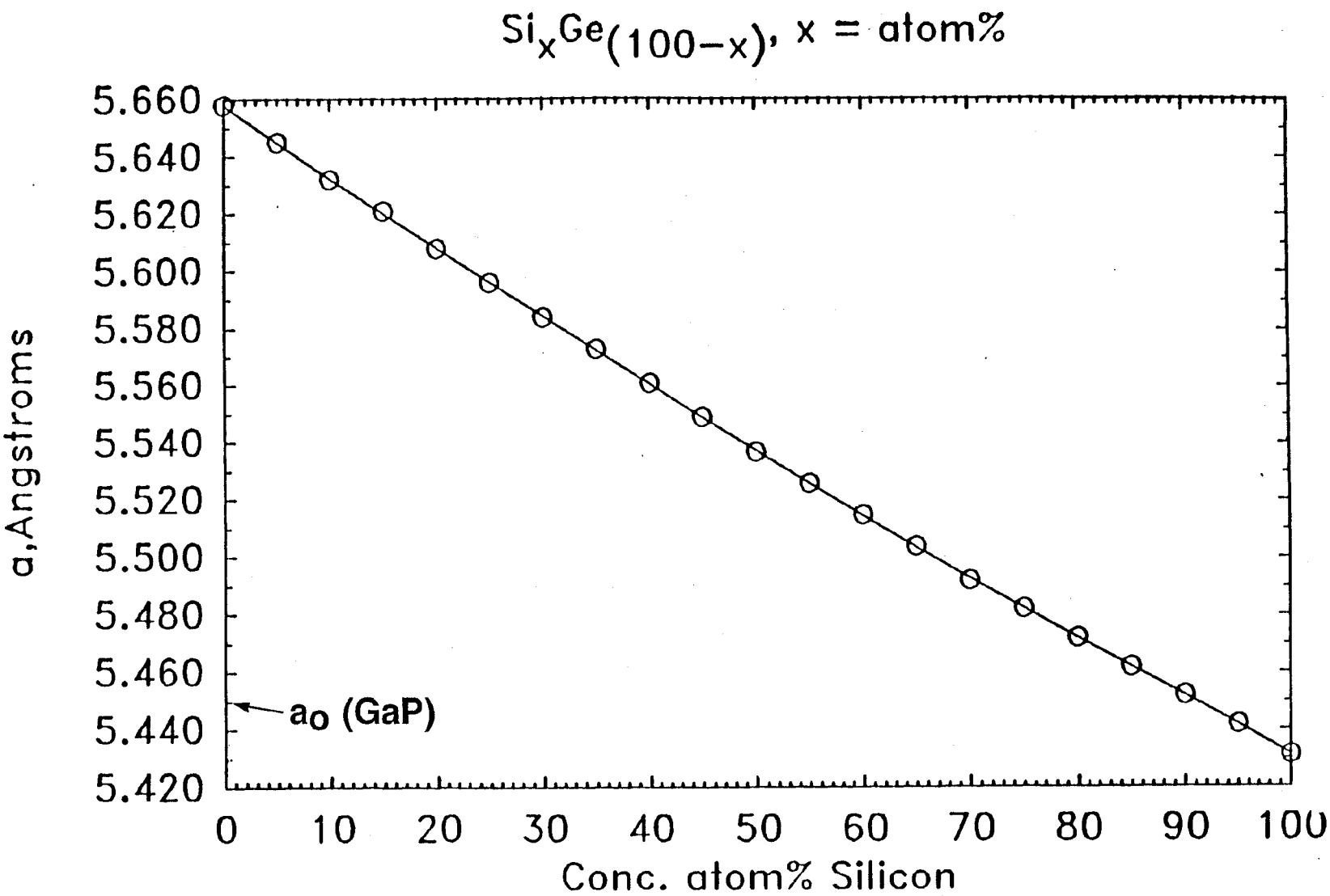

Figure 5-7. Lattice Parameter vs. Silicon Concentration in Si_xGe_y

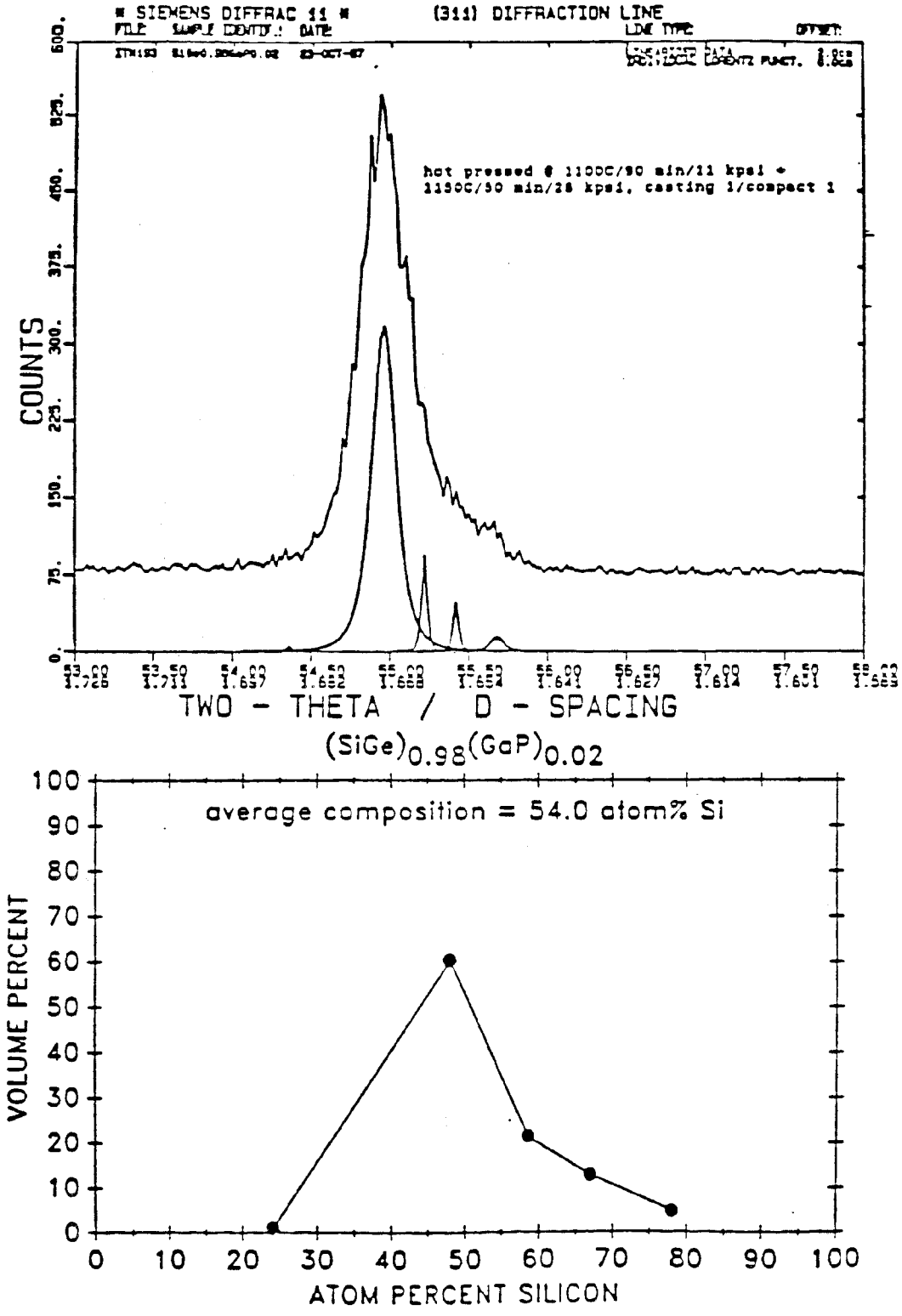

Figure 5-8. Compositional Range (From X-Ray Diffraction Data) for As-Pressed ITM-193

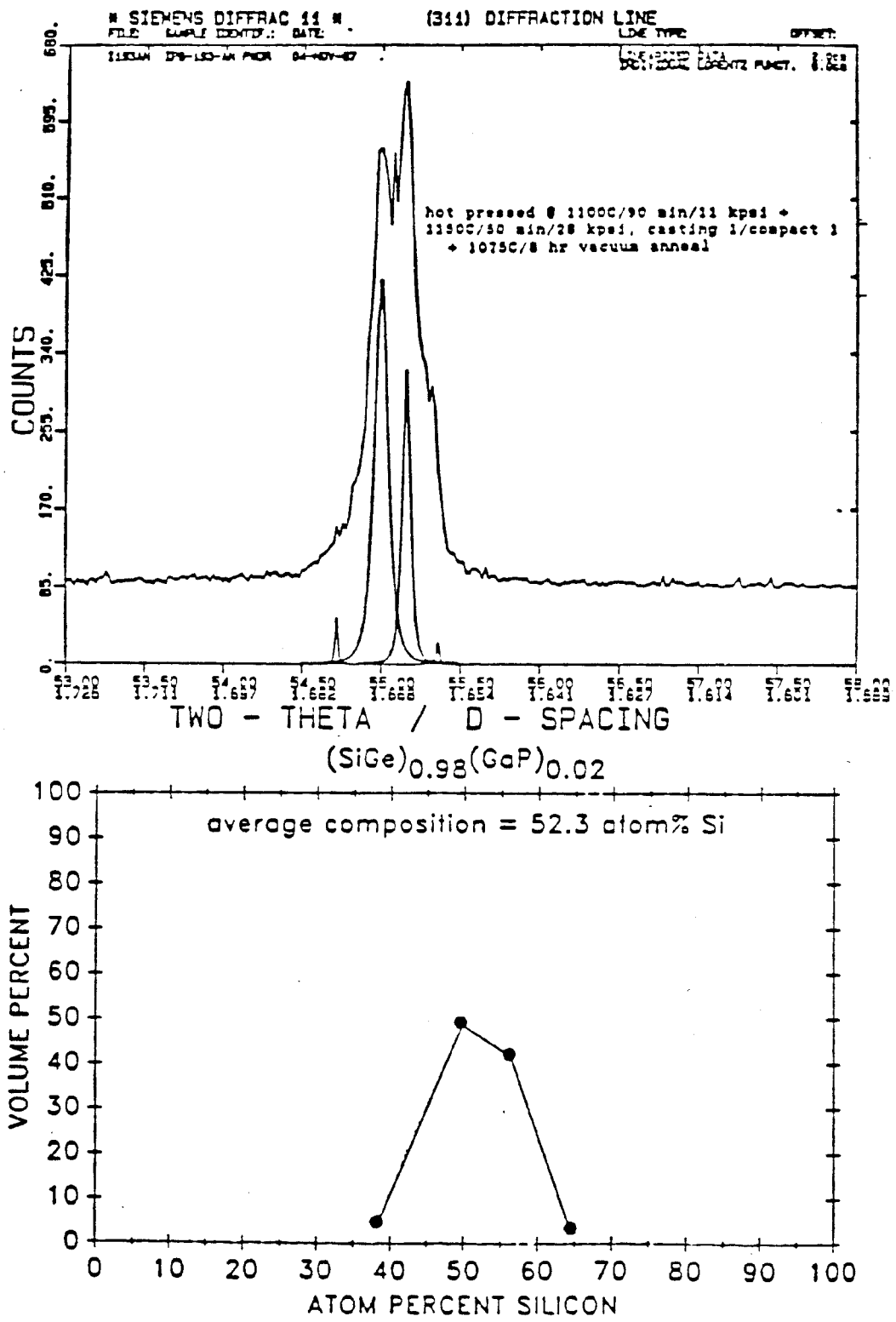

Figure 5-9. Compositional Range for ITM-193 with Additional Heat Treatment

The as-pressed compact can be seen to have a composition ranging from about 24 to 78 atom percent Si, with three specific compositions centered about 48, 58 and 67 atom percent Si. The weighted average composition of this material, as determined from x-ray diffraction data, is 54.0 atom percent Si. The heat treated specimen has a narrower range of compositions, from about 38 to 65 atom percent Si, primarily in two compositions centered about 49 and 57 atom percent Si. The weighted average composition for this material is 52.3 atom percent Si.

These x-ray diffraction data indicate that the materials become increasingly homogeneous after heat treatment. In addition, the diffraction patterns were void of peaks corresponding to GaP and it was concluded that GaP appears to be soluble in 50/50 Si-Ge at concentrations up to at least 16 Mol percent.

Scanning electron microscopy (SEM) in the backscattered electron imaging mode and energy dispersive spectroscopy (EDS) were used to study the microstructure of the thermally processed 50/50 Si-Ge compacts containing 2, 4 and 8 Mol percent GaP. The specimens were mounted, ground and polished using standard metallographic techniques. Argon sputter etching was subsequently used to remove both surface contaminants and material smeared during grinding and polishing. A 200 angstrom layer of carbon was vapor deposited onto the specimen surface to provide a electrically conductive path. Examination of the surfaces at various magnifications was done in order to access compositional homogeneity. Average compositions were also determined by performing quantitative standardless EDS elemental analyses at four randomly selected regions at 500x magnification. ITM-191 (8 Mol percent GaP in 50/50 Si-Ge) was selected to illustrate the SEM/EDS capabilities and to assess the degree of homogeneity. At magnifications below 300x, this material, as well as the other materials appear to be featureless with the exception of a few voids. Only at magnifications of 500x and above can microstructural features be discerned. This fact is an indication of a high degree of compositional homogeneity.

If the material were very inhomogeneous one would expect, based on previous experiences with this type of material, to see contrast differences in the SEM images which are indicative of compositional variations. However, in the case

of the materials studied here the observed contrast variations are very slight. Thus, one would not expect to find large compositional variations in subsequent element analyses.

Two typical 500x magnification fields randomly selected on the surface of this material are presented in Figure 5-10. The results of the EDS analyses from four such fields are shown in Table 5-2.

Table 5-2. ITM-191 Composition (Atomic % from four 500x Fields)

Field	1	2	3	4	Av.	sigma
Si	52.10	51.33	51.72	52.14	51.82	0.38
P	4.51	4.71	4.50	4.65	4.59	0.10
Ga	3.66	3.88	3.70	3.56	3.70	0.13
Ge	39.74	40.08	40.08	39.65	39.89	0.22

The results of these analyses indicate that the compositions of four randomly selected areas (each approximately 230 microns x 170 microns) are very similar. The specimen is homogeneous. The nominal composition of this material was:

$$Si_{46}Ge_{46}Ga_4P_4$$

The composition of this material, as determined from this EDS analysis is:

$$Si_{51.8}Ge_{39.9}Ga_{3.7}P_{4.6}$$

Thus, this material appears to have lost germanium and gallium during hot pressing (squeeze out) and thermal treatments. When compositional maps for Si, Ge, Ga and P were made at magnifications of about 5000x, they were found to be featureless. This fact, again, points to the homogeneous character of the material.

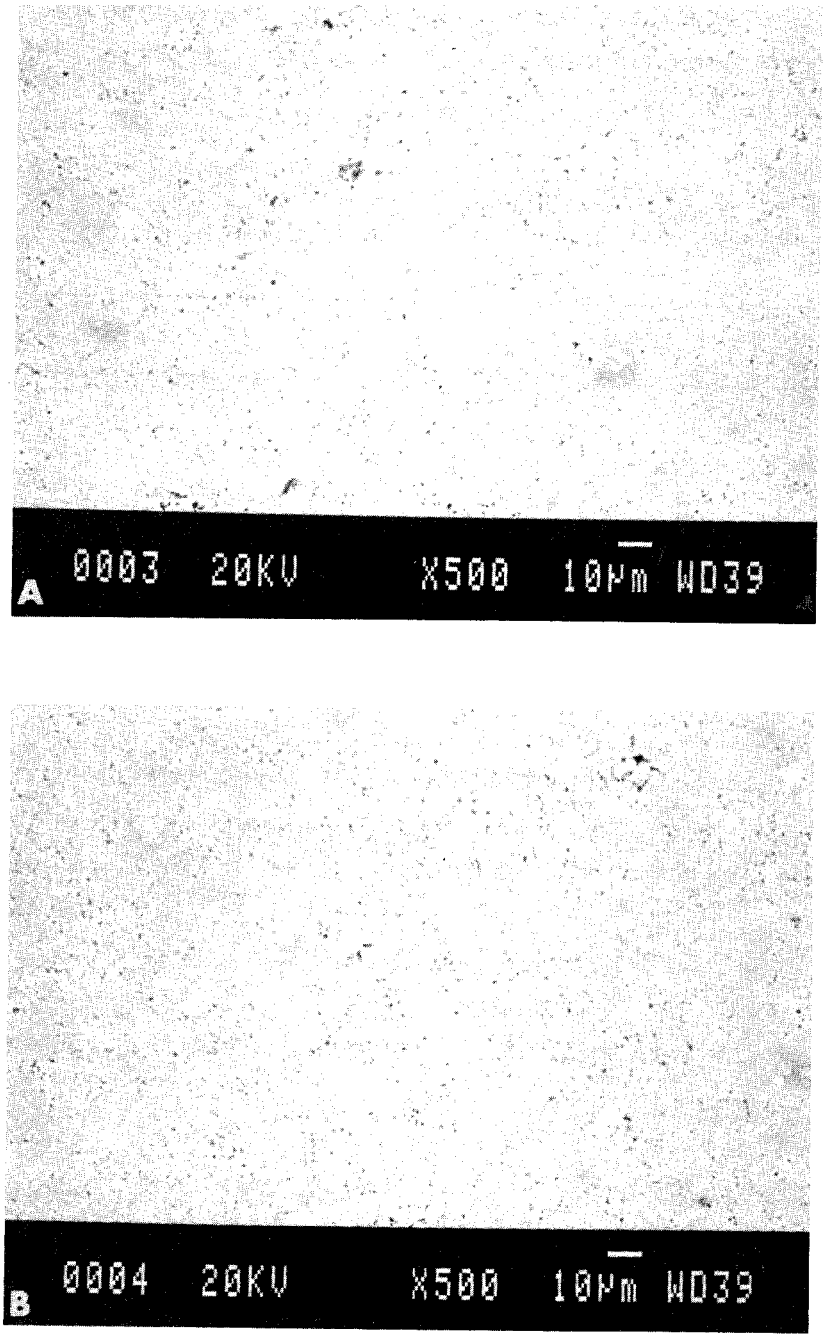

Figure 5-10. SEM photomicrographs prepared from two typical regions on the surface of specimen ITM-191. The lack of contrast difference indicates homogeneity. Magnification = 500x

If one carefully examines the SEM photomicrographs in Figure 5-10, small dark spots can be found in grain boundaries. When elemental analyses of individual dark spots were made, it was determined that they contained oxygen and silicon -- probably silicon oxide, SiO_y.

The SEM/EDS results indicate that the homogeneity of 50/50 Si-Ge doped with 2, 4 and 8 Mol percent GaP are superior to standard Si-Ge alloys. Some porosity was observed and oxide particles were found to be primarily concentrated in grain boundaries. In addition, the EDS analyses indicate that some germanium and gallium are lost during the hot pressing/annealing steps.

5.2.1.3 Thermoelectric Properties

Room temperature and high temperature thermoelectric properties were measured on samples containing 2, 4 and 8 Mol percent GaP. Table 5-3 is a summary of the room temperature electrical properties. The Seebeck coefficient was measured on a bar specimen, 1/4" x 1/4" x 2", while the resistivity, mobility and carrier concentration were measured on a 1/2" diameter x 0.030" thick disk specimen using the Hall effect method.

Table 5-3. Summary of Results for GaP Doped 50/50 Si-Ge Test Specimens

SAMPLE ID	NOMINAL COMPOSITION	ROOM TEMPERATURE				
		SEEBECK (μV/°C)	RHO (HALL) (mΩ-cm)	MOBILITY (cm^2/V-sec)	CARRIER CONC. (1/cc)	DENSITY (g/cc)
ITM-191	$(SiGe)_{0.92}(GaP)_{0.08}$	-160	6.82	19.08	4.80E+19	3.86
ITM-192	$(SiGe)_{0.96}(GaP)_{0.04}$	-168	5.01	26.36	4.74E+19	3.92
ITM-193	$(SiGe)_{0.98}(GaP)_{0.02}$	-183	5.50	27.54	4.12E+19	3.90

These data indicate that the alloys have high electrical resistivities due primarily to lower carrier concentrations and somewhat reduced mobilities. This probably results from the fact that the lower melting points of the Ge rich alloys make it difficult to maintain the excess phosphorus in solid solution to provide the required number of active charge carriers. About 10%

of the excess phosphorus is in solution and the remainder probably present as SiP inclusions. The Seebeck coefficients are increased due primarily to the lower carrier concentrations and the solution of the higher band-gap GaP compound.

High temperature electrical property measurements were obtained by instrumenting a bar specimen as described in Section 3. The high temperature Seebeck coefficients and electrical resistivities of the 2, 4 and 8 Mol percent GaP doped 50/50 Si-Ge alloys are shown in Figures 5-11 and 5-12. Data are normally taken at 10°C increments and the gaps in the curves represent data that are experimentally inconsistent with overall trends.

The Seebeck coefficients are in an excellent range with values up to about 300 μV/°C. However, the electrical resistivities are also high (about seven times higher than for the more conventional 80/20 SiGe-GaP alloys). The resistivities vary nearly linear with increasing temperature until about 700°C at which time intrinsic conduction or phosphorus dissolution occurs. Thus, electrical power factors are below 15 $\mu W/cm°C^2$ from room temperature up to 900°C. The poor electrical properties appear to be due primarily to low carrier concentrations. Thus, specific annealing treatments were used in an attempt to obtain more favorable combinations of thermoelectric properties.

5.2.1.4 Aging/Heat Treatment Studies

In an attempt to improve the electrical properties by the removal of Ga by oxidation and dissolution of additional phosphorus, wafers 1/2" in diameter and 0.030" thick were heat treated in flowing oxygen at one atmosphere pressure of 100 cc/min at 700, 800, 900 and 1000°C. After a specified time, the samples were allowed to cool slowly to room temperature. The surfaces had either a gold or blue tint indicating a small but finite degree of surface oxidation.

The thin oxide layer was readily removed by grinding with SiC paper and distilled water. Room temperature Hall effect and Seebeck coefficient measurements were repeated. The room temperature electrical properties from these oxidation experiments are shown in Tables 5-4 through 5-6 for the alloys. In the 8 m/o GaP alloy (ITM-191), the 1000°C heat treatment was

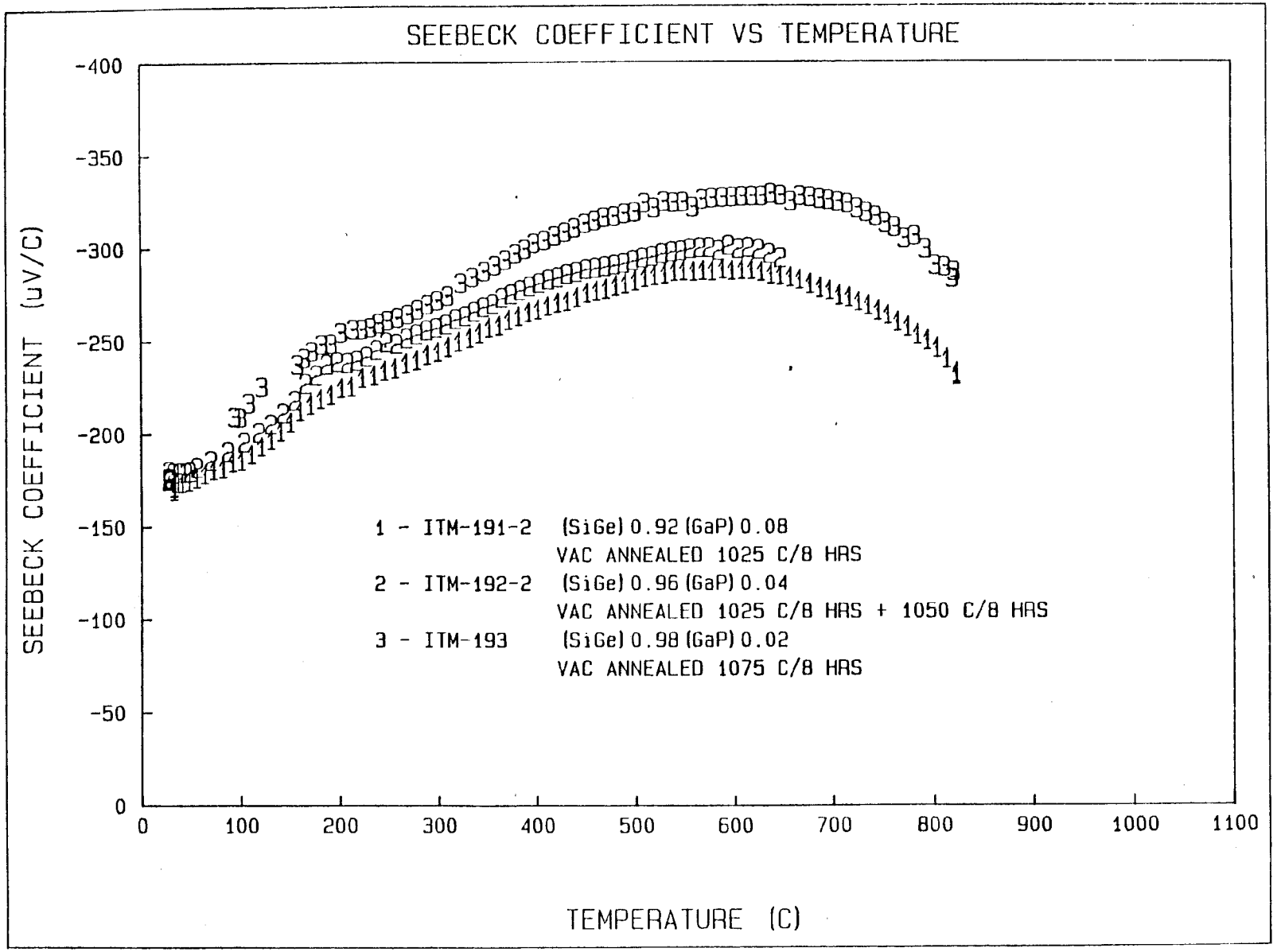

Figure 5-11. First Heat Temperature Dependence of the Seebeck Coefficients for ITM 191, ITM 192 and ITM 193 SiGe-GaP Alloys

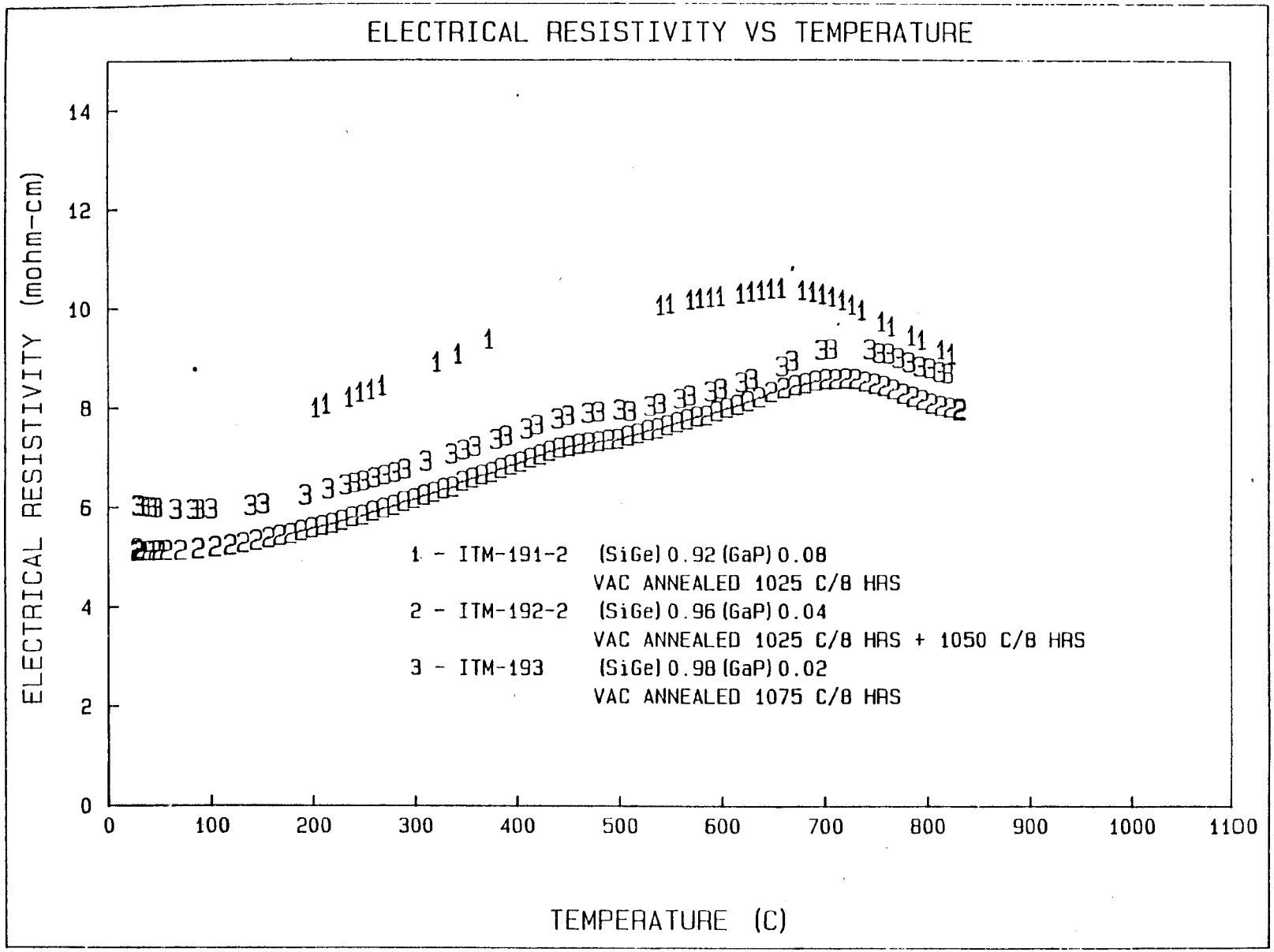

Figure 5-12. First Heat Temperature Dependence of the Electrical Resistivities for ITM 191, ITM 192 and ITM 193 SiGe-GaP Alloys. The gaps in the curves represent data that are not experimentally consistent with overall trends.

Table 5-4. Room Temperature Electrical Properties of ITM 191, (SiGe) 0.92 (GaP) 0.08, as a Function of Time and Temperature of Annealing in an Oxygen Flow of 100 cc/min

ROOM TEMPERATURE	*AS HOT PRESSED	25 700	100 700	200 700	25 800	50 800	100 800	15 900	50 900	5 1000	25 1000	TIME (HRS.) TEMP (^{o}C)
$S(\mu V/^{o}C)$	-160	-181	-182	-179	-161	-150	X	-65	X	-175	-165	
S^2/ρ ($\mu W/cm^{o}C^2$)	3.75	3.03	2.60	2.31	1.58	0.77	X	0.13	X	4.00	5.31	
ρ_H(m ohm cm)	6.82	10.80	12.74	13.88	16.35	29.15	X	31.09	10.62	7.66	5.13	
$n(x10^{20}/cm^3)$	0.48	0.32	0.30	0.22	0.37	0.34	X	0.30	1.43	0.27	0.36	
$\mu(cm^2/V.s)$	19.08	17.96	16.34	20.26	10.38	6.39	X	6.60	4.13	29.73	34.17	

* S and Hall effect not measured on actual sample heat treated

x = nonuniform result

Table 5-5. Room Temperature Electrical Properties of ITM 192 (SiGe) 0.96 (GaP) 0.04, as a Function of Time and Temperature of Annealing in an Oxygen Flow of 100 cc/min

ROOM TEMPERATURE	*AS HOT PRESSED	25 700	100 700	200 700	25 800	50 800	100 800	15 900	50 900	5 1000	25 1000	TIME (HRS.) TEMP (^{o}C)
$S(\mu V/^{o}C)$	-170	-187	-190	-190	-180	-185	-178	-162	-143	-173	-159	
S^2/ρ ($\mu W/cm^{o}C^2$)	5.77	6.32	5.83	5.59	3.84	2.76	2.02	1.28	0.892	1.10	1.70	
ρ_H(m ohm cm)	5.01	5.53	6.19	6.46	8.43	12.42	15.65	20.53	22.92	27.22	14.84	
$n(x10^{20}/cm^3)$	0.47	0.32	0.34	0.33	0.34	0.30	0.31	0.28	0.25	0.087	0.10	
$\mu(cm^2/V.s)$	26.36	35.86	29.69	29.27	21.88	16.54	12.99	11.06	10.83	26.43	40.73	

* S and Hall effect not measured on actual sample heat treated

Table 5-6. Room Temperature Electrical Properties of ITM 193 (SiGe) 0.98 (GaP) 0.02, as a Function of Time and Temperature of Annealing in an Oxygen Flow of 100 cc/min

ROOM TEMPERATURE	*AS HOT PRESSED	25 700	100 700	200 700	25 800	50 800	100 800	15 900	50 900	5 1000	25 1000	TIME (HRS.) TEMP (^{o}C)
$S(\mu V/^{o}C)$	-175	-197	-204	-202	-188	-196	-194	-161	-155	-168	-171	
S^2/ρ ($\mu W/cm^{o}C^2$)	5.57	5.30	5.04	4.35	4.36	3.39	2.84	0.73	0.21	0.73	X	
ρ_H(m ohm cm)	5.50	7.32	8.26	9.37	8.11	11.34	13.26	35.41	113.7	38.44	X	
$n(x10^{20}/cm^3)$	0.41	0.27	0.30	0.28	0.33	0.29	0.27	0.18	0.25	0.073	X	
$\mu(cm^2/V.s)$	27.54	31.56	25.65	23.99	23.33	18.82	17.59	10.03	2.19	22.23	X	

*** S and Hall effect not measured on actual sample heat treated**

x = nonuniform result

partially effective in increasing the electrical power factor due to an increase in the carrier mobility. In all three samples, the carrier concentration started off low and continually decreased with heat treatment. This strongly indicates the reprecipitation of electrically active phosphorus atoms by slow cooling. Rapid cooling could have possibly kept the excess phosphorus in solid solution.

5.2.1.5 Summary of Results

The solubility of GaP in 50/50 Si-Ge is at least 16 Mol percent as determined from x-ray diffraction analysis. The materials prepared in this study by chill casting, grinding, hot pressing and vacuum annealing have been relatively homogeneous as determined from x-ray diffraction and SEM/EDS analyses.

Additives such as GaP to 50/50 Si-Ge alloys do significantly increase their high temperature Seebeck coefficients. However, this was accomplished with sharply increased electrical resistivity values. The resistivity increases appear to result from a combination of low concentrations of electrically active n-type charge carriers and somewhat lower charge carrier mobilities.

It has been proposed that heat treatment of the alloy powders in a phosphorus containing atmosphere could produce more effective compensation of excess gallium atoms and increase the number of electrically active phosphorus atoms in solution.

5.2.2 THE EFFECT OF GaP DOPING ON 80/20 Si-Ge ALLOYS

Residual material from the 50/50 Si-Ge alloys with the GaP contents described above were ground to a controlled particle size and subsequently hot pressed after being blended with controlled size particles of P doped Si. The goal was to produce a series of 80/20 Si-Ge alloys with 1/2, 1, 2 and 4 Mol percent GaP and to have more P than Ga in solution so as to produce n-type alloys. Table 5-7 shows the nominal composition of the samples fabricated. Fabrication was carried out in a manner which would retain the GaP within the grains as either a supersaturated solid solution and/or as a fine dispersion of GaP particles.

Table 5-7. Nominal Composition of GaP Doped 80/20 Si-Ge

Sample Number	Atomic Fraction			
	Si	Ge	Ga	P
199	0.779	0.195	0.004	0.022
198	0.773	0.193	0.008	0.026
197	0.760	0.190	0.016	0.034
196	0.731	0.183	0.035	0.052

5.2.2.1 Fabrication

Figures 5-13 through 5-16 summarize the process details for the fabrication of the four 3 inch diameter by 3/4 inch thick compacts produced. Figure 5-17 provides typical details for the hot pressing of all four blended powder compacts.

The phosphorus doped silicon powder blend having a nominal P content of 3 atomic percent was prepared by chill casting a silicon melt to which phosphorus chunks were added, followed by mechanical crushing to a median particle size near 5 microns.

5.2.2.2 Material Characterization

X-ray diffraction and SEM/EDS analyses were performed on pieces cut from the as-pressed compacts in order to assess the degree of compositional homogeneity. Again, the (311) diffraction profile was examined in detail. It appears that GaP is present when the diffraction profiles are deconvoluted into their Lorentz functions. As shown in Figure 5-18, each of the materials was found to yield a Lorentz function coincident with the position of GaP. In this figure, Lorentz function intensities for three of the compositions are plotted versus diffraction angle. Also included is the diffraction profile for GaP in this diffraction range; note the overlap of the Lorentz data with the GaP diffraction profile at about 56.1 degrees. The data confirm the limited solubility of GaP in the 80/20 Si-Ge composition. The estimated maximum solubility is about 1 to 2 Mol percent. It is also noted that the GaP diffraction position indicates very little solid solubility of Ge or Si in the GaP lattice.

The (311) diffraction profile and the deconvoluted Lorentz functions are shown in Figure 5-19 for ITM 197. The corresponding plot of composition in atom percent Si versus volume percent is also shown, indicating excellent homogeneity (only one major Lorentz function).

SEM/EDS analyses were made on polished surfaces of the four GaP doped 80/20 Si-Ge alloys. Specimens were prepared similar to that used for the 50/50 SiGe-GaP alloys. All the samples evaluated, with the exception of ITM 196, were found to be very homogeneous in Si and Ge distributions.

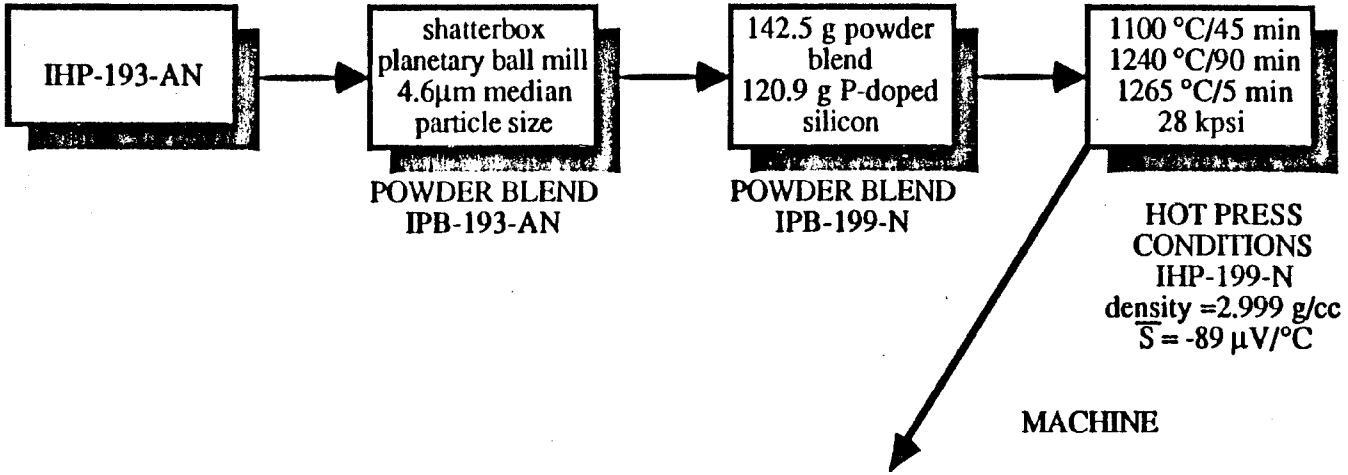

Figure 5-13. ITM 199, Normalized Composition of $Si_{0.779}Ge_{0.195}Ga_{0.004}P_{0.022}$

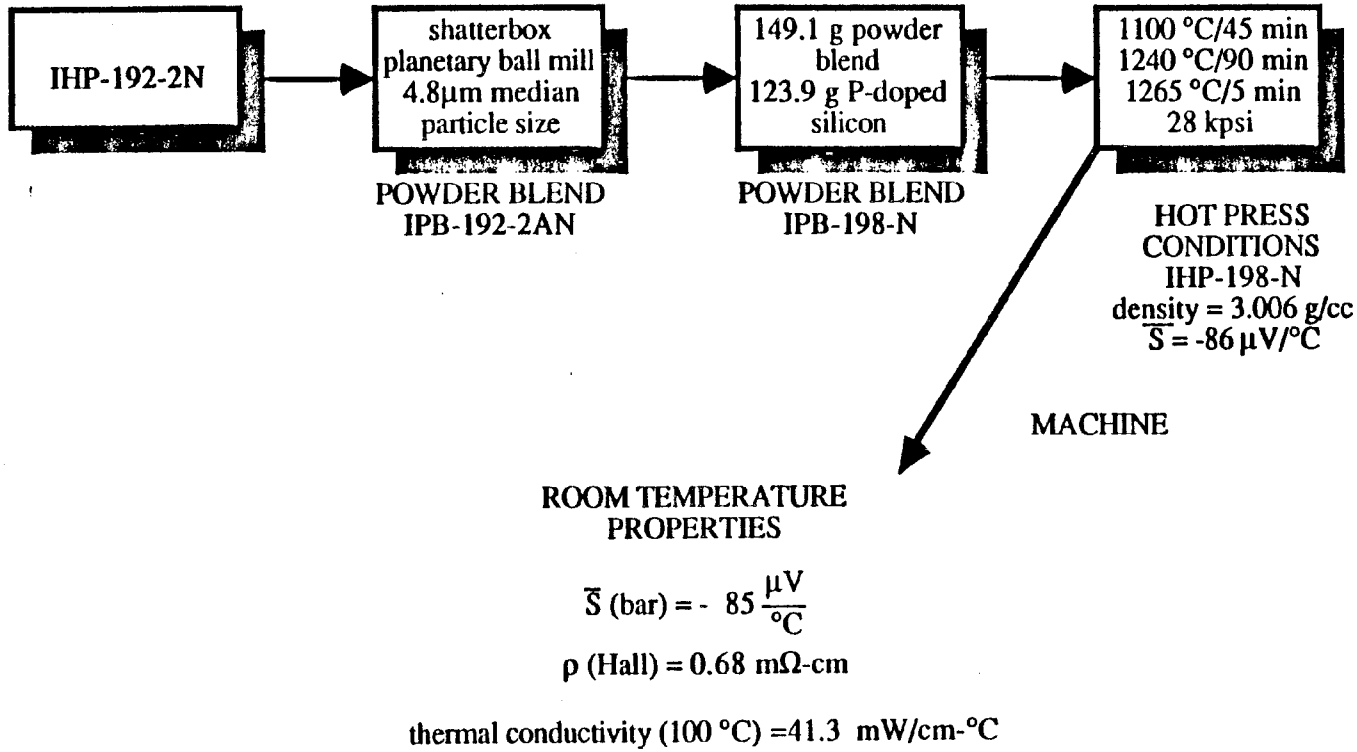

Figure 5-14. ITM 198, Normalized Composition of $Si_{0.773}Ge_{0.193}Ga_{0.008}P_{0.026}$

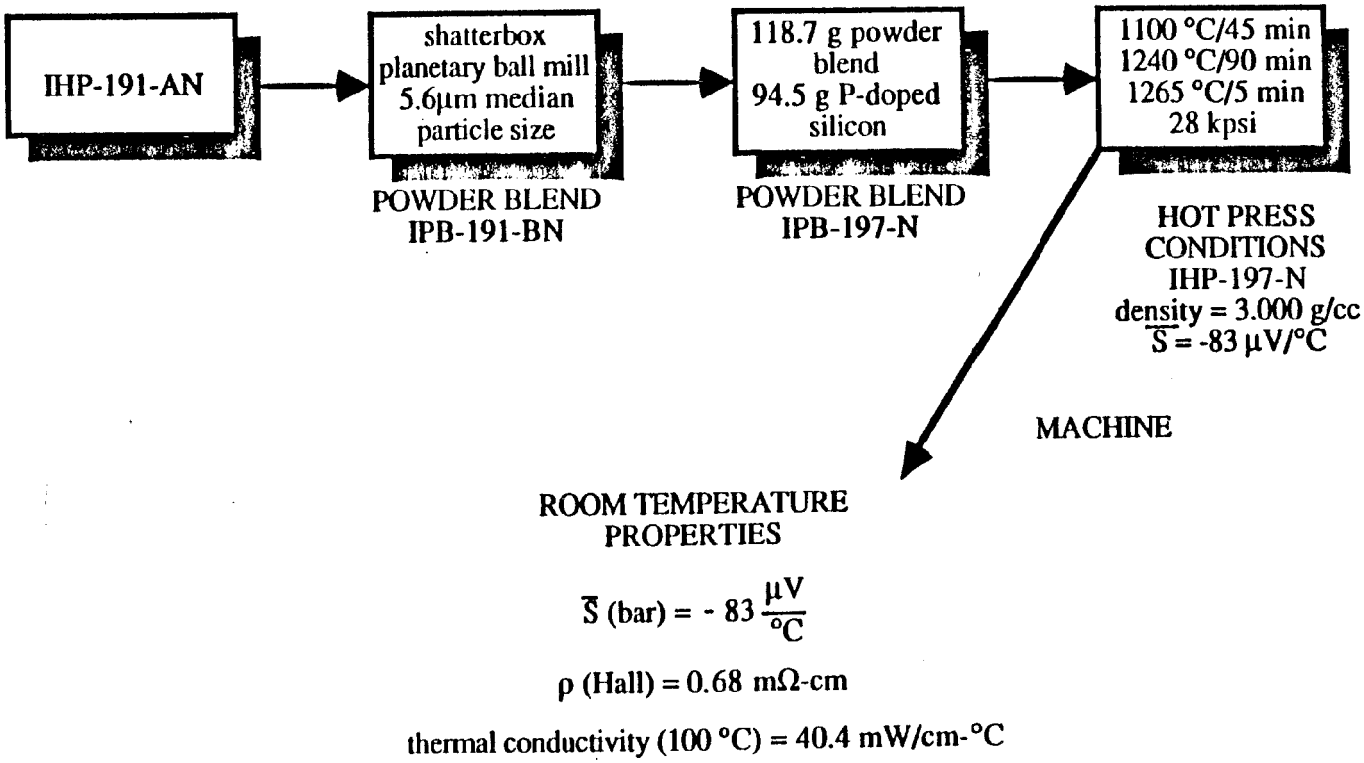

Figure 5-15. ITM 197, Normalized Composition of $Si_{0.760}Ge_{0.190}Ga_{0.016}P_{0.034}$

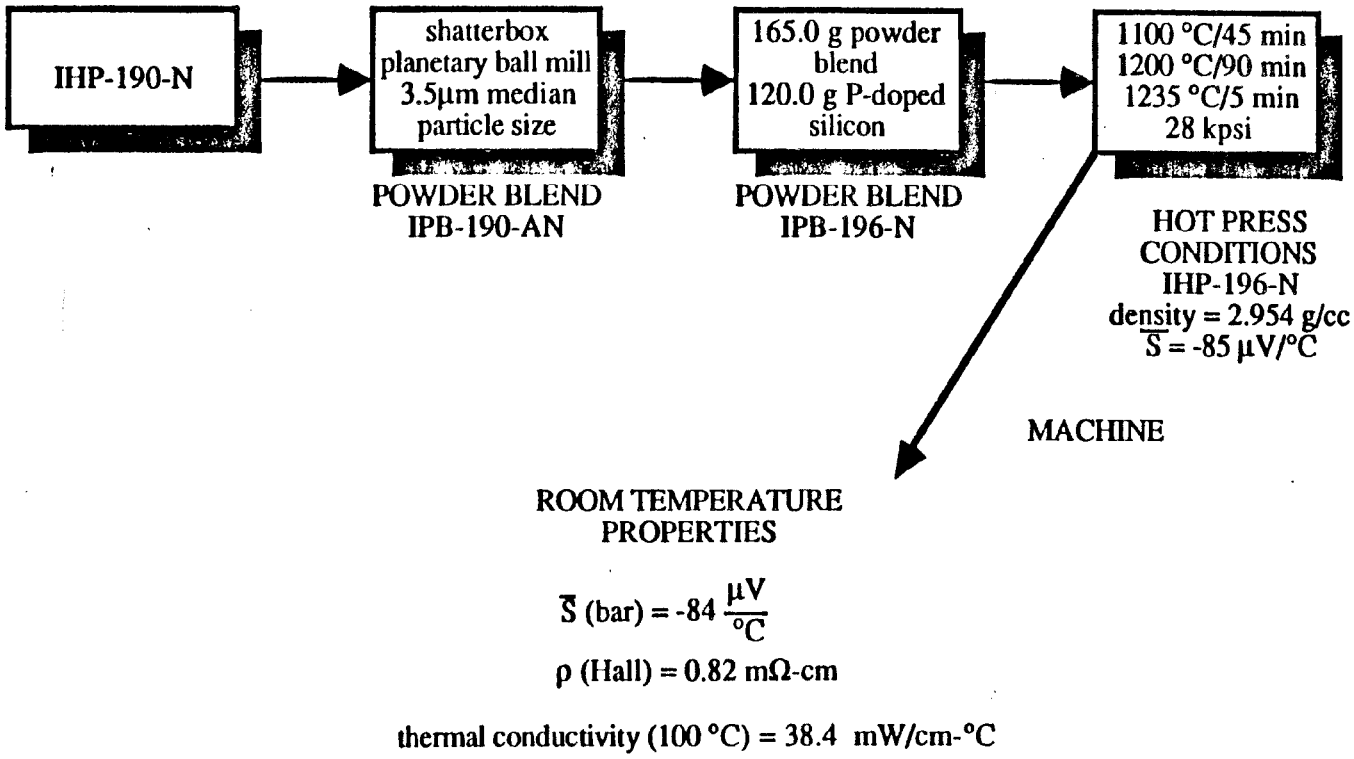

Figure 5-16. ITM 196, Normalized Composition of $Si_{0.731}Ge_{0.183}Ga_{0.035}P_{0.052}$

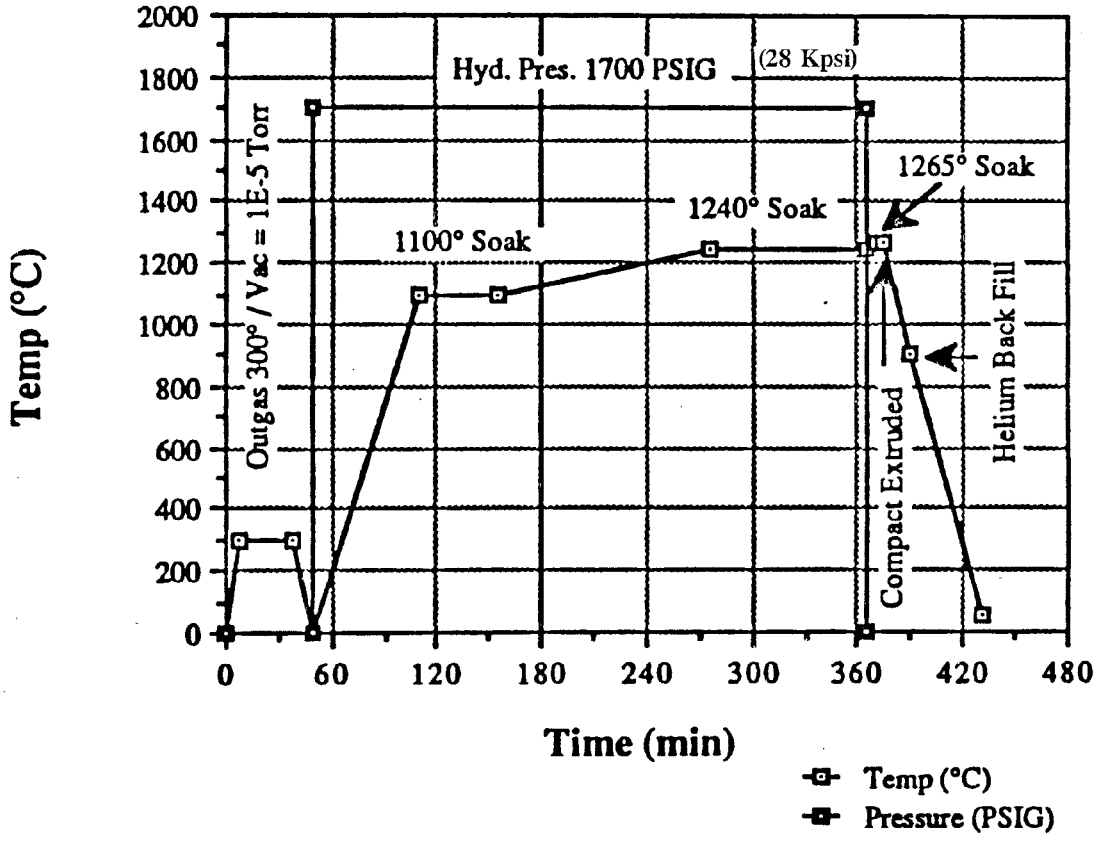

Figure 5-17. Hot Press Cycle for Lot ITM 197, ITM 198 and ITM 199. Slightly Lower Temperatures Were Used to Hot Press ITM 196

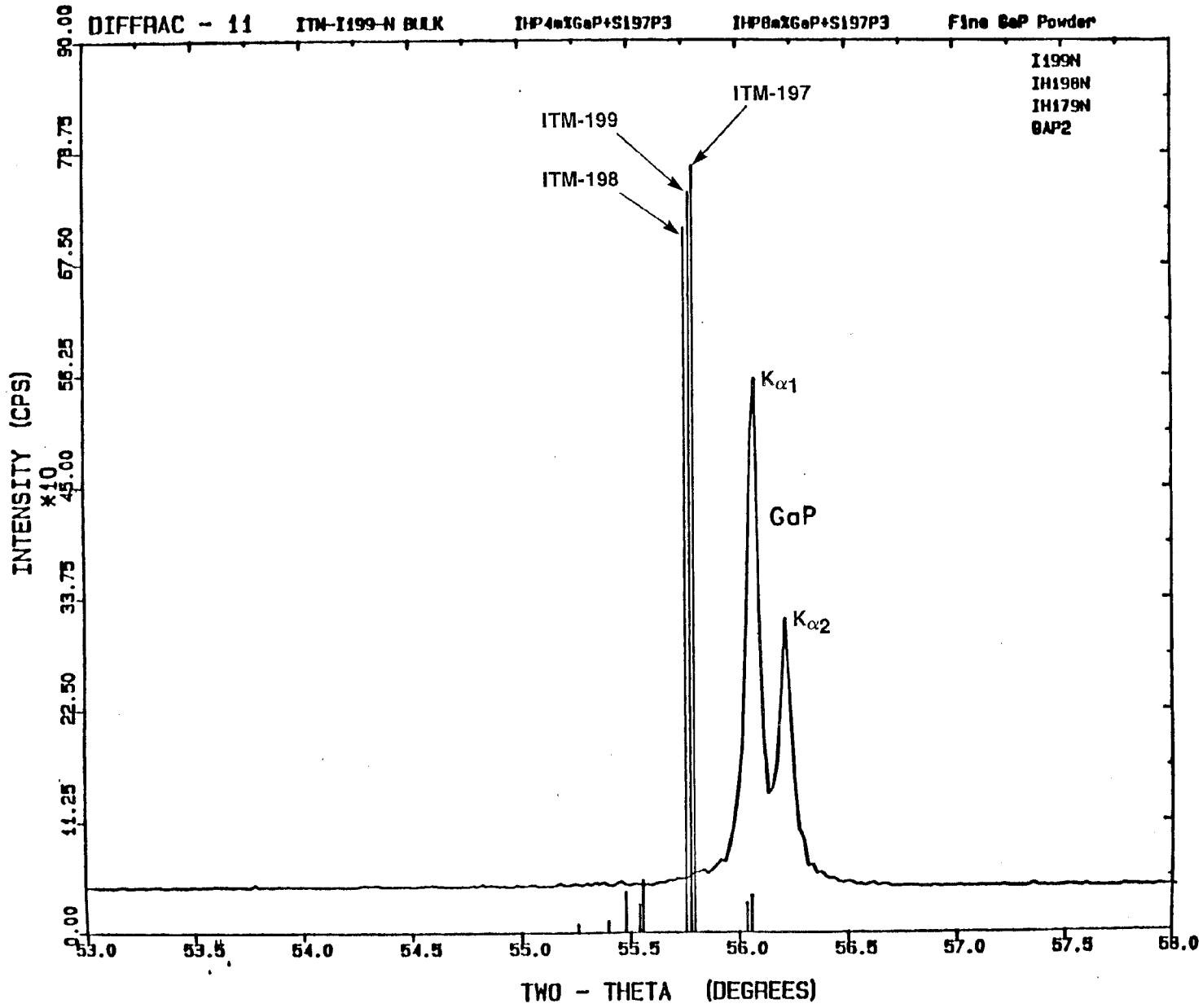

Figure 5-18. Positions of Lorentz deconvoluted x-ray diffraction $K_{\alpha 1}$ data for the (311) lines from ITM 197, 198 and 199. Also included is the diffraction profile ($K_{\alpha 1}$ and $K_{\alpha 2}$) for GaP. Note the presence of $K_{\alpha 1}$ for GaP in each of the Si-Ge materials.

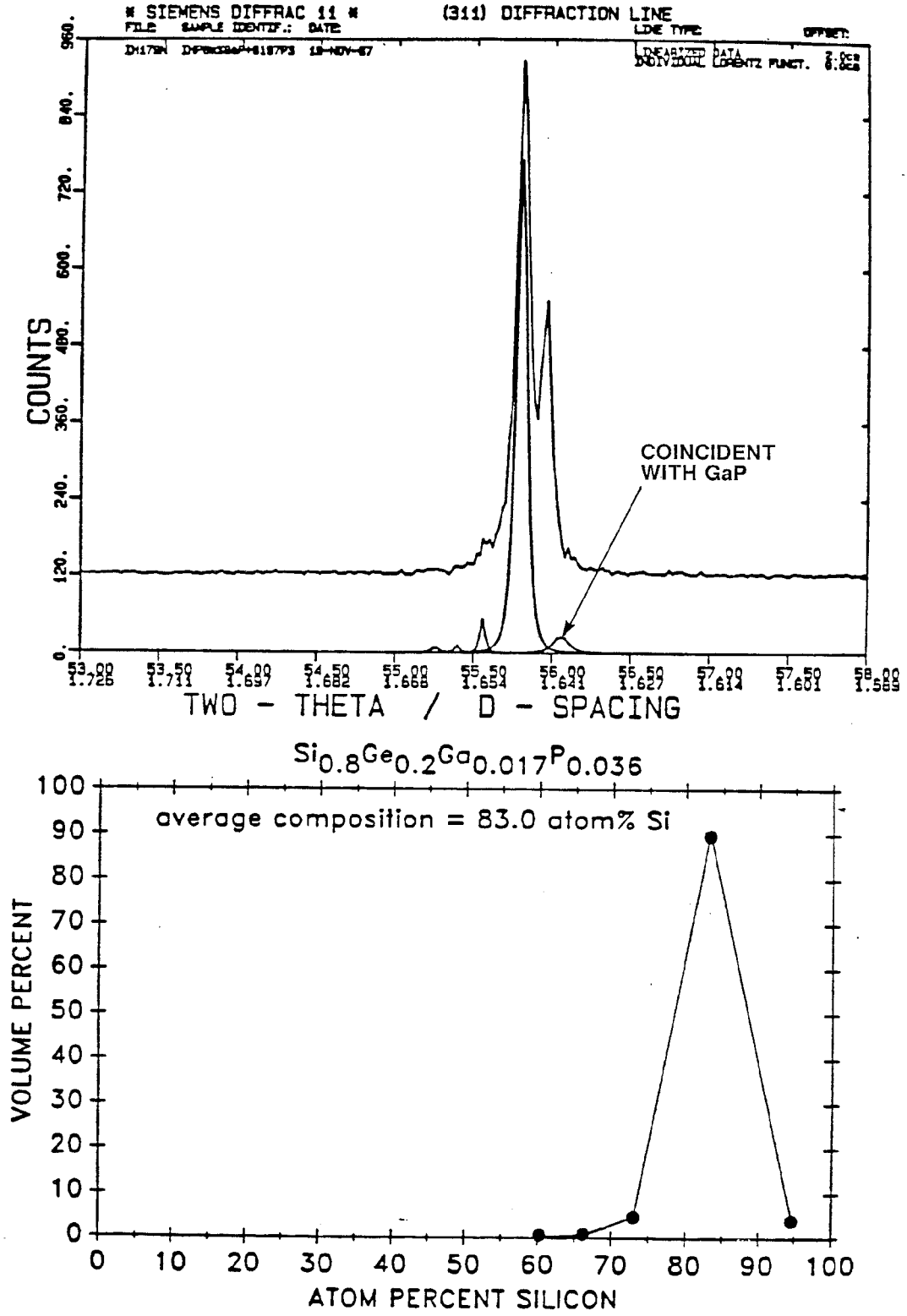

Figure 5-19. Si-Ge Compositional Distribution for ITM 197. The Lorentz function at 56.1 degrees 2-theta is coincident with the GaP diffraction profile.

The results for ITM 197 will be discussed as a typical example.

With the exception of relatively minor porosity, SEM images at magnifications below 300x were void of detail. At magnifications above 300x only very slight contrast differences in the SEM image was observed. This lack of contrast is an indication of a high degree of homogeneity. Dark spots, about 0.5 micrometer in diameter, were observed primarily in grain boundaries. Two randomly selected, 500x magnification, fields are shown in Figure 5-20. The composition as determined using EDS is listed in Table 5-8.

Table 5-8. ITM 197 Composition (Atomic % from Four 500x Fields)

Field	1	2	3	4	Av.	sigma
Si	78.76	78.99	78.40	78.74	78.72	0.24
P	3.75	3.96	3.68	3.66	3.76	0.14
Ga	1.63	1.54	1.68	1.66	1.63	0.06
Ge	15.86	15.78	16.24	15.94	15.96	0.20

The nominal composition for this material was:

$$Si_{76.0}Ge_{19.0}Ga_{1.6}P_{3.4}$$

The average composition from Table 5-8 is:

$$Si_{78.7}Ge_{16.0}Ga_{1.6}P_{3.8}$$

The indication is that this material lost Ge during its formation. However, it does not appear as though any significant quantity of Ga or P was lost.

The dark spots in grain boundaries were found to contain silicon and oxygen, again suggesting SiO_2 inclusions.

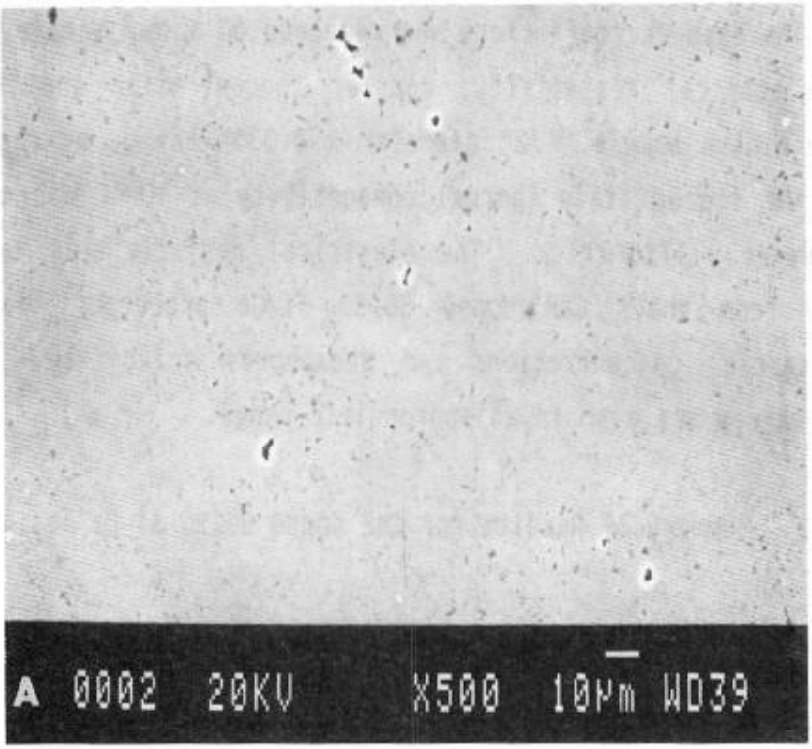
A 0002 20KV X500 10µm WD39

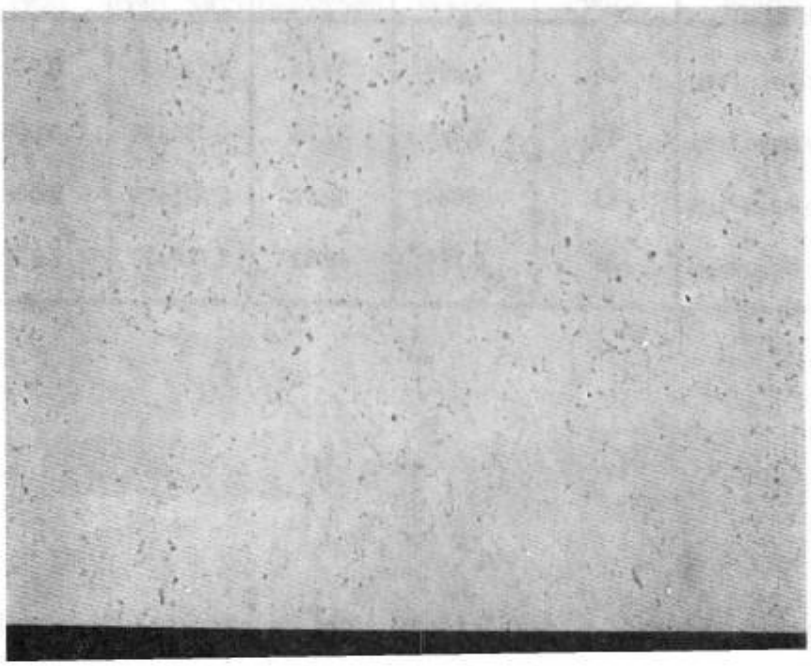

5.2.2.3 Thermoelectric Properties

Room temperature and high temperature thermoelectric properties were measured for the four alloys. The hot pressing procedures used in their fabrication resulted in extremely uniform room temperature Seebeck coefficients and microstructures. Table 5-9 is a summary of the room temperature electrical properties. The Seebeck coefficient was measured on a bar sample, 1/4" x 1/4" x 2", the electrical resistivity, carrier concentration and mobility were determined on a disk sample, 1/2" diameter x 0.030" thick, by the Hall effect method, and the steady state thermal conductivity at 100°C was measured on a puck, 2" diameter x 1/2" thick. The electrical resistivities have decreased significantly from their GaP doped 50/50 Si-Ge precursors due to higher mobilities, carrier concentrations and phosphorus solubility. The thermal conductivity values are also in an appropriate range.

Table 5-9. Summary of Results for GaP doped 80/20 Si-Ge Test Specimens

SAMPLE ID	NOMINAL COMPOSITION	ROOM TEMPERATURE					100°C -THERMAL CONDUCTIVITY (mW/cm-°C)
		SEEBECK (μV/°C)	RHO (HALL) (mΩ-cm)	MOBILITY (cm^2/V-sec)	CARRIER CONC. (1/cc)	DENSITY (g/cc)	
ITM-196	$Si_{0.731}Ge_{0.183}Ga_{0.035}P_{0.052}$	-84	0.824	34.29	2.21E+20	2.954	38.43
ITM-197	$Si_{0.750}Ge_{0.190}Ga_{0.016}P_{0.034}$	-83	0.675	37.45	2.47E+20	3.000	40.45
ITM-198	$Si_{0.773}Ge_{0.193}Ga_{0.008}P_{0.006}$	-85	0.684	39.36	2.32E+20	3.006	41.27
ITM-199	$Si_{0.779}Ge_{0.195}Ga_{0.004}P_{0.022}$	-89	0.724	40.92	2.11E+20	2.999	41.27

High temperature Seebeck coefficients and electrical resistivities were measured on as-pressed samples by Ames Laboratory, Battelle-Columbus and GE-ASD. High temperature thermal diffusivity was measured by Battelle-Columbus and GE-ASD.

Figure 5-21 is a plot of the Seebeck coefficients versus temperature in which the GE-ASD first heat curves for the four alloys are superimposed. It is interesting to note that the Seebeck coefficients are independent of porosity and GaP content, which ranges from 0.4 to 3.5 Mol percent. ITM sample 196 contained an appreciable volume fraction of voids due to the large phosphorus overpressure during hot pressing. The similarity of the Seebeck coefficient values could be due to the similarity in the carrier concentration since S is inversely proportional to the log of the carrier concentration. The measured carrier concentrations ranged from 2.11 to 2.47 x $10^{20}/cm^3$ at room temperature.

Also included in Figure 5-21 is a tabulation of the integrated average Seebeck coefficient between 300 and 1000°C and between 600 and 1000°C. Within experimental error they are identical.

Figure 5-22 is a plot of the Seebeck coefficient for ITM 197 as measured by the various laboratories. There is satisfactory agreement between the laboratories. Ames and Battelle data are lower with respect to GE data, as was previously observed in the round robin testing (Section 3.4).

Figure 5-23 is a plot of the Battelle electrical resistivity data exhibiting a linear increase with temperature and bending over near 800°C due to the onset of intrinsic conduction or increased phosphorus solubility. ITM 196 has the highest resistivity due to a lower carrier mobility and mean free path because of the presence of porosity as discussed above. The integrated average values between 300 and 1000°C and between 600 and 1000°C are also included. These data clearly show that ITM 196 has the highest electrical resistivity and ITM 197 the lowest. These electrical properties are not any different from that measured in Phase I of this Program for n-type 80/20 Si-Ge since a plot of the Seebeck coefficient vs. electrical conductivity is the same as that shown in Figure 4-6.

The electrical power factor was calculated using GE-ASD Seebeck and Battelle electrical resistivity measurements. Figure 5-24 shows the temperature dependence of the electrical power factors. Between 600 and 1000°C, ITM 197 and ITM 199 have a maximum power factor of about 40 $\mu W/cm°C^2$ and an

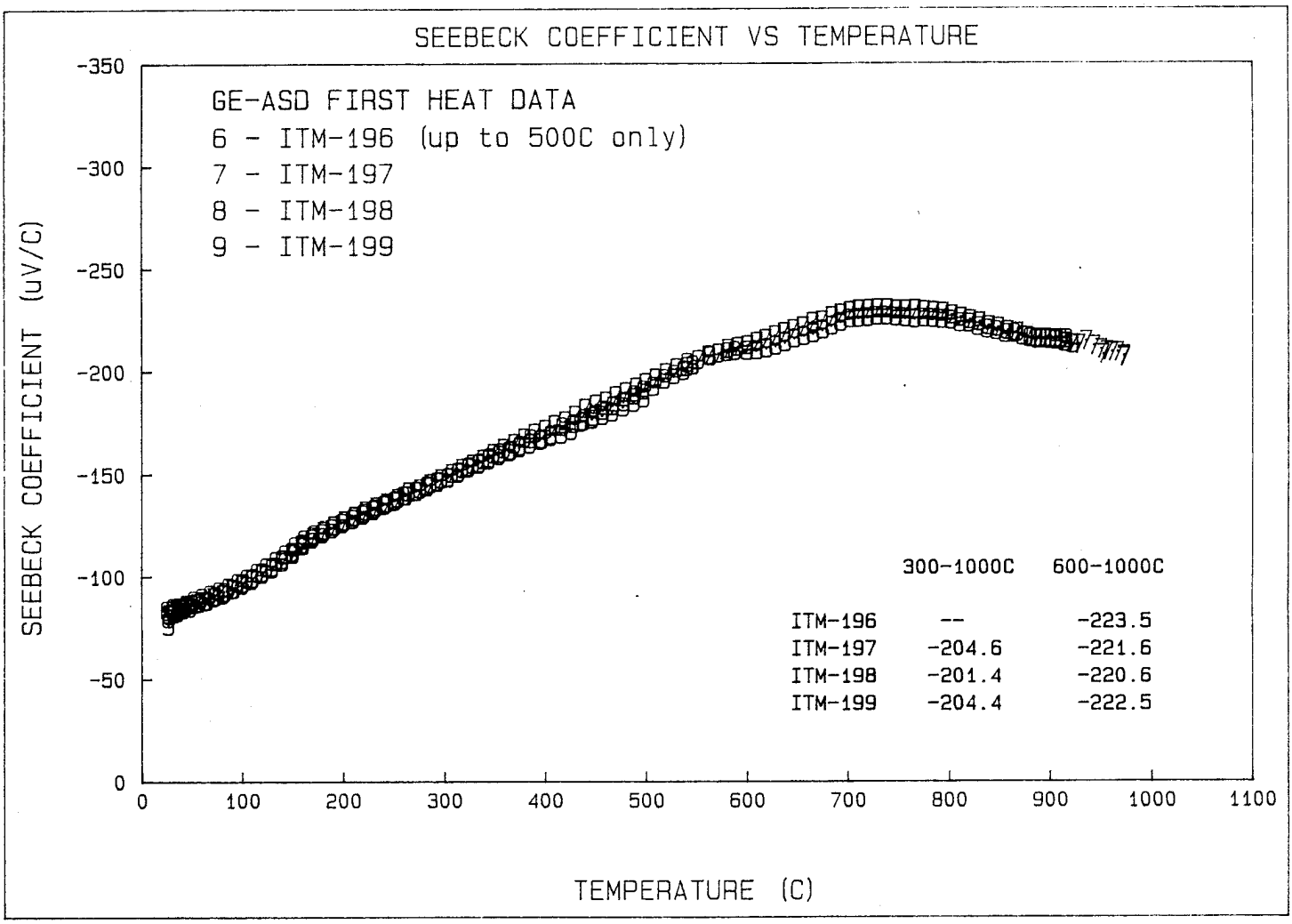

Figure 5-21. High Temperature Seebeck Coefficients of As-Pressed ITM 196 through ITM 199

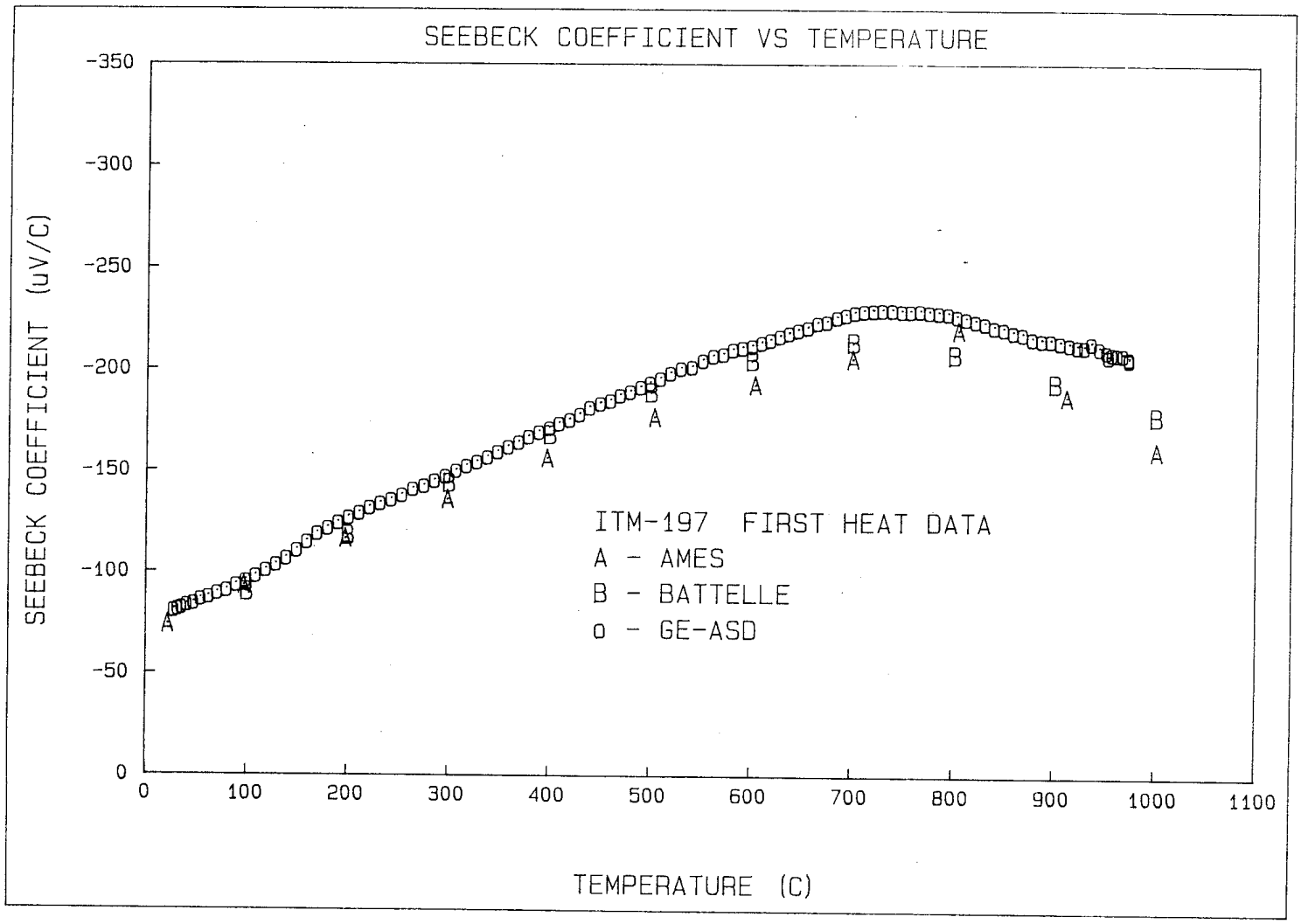

Figure 5-22. High Temperature Seebeck Coefficient of As-Pressed ITM 197

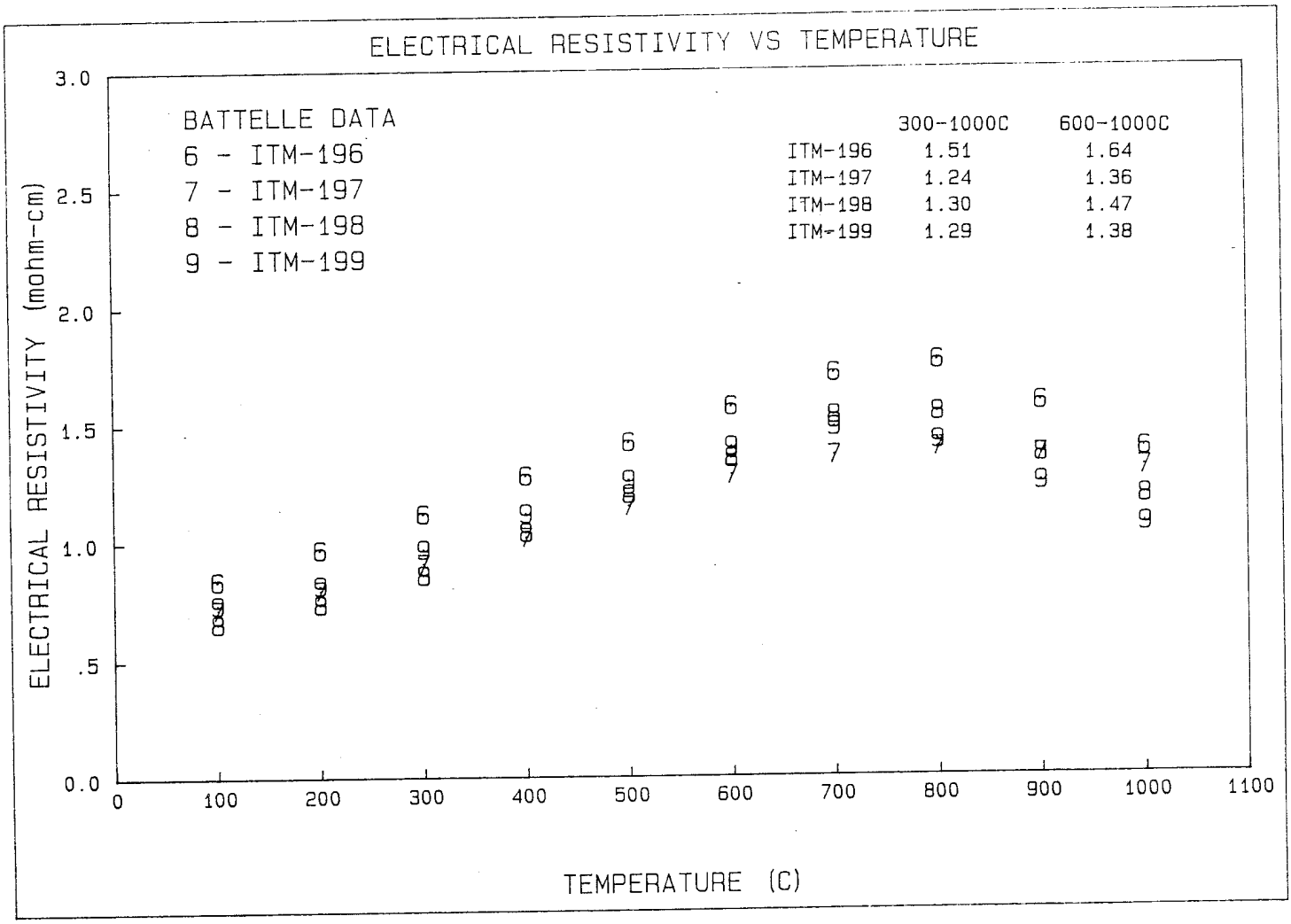

Figure 5-23. High Temperature Electrical Resistivity of As-Pressed ITM 196 through ITM 199

integrated value near 36 $\mu W/cm°C^2$. The integrated values between 300 and 1000°C are also included in Figure 5-24. The value for ITM 196 is an estimate since an integrated average Seebeck coefficient in this temperature range was not determined and a value of -204 μV/°C was estimated.

Thermal diffusivity, measured at GE-ASD by the laser flash technique, was combined with heat capacity data from Ames (for 2 Mol percent GaP in 80/20 Si-Ge) and experimentally determined density to calculate the thermal conductivity values.

Figure 5-25 is a plot of the temperature dependence of the thermal conductivities of the four alloys. ITM 196 has the lowest thermal conductivity consistent with the observation of voids in the microstructure. The data between 600 and 1000°C are considered very reliable and the integrated average thermal conductivity is shown to decrease with increasing GaP content. The calculated lattice thermal conductivities are compared to those of n-type 80/20 Si-Ge and are listed in Table 5-10. The lattice thermal conductivities are seen to be lower for the GaP containing alloys. Improved phonon scattering (e.g., second phase scattering) is thought to be responsible for this reduction.

Table 5-10. Calculated Lattice Thermal Conductivities of n-SiGe and n-SiGe-GaP Samples Prepared on this Program

Sample	Temperature °C				
	200	400	600	800	1000
n-SiGe	37.4	30.3	29.5	28.7	32.6
ITM-196	30.9	29.3	24.6	18.5	15.1
ITM-197	33.7	30.9	25.5	19.6	22.1
ITM-198	34.1	31.3	26.9	22.6	21.5
ITM-199	35.7	33.1	29.3	25.5	18.7

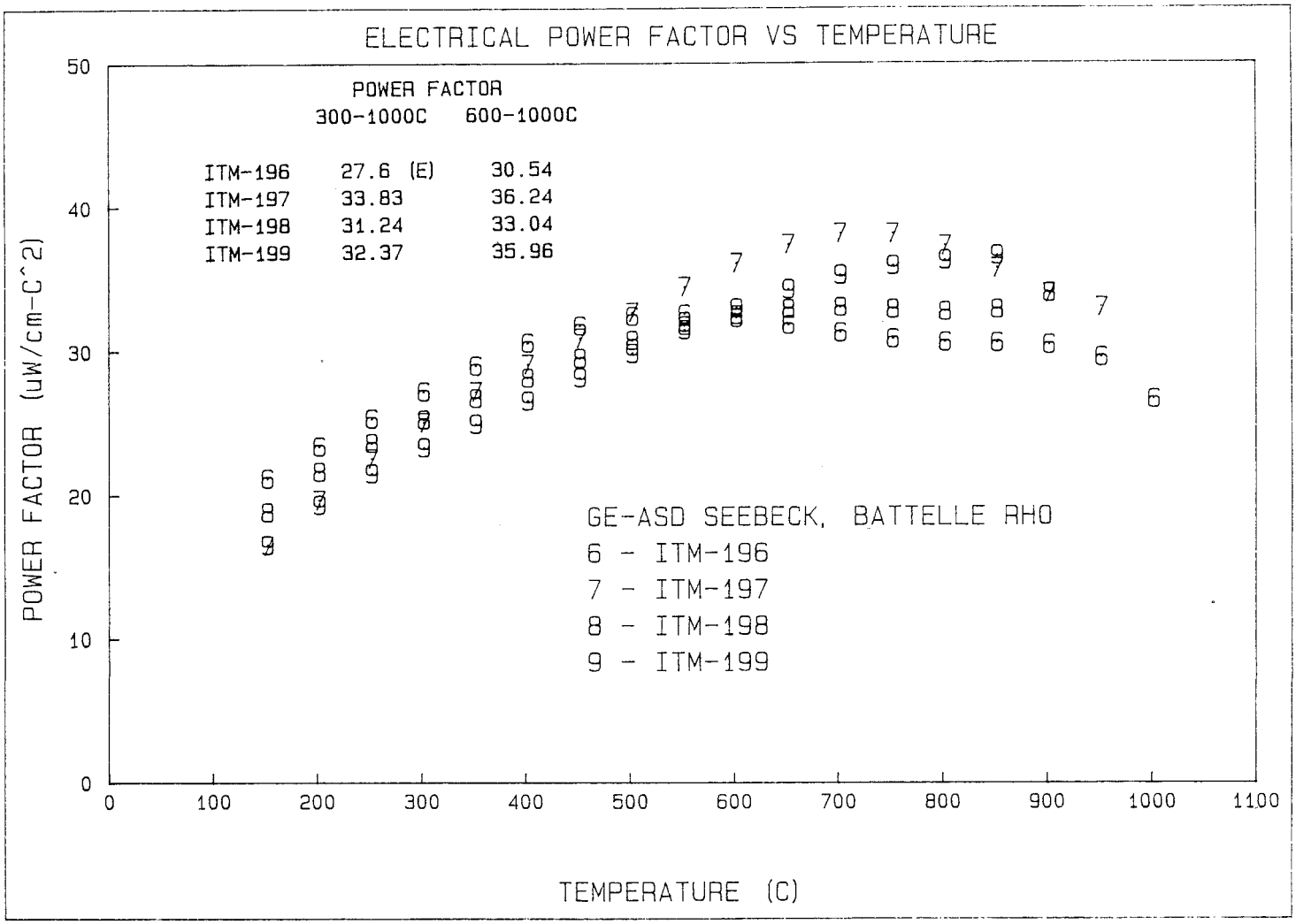

Figure 5-24. High Temperature Electrical Power Factor of As-Pressed ITM 196 through ITM 199

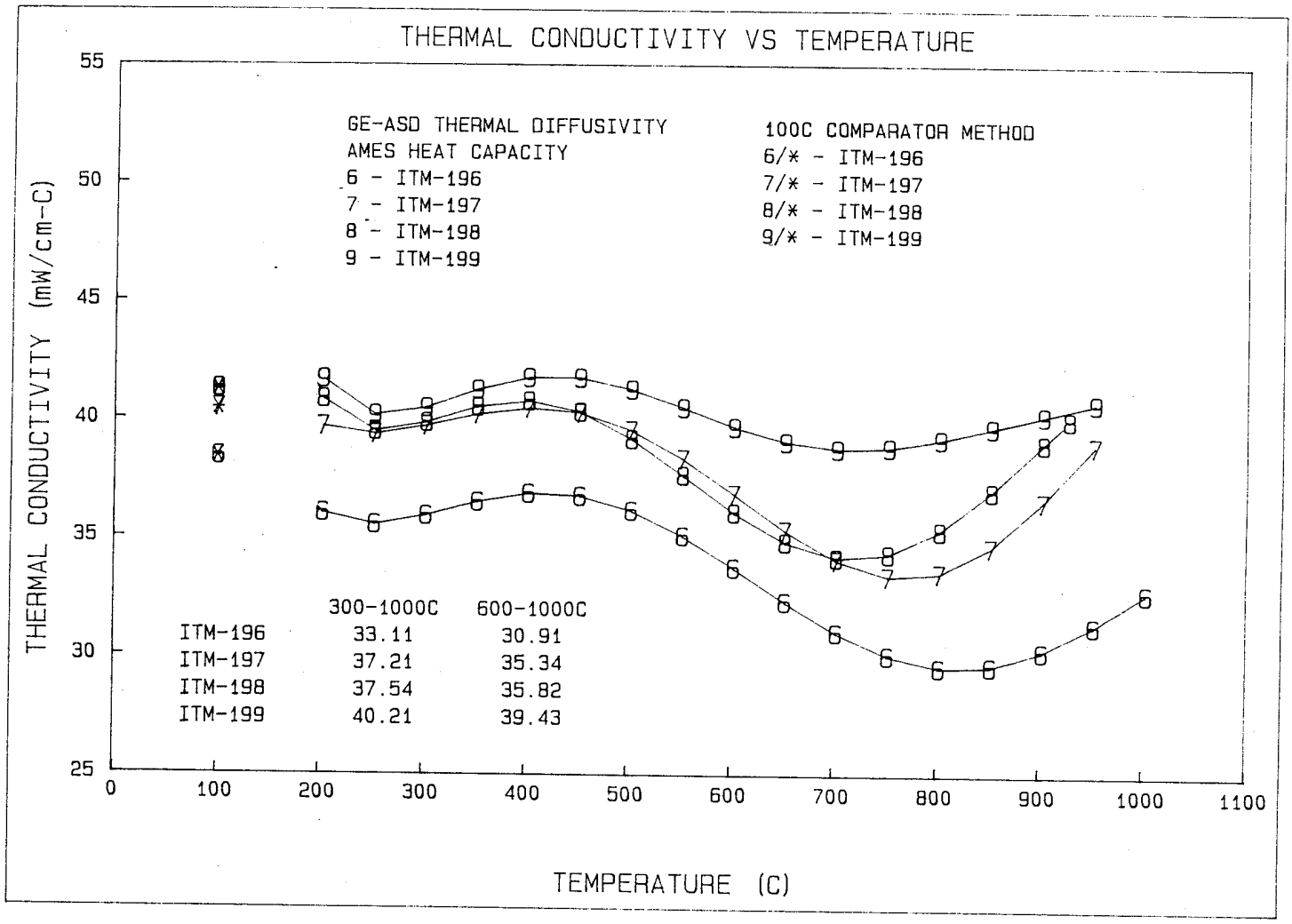

Figure 5-25. High temperature thermal conductivity measured at GE by the comparator method at 100°C and calculated from GE thermal diffusivity data and Ames heat capacity for ITM 196 through ITM 199.

Combining the electrical power factor with the thermal conductivity data results in the temperature dependence of the figure-of-merit trends as shown in Figure 5-26. ITM samples 196 and 197 with 3.5 and 1.6 Mol percent GaP, respectively, possess figure-of-merit values near 1 x 10^{-3}/°C. Integrated values between 300 and 1000°C are about 10-20% lower as is expected from the temperature dependence of the thermoelectric properties.

Figure 5-27 is a comparison of the temperature dependence of the figure-of-merit of ITM 197, which is considered to contain the optimum GaP content in 80/20 Si-Ge, with respect to the improved materials developed on the SP-100 Program (T106, T366, T373). The SP-100 samples were fabricated by Thermo Electron and were heat treated in air to homogenize the constituents. Elaborate air heat treatments up to 1320°C were performed to achieve these improvements, however, this technique has been shown to be non-reproducible. This plot leads one to believe that improved n-SiGe-GaP materials can be obtained by two different methods; namely, (1) the vacuum melting/chill casting/grinding/double hot pressing technique and, (2) the elemental approach combined with air heat treatment.

5.2.2.4 Thermal Treatments of 80/20 SiGe-GaP Alloys

Wafers, 1/2" in diameter and 0.030" thick, were thermally treated in an air furnace in an attempt to duplicate the further improvement in the electrical power factors reported by NASA-JPL and Thermo Electron. The room temperature Seebeck coefficient and Hall effect were measured in the as-pressed condition, after 98 hours at 1200°C, after 25 hours at 1275°C and 25 hours at 1320°C. The data are tabulated in Table 5-11. After each heat treatment, the white gallium oxide layer was removed by grinding with 600 grit SiC paper and distilled water. The edges were also sanded in order to obtain reproducible Hall effect results. After each heat treatment, the Seebeck coefficient, electrical resistivity and power factors increased. The increase in power factor was about 20%. The charge carrier concentration continually decreased although the carrier mobility increased significantly.

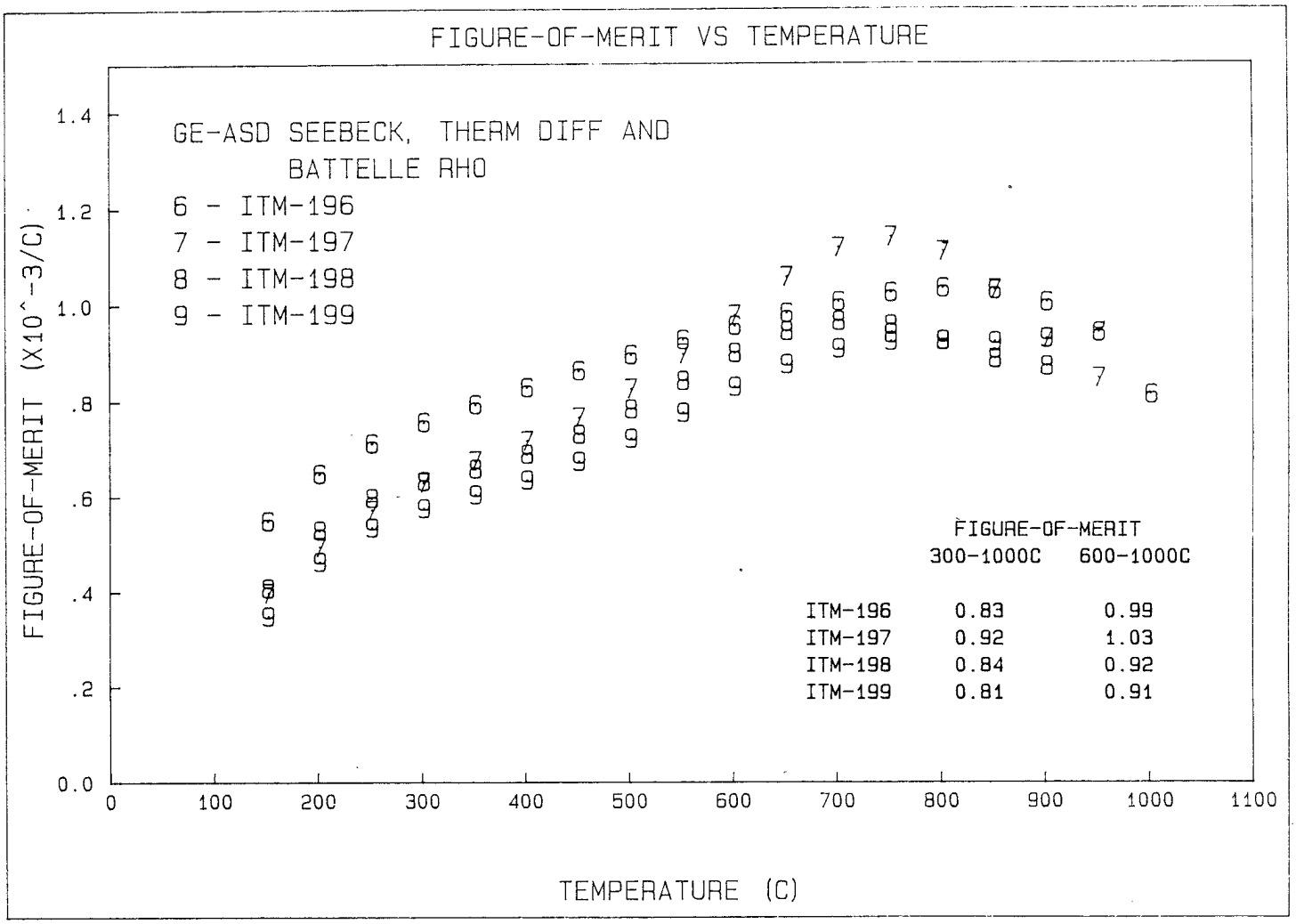

Figure 5-26. High Temperature Figure-of-Merit of As-Pressed ITM 196 through ITM 199

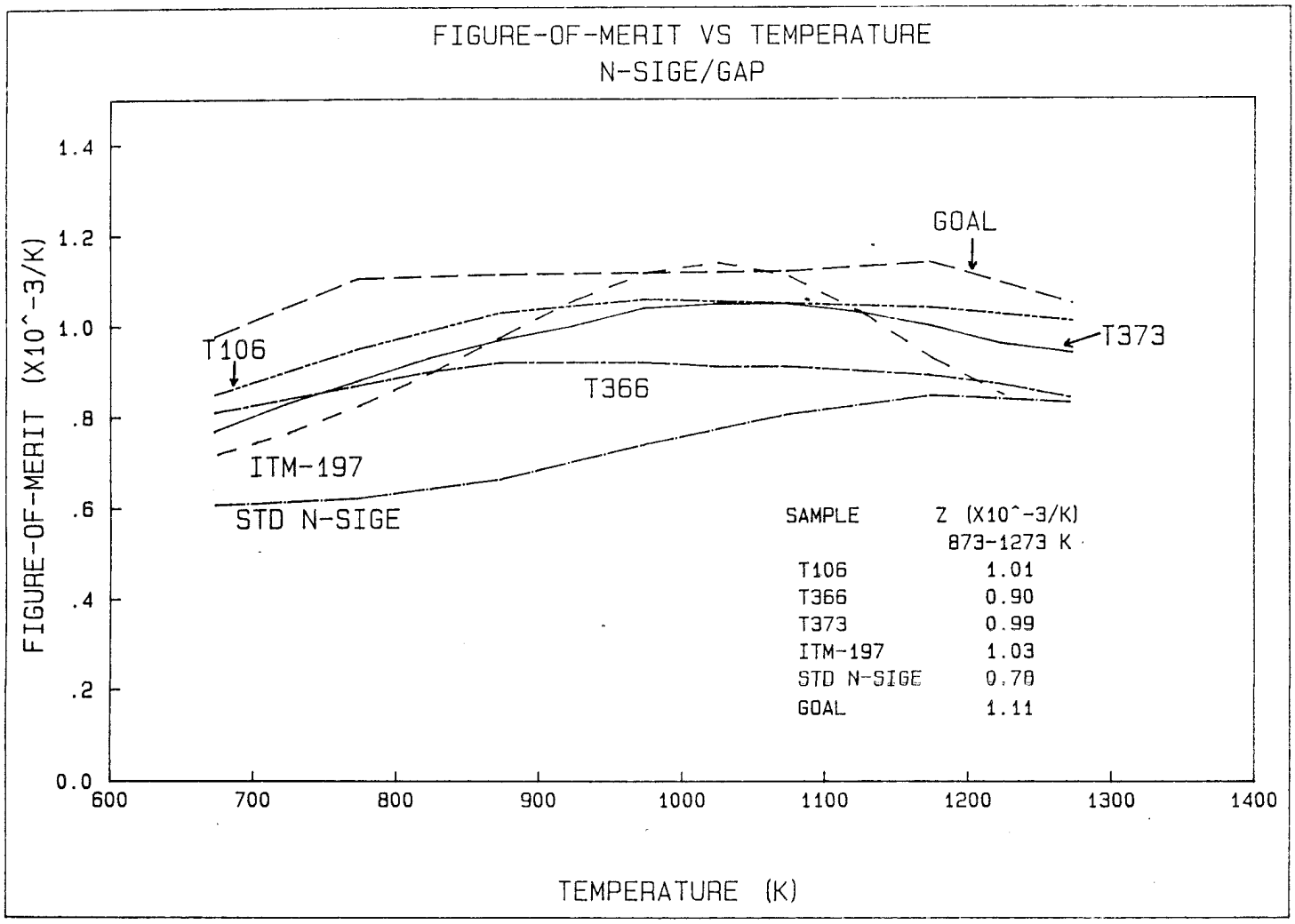

Figure 5-27 Comparison of the figure-of-merit of improved n-SiGe-GaP materials developed on the SP-100 Program (T106, T366, T373) and the ITM Program (ITM 197)

Table 5-11. Room Temperature Seebeck Coefficient and Hall Effect Measurements of GaP Doped 80/20 Si-Ge Alloys After a Sequence of Thermal Treatments

GE-ASD DATA	AS HOT PRESSED				AIR 1200°C/98 HRS				AIR 1275°C/25 HRS				AIR 1320°C/25 HRS			
ROOM TEMPERATURE	S	ρ_H	n	μ	S	ρ_H	n	μ	S	ρ_H	n	μ	S	ρ_H	n	μ
SAMPLE ID	μV/°C	mΩcm	$\times 10^{20}$ cm^{-3}	cm^2/V-s	μV/°C	mΩcm	$\times 10^{20}$ cm^{-3}	cm^2/V-s	μV/°C	mΩcm	$\times 10^{20}$ cm^{-3}	cm^2/V-s	μV/°C	mΩcm	$\times 10^{20}$ cm^{-3}	cm^2/V-s
$Ga_{0.038}P_{0.057}$		(8.81)				(10.01)				(10.23)						
1. ITM-196	-85	0.82	2.21	34.3	- 97	0.94	1.58	42.0	-108	1.14	1.18	46.8	—	1.31	1.08	44.2
$Ga_{0.017}P_{0.036}$		(10.13)				(11.83)				(12.40)						
2. ITM-197	-83	0.68	2.47	37.4	-106	0.95	1.37	47.8	-113	1.03	1.18	51.6	—	1.12	1.06	52.6
$Ga_{0.008}P_{0.027}$		(10.88)				(12.88)				(13.07)						
3. ITM-198	-86	0.68	2.32	39.4	-104	0.84	1.50	49.5	-112	0.96	1.22	53.2	—	1.09	1.07	53.9
$Ga_{0.004}P_{0.023}$		(11.00)				(13.60)				(13.25)						
4. ITM-199	-89	0.72	2.11	40.9	-110	0.89	1.33	52.7	-108	0.88	1.28	55.2	—	1.02	1.10	55.7

NUMBERS IN PARENTHESES ARE S^2/ρ VALUES

FOR OXIDIZED SAMPLES, PROPERTY MEASUREMENTS WERE TAKEN AFTER THE OXIDE LAYER WAS REMOVED BY GRINDING ON 600 grit SiC PAPER WITH DISTILLED WATER

After the third heat treatment at 1320°C for 25 hours, there was no white gallium oxide coating. The gallium content was depleted and a glossy SiO_2 surface remained together with the formation of a surface exudation. This surface exudation was identified to be SiP by SEM/EDS analysis.

The room temperature results of the heat treatment are inconsistent with Thermo Electron's (TECO's) observations: the Seebeck coefficients increased here while no change was measured in TECO's samples and the electrical resistivities here increased while TECO measured an appreciable decrease. However, the thermal treatment in both programs do appear to improve the thermoelectric properties. The ITM data suggest a potential improvement of up to 20 percent in figure-of-merit through factors such as carrier mobility increases, more complete densification and/or reduction in grain boundary effects.

Due to the promising trends in room temperature properties resulting from thermal treatments, it is highly recommended that high temperature thermoelectric property measurements be performed on the samples.

5.2.2.5 Long Term Thermal Stability

Ames Laboratory, of Iowa State University, sealed as-hot-pressed specimens of the ITM materials in quartz ampoules and heat treated them at 1000°C for three days. An as-hot-pressed piece of ITM 197 was also heat treated at 1000°C for 49 days. The high temperature Seebeck data for ITM 197 are shown in Figure 5-28. After 49 days at 1000°C, the high temperature Seebeck coefficients were decreased from the three day data, however, they were still higher than the as-pressed data. These data indicate that the relative thermal stability of ITM 197 is good.

The corresponding electrical resistivities for ITM 197 are shown in Figure 5-28. The low temperature resistivities after heat treatment are decreased from that for the as-pressed condition; a trend which will improve the figure-of-merit averaged between 300 and 1000°C assuming the thermal conductivity is constant. It is conjectured that the thermal conductivity will only be dependent on grain size and, hence, not be susceptible to change

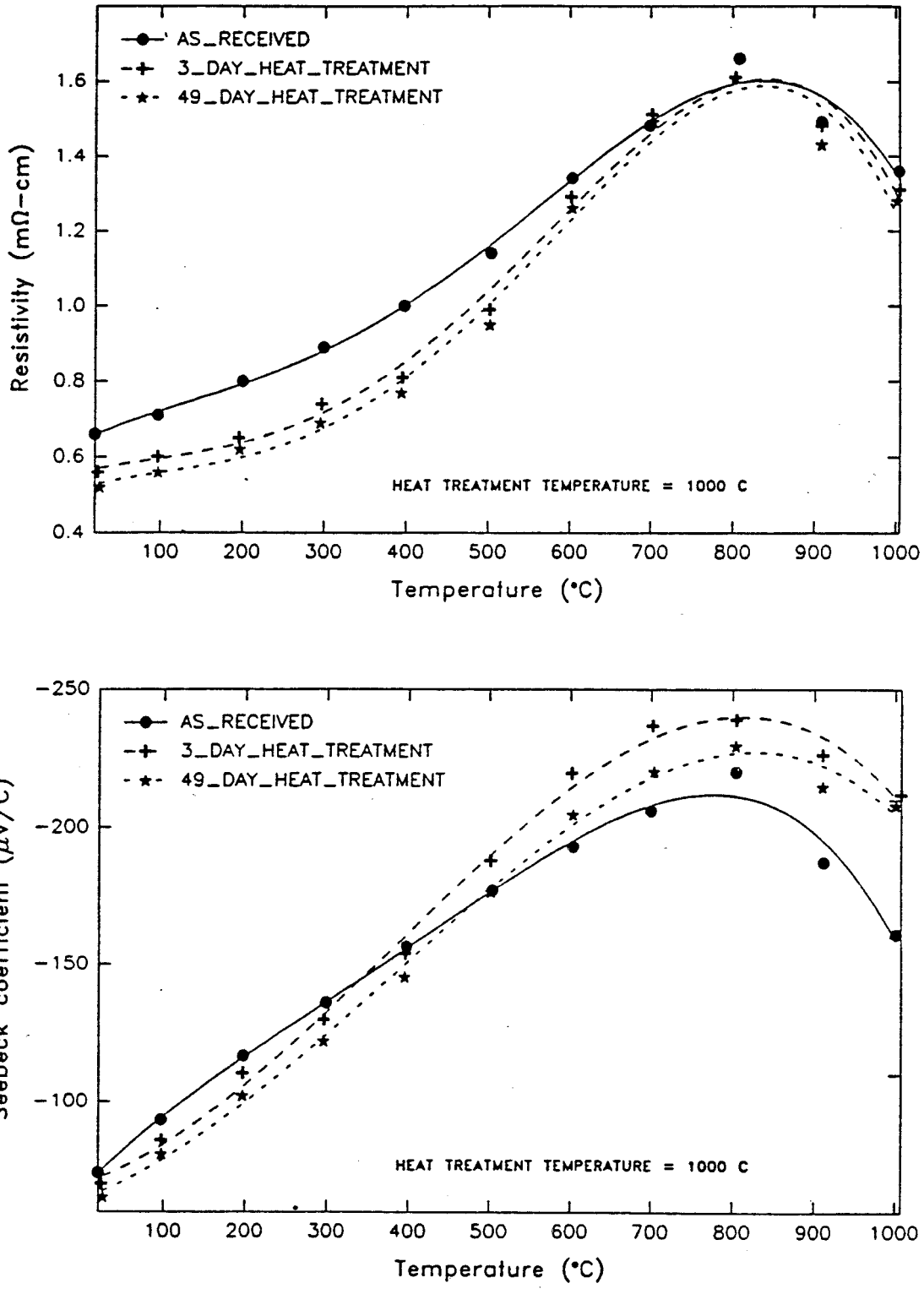

Figure 5-28. Resistivity and Seebeck Coefficient Heating Curves for ITM 197, after 1000°C Heat Treatment As Measured by Ames Laboratory

during heat treatments. Thermal aging beyond three days does not further affect the electrical resistivity.

Figure 5-29 is a plot of the power factor of ITM 197 after three and 49 days at 1000°C. The data indicate that the figure-of-merit can be improved by judicious heat treatment.

Table 5-12 lists the average electrical power factors (from data obtained by Ames Laboratory) of the four 80/20 SiGe-GaP alloys before and after long term heat treatment at 1000°C. Only ITM 197 has responded favorably; that is, the electrical properties have improved 23% between 300 and 1000°C with isothermal heat treatment. No significant improvement was observed for the remaining three samples.

Table 5-12. The Effect of Heat Treatment on the Average Electrical Power Factor ($\mu W/cm°C^2$) as Measured by Ames Laboratory

	AS-PRESSED		POST 49 DAYS @ 1000°C IN QTZ	
SAMPLE	300-1000*	600-1000*	300-1000*	600-1000*
ITM-196	24.8	26.2	24.4	27.3
ITM-197	22.3	25.6	27.4	32.9
ITM-198	24.4	29.0	22.7[a]	27.2[a]
ITM-199	27.4	32.6	22.6[b]	26.8[b]

* °C

[a] 54 days at 1000°C in quartz

[b] 36 days at 1000°C in quartz

Battelle-Columbus has completed in-gradient leg tests using ITM samples 197 and 198, in which the Seebeck coefficient and electrical resistivity were monitored as a function of time. Each sample was instrumented with three W5Re-W26Re thermocouples and the current leads were placed at opposite ends of the sample. The hot and cold ends were maintained at 915 and 400°C,

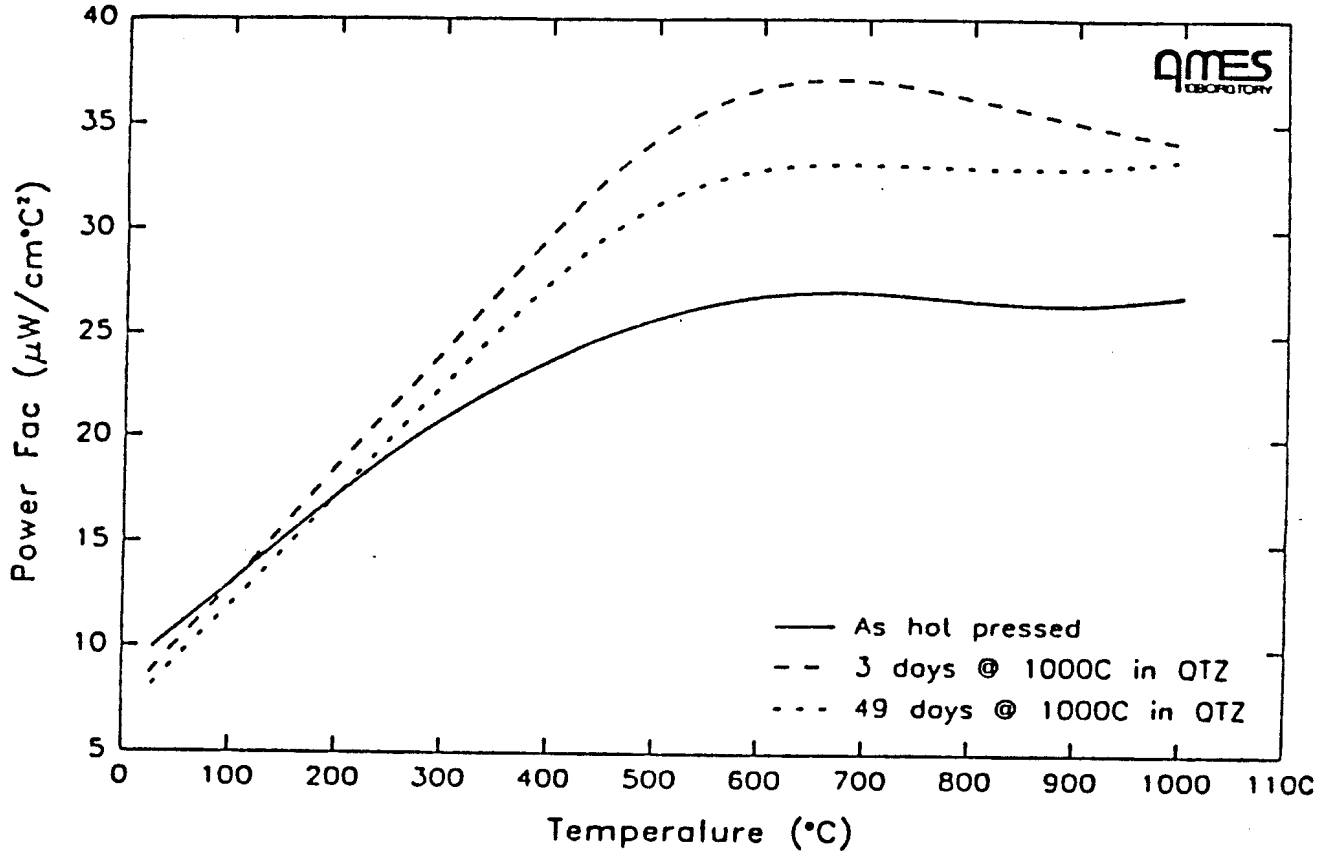

Figure 5-29. Effect of 1000°C Heat Treatments on the Electrical Power Factor of ITM 197

respectively. The Seebeck coefficients were determined by evaluating the quotient Delta V/Delta T and the resistivities were determined by the 4-point AC method between adjacent thermocouples. A schematic of the setup is shown in Figure 5-30.

Figure 5-31 shows the time dependence of the Seebeck coefficients and Figure 5-32 shows the time dependence of the electrical resistivities. Both properties have increased from their as-pressed values. However, they have stabilized after 40 days. Figure 5-33 is a plot of the electrical power factors using only Battelle Columbus data. The curves are representative of the as-pressed condition and the symbols represent values at day 1 and 59. There is no degradation after 59 days for ITM 197 and a remarkable improvement for ITM 198.

Preliminary long term aging tests and thermal treatment studies at Ames and Battelle Laboratories suggest that the 80/20 SiGe-GaP enhanced performance alloys are (1) remarkably stable and (2) may be amenable to substantial property improvements by thermal treatments. However, much additional effort will be required to quantify the trends.

5.3 REPRODUCIBILITY DEMONSTRATION OF ENHANCED PERFORMANCE 80/20 SiGe-GaP ALLOYS

5.3.1 COMPACT FABRICATION

Three additional compacts were fabricated to demonstrate the reproducibility of property improvements achieved on ITM 197. ITM 232 is a duplicate of ITM 197 and was prepared from a powder blend consisting of 8 Mol percent GaP in 50/50 Si-Ge and phosphorous doped silicon. The nominal composition of ITM 232 is $Si_{0.760}Ge_{0.190}Ga_{0.016}P_{0.034}$. The second compact, ITM 234, is a duplicate of ITM 197 with additional phosphorous. The extra phosphorous was added to the initial vacuum casting of 8 Mol percent GaP in 50/50 Si-Ge. The nominal composition of ITM 234 is $Si_{0.747}Ge_{0.187}Ga_{0.016}P_{0.050}$. The third compact, ITM 237, has a nominal composition of $Si_{0.769}Ge_{0.192}Ga_{0.016}P_{0.022}$ and was prepared from a powder blend consisting of Si-Ge and Ge-GaP master alloys.

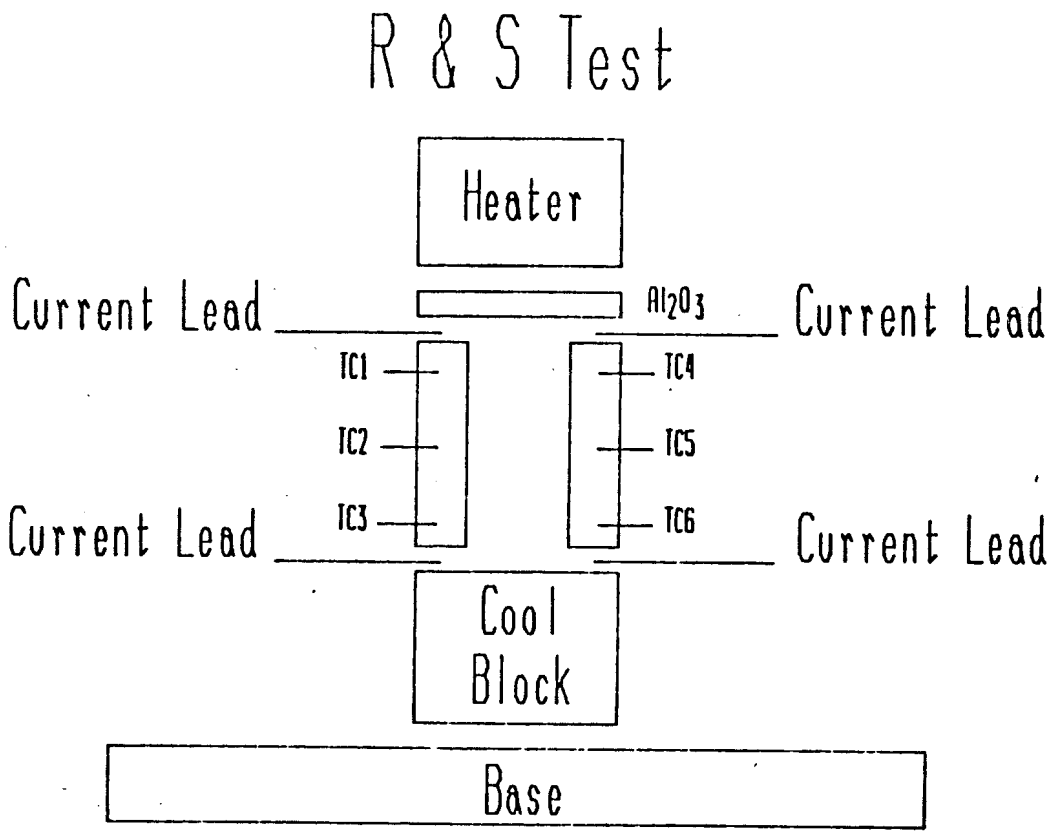

Heater Temp	1000 C	TC3 (197)	491 C
Hot End Temp	915 C	TC4 (198)	796 C
TC1 (197)	835 C	TC5 (198)	641 C
TC2 (197)	680 C	TC6 (198)	505 C
	Cold End Temp	400 C	

Figure 5-30. Schematic of the In-gradient Leg Test at Battelle-Columbus

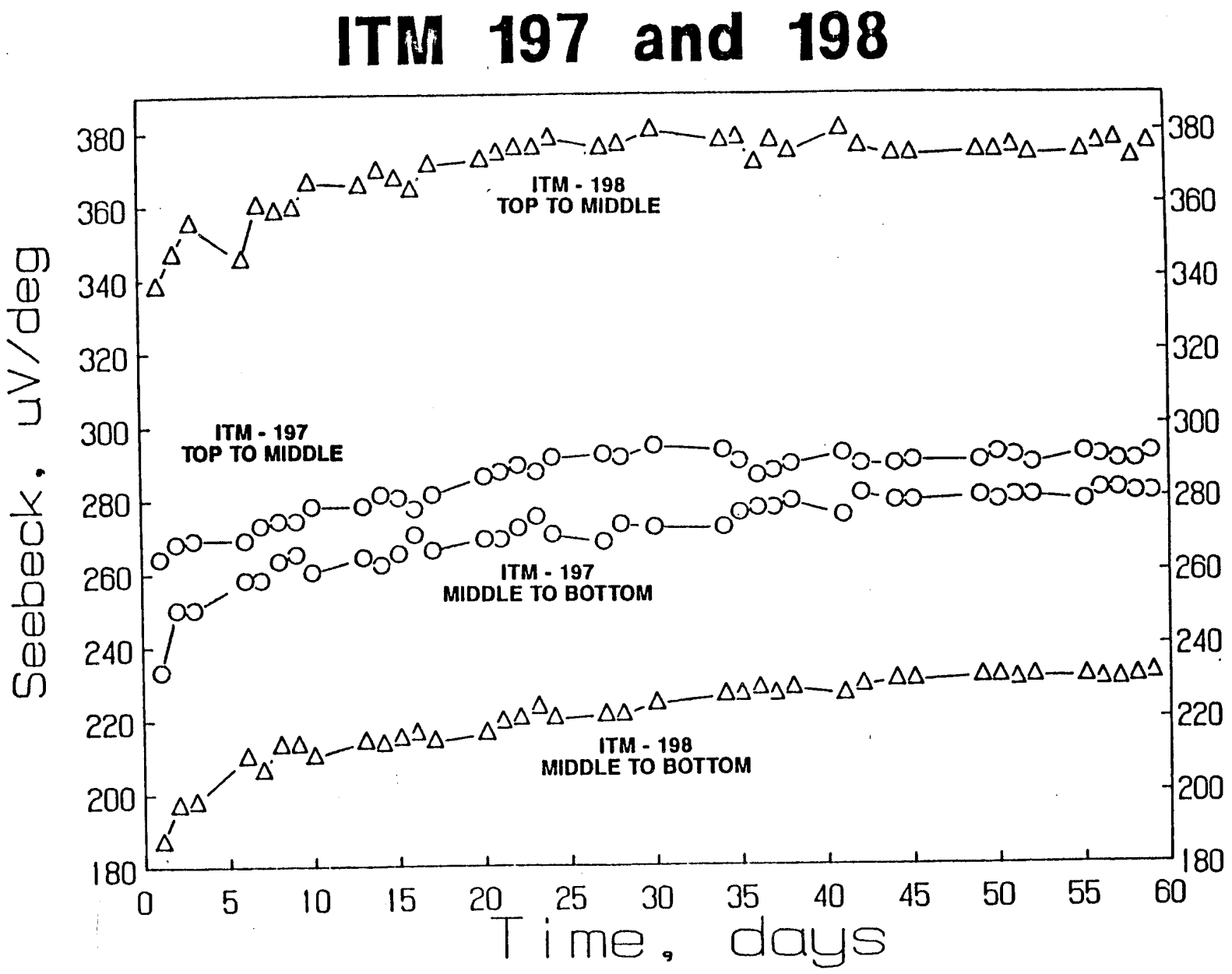

Figure 5-31. Seebeck Coefficient as a Function of Time for ITM 197 and 198 from Battelle In-gradient Leg Test

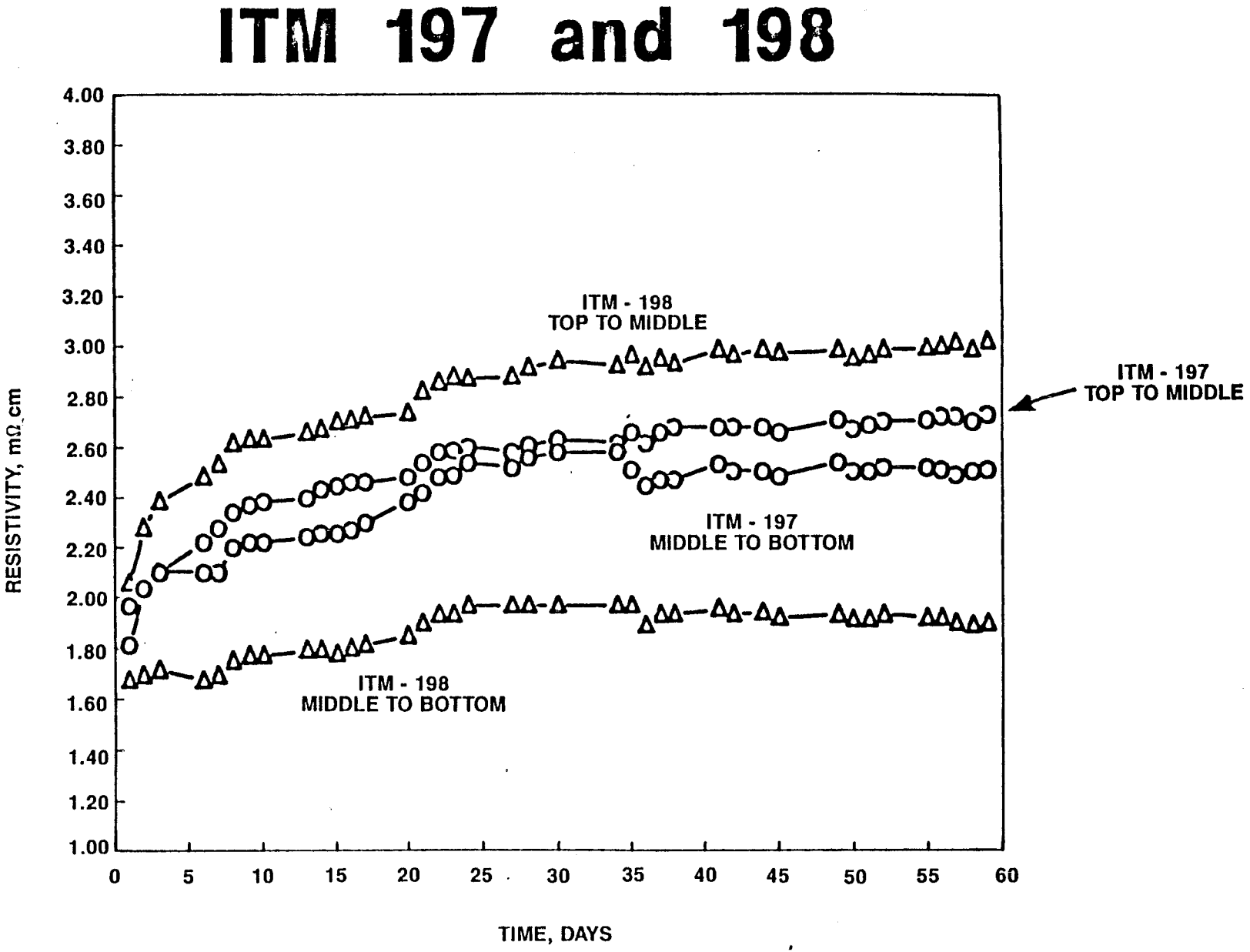

Figure 5-32. Electrical Resistivity as a Function of Time for ITM 197 and 198 from Battelle In-gradient Leg Test

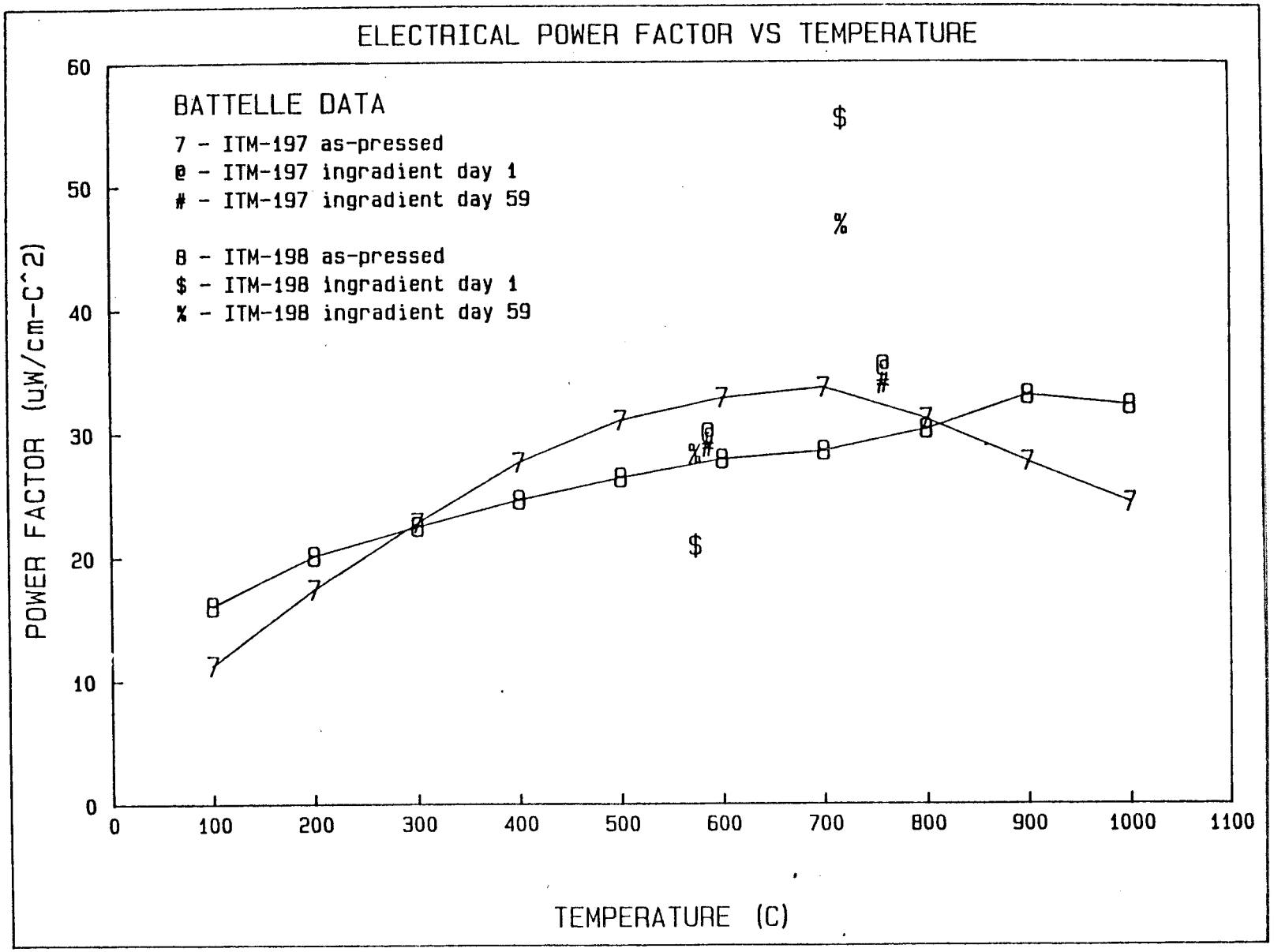

Figure 5-33. Electrical Power Factor as a Function of Time for ITM 197 (586° and 758°C) and ITM 198 (573° and 718°C) from Battelle In-gradient Leg Test

Figures 5-34 to 5-36 provide flow diagrams to describe the fabrication processes for the three compacts. After vacuum hot pressing, the room temperature Seebeck coefficients were carefully measured on the top and bottom surfaces of the 3" diameter compacts. The Seebeck values varied by only 3 μV/°C at most, which is a good indicator of a high degree of homogeneity.

5.3.2 MATERIAL CHARACTERIZATION

The density and room temperature Hall effect of the compacts were measured and the results are tabulated in Table 5-13, along with the results for ITM 197. The data for ITM 232 are the same as ITM 197 within experimental error. This clearly shows GE's ability to reproduce materials. The trend in carrier concentration with the electrical resistivity and Seebeck coefficient is consistent with that expected from the nominal composition. Though the carrier concentration is lowest for ITM 237, the room temperature power factor is about 10% larger than the corresponding values for the other two samples. This is possible since the increase in the Seebeck coefficient squared more than compensates for the increase in the electrical resistivity.

The compositional homogeneity of the three materials listed in Table 5-13 was studied using x-ray diffraction methods. The procedure used consisted of analyzing the (311) x-ray diffraction profiles obtained for each of the materials.

Two specimens were evaluated from the ITM 232 compact. A 0.5 inch diameter core was taken through the thickness of the compact. One of the specimens examined was taken from the top of the core, the other from the bottom. The top and bottom slices were found to be very similar. They both have a very narrow compositional range. This narrow range of composition indicates a high degree of homogeneity. The average composition of the top slice is slightly greater in silicon concentration than is the bottom slice and both slices have similar ranges in composition. It is concluded that the variation between the top and bottom of the compact, in terms of homogeneity and composition, is probably insignificant.

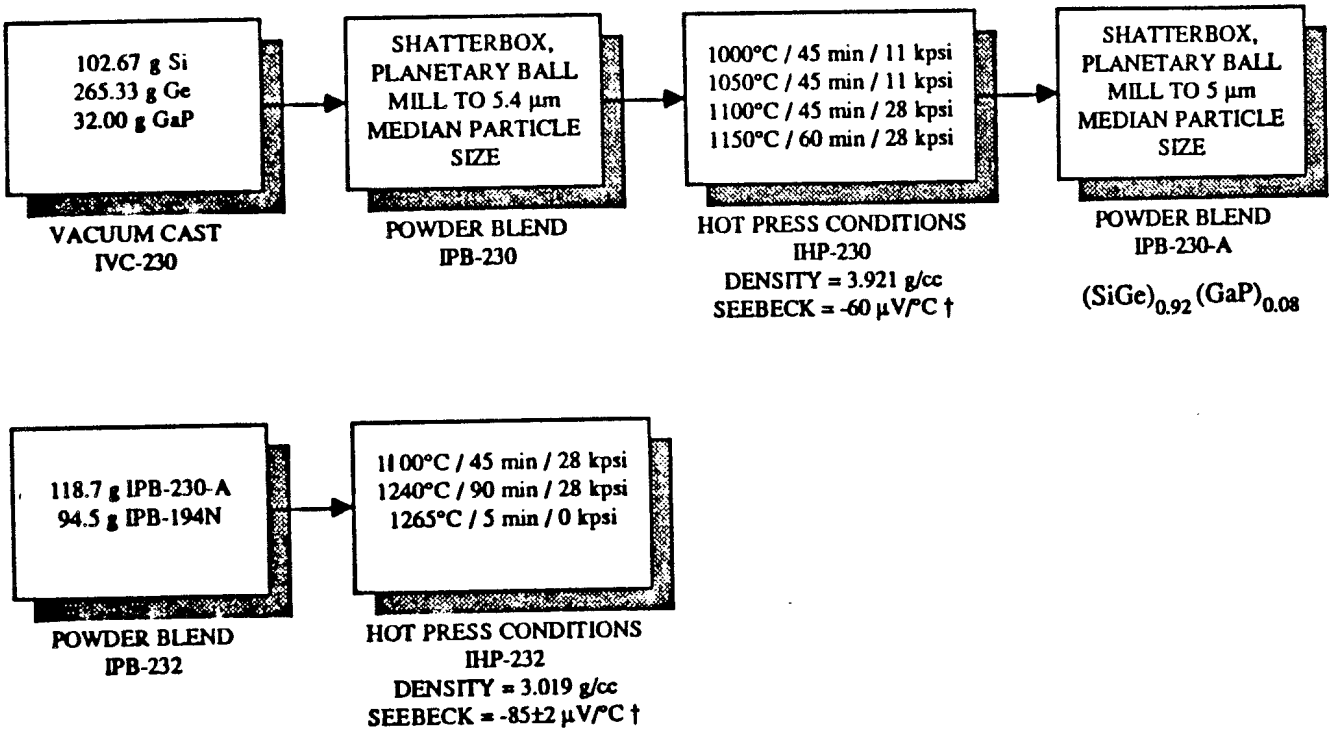

† AVERAGE SEEBECK MEASURED ON TOP AND BOTTOM SURFACES OF COMPACT

Figure 5-34. Fabrication Process for ITM 232
$Si_{0.760}Ge_{0.190}Ga_{0.016}P_{0.034}$

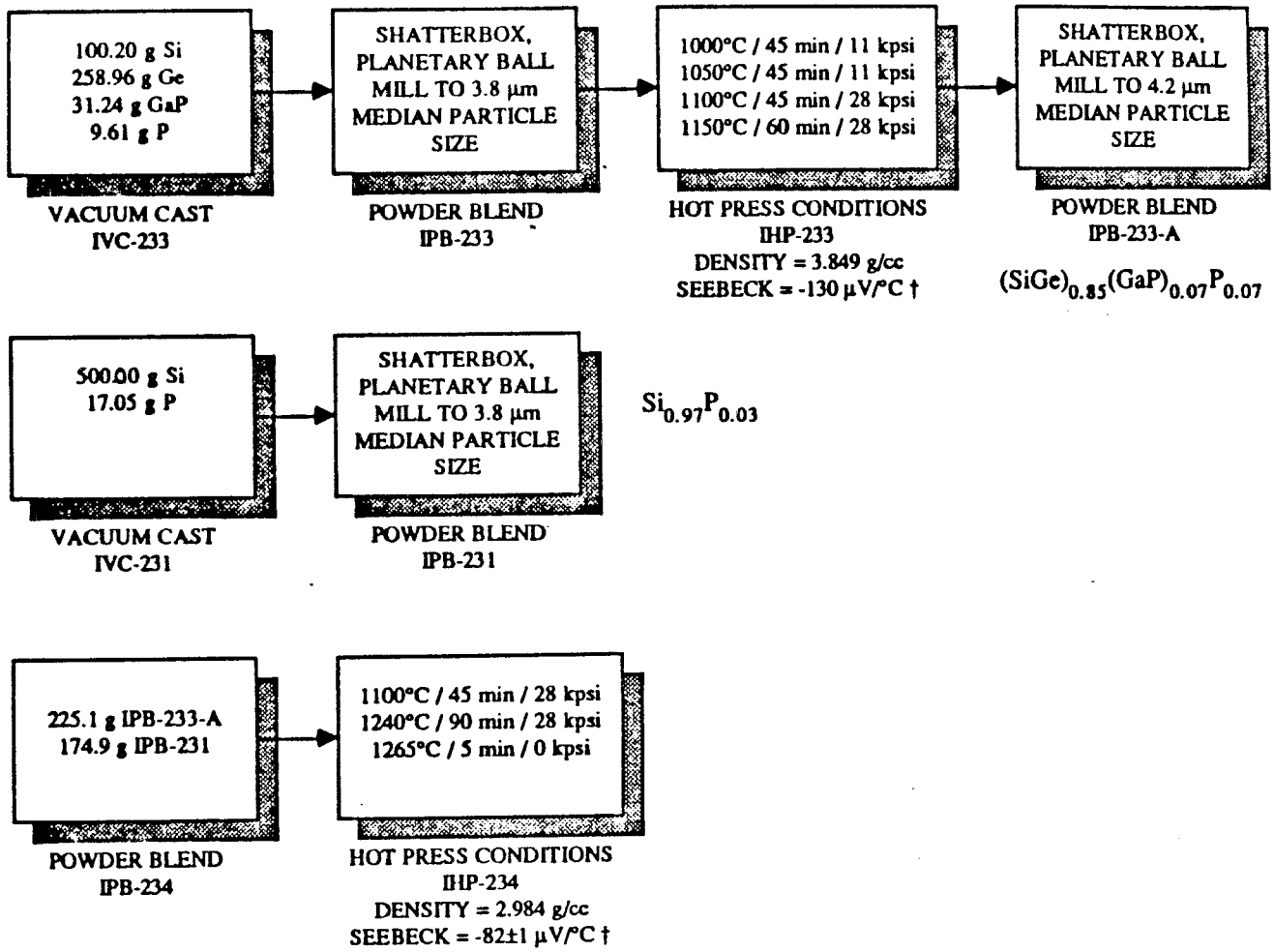

† AVERAGE SEEBECK MEASURED ON TOP AND BOTTOM SURFACES OF COMPACT

Figure 5-35. Fabrication Process for ITM 234 $Si_{0.747}Ge_{0.187}Ga_{0.016}P_{0.050}$

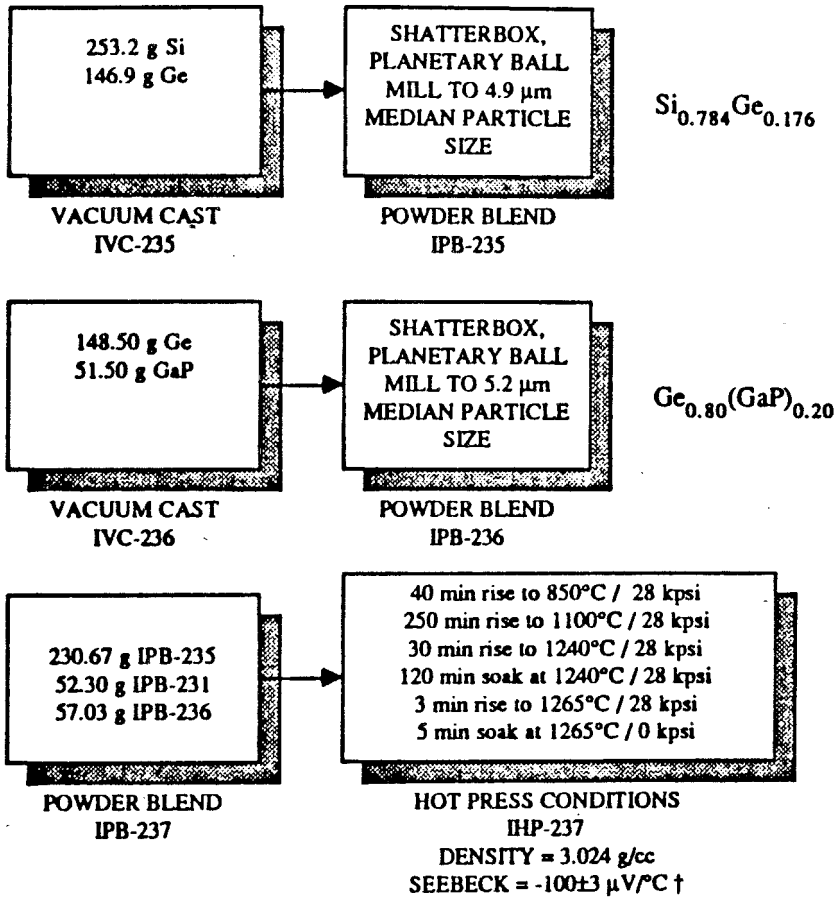

† AVERAGE SEEBECK MEASURED ON TOP AND BOTTOM SURFACES OF COMPACT

Figure 5-36. Fabrication Process for ITM 237
$Si_{0.769}Ge_{0.192}Ga_{0.016}P_{0.022}$

Table 5-13. Summary of Room Temperature Results for GaP Doped 80/20 Si-Ge

COMPACT	NOMINAL COMPOSITION	SEEBECK ($\mu v/^oC$)	RHO(HALL) ($m\Omega cm$)	MOBILITY ($cm^2/V-s$)	CARRIER CONC (1/cc)	DENSITY (g/cc)
ITM-232	$Si_{0.760}\ Ge_{0.190}\ Ga_{0.016}\ P_{0.034}$	-85	0.677	38.22	$2.43x10^{20}$	3.019
ITM-234	$Si_{0.747}\ Ge_{0.187}\ Ga_{0.016}\ P_{0.050}$	-82	0.603	40.62	$2.55x10^{20}$	2.984
ITM-237	$Si_{0.769}\ Ge_{0.192}\ Ga_{0.016}\ P_{0.022}$	-100	0.834	41.31	$1.82x10^{20}$	3.024
ITM-197	$Si_{0.760}\ Ge_{0.190}\ Ga_{0.016}\ P_{0.034}$	-83	0.675	37.45	$2.47x10^{20}$	3.000

One reason that compact ITM 232 was produced was to show that ITM 197 could be duplicated. The x-ray diffraction profiles from both of these materials are presented for comparison in Figure 5-37. Since the profiles are seen to be very similar, it is concluded that the degree of compositional homogeneity for these two materials is also very similar. The Lorentz function at 56.1 degrees 2-theta is also in the deconvolution for ITM-232 which is coincident with the GaP diffraction profile.

Examination of the (311) diffraction profile obtained for ITM 234 and ITM 237 also indicated a high degree of compositional homogeneity. Narrow diffraction profiles with a corresponding single large Lorentz function and only a very few small side Lorentz functions attest to the narrow range of compositions.

5.3.3 THERMOELECTRIC PROPERTIES

Samples from compacts ITM 232, 234 and 237 were supplied to Ames Laboratory for evaluation. The compacts were fabricated to demonstrate that the vacuum melting/chill casting/grinding/hot pressing method of compact fabrication was capable of providing reproducible improvement in properties.

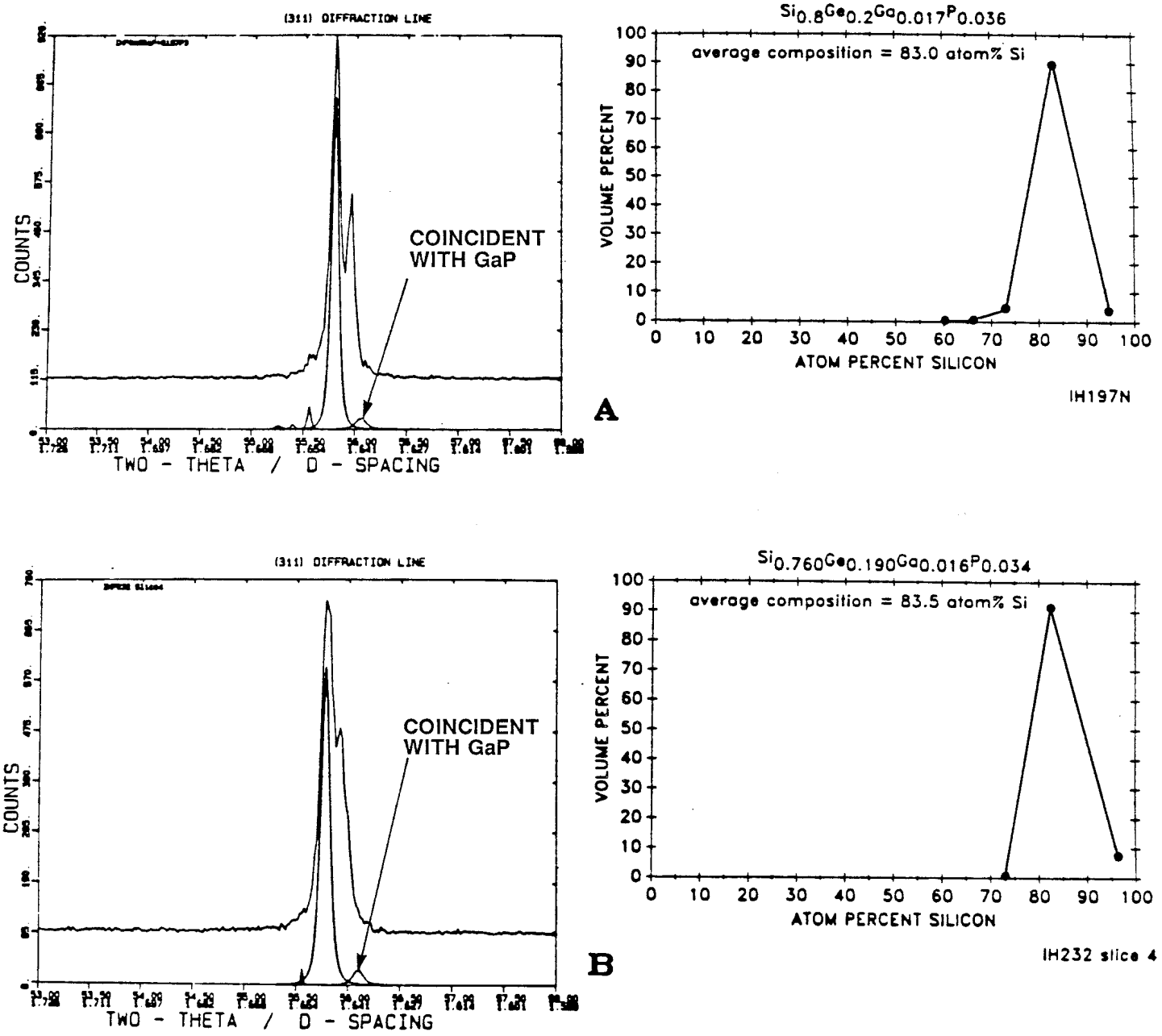

Figure 5-37. (311) X-ray Diffraction Profiles (with Lorentz Functions) and Compositional Distributions for:(a) Region in Compact ITM 197; and (b) from Region in Compact ITM 232. The Lorentz function at 56.1 degrees 2-theta is coincident with the GaP diffraction profile.

Figures 5-38 through 5-40 show the temperature dependence of the Seebeck coefficients, electrical resistivities and electrical power factors, respectively, as measured by Ames Laboratory for sample ITM 232 in comparison with ITM 197. There is excellent agreement in the data except that the Seebeck coefficients at 900 and 1000°C are 11% and 25% higher, respectively, for ITM 232. This, in turn, results in an 18% improvement in the integrated average power factor between 300 and 1000°C. The duplication of the high temperature electrical properties clearly demonstrates fabrication reproducibility.

Figures 5-41 and 5-42 compare the high temperature electrical properties of ITM samples 232, 234 and 237. The n-SiGe-GaP samples possessing phosphorus to gallium ratios in excess of 1.5 (ITM 232 and 234) have lower Seebeck coefficients and electrical resistivities due to their higher carrier concentrations. A plot of the Seebeck coefficient vs. the log of the electrical conductivity is the same as shown in Figure 4-6 for n-type 80/20 Si-Ge. This indicates that the electrical properties are not affected by the addition of GaP.

The calculated electrical power factors are compared in Figure 5-43. Also, the integrated average electrical power factors between 300 and 1000°C and 600 and 1000°C are compiled in Table 5-14.

ITM 234 possesses the highest power factors due to increased carrier concentration and correspondingly lower electrical resistivities.

Table 5-14. Electrical Power Factors for n-SiGe-GaP Samples ITM 232, 234 and 237

	S^2/ρ ($\mu W/cm^oC^2$)	
N-SiGe-GaP	300-1000°C	600-1000°C
ITM-232	26.4	28.2
ITM-234	32.9	34.6
ITM-237	31.1	32.0

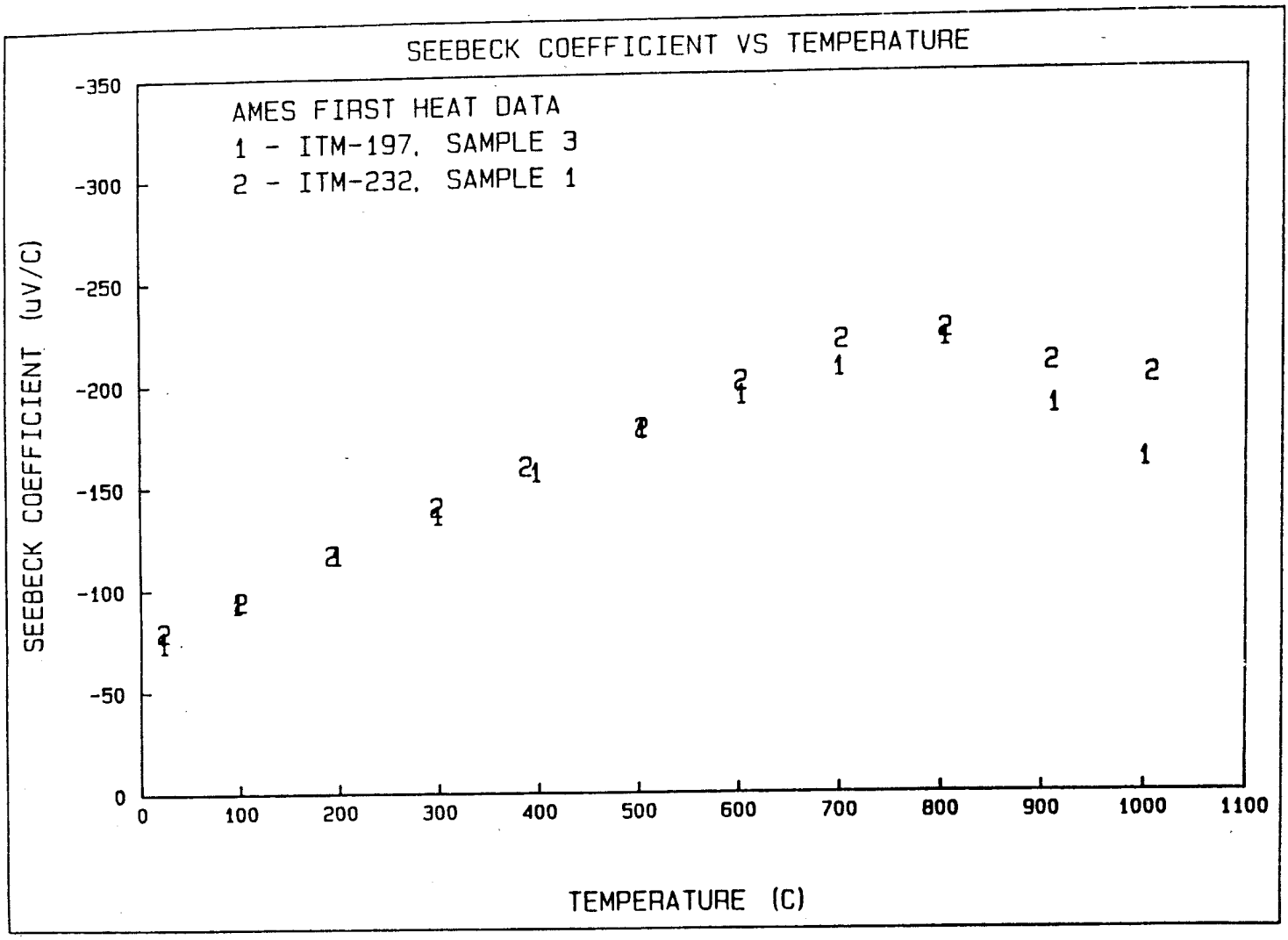

Figure 5-38. Seebeck Coefficients for Samples from Compacts ITM 197 and 232 with the Same Fabrication Procedures

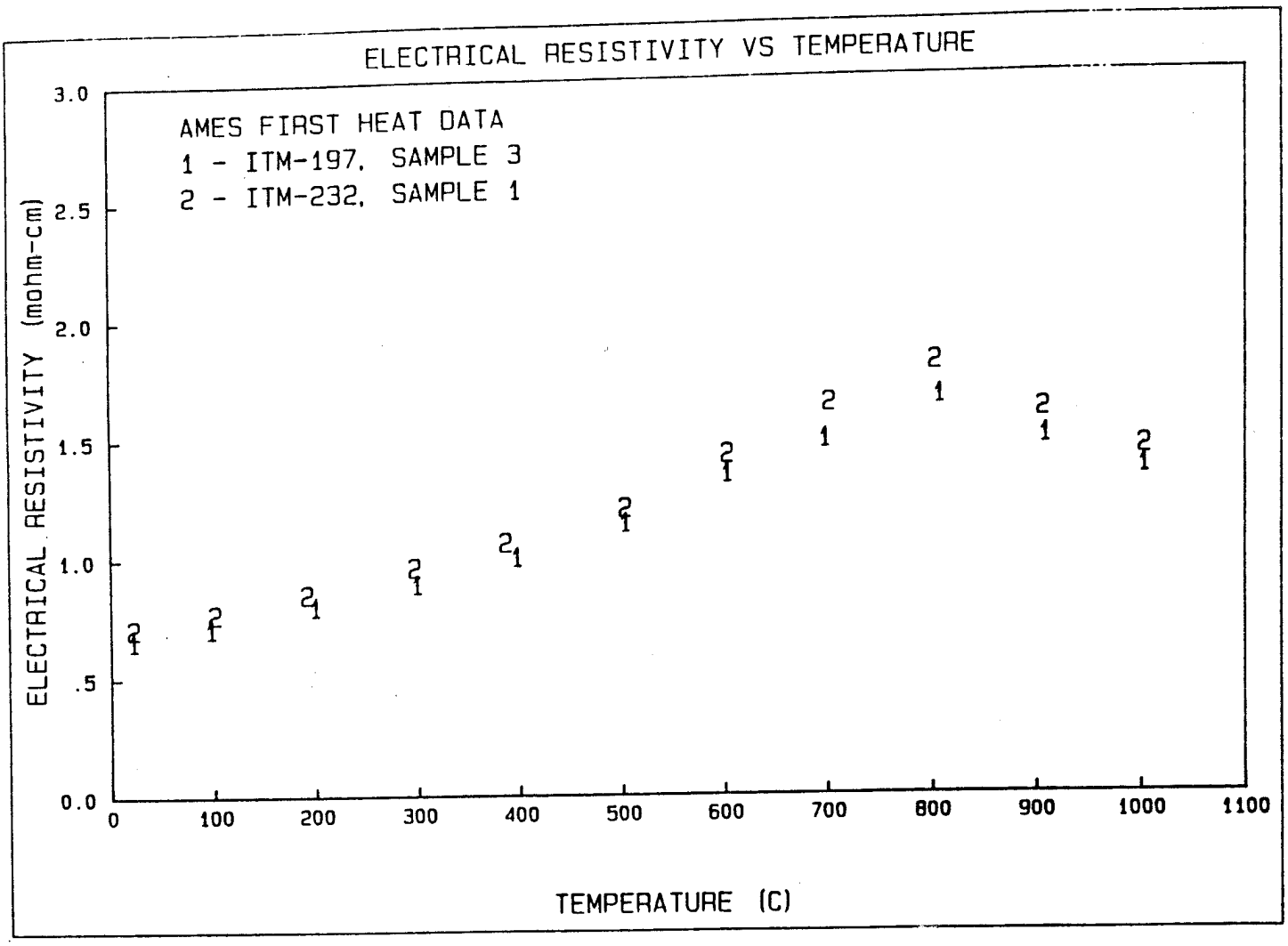

Figure 5-39. Comparison of the Electrical Resistivities for Samples from ITM 197 and 232 with the Same Fabrication Procedures

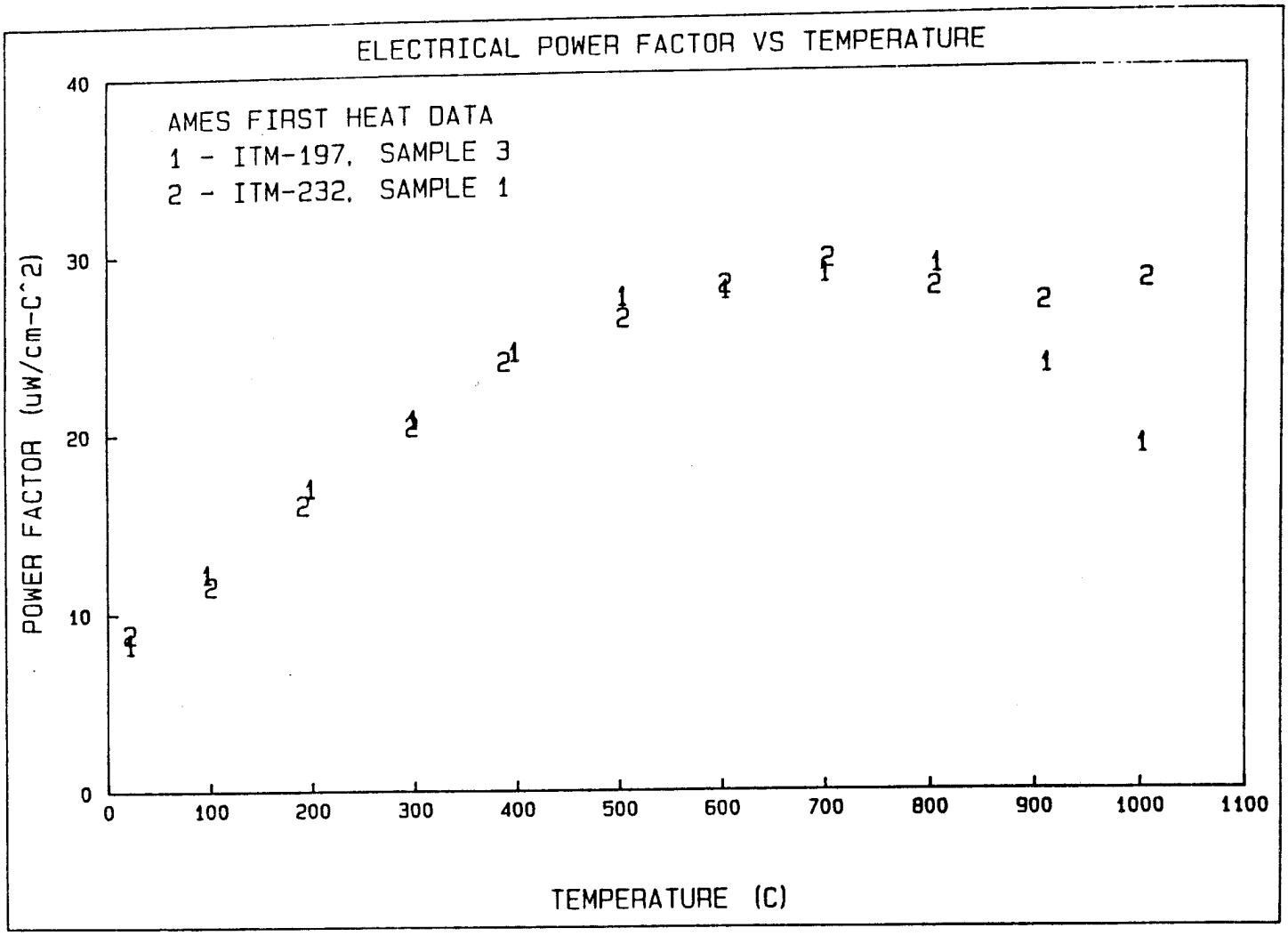

Figure 5-40. Comparison of the Electrical Power Factor for Compacts ITM 197 and 232 with the Same Fabrication Procedures

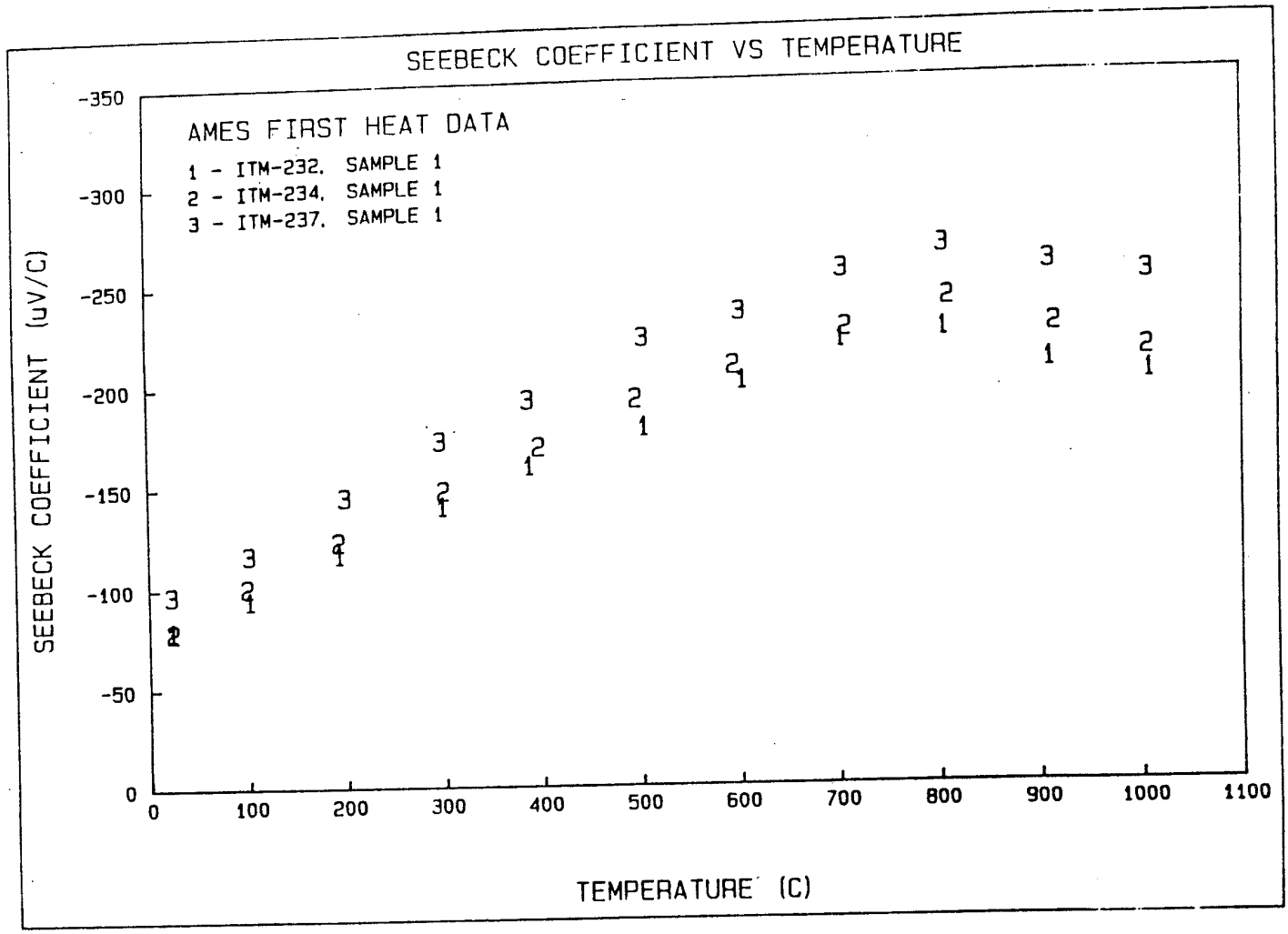

Figure 5-41. Temperature Dependence of the Seebeck Coefficient of ITM Samples 232, 234 and 237 as Measured by Ames Laboratory

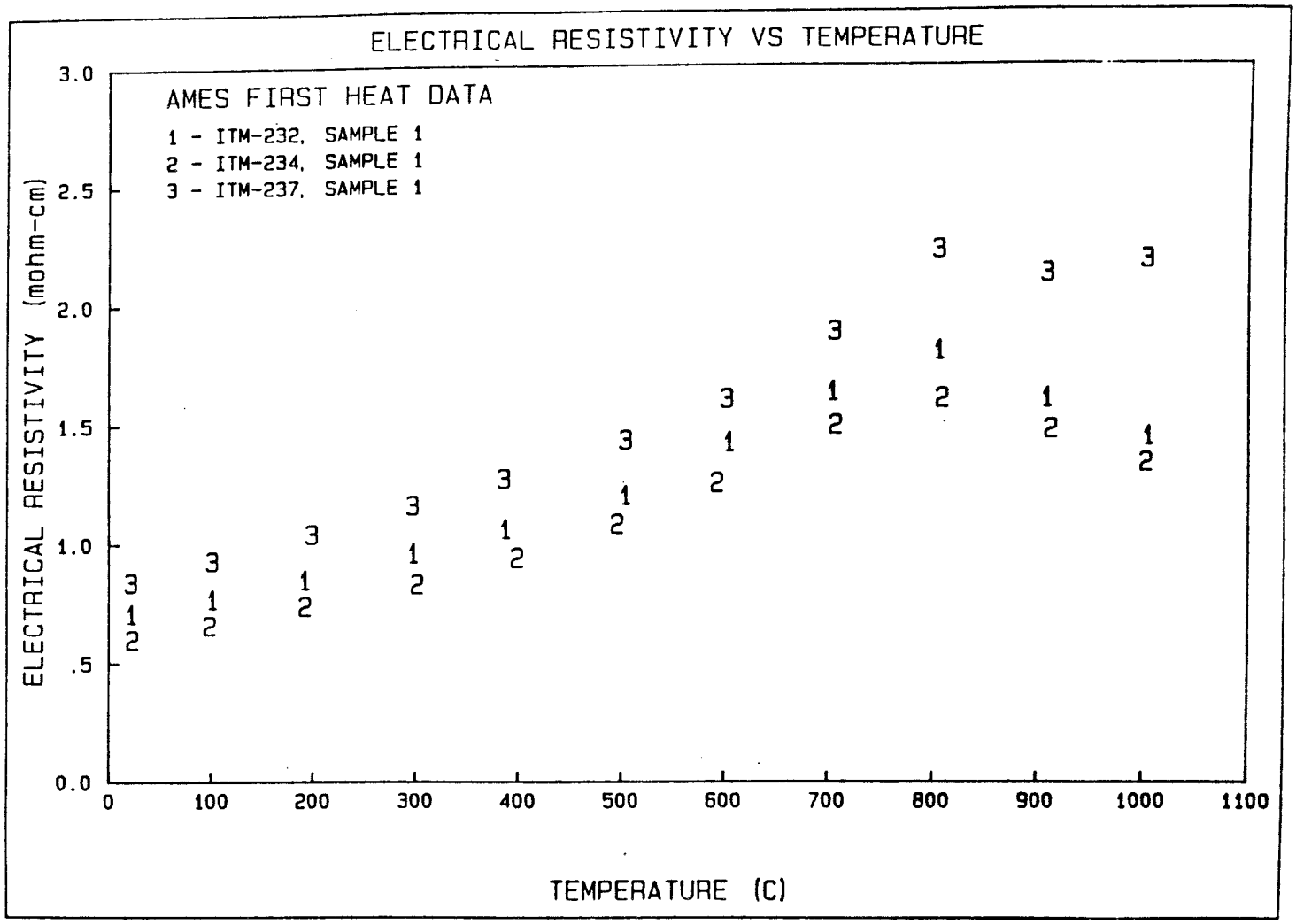

Figure 5-42. Temperature Dependence of the Electrical Resistivity of ITM Samples 232, 234, and 237 as Measured by Ames Laboratory

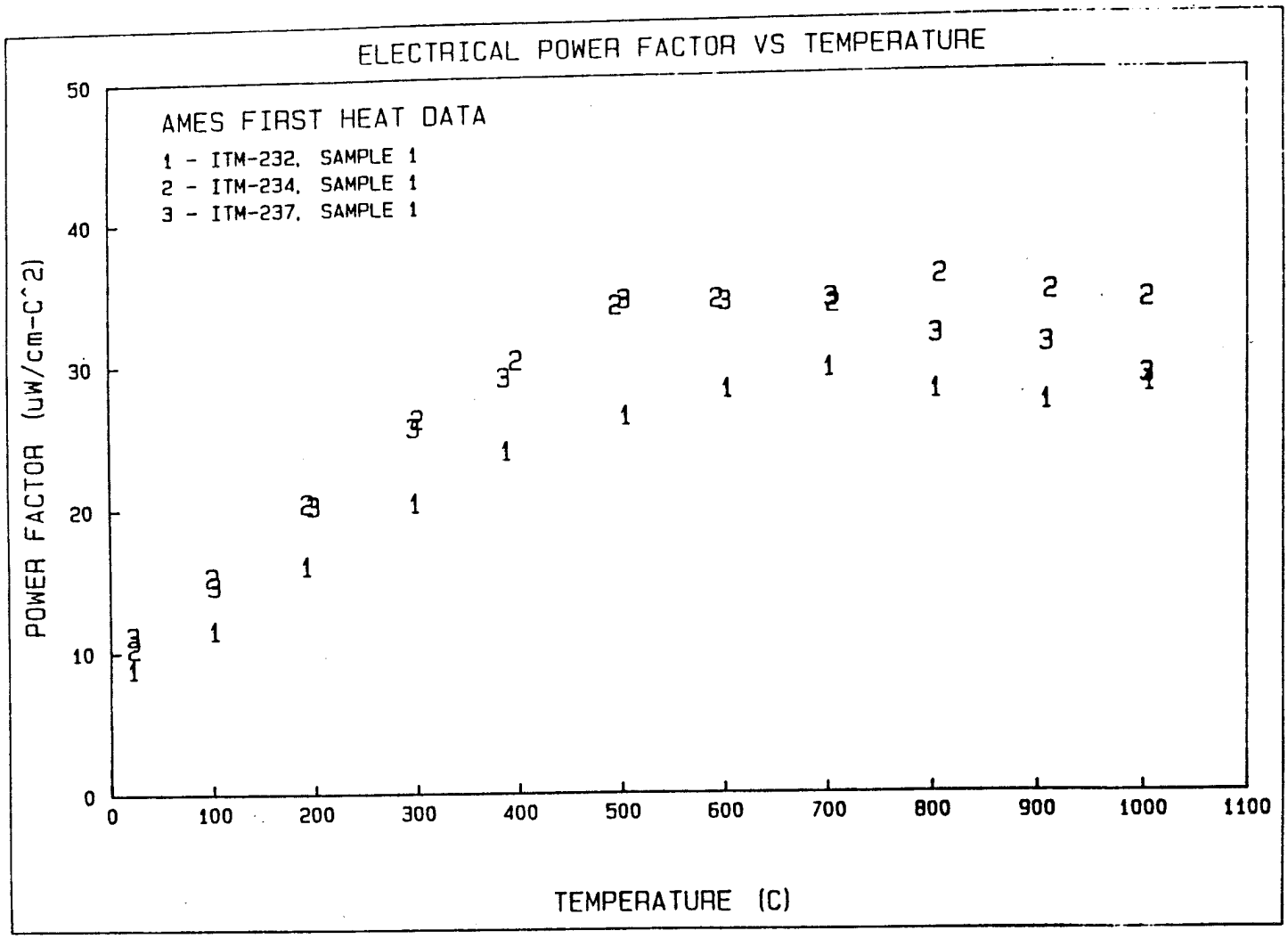

Figure 5-43. Temperature Dependence of the Electrical Power Factor of ITM Samples 232, 234, and 237 as Calculated from Properties Measured by Ames Laboratory

Thermal diffusivity was also measured by Ames Laboratory between 400 and 1000°C on 1/2" diameter disks. A laser flash technique was employed and the data were corrected for heat loss using an algorithm developed jointly by Thermo Electron and JPL. The thermal conductivity was calculated by multiplying the corrected thermal diffusivity, heat capacity (as measured by Ames Laboratory using the drop calorimetry technique on a similar SiGe-GaP sample) and density corrected for thermal expansion. The resultant thermal conductivities are plotted as a function of temperature in Figure 5-44. The curves have a shape that is consistent with theory. The minimum thermal conductivity occurs at 700°C with a value near 32 mW/cm°C for ITM 232 and ITM 234, and 36 mW/cm°C for ITM 237. The lattice component of the thermal conductivity was calculated and is tabulated in Table 5-15. Between 600 and 1000°C they are lower than that of n-type 80/20 Si-Ge. GaP additions reduce the lattice thermal conductivity by enhancing the scattering of phonons by GaP precipitates.

Table 5-15. Calculated Lattice Thermal Conductivities of n-SiGe and n-SiGe-GaP Samples Prepared on this Program

Sample	Temperature °C				
	200	400	600	800	1000
n-SiGe	37.4	30.3	29.5	28.7	32.6
ITM-232	--	32.9	27.0	21.6	22.8
ITM-234	--	32.6	20.7	21.7	21.6
ITM-237	--	37.0	32.0	27.4	29.9

The figure-of-merit curves are shown in Figure 5-45. ITM 234 appears to have very favorable properties. The maximum figure-of-merit is 1.07 x 10^{-3}/°C at 700°C and the average value between 400 and 1000°C is 0.94 x 10^{-3}/°C. For ITM 232 and 237, the maximum Z occurs at 700°C with values of 0.91 and 0.96 x 10^{-3}/°C, respectively.

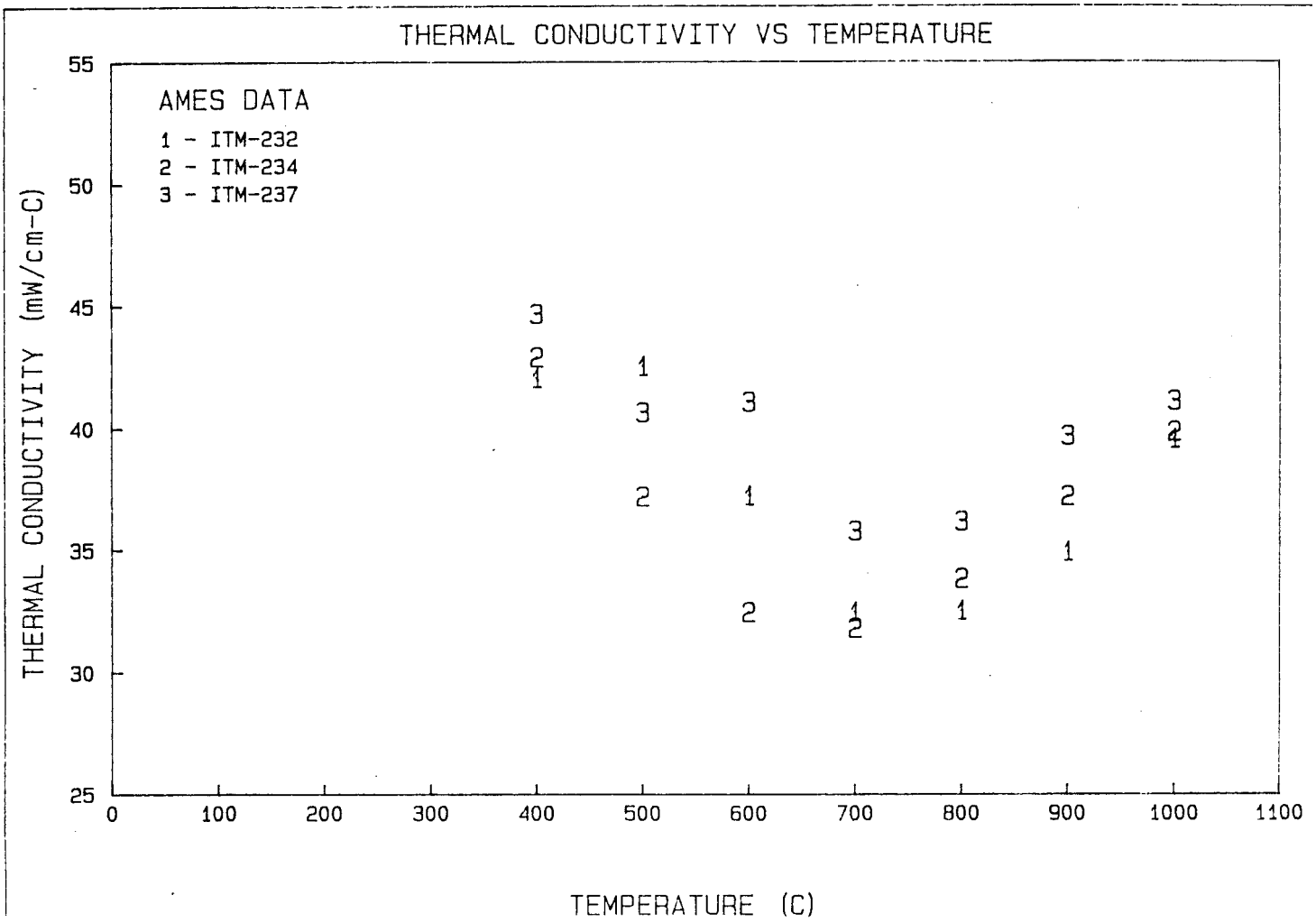

Figure 5-44. Temperature Dependence of the Thermal Conductivity on ITM samples 232, 234, and 237 Calculated from the Thermal Diffusivity Measured by Ames Laboratory

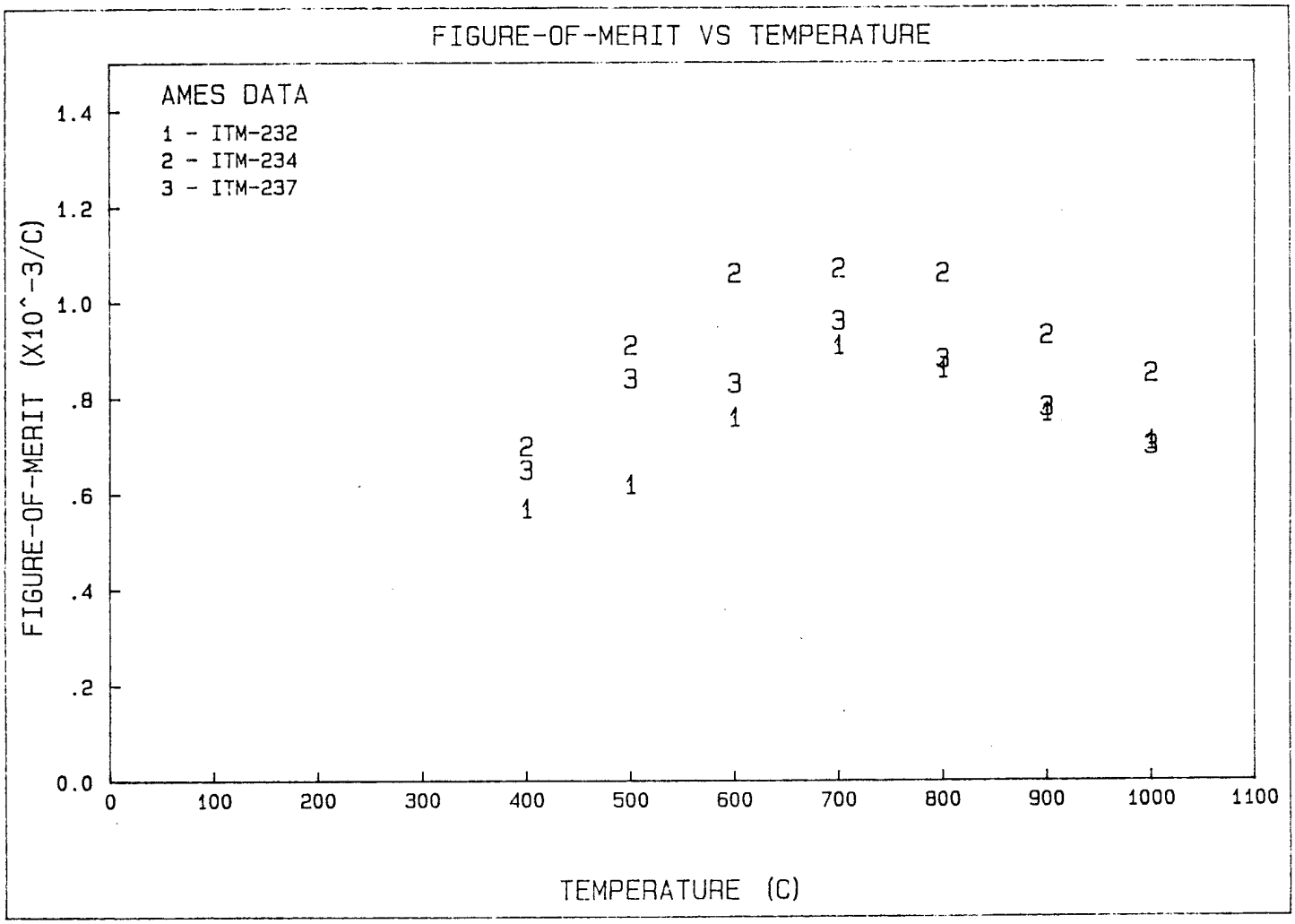

Figure 5-45. Temperature Dependence on the Figure-of-Merit of ITM Samples 232, 234 and 237 Calculated from Properties Measured by Ames Laboratory

Further improvement may be realized by conducting a heat treatment study on these samples since previous results have indicated improvement in Z above 800°C. The power factor was observed to increase such that the temperature dependence curve was flat above 600°C.

5.4 COMPARISON OF VACUUM MELTING/CHILL CASTING/GRINDING/HOT PRESSING WITH THE ELEMENTAL APPROACH FOR ADDING GaP TO 80/20 Si-Ge ALLOYS

5.4.1 ELEMENTAL (OR UNREACTED MIXED POWDER) APPROACH COMPACT FABRICATION

In addition to preparing GaP doped 80/20 Si-Ge alloys by the vacuum melting/chill casting/grinding/hot pressing method, two compacts were fabricated using the elemental method. Two first pressing compacts composed of -325 mesh Si and Ge powders in the proper 80/20 stoichiometry were hot pressed as indicated in Figure 5-46. One compact, ITM 212, was hot pressed from a powder blend containing GaP and first pressing 80/20 Si-Ge. The second compact, ITM 213, was hot pressed from a powder blend containing Ga_2O_3, GaP and first pressing 80/20 Si-Ge. The purpose of the second compact was to determine if figure-of-merit improvements could have been due to the formation of high band-gap Ga_2O_3 during high temperature air heat treatments. The hot pressing cycle used for preparing compacts ITM 212 and 213 is shown in Figure 5-47.

5.4.2 THERMOELECTRIC PROPERTIES

Table 5-16 summarizes the nominal composition and the room temperature thermoelectric properties. The presence of high band-gap Ga_2O_3 increases the Seebeck coefficient but at the same time increases the electrical resistivity significantly. Both of these ITM samples have low carrier concentrations and mobilities, especially ITM-213 which contains Ga_2O_3.

Disk shaped samples were heat treated in air similar to that performed on the GaP doped 80/20 Si-Ge alloys prepared by vacuum melting/chill casting/grinding/ hot pressing. Table 5-17 tabulates the room temperature electrical properties after a series of air heat treatment at 1200°C, 1275°C and 1320°C. This heat treatment schedule was similar to that developed by Thermo Electron which yielded figure-of-merit improvements on two n-SiGe-GaP samples prepared by the elemental method. After each heat treatment, the room

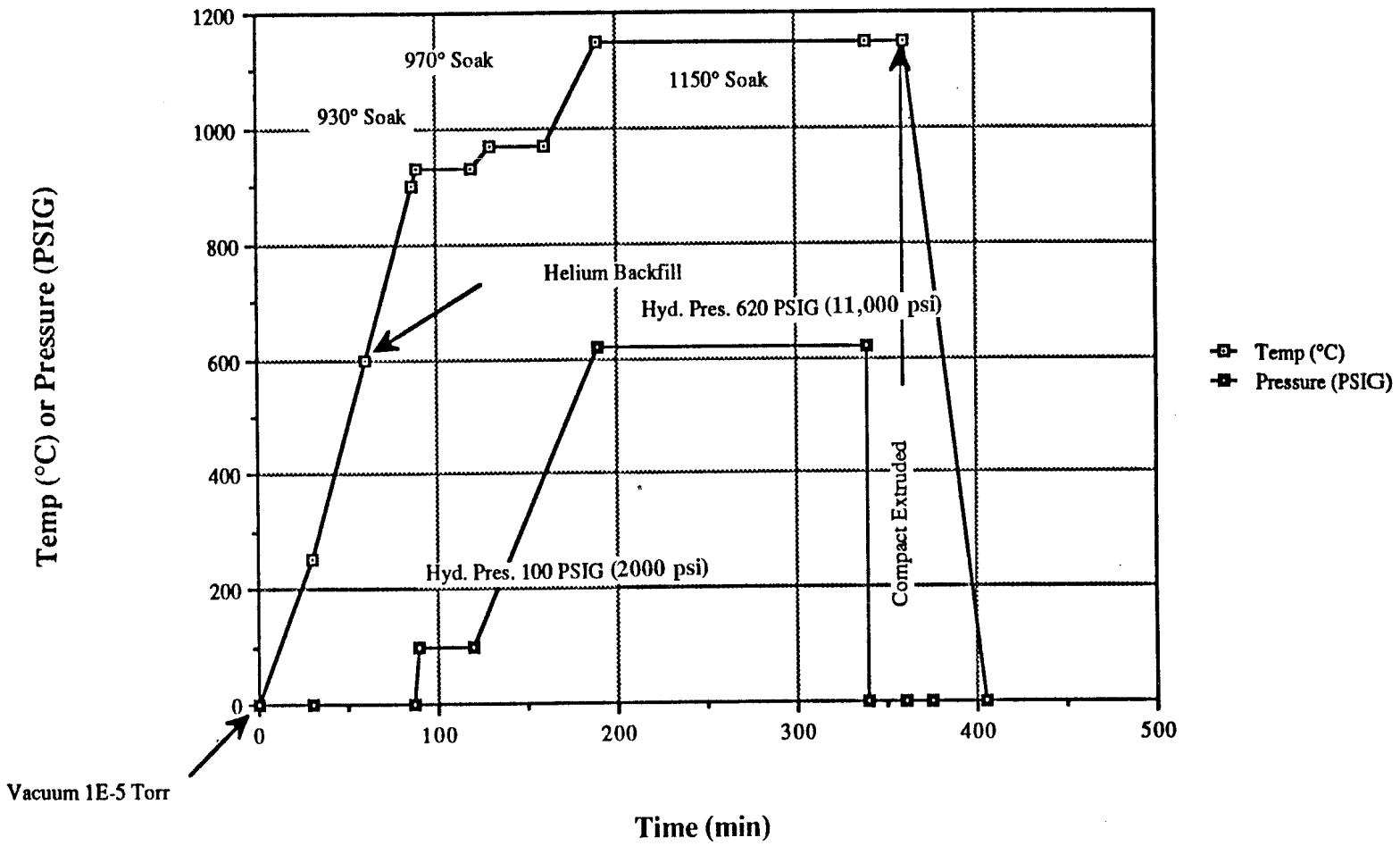

Figure 5-46. Hot Press Cycle for First Pressing 80/20 Si-Ge (ITM 210A and ITM 210B)

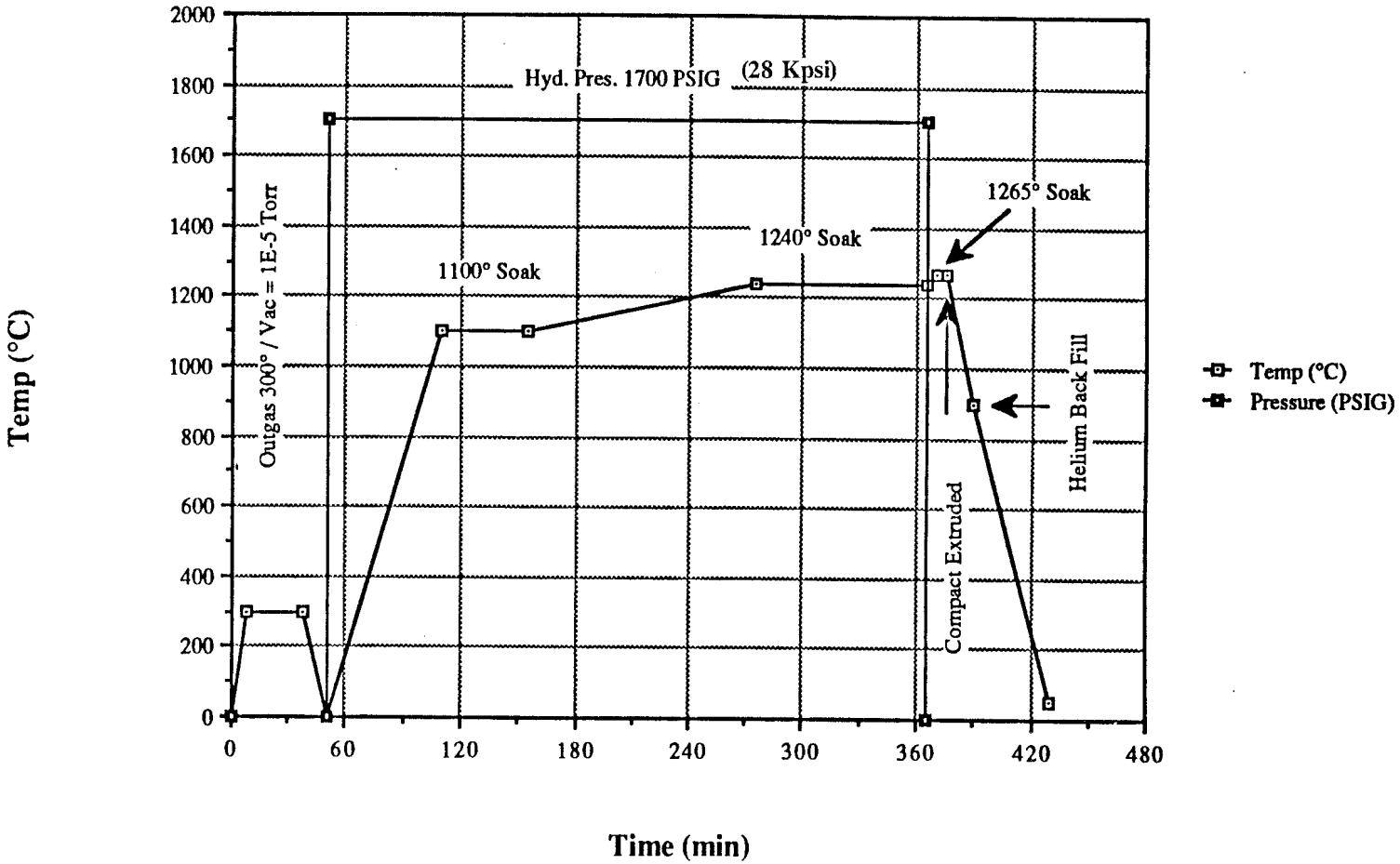

Figure 5-47. Hot Press Cycle for Compacts ITM 212 and ITM 213

Table 5-16. Summary of Room Temperature Results for GaP Doped 80/20 Si-Ge Prepared by the Elemental Method

COMPACT	NOMINAL COMPOSITION	SEEBECK (μV/°C)	Rho(HALL) (mΩcm)	MOBILITY (cm^2/V-s)	CARRIER CONC (1/cc)	DENSITY (g/cc)	THERMAL CONDUCTIVITY AT 100°C (mW/cm°C)
ITM-212	$Si_{0.784}Ge_{0.196}(GaP)_{0.02}$	-130	2.08	25.8	1.16×10^{20}	2.953	46.58
ITM-213	$Si_{0.788}Ge_{0.197}Ga_{0.02}$ $P_{0.001}O_{0.015}$	-170	15.2	9.49	0.44×10^{20}	2.946	51.40

temperature electrical properties improved remarkably. This was probably due to a combination of factors; namely, the carrier concentration increased indicating more dopants were going into solution and the mobility increased indicating that the amount of intergranular resistive barriers were decreasing. The room temperature power factors after heat treatment have increased to a value (approximately 10 $\mu W/cm°C^2$) similar to that for the as-pressed GaP doped 80/20 Si-Ge alloys prepared by the vacuum melting/chill casting/grinding/hot pressing method. These data illustrate that improved properties can be realized by two different methods; i.e., elemental method coupled with elaborate high temperature air heat treatment and diluting GaP doped 50/50 Si-Ge alloys prepared by the chill casting method. The advantage of the latter method is that the chemistry is more controllable and, hence, the process can be easily reproduced.

5.5 SUMMARY OF RESULTS

The maximum solubility of GaP in 80/20 Si-Ge is estimated to be about 1 to 2 Mol percent as determined from x-ray diffraction analysis. The compacts prepared in this study which involved double hot pressing produced the most homogeneous materials seen heretofore as determined by x-ray diffraction and SEM/EDS examinations.

The high temperature Seebeck coefficients as measured by GE on bar samples were independent of porosity and GaP content, which ranged from 0.4 to 3.5 Mol percent. The electrical resistivities were highest for ITM 196 due to the

Table 5-17. Room Temperature Seebeck Coefficient and Hall Effect Measurements After a Sequence of Thermal Treatments of GaP Doped 80/20 Si-Ge Alloys

GE-ASD DATA	AS-RECEIVED				AIR 1200°C/98 HRS.				AIR 1275°C/25 HRS.				AIR 1320°C/25 HRS.			
ROOM TEMPERATURE	S	ρ_H	n	μ	S	ρ_H	n	μ	S	ρ_H	n	μ	S	ρ_H	n	μ
SAMPLE ID	μV/°C	mΩcm	$X10^{20}$ cm^{-3}	cm^2/V-s	μV/°C	mΩcm	$X10^{20}$ cm^{-3}	cm^2/V-s	μV/°C	mΩcm	$X10^{20}$ cm^{-3}	cm^2/V-s	μV/°C	mΩcm	$X10^{20}$ cm^{-3}	cm^2/V-s
1. ITM-212 $(GaP)_{0.02}$	-130	(8.12) 2.08	1.16	25.8	-100	(11.63) 0.86	1.39	52.2	-92	(12.82) 0.66	1.77	53.4	—	0.87	1.29	55.4
2. ITM-213 $Ga_{0.02}P_{0.01}O_{0.015}$	-170	(1.90) 15.2	0.44	9.49	-130	(5.73) 2.95	0.65	32.5	-118	(9.28) 1.50	0.99	42.1	—	0.87	1.24	57.9

NUMBERS IN PARENTHESES ARE S^2/ρ values

FOR OXIDIZED SAMPLES, PROPERTY MEASUREMENTS WERE TAKEN AFTER THE OXIDE LAYER WAS REMOVED BY GRINDING ON 600 GRIT SiC PAPER WITH DISTILLED WATER

presence of porosity and lowest for ITM 197. The thermal conductivity was observed to decrease with increasing GaP content. The combination of these properties for each sample resulted in figures-of-merit ranging from 0.8 x 10^{-3}/°C (ITM 199, ITM 198, ITM 196) to 0.9 x 10^{-3}/°C (ITM 197) averaged between 300 and 1000°C.

ITM 197 was seen to possess the most desirable thermoelectric properties and a further 20-25% improvement in room temperature properties was achieved by thermal processing in air. The addition of phosphorous to 2 Mol percent GaP in 80/20 Si-Ge (ITM-234) produced further improvement in Z due to higher carrier concentrations and mobilities. It is recommended that additional work be directed towards reproducing these results.

The results show that the methods used here have a high degree of reproducibility for uniform, improved property compact fabrication. Compact ITM-234 is believed to have the highest level of thermoelectric figure-of-merit properties of the candidate alloys as noted above. Appendix D provides a detailed summary of the fabrication procedures used for this compact.

5.6 REFERENCES

(1) R.K. Pisharody and L.P. Garvey, in Proceedings of 13th Intersociety Energy Conversion Engineer Conference, (Society of Automotive Engineers, 1978) p. 1963.

(2) A.F. Ioffe, S.V. Airapetiants, A.V. Ioffe, N.V. Kolomoets and L.S. Stilbans, Dokl. Akad. Nauk. SSSR 106, 198 (1956).

(3) J.P. Dismukes, L. Ekstrom and R.J. Paff, RCA Technical Report, PTR-1533, p. 13, Dec. 1963.

SECTION 6
MATERIALS ANALYSIS AND CHARACTERIZATION USING ADVANCED TECHNIQUES

6.1 BACKGROUND

In this Program, careful attention was paid to analysis and characterization of the materials prepared. This was done to ensure reproducibility and to establish a reliable basis for interpretation of results. Specifically, samples of the materials were examined by conventional techniques such as light and scanning electron microscopy and X-ray diffraction to evaluate grain size and chemical and structural homogeneity. For a better understanding, some advanced techniques were used to evaluate crystal structure, GaP concentration and distribution, effects of contamination such as oxygen, and evidence for microprecipitation. These techniques included extended x-ray absorption fine structure (EXAFS), transmission electron microscopy (TEM), nuclear magnetic resonance (NMR) and Raman scattering. A description of each technique as well as some of the significant observations are summarized below.

6.2 EXAFS

GE-CR&D has successfully applied the EXAFS technique to characterize the local atomic environment of Ga in both p-type and n-type Si-Ge alloys initially doped with GaP by a hot pressing and sintering process. This technique[1] is element selective since each chemical element has its own characteristic X-ray absorption energy. The fine structure on the high energy side of the absorption edge arises from backscattering of the photo-ejected core electron from a central atom by its atomic neighbors to yield an interference pattern (the EXAFS) which contains information about bond distance, coordination and chemical nature of the neighbors. Using intense synchrotron X-radiation as a light source with intensity 4 to 5 orders of magnitude higher than a conventional X-ray tube, the technique is capable of structure determination of dilute species using a fluorescence mode of detection[2].

The room temperature EXAFS spectra of three specimens were measured at Stanford Synchrotron Radiation Laboratory (SSRL). These were:

1. Pure GaP used as a standard to model the Ga environment in the Si-Ge alloys,

2. MHPG-006P: p-type B, GaP-doped Si-Ge alloy having the following composition (atomic %) - Si=71, Ge=18, Ga=1, P=1.6 and B=8.4,

3. MHPG-008N: n-type GaP-doped Si-Ge alloy with Si=76.4, Ge=19.1, Ga=1.96 and P=2.53.

The room temperature experimental scans of Ga K-edge EXAFS for the three specimens are shown in Figure 6-1. These are plotted as absorption intensity versus energy with respect to the Ga K-edge energy (at 10367 eV) taken as zero. The sharp rise corresponds to the K-edge discontinuity. The EXAFS is on the high energy side of the absorption edge and extends from about 40 eV to a few hundred eVs. The spectrum for the n-type material shown in Figure 6-1(b) is quite similar to that of pure GaP shown in Figure 6-1(a), but that of the p-type materials shown in Figure 6-1(c) is quite different.

The absorption intensities were normalized, Fourier transformed and back transformed to reciprocal space to yield X^F vs. k plots. Computer simulation was performed using the single scattering approximation[2] to quantify the structural differences of the Ga environment in the two SiGe-GaP alloys.

Figure 6-2(a) shows comparison of the simulated (points) first shell EXAFS in pure GaP with the experimental data (line). The simulation was made using the known Ga-P separation of 2.36 angstroms and a coordination of 4 together with parametric phase functions[3]. Similar simulations were performed for the Ga sites in both n-type (Figure 6-2(b)) and p-type (Figure 6-2(c)) materials. The results, tabulated in Table 6-1, show that in the n-type material, Ga is coordinated by four P atoms at a distance of 2.36 angstroms identical to the case in pure GaP. A measure of structural disorder about the Ga-P coordination sphere with respect to that in pure GaP is also tabulated.

In the p-type material, simulations of the Ga environment with a single P, or Si or Ge neighbor type did not produce a convergent solution and fit with experimental data. Reasonable fits with physically meaningful parameters were obtained when a mixed coordination of Si and Ge was used. Again, the Ga is

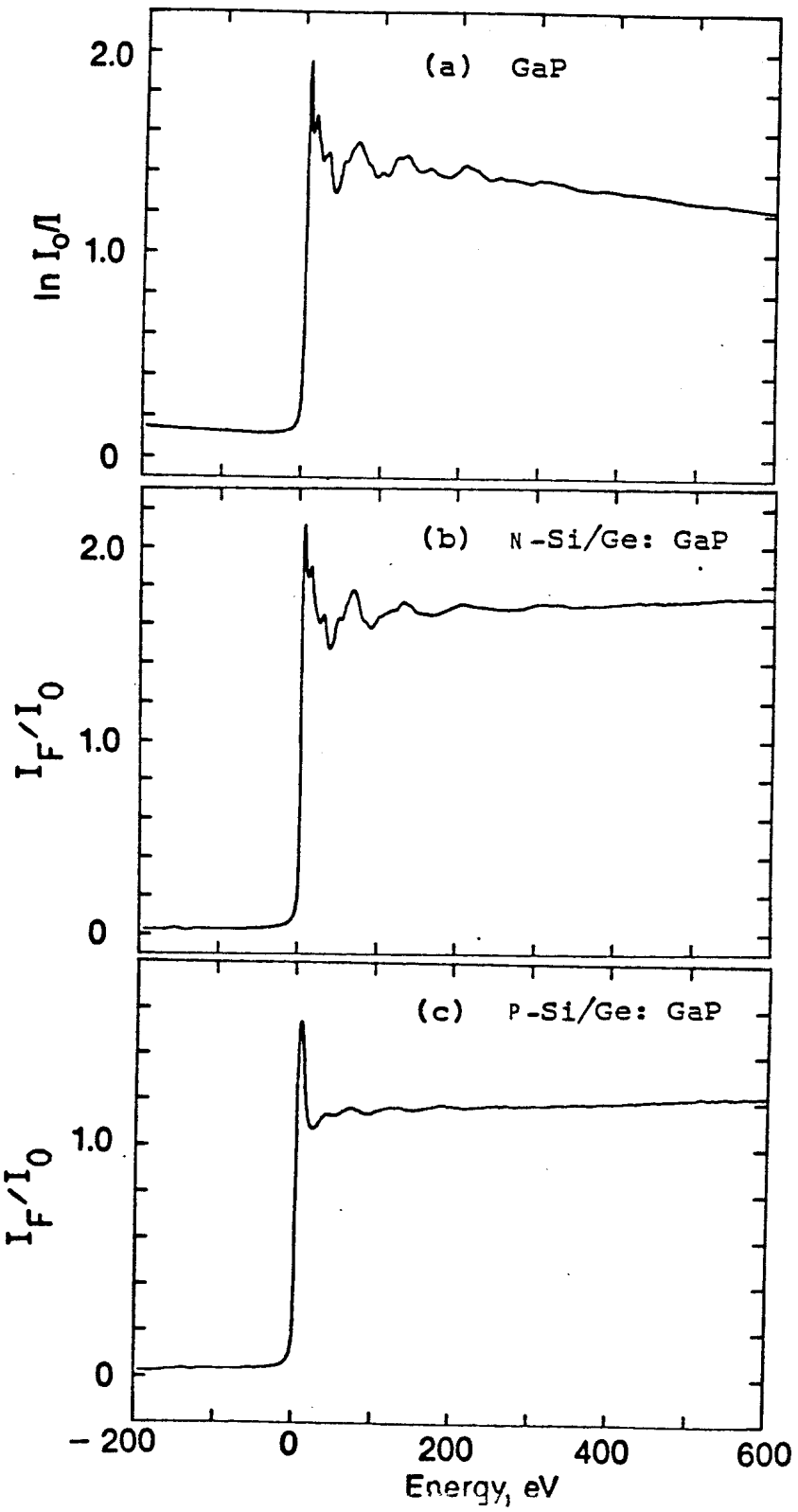

Figure 6-1. Room Temperature Experimental Scans of Ga K-edge EXAFS in (a) GaP, (b) n-type GaP-doped Si-Ge Alloy and (c) p-type B, GaP-doped Si-Ge Alloy. The Energy Scale is with Respect to the Ga K-edge Energy (10367 eV) Taken as Zero.

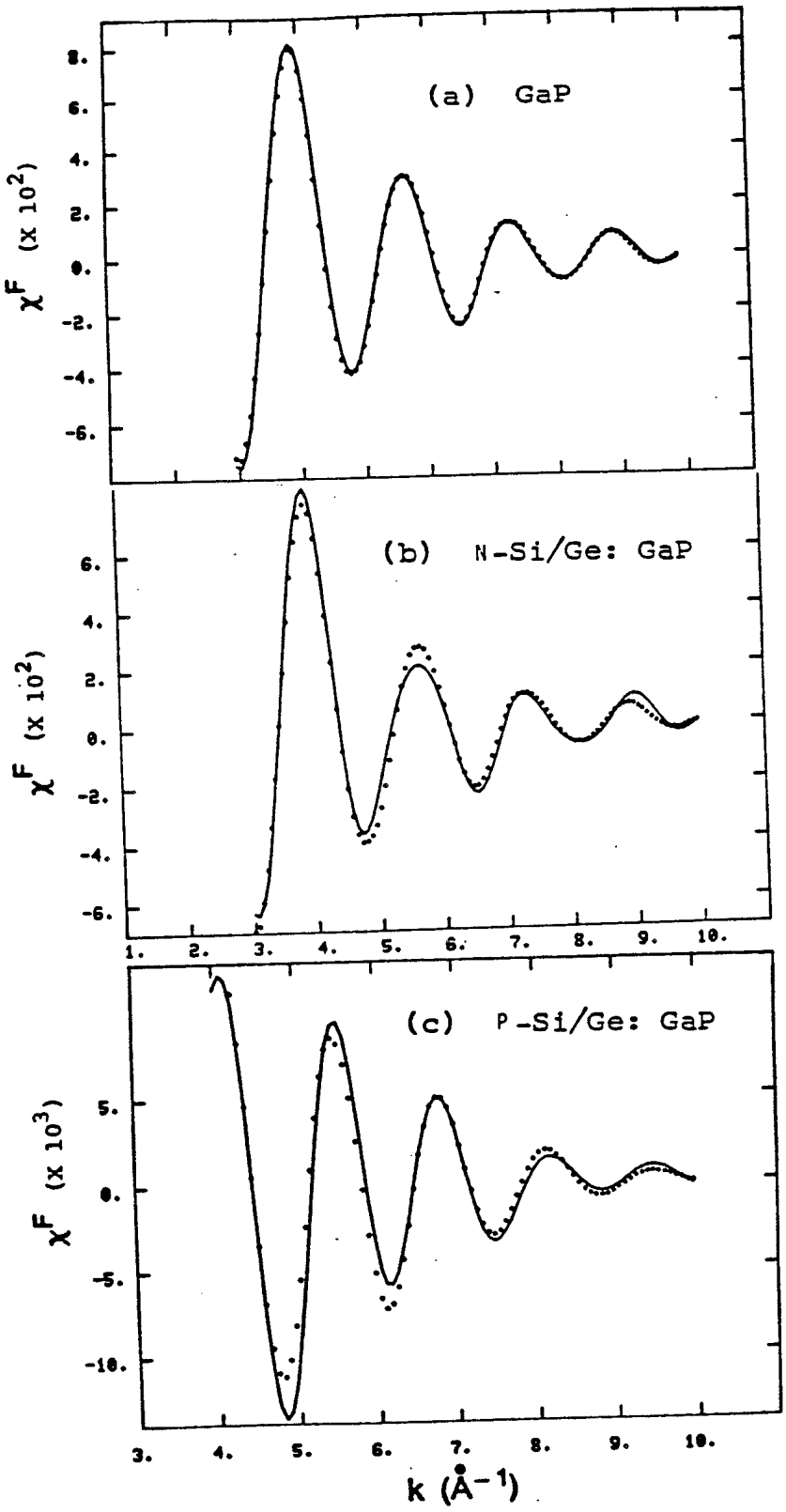

Figure 6-2. Experimental (Line) and Simulated (Points) EXAFS from the First Coordination Sphere in (a) GaP, (b) n-type Material, and (c) p-type Material.

Table 6-1. Coordination Number, N, Bond Distance, r, and Type of Nearest Neighbors about Ga in Si-Ge Alloys Initially Doped with GaP

Sample	Neighbor	N	r(Å)	Std. Dev.
MHPG-006P	Si	3.2	2.37	
	Ge	0.8	2.65	7.5%
MHPG-008N	P	4	2.36	4.4%

4-fold coordinated. The best fit yields a mixed coordination of Si and Ge in a ratio of 4 to 1 which is that of the bulk Si-Ge matrix composition. As shown in Table 6-1, the values for both the Ga-Si and Ga-Ge distances are large, indicative of structural and thermal disorder in the material.

The structural data about the Ga sites in the Si-Ge alloys were also compared with the absorption features within about 40 eV about the X-ray absorption edge. This region of the spectrum is called XANES (X-ray absorption near-edge structure) and is non-EXAFS in origin, but is associated with transitions of the core electron (the K electron in our case) to various final, allowed states before the continuum. Hence, the XANES spectra give electronic information and reflect the chemical bonding about the central X-ray absorbing atom with its neighbors[4]. As seen in Figure 6-3, the XANES spectrum of Ga in the n-type material is identical to that of pure GaP and consists of a number of well-defined absorption features at 7.2, 16 and 32 eV, reflective of the P coordination about the central Ga atom. The XANES spectrum of the p-type material (Figure 6-3(c)) is quite different and consists basically of a broad line at 7.9 eV. These observations in turn support the EXAFS findings that the Ga environment in the p-type material is quite different from that of the n-type material.

In summary, the EXAFS and XANES results indicate that at least Ga from the GaP added to the Si-Ge powder blend prior to the second hot pressing remain in discrete GaP particles or at least in local 5-atom clusters of GaP_4 in the n-type alloy and is in random solid solution in the p-type alloy.

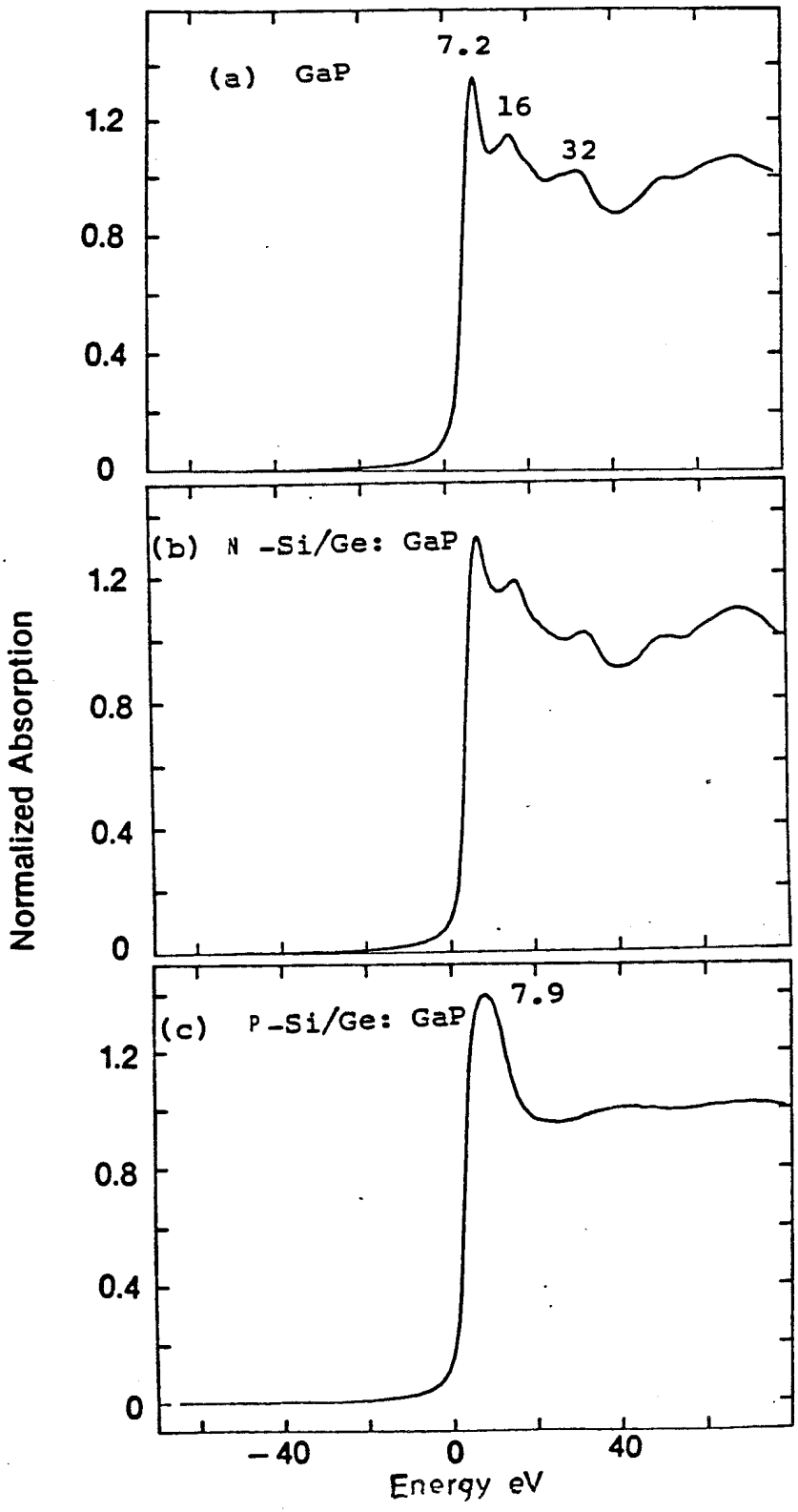

Figure 6-3. Ga K-edge XANES Spectra in (a) GaP, (b) n-type Material and (c) p-type Material

6.3 TEM

Transmission electron microscopy investigations on Si-Ge and SiGe-GaP alloys were performed at GE-CR&D and the Department of Materials Science and Electrical Engineering at the University of Virginia. From these microstructure studies the distribution of grains, GaP and oxygen was assessed and some insight into the compositional homogeneity, secondary phase or precipitate distribution and dislocation density was provided.

Three classes of SiGe-GaP alloys were examined (Table 6-2). One class (Method I) was as- hot pressed alloys prepared by first alloying the Si, Ge and P or B dopants in the liquid state. The alloy was chill cast and then comminuted into a powder. The powder was hot pressed to form a compact which was then recomminuted into powder. The Si-Ge powder (P or B doped) was then blended with GaP powder and hot pressed to form the final compact. Hot pressing was nominally performed for 30 minutes at 1240°C using 180 KPa pressure. This procedure was used for compacts ITM-62, MHPG-006P, MHPG-007N and MHPG-008N.

The second class (Method II) of alloys was also as-pressed, however the GaP was added to a melt containing a higher Ge content. The silicon content was brought up to the more typical 80 atomic percent level by adding phosphorous doped Si powder prior to the second hot pressing. This procedure was used for compacts ITM-232 and ITM-234.

The third class (Method III) of alloys* was prepared by Thermo Electron using the elemental approach in which silicon and germanium powders were first hot pressed then comminuted into a powder. This powder was then blended with GaP powder and hot pressed into the final compact. This compact was subsequently heat treated in air at temperatures above 1100°C. This procedure was used for samples T111 and T118 which showed a 15-30% improvement in the figure-of-merit over the values for more conventionally processed Si-Ge alloys.

* Provided by Dr. J. Vandersande of NASA-Jet Propulsion Laboratory, Pasadena, CA

Table 6-2. Silicon Germanium Alloys Examined by Transmission Electron Microscopy at GE-CR&D and University of Virginia

Specimen Number	Nominal Composition Atomic %					Preparation Method
	Si	Ge	Ga	P	B	
ITM-62	79.8	20.0	-	-	0.2	I
MHPG-006P	71.7	17.9	0.99	0.99	8.4	I
MHPG-007N	76.4	19.1	1.96	2.53	--	I
MHPG-008N	76.4	19.1	1.96	2.53	--	I
ITM-232	76.0	19.0	1.6	3.4	--	II
ITM-234	74.7	18.7	1.6	5.0	--	II
T111	76.9	19.2	1.92	1.92	--	III
T118	76.9	19.2	1.92	1.92	--	III

I. Chill cast (Si, Ge, B or P), pulverize, hot press, pulverize, blend with GaP, hot press.

II. Chill cast (Si-Ge, GaP), pulverize, hot press, pulverize, blend with P-doped Si, hot press.

III. Hot press (Si, Ge), pulverize, blend with GaP, hot press, heat treat in air.

The size of the grains in the compact was measured from micrographs obtained by optical metallography (OM) and TEM. The measurements by both techniques agreed within a factor of about 3 in the same grain size range. It was possible to measure grains as small as one micrometer from optical micrographs taken at about 1000 times magnification. The smaller grain sizes were reliably measured from TEM micrographs taken at about 20,000 times magnification.

The specimens prepared by Method I exhibited a grain size distribution that can be characterized as mottled or bimodal. There is a population of small grains and one of large grains. The small grain population has a very high areal number density as compared to the large grains. In order to fully represent these population groups, a histogram of the areal number density of

grains was plotted against the size range of the grains. One of the largest changes in population density occurred in a GaP containing specimen, MHPG-007N, whose data are shown in Figure 6-4.

There is a sharp fall in the number density of grains just beyond the small size ranges. This rise is so steep that the scale is broken to represent both data for the coarse grains as well as the fine grains. The existence of two distinct grain size groups is clearly seen in Figure 6-4 for specimen MHPG-007N. A gap in the grain size is present between 0.6 μm and 1.5 μm.

The corresponding grain distribution for MHPG-007N is shown in a high magnification (x 60,000) TEM micrograph (Figure 6-5). It can be seen that the fine grains occur at the grain boundaries of the large grains. This observation suggests that the electrical and thermal properties can be tailored by controlling the uniformity of the grain size distributions.

Dislocations within grains were also observed by TEM for samples with and without GaP prepared by Methods I and II (chill cast/pulverized/hot pressed).

In addition to dislocations, the TEM micrographs of the GaP containing alloys showed spherical or globular precipitates within the grains and in some grain boundaries. A typical micrograph is shown in Figure 6-6 which is a 20,000X magnification of ITM-232.

The chemical composition of individual precipitates and grains could be determined by performing X-ray spectroscopy in the TEM microscope. The precipitates identified in the SiGe-GaP alloys were:

- GaP associated with a 2:1 Si-Ge matrix
- P associated with Si enrichment
- Ga associated with Ge enrichment
- SiO_x

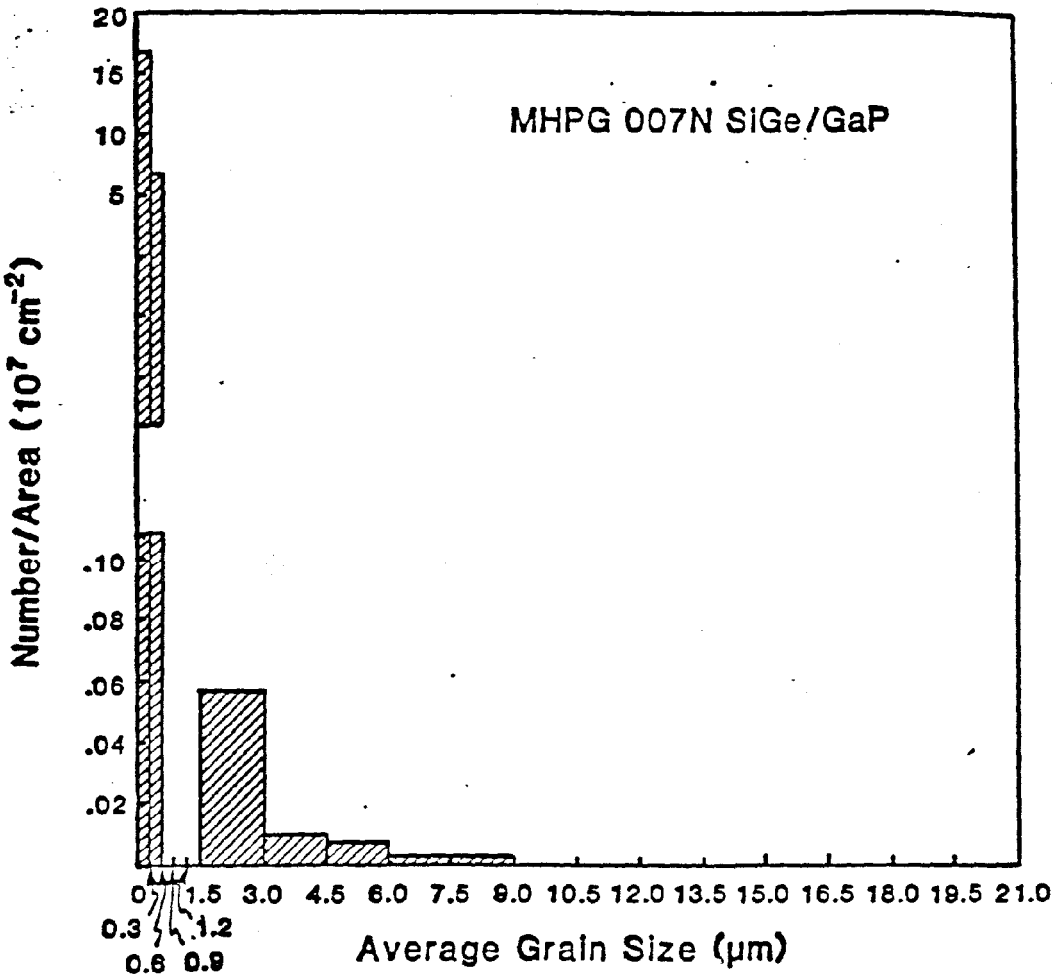

Figure 6-4. Number of Grains per Area Versus Average Grain Size in n-SiGe-GaP (MHPG 007N).

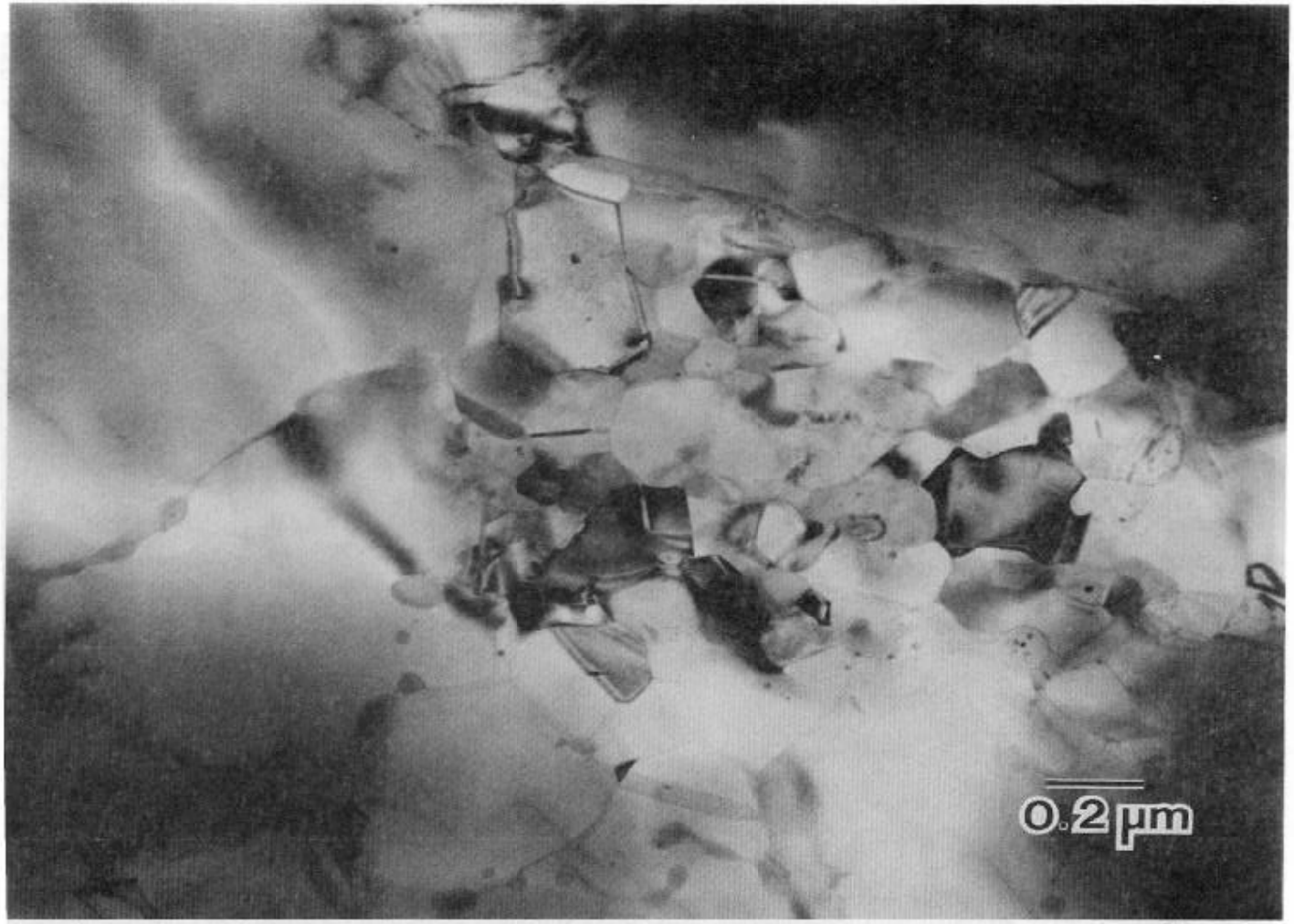

Figure 6-5. TEM Micrograph (X 60K) of Sample MHPG-007N Showing 50-200 nm Grains. Note the Fine Grains at Grain Boundaries of Large Grains.

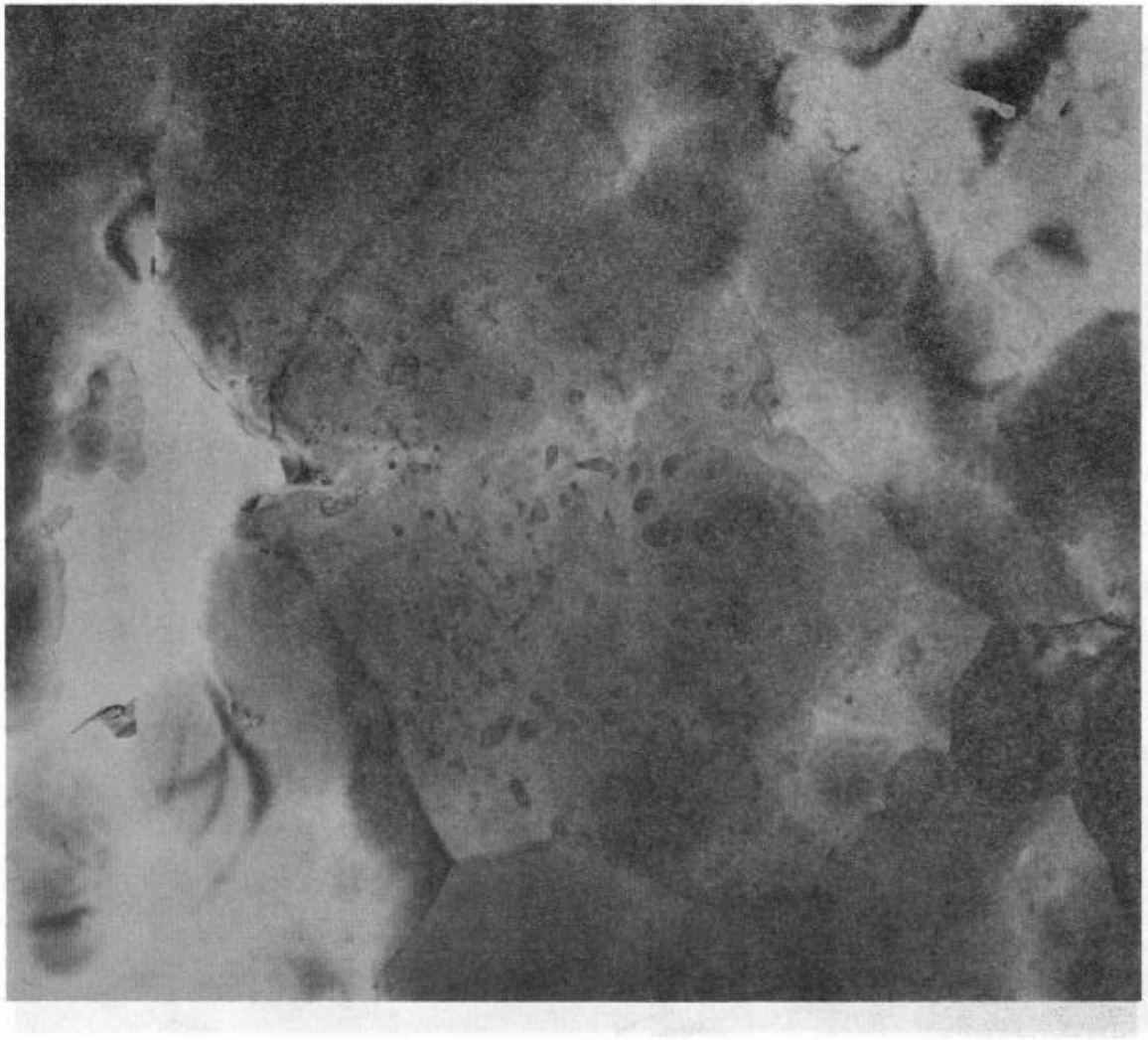

Figure 6-6. TEM Micrograph of Sample ITM-232 Showing Spherical Precipitates within Grains and on Grain Boundaries (20KX Magnification)

The GaP precipitate identified with a 2:1 Si-Ge matrix may be indicative of silicon depletion surrounding the precipitate or alternatively a GaP precipitate in a Ge rich region. The most frequent precipitates were identified as SiO_x and the remaining three types were rarely found.

A typical micrograph containing three chemically different precipitates is shown in Figure 6-7. Area 37 contains high Si and P and essentially no Ga. Area 39 corresponds to an SiO_2 particle and area 40 contains high Ga and P in a Si-Ge matrix.

The Ga and P distributions were also examined in the as-pressed specimens and they were found to be randomly distributed in the Si-Ge matrix. The concentration of Ga and P varied throughout the matrix from essentially non-detectable levels to levels sufficient to dominate the X-ray signal from the Si-Ge matrix. Additionally, the ratio of the Ga to P also varied from region to region.

Professors W.A. Jesser, F.D. Rosi and J.C. Liu of the Departments of Materials Science and Electrical Engineering of the University of Virginia conducted a SEM and TEM study of the high power factor (45 $\mu W/cm°C^2$) annealed/oxidized samples T111 and T118 developed by Thermo Electron and NASA-JPL. These samples were supplied by Dr. J. Vandersande of NASA-JPL and were to be used to help assess the effects of annealing/oxidation treatments on Si-Ge alloy microstructures in comparison with that for similar materials processed by more conventional casting/grinding/hot pressing and sintering techniques.

The observed improvements in thermoelectric behavior of n-type SiGe-GaP after undergoing high temperature oxidation thermal treatments are illustrated in Figure 6-8[5]. The observed changes represent improvements of about 15 to 30 percent over the values for more conventionally processed Si-Ge alloys.

When the results of T111 and T118 are compared to the as-pressed SiGe-GaP alloys prepared by casting/grinding/hot pressing, the following observations can be made:

Figure 6-7. TEM Micrograph of Sample ITM-232 Containing Precipitates on Grain Boundaries (20KX Magnification)

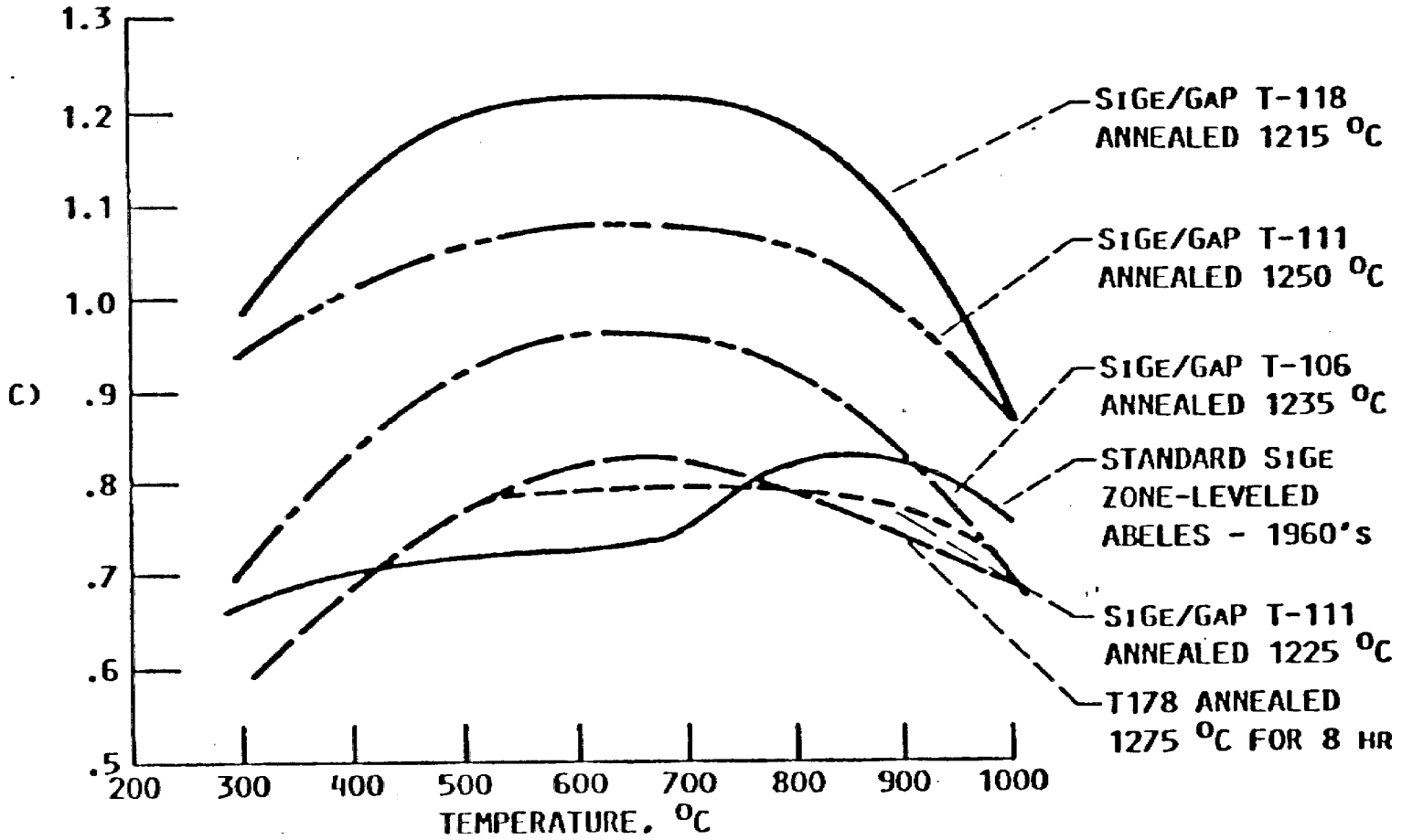

Figure 6-8. Figure-of-Merit, Z, of Annealed n-type SiGe-GaP as a Function of Temperature (Taken from Reference 5)

- Level of porosity is significantly higher and varies across the thickness of the specimen.
- Grain size is rather uniform and equiaxed, 10 μm in diameter.
- Fewer precipitates.
- Small dislocation loops (approximately 200 angstroms in size) were observed to form after 20 minutes of electron bombardment in the (110) or (100) direction, and their number density increased significantly with increasing time.

TEM has been shown to be a valuable tool in characterizing microstructure features in Si-Ge alloys. The differences in the distribution of grains and precipitate phases as well as compositional homogeneity were clearly illustrated. These microstructural features can influence the thermoelectric properties and careful correlation studies will be helpful in guiding the process to reproducibly fabricate high Z materials.

6.4 NMR AND RAMAN SPECTROSCOPY

NMR (Nuclear Magnetic Resonance) and Raman scattering techniques were recently identified as possible tools for determining the extent of homogeneity in Si-Ge alloys. NMR probes the local atomic environment of Si or Ge in much the same way as EXAFS does, however, on a much larger volume of sample (approximately 1 gram).

The ^{29}Si isotope is the only silicon atom with a nuclear magnetic moment. It is possible to observe the nucleus with nuclear magnetic resonance (NMR) techniques using magic-angle sample spinning[6]. The exact resonance frequency is sensitive to the local environment of the ^{29}Si atom. Thus it is possible to see small changes in the local environment. Si-Ge alloys have been examined in order to determine the number of Ge atoms around a ^{29}Si nucleus. Other Si compounds such as pure Si, SiP, α-Si_3N_4, ß-SiC, and α-SiO_2 have also been studied for comparison.

The measurements were made at the "Regional NMR Center" at Colorado State University under the direction of Dr. Charles Bronnimann and at GE-CR&D by Dr. E. Williams. The measurements were made on powdered samples at a frequency of 39.8×10^6 Hz (Colorado) or 59.6×10^6 Hz (GE) at room

temperature. The data are recorded as frequency shifts in parts per million from the resonance frequency of ^{29}Si in tetramethyl silane:$Si(CH_3)_4$. Table 6-3 gives a summary of the results. The results for Si are for ^{29}Si in pure, high resistivity undoped Si powder. The results for Ge are for dilute ^{29}Si in a pure, undoped Ge matrix.

Table 6-3. Measured ^{29}Si Resonance Frequency Shifts in PPM for Various Crystals

Compound	Shift
α-SiO_2	-108.3
α-Si_3N_4	-45.3
SiP*	-22.8±8
β-SiC	-13.3
Si	-79.5
Ge	-23.0

* In this crystal there are 6 different Si sites, so the peak is rather broad.

From Table 6-3 a ^{29}Si atom in a pure Si crystal has a shift of -79.5 ppm while in a Ge crystal with all Ge neighbors has a shift of -23.0 ppm. In Si-Ge mixed crystals it is expected that the shift will depend on the number of Ge nearest neighbors. If the shift is linear in the number of Ge neighbors, n, then it is expected that

$$\text{shift} = -79.5 + \frac{n}{4}(79.5 - 23.0)\ \text{ppm},\ 0 \leq n \leq 4 \qquad (1)$$

This means that the shifts would occur at discrete intervals of 14.13 ppm between -79.5 ppm and -23.0 ppm. Table 6-4 shows the resonance peaks observed in a number of chill-cast Si-Ge alloys, and an indication of their relative strengths (S = strong, M = medium, W = weak). The peak height for the particular resonance is proportional to the number of Si atoms in the sample with the particular number of Ge neighbors. Note that the observed peak positions in Table 6-4 are in good agreement with Equation (1). Figure 6-9 shows the measured spectrum of an as-cast sample of a 50 atom% Si + 50 atom% Ge alloy. If the specimen was homogeneous, the highest peak would be at

Table 6-4. Observed Frequency Shifts in PPM from TMS for NMR Peaks Seen in a Number of As-Cast Si-Ge Alloys

No. Ge Nearest → Neighbors	4	3	2	1	0
Nominal Shift →	-23.0	-37.1	-51.2	-65.4	-79.5
Melt Composition ↓ Atom % Si	Observed Shifts				
100	---	---	---	---	-79.5 S
80	-27±8 W	-40±2 W	-57 W	-68 M	-79.7 S
50	---	-39±1 W	-52.0 M	-63.7 S	-73 M
35	-24.9 S	---	-50.7 S	-64±3 M	---
20	-22.8 S	-40 W	-55 W	---	---
5	-23.1 S	-39 M	-55 W	---	---

S = strong, M = medium, W = weak

-51.2 ppm where a ^{29}Si atom has 2Si and 2Ge neighbors. The peak distribution on either side of this should be symmetrical. Clearly this is not the case. The highest peak occurs for Si atoms with 3Si + 1 Ge neighbors at -63.7 ppm. Thus the as-cast sample appears to contain more silicon than the liquid phase did originally.

The Si-Ge phase diagram has been studied by Stohr and Klemm[7], who showed a large separation between the liquidus and solidus lines. According to their results the first solid to freeze out of a 50/50 liquid mixture will have a composition of 80 atom% Si + 20 atom% Ge. We can use the NMR observations in Table 6-5 to estimate the relative numbers, N, of Si and Ge atoms in the as-cast material as follows:

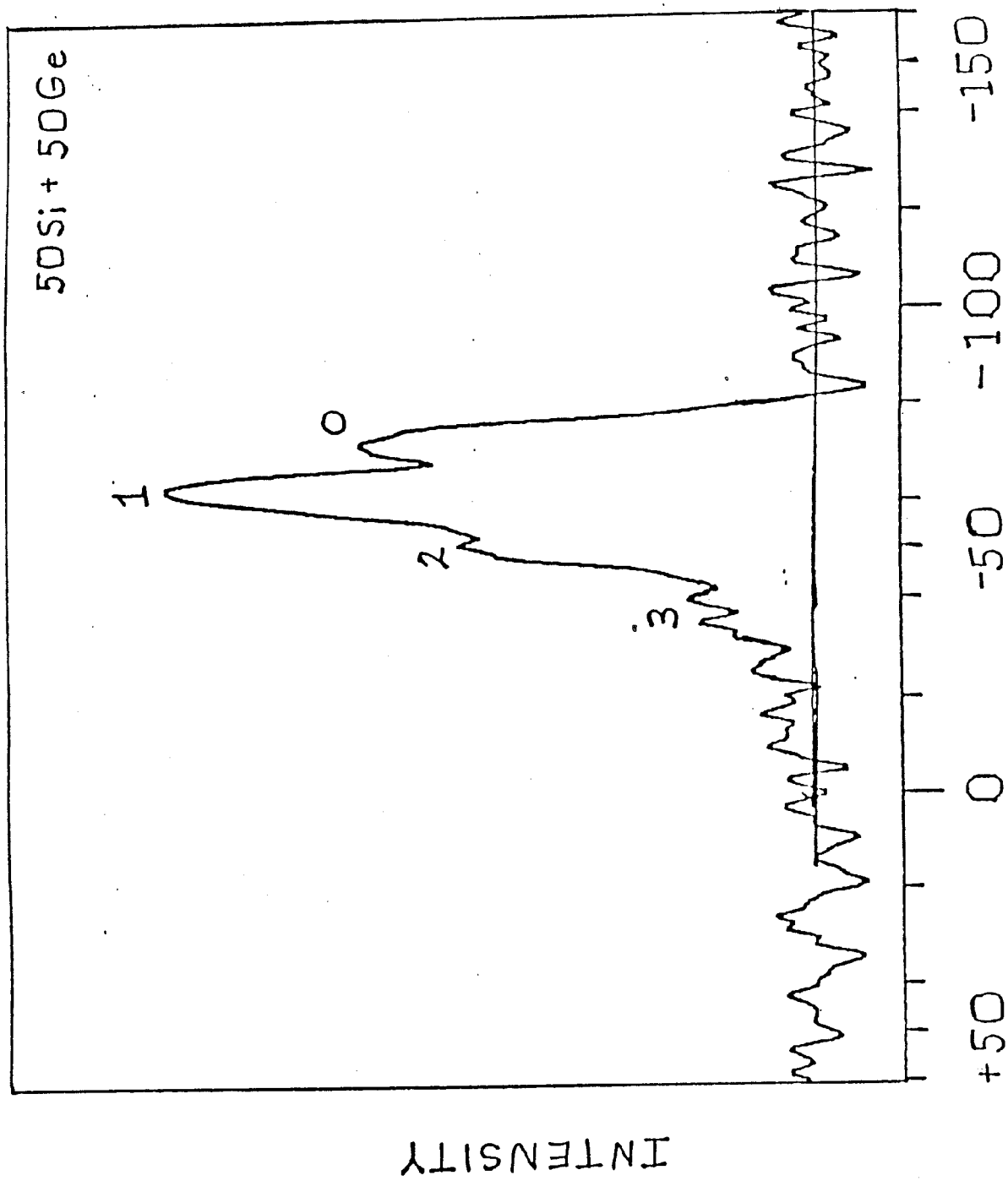

Figure 6-9. NMR Frequency Shifts in ppm for an as-cast 50/50 Si-Ge Alloy. The Peaks are Labeled with the Number of Ge Nearest Neighbors.

Table 6-5. Observed and Predicted Relative Peak Heights for a 50 Si + 50 Ge Alloy

Number of Nearest Ge Neighbors	Predicted Height	Observed Height
0	0.16	0.71
1	0.67	1.00
2	1.00	0.55
3	0.67	0.19
4	0.16	<0.1

$$N(Si) = 4(0.71) + 3(1.00) + 2(0.55) + 1(0.19) + 0$$
$$N(Ge) = 0 + 1(1.00) + 2(0.55) + 3(0.19) + 4(0.05)$$

and the ratio is:

$$\frac{N(Si)}{N(Ge) + N(Si)} = \frac{7.13}{10.00} = 71.3 \text{ atom\% Si}$$

This means that the NMR results are in reasonable agreement with Stohr and Klemm. From this it is concluded that the remainder of the Ge in the sample freezes last as almost pure Ge with little or no ^{29}Si atoms in it that yield an NMR signal. The majority of the Si freezes out in a rather Si-rich alloy. In Table 6-4 it was observed that for the 35 atom% Si alloy the peak for 3Ge + 1Si neighbors is actually missing (or very weak), whereas the 2Ge- and 4Ge-neighbor peaks are strong. On freezing, the system seems to bypass the intermediate compositions ending up at nearly pure Ge as the last to freeze. For this reason such as-cast material should be thermally homogenized in order to interdiffuse the Si and Ge atoms in order to make a homogeneous sample for the thermoelectric devices.

The local atomic environment of Si-Ge alloys was also probed by Raman scattering. Dr. Peter Codella performed the analyses using the GE-CR&D spectrometer operating at a laser wavelength of 514 nm.

Pure Si and Ge were first run to confirm that the system was operating properly. Two different specimens of nominal composition Si(0.5)Ge(0.5) + 8 Mole% GaP, cut from sample IHP-191-AN, were subsequently examined using the usual reflecting mode of the spectrometer.

In addition a specimen of undoped, chill cast alloy of nominal composition Si(0.5) Ge(0.5) was cut and polished for analysis. Microscopic examination of the polished surface revealed areas of light and dark contrast presumably indicating regions having different Si-Ge ratios. The light areas are Ge rich, the dark ones Si rich. Figure 6-10 shows the spectrum obtained when the beam spot was on a dark area. The shift at around 500 cm^{-1} is due to Si-Si vibrations while that around 400 cm^{-1} is due to Si-Ge vibrations and the line near 300 cm^{-1} is Ge-Ge vibrations. Comparison with the curves shown in Figures 2 and 3 in the paper by Ishidate et al.[8] lead to the conclusion that the local composition in the region examined was around (Si(0.8)-Ge(0.2)), in agreement with the phase diagram of Stohr and Klemm[7]. Thus these results agree well with NMR data on the same material. The light area gave the spectrum shown in Figure 6-11 where the line around 300 cm^{-1} is caused by Ge-Ge pairs and the line at approximately 400 cm^{-1} is Si-Ge pairs.

The GaP doped 50/50 Si-Ge alloy, IHP-191-AN, which was hot-pressed and annealed, shows all 3 lines at more or less equal intensity in Figure 6-12. In a homogeneous sample containing Si with atom fraction q and Ge with atom fraction p the following relationships apply:

$$p + q = 1$$

$$\text{Relative Intensity (500 cm}^{-1}\text{ line)} = q^2$$
$$\text{Relative Intensity (400 cm}^{-1}\text{ line)} = 2pq$$
$$\text{Relative Intensity (300 cm}^{-1}\text{ line)} = p^2$$

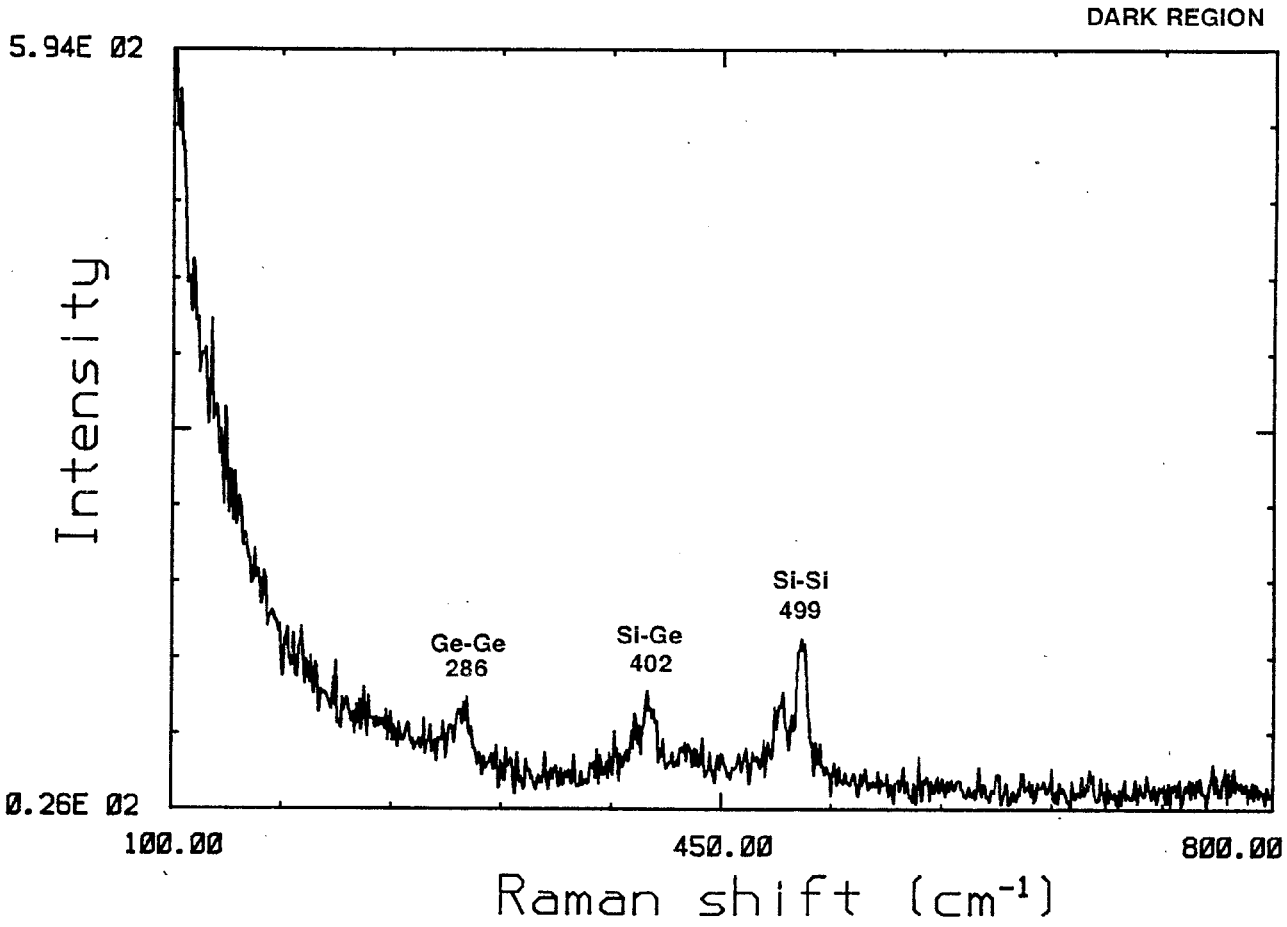

Figure 6-10. Raman Spectrum of a Dark Contrast Area of an As-cast Specimen of 50/50 Si-Ge.

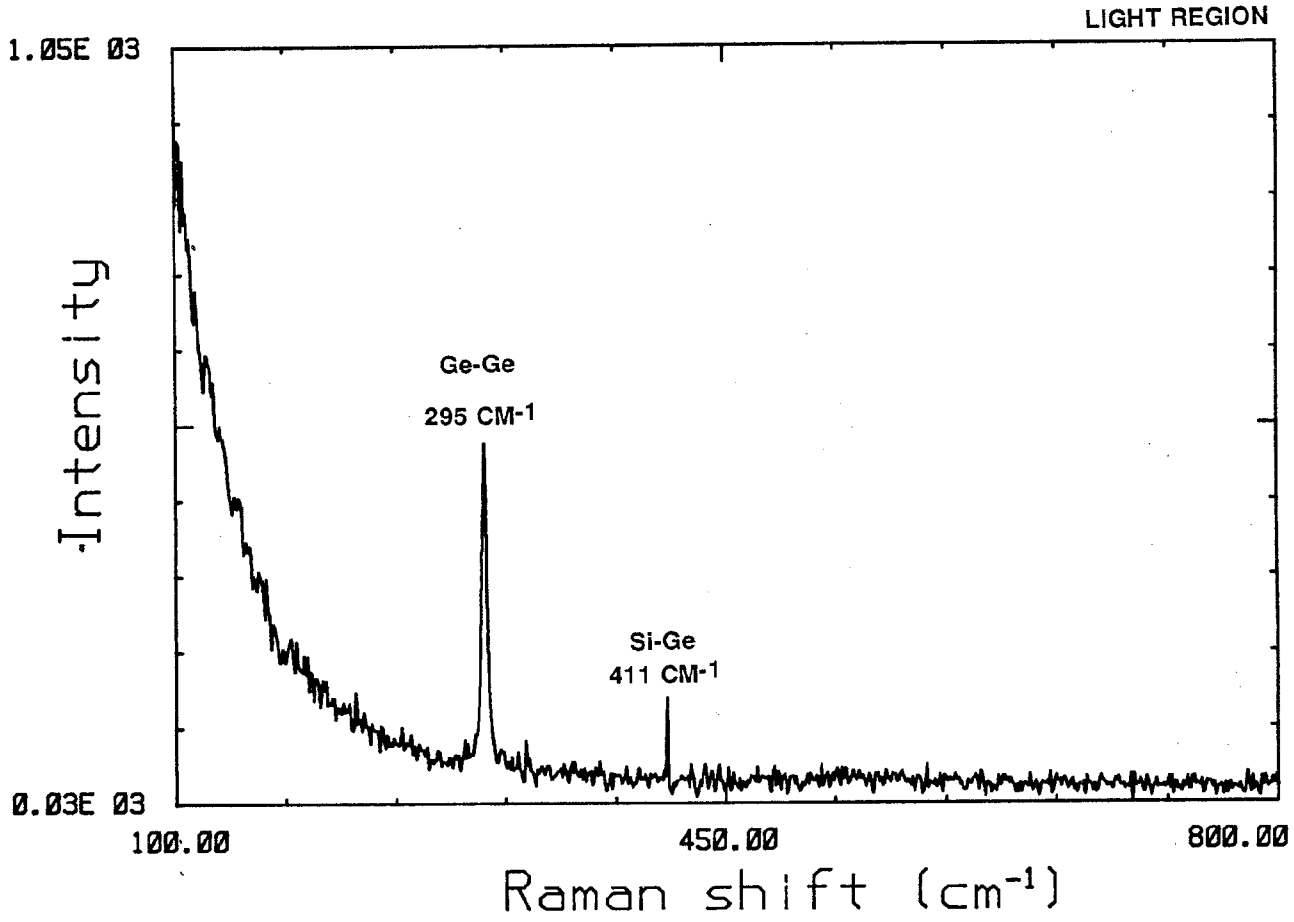

Figure 6-11. Raman Spectrum of a Light Contrast Area of an As-cast Specimen of 50/50 Si-Ge.

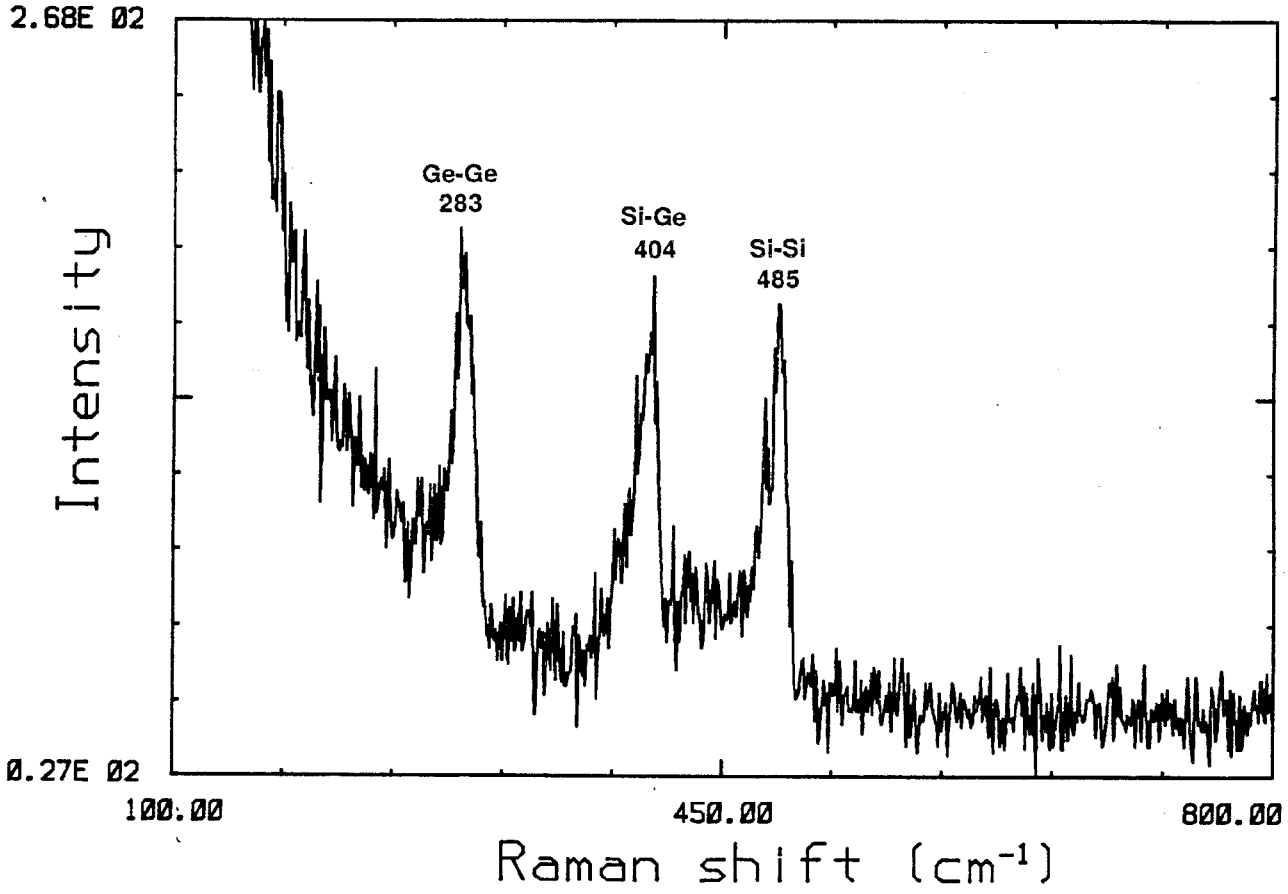

Figure 6-12. Raman Spectrum of 8 Mole Percent GaP in 50/50 Si-Ge Hot Pressed and Annealed Compact (IHP-191-AN)

Thus, at the 50/50 Si-Ge composition, the relative line intensities should be 1:2:1. In Figure 6-12 the ratio is closer to 1:1:1, but the agreement isn't bad.

From these preliminary examinations it is apparent that specimens of both undoped and heavily doped samples can be studied effectively in air with a laser spot size of about 1 micron, and that the local Si-Ge composition can be measured. The electron beam microprobe can accomplish the same thing, but requires samples in a vacuum chamber. This technique appears to have some promise.

6.5 SUMMARY

From the EXAFS study it was determined that the Ga atoms in n-SiGe-GaP have the same four nearest neighbor P atoms as molecular GaP while in p-SiGe-GaP there are three nearest neighbor Si atoms and one nearest neighbor Ge atom. These observations indicate that, in the presence of Boron in the p-type alloy, GaP has a tendency to dissociate and the Ga is readily assimilated into the Si-Ge matrix.

The TEM study of as-pressed samples prepared by the chill cast/pulverized/hot pressed method indicated a mottled or bimodal grain structure, with fine grains occuring predominantly at the grain boundaries of the coarse grains. This effect was more pronounced for the GaP doped samples. SiO_2 precipitates were also detected in the grain boundaries. The Ga and P distribution was not uniform and only an occasional GaP particle was detected. These observations strongly suggest the potential of using grain size to tailor the thermal conductivity characteristics of the alloys and the second phase precipitation process to tailor the electrical properties. The TEM results of heat treated n-SiGe-GaP samples prepared by Thermo Electron indicated a more uniform grain size distribution, higher porosity and fewer precipitates.

Preliminary NMR and Raman scattering results of undoped and GaP doped 50/50 Si-Ge alloys suggest the possible potential of these tools for probing the local environment of Si or Ge atoms. The relative position and intensity of the characteristic fingerprint give some indication of the kind and number of

nearest neighbor atoms just as EXAFS is capable of providing. EXAFS would be considered a microstructure tool while NMR is considered a bulk tool. The application to a variety of GaP containing alloys is necessary since the effect of Ga and P have not been fully revealed.

6.6 REFERENCES

(1) J. Wong, Mater. Sci. and Eng. __, (1986).

(2) J. Jaklevic et al., Solid State Comm. 12, 679 (1977).

(3) P.A. Lee et al., J. Amer. Chem. Soc. 99, 3856 (1977).

(4) J. Wong et al., Phys. Rev. B30, 5596 (1984).

(5) S. Draper, M.S. Thesis, Case Western Reserve, April 1987.

(6) G.L. Turner, R.J. Kirkpatrick, S.H. Risbud and E. Oldfield, Bull. Am. Ceram. Soc. 66, 656 (1987).

(7) H. Stohr and W. Kelmm, Z. Anorg. Allgem. Chem. 241, 305 (1939).

(8) T. Ishidate, S. Katagari, K. Inoue, M. Shibuya, K. Tsuji and S. Minomura, J. Phys. Soc. Japan 53, 2584 (1984).

SECTION 7
SiP FOR CHARGE CARRIER CONCENTRATION CONTROL

7.1 BACKGROUND

The importance of doping concentrations in the optimization of thermoelectric properties was demonstrated by Dismukes et al.[1] The trends observed by them are illustrated in Figure 7-1, when the dimensionless figure-of-merit (ZT) is plotted against temperature for n-type 70/30 Si-Ge alloys with different carrier concentrations. In addition, C. Vining[2] has hypothesized that overdoping of Si-Ge alloys up to perhaps 10^{21} carriers/cm^3 may reduce the ambipolar effects and improve Z by as much as 45 percent. These improvements due to excess phosphorus doping may result from (1) improvement of electrical properties because of the larger number of charge carriers and/or (2) the precipitation of the excess phosphorus to provide phonon scattering sites and reduced thermal conductivity.

Phosphorus is the major element used for doping n-type Si-Ge alloys. It is added either by the solution of elemental P or molecular GaP. One drawback with using GaP is that it is a compensated dopant which requires dissociation and preferential solid solution of the phosphorus to produce the active charge carriers. If dissociation does not occur, the active change carrier concentration may be much less than the amount of phosphorus added to the Si-Ge alloy.

Silicon phosphide, SiP, may be a more suitable n-type dopant since it dissociates at a lower temperature than GaP. In addition, the phosphorus is not compensated by the silicon.

SiP is not available commercially and some preliminary synthesis efforts were conducted in two laboratories to produce it by reacting the elements in sealed quartz tubes. SiP was synthesized on the Program but no compacts were fabricated.

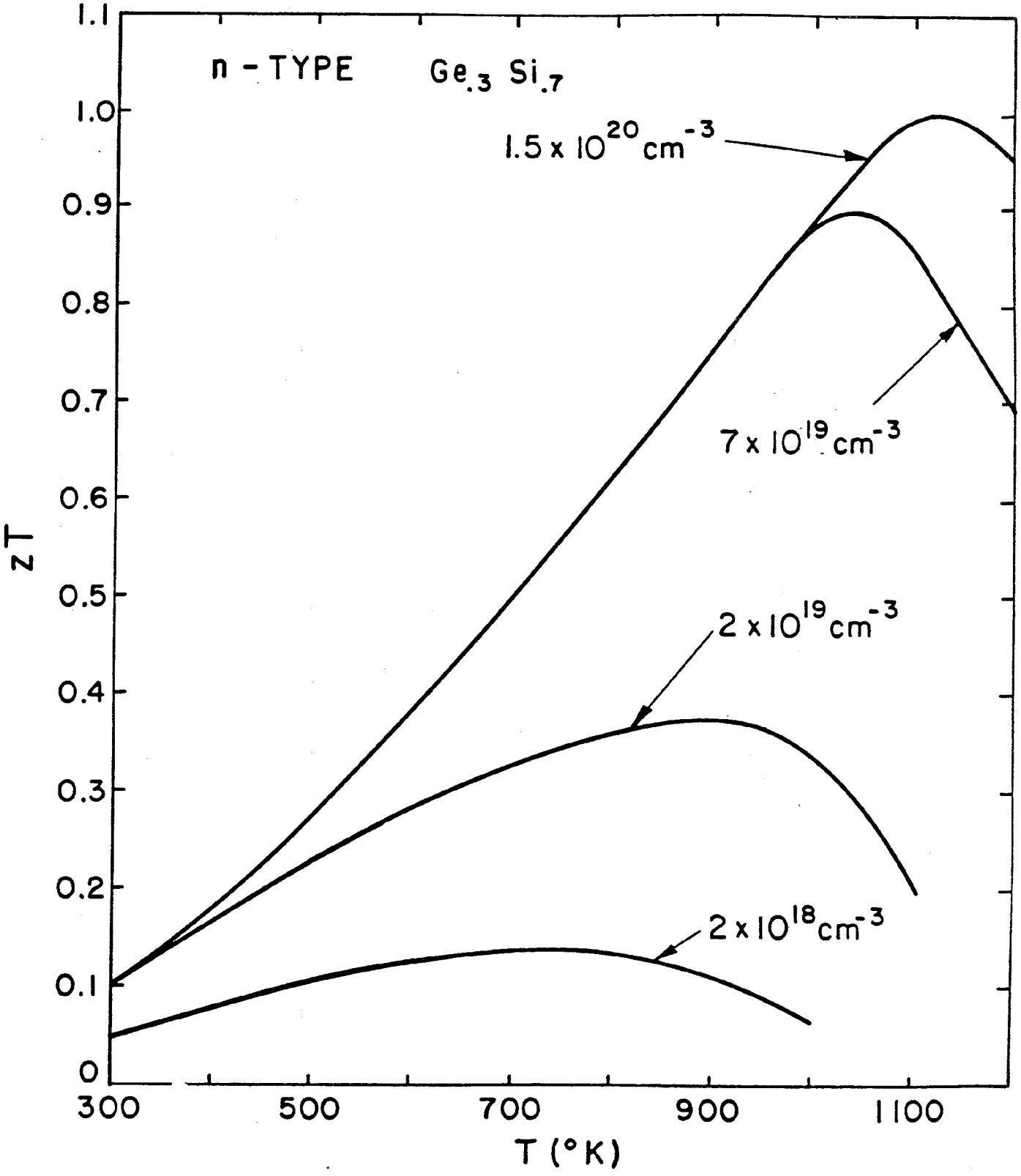

Figure 7-1. Dimensionless Figure-of-Merit Trends as a Function of Charge Carrier Concentration for 70/30 Si-Ge Alloys (After Dismukes et al.[1])

7.2 SiP SYNTHESIS

Both GE-CR&D and Thermo Electron prepared small quantities of SiP by reacting finely divided silicon with lumps of red phosphorus by vapor phase transport. The silicon powder used at CR&D was 8.0 microns median particle diameter while -625 mesh (20 microns) powder was used at Thermo Electron.

The experimental setup employed at GE-CR&D is shown in Figure 7-2. The silicon powder was contained in a high purity alumina boat at the hot end of the furnace. The phosphorus was placed at the cold end of the furnace in direct contact with the fused quartz. The hot and cold zones were separated by a section of quartz wool to reduce heat transfer. The quartz tube assembly was evacuated to 10^{-6} torr and sealed before heating.

The reaction furnace was run for a total of 120 hours (5 days) with the phosphorus temperature held at 400°C and the silicon temperature at 1000°C for 3 days, then at 1050°C for 2 days. The calculated phosphorus pressure was 0.7 atmospheres.

A total of 10 gm of SiP product was made in this run since the unreacted Si powder is only packed to about 30% of theoretical density.

The procedure used by Thermo Electron is similar to GE-CR&D except that an "L" shaped quartz tube was used as shown in Figure 7-3. About 27 grams of -625 mesh Si powder were loaded into the horizontal section and about 33 grams of lump red phosphorus were loaded into the narrower vertical section. A baffle was positioned at the elbow to prevent the silicon from coming into contact with the phosphorus. The quartz tube was evacuated to 5×10^{-6} torr and placed into a tube furnace with flowing argon in order to minimize oxygen diffusion. The phosphorus segment was heated by a separate resistance heater. The silicon was kept between 950 and 1000°C while the phosphorus was kept at 500°C for six hours. After this heating period, power was turned off and the system was allowed to cool overnight. The silicon powder was agitated to expose a fresh unreacted surface and the six hour heating cycle was repeated. This heating/cooling/agitating process was continued until no change was observed in the phosphorus level which took approximately one week for the synthesis of 50 grams.

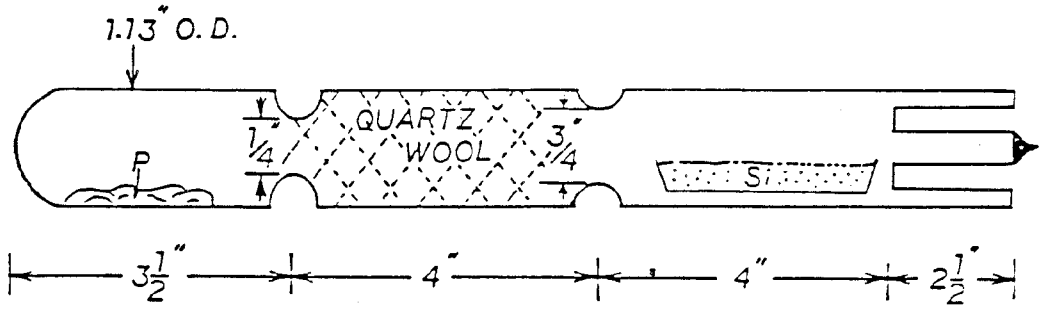

Figure 7-2. The Sealed Fused-Quartz Tube Assembly Used for Making SiP at GE-CR&D

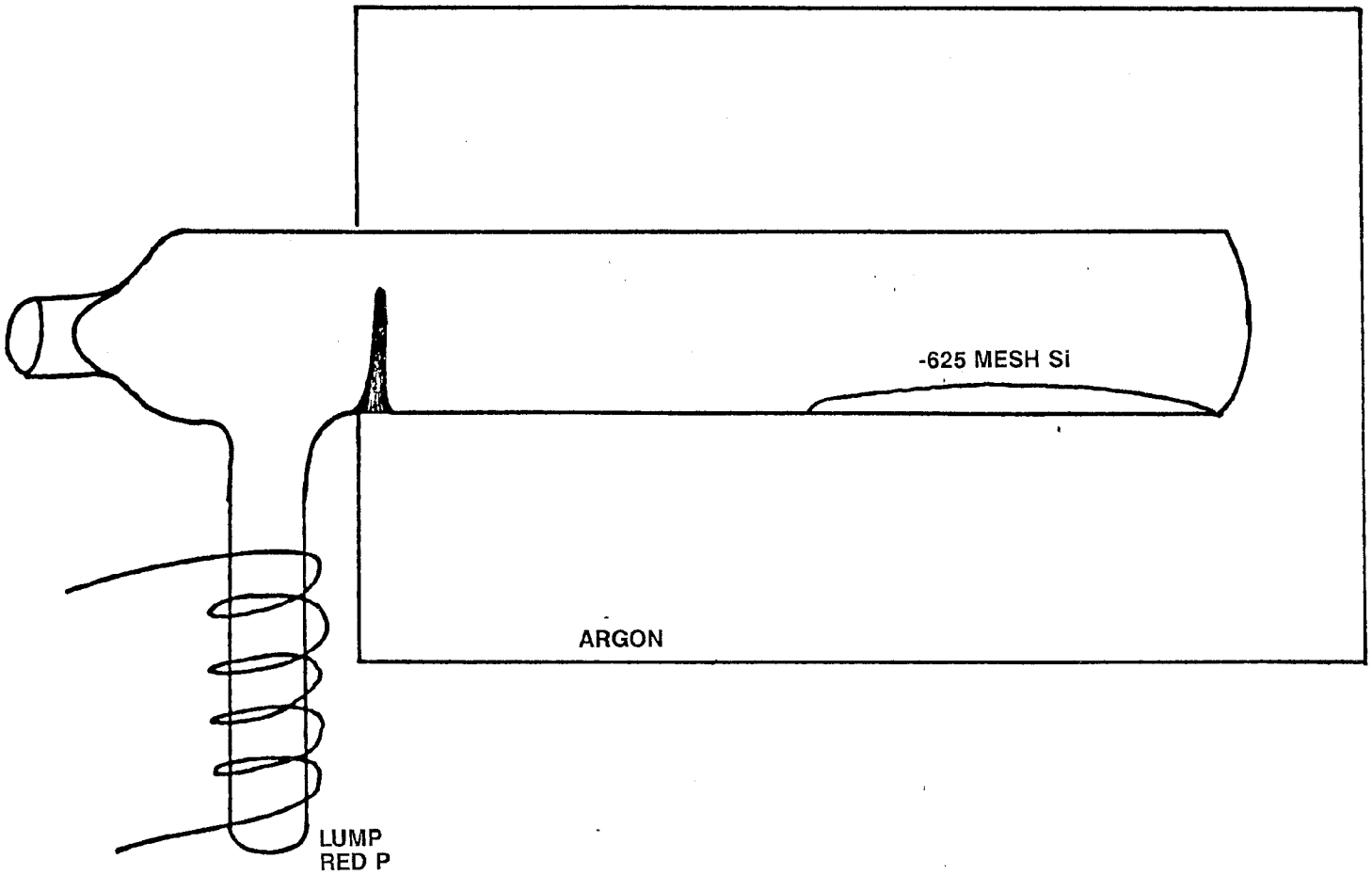

Figure 7-3. SiP Synthesis Setup at Thermo Electron

7.3 SiP CHARACTERIZATION

X-ray diffraction and SEM/EDS analyses were performed at GE-ASD on these powders. X-ray diffractograms were obtained between 15 and 115 degrees 2-theta on a Siemens D500 automatic diffractometer using copper radiation. Figure 7-4 shows the diffraction patterns between 15 and 65 degrees 2-theta. The top pattern is that of GE-CR&D's SiP and the bottom is that of Thermo Electron's SiP. The patterns are identical and correspond to a mixture of orthorhombic SiP and cubic Si.

Figure 7-5 shows the backscattered electron images. The CR&D product is more finely divided with a crust-like appearance while cleavage planes can be seen on the large particles of Thermo Electron's product. Energy dispersive spectroscopy results indicate that CR&D's material is very nearly stoichiometric (50.5 a/o Si, 49.5 a/o P) while Thermo Electron's has a much higher Si to P ratio (57.8 a/o Si, 42.2 a/o P).

7.4 SUMMARY

The feasibility of synthesizing SiP for more effective charge carrier concentration control was demonstrated. It is recommended that compacts be processed with these materials and the thermoelectric properties compared with GaP doped alloys.

7.5 REFERENCES

(1) J.P. Dismukes, L. Ekstrom, E.F. Steigmeier, I. Kudman and D.S. Beers, J. Appl. Phys. 35, 2899 (1964).

(2) C. Vining, private communication.

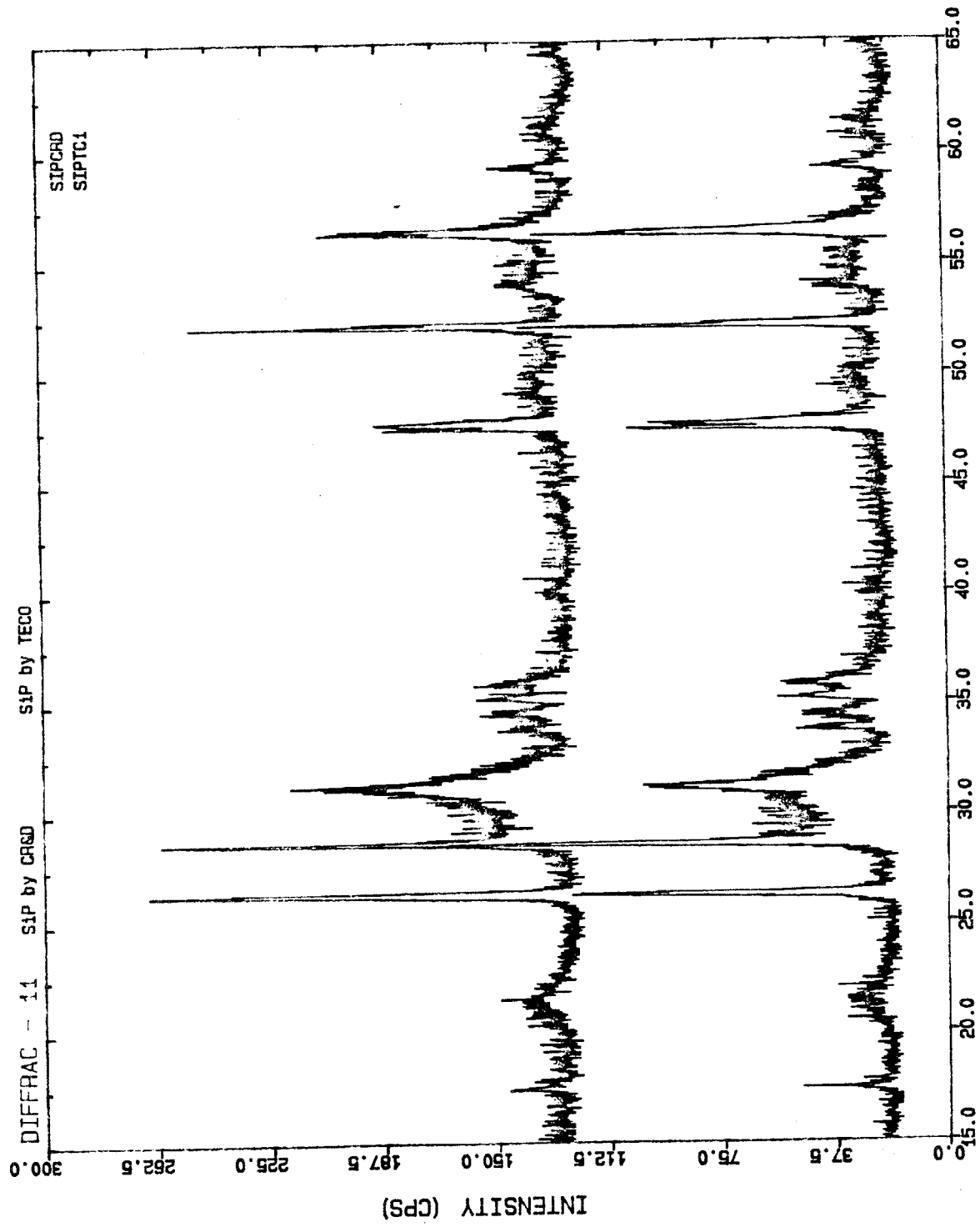

Figure 7-4. X-ray Diffraction Patterns of a Mixture of SiP and Si Synthesized by CR&D (Top) and Thermo Electron (Bottom)

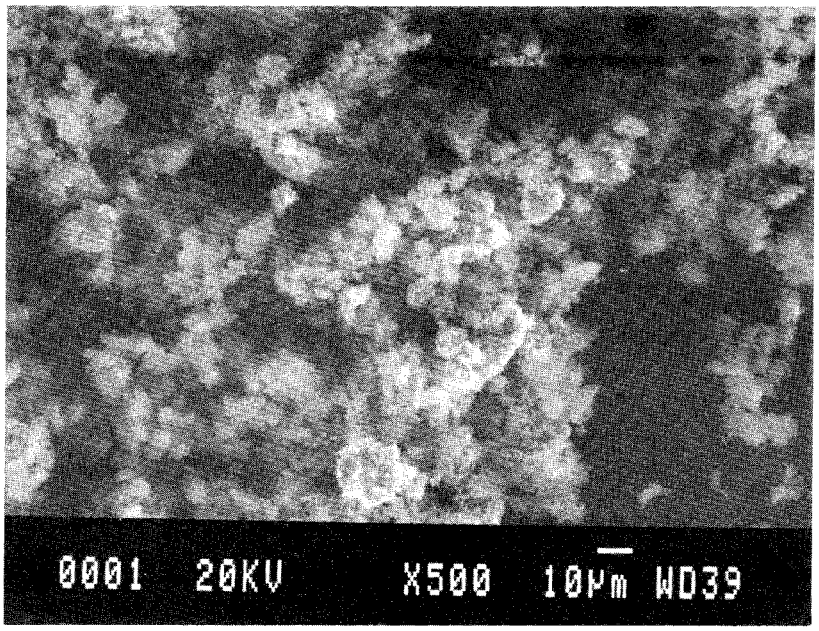

A. GE-CR&D 50.5 a/o Si, 49.5 a/o P

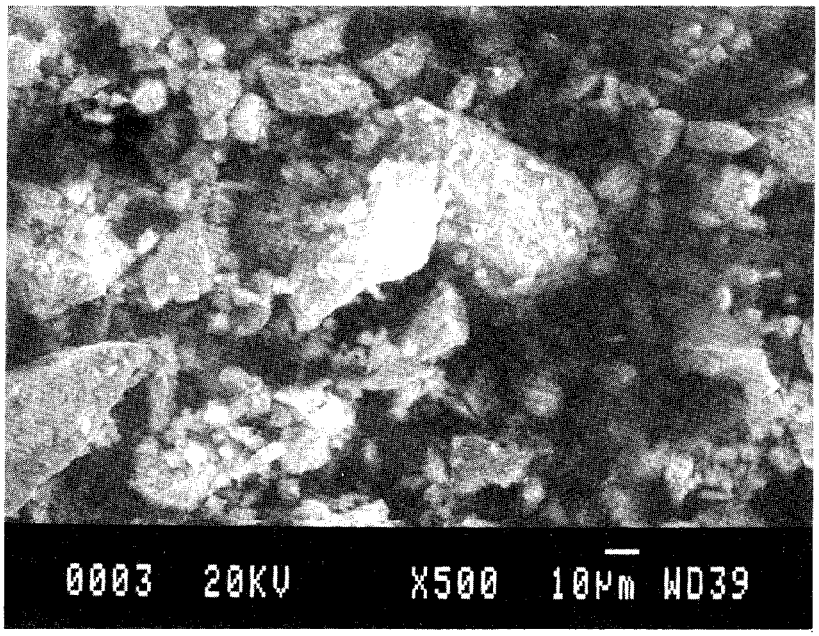

B. Thermo Electron 57.8 a/o Si, 42.2 a/o P

Figure 7-5. Backscattered Electron Image of Silicon Phosphide

SECTION 8
MICROSTRUCTURE CONTROL IN p-TYPE MATERIALS

8.1 BACKGROUND

Studies were conducted of approaches for reducing the lattice thermal conductivity of Si-Ge alloys as the means of improving their performance in thermoelectric generators. It was concluded that the best method for decreasing the lattice thermal conductivity of Si-Ge alloys below their present value of about 50 milliwatt/cm deg at 300K is to introduce scattering of phonons from thermally stable second phase inclusions with a particle diameter of about 50 angstroms and a concentration of a few volume percent. GE-CR&D undertook several approaches for manufacturing suitable samples with particular emphasis on trying to improve p-type Si-Ge alloys.

8.1.1 SEMICONDUCTOR INCLUSIONS

It seemed reasonable to use particulate inclusions which do not drastically alter the semiconducting properties of the matrix. Thus it was felt that the particles should be either insulating or semiconducting, but should not be metallic. A number of choices of metal silicides which are semiconducting exist. Some examples are: $BaSi_2$, $CrSi_2$, Mg_2Si, $Mn_{11}Si_{19}$, $FeSi_2$, $ReSi_2$, and $OsSi_2$. These metals all have very low (<10 ppm atomic) solid solubilities at equilibrium in solid silicon. $OsSi_2$ was chosen as the most useful compound from this collection because of its high density and large bandgap.

8.1.2 CHILL-BLOCK CASTING

A technique for chill-block casting of ribbons (CBCR) was developed at GE-CR&D by Walter [1,2]. In this technique, a small diameter stream of the melt is directed to impinge on a rapidly rotating, cold copper drum. The cooling rates so obtained near the melting point are of the order of 10^6 to 10^7K/sec. For the silicon ribbons studied here, the 1.5 gm melt was held in a fused quartz tube 0.6 cm in diameter and 15 cm long which had a capillary tube orifice 0.075 cm in diameter. The melt was held at 1450°C and then extruded using 12 psig of argon gas onto a 15 cm diameter copper drum rotating so that the surface speed was 3000 cm/sec. The resulting ribbon was 2×10^{-3} cm thick and 2×10^{-1} cm wide. The production rate of a length

of the ribbon was calculated to be 250 cm/sec. To establish the potential and feasibility of this approach, two different additives were used in the silicon melts, namely osmium and boron.

8.1.3 RAPID-QUENCHING STUDIES

Si-Ge alloys were quenched in very short times by squirting them from a fused-quartz hypodermic needle onto a rapidly rotating copper drum. These samples, cooled by this chill-block casting-of-ribbon (CBCR) technique, cool at a rate of about 3×10^6K/sec. This resulted in non-equilibrium concentrations of the various elements.

8.1.4 UNDOPED ALLOYS

Two undoped Si-Ge alloys were studied containing 80/20 and 50/50 Si to Ge atom ratios. The results are shown in Figure 8-1 as the curve labeled at CBCR. The segregation coefficient, k, is the ratio of the Ge content in the first solid to freeze to that in the initial melt.

$$k = \frac{\text{Ge content in solid}}{\text{Ge content in liquid}}$$

The equilibrium phase diagram of the Si-Ge system has been worked out by Stohr and Klemm[3]. From their data the equilibrium values of k in Figure 8-1 have been calculated. For materials which have been rapidly cooled the value of k is considerably larger; however, it is not unity. If the melt froze instantaneously, k = 1, and it does not. However, from Figure 8-1 it can be seen that large deviations from equilibrium can be achieved which results in more Ge being retained in the solid than would be possible during slow cooling. X-ray diffraction studies of lattice parameter on these Si-Ge alloys showed that the rapid freezing tended to produce two distinct regions in the solidified deposit. One is a Si rich region and the second is almost pure Ge. There is very little material of intermediate composition. For example, a 50/50 liquid alloy under CBCR solidified into:

Region 1: 63.0 atom% Si + 37.0 atom% Ge
Region 2: 1.0 atom% Si + 99.0 atom% Ge

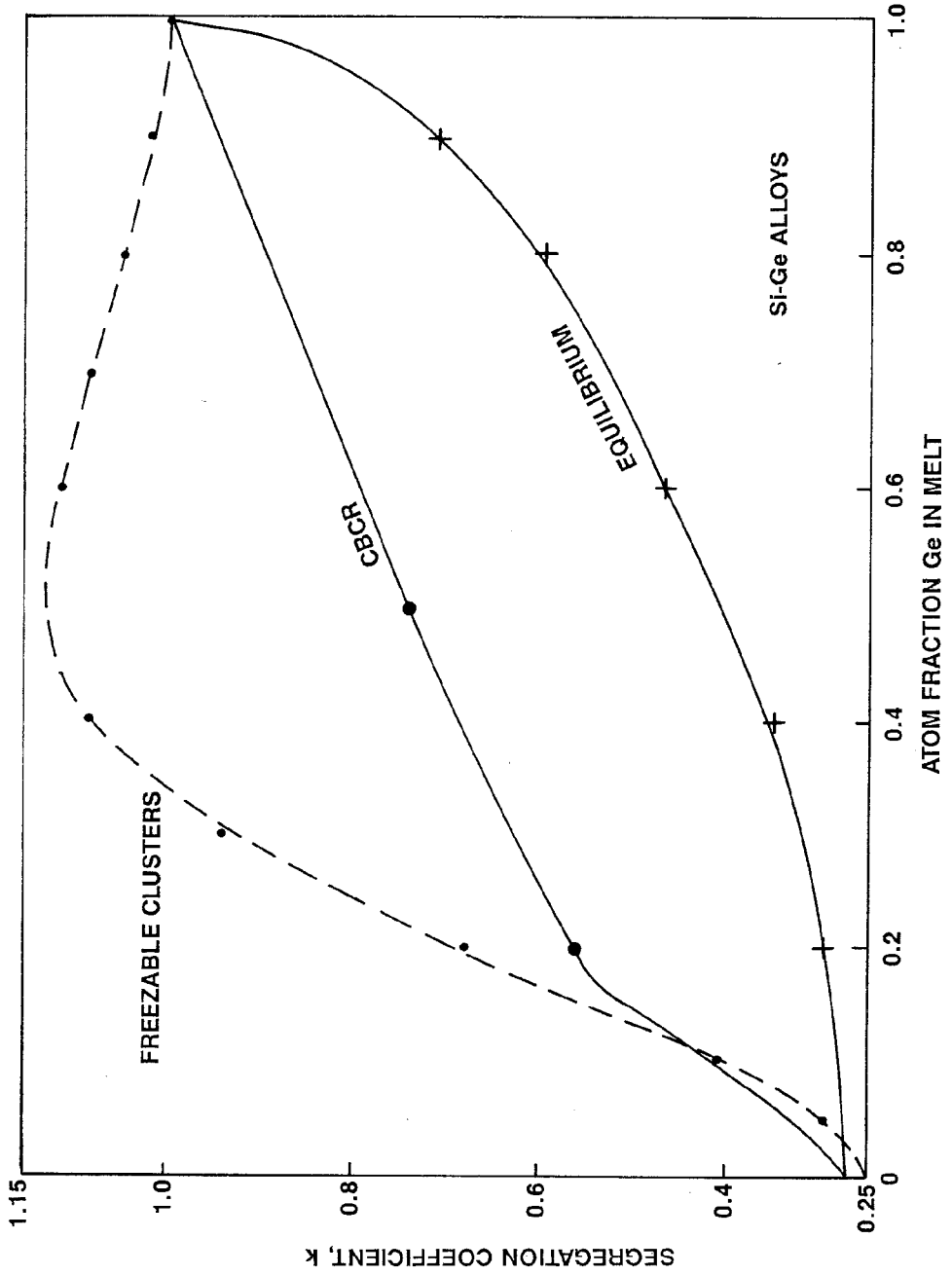

Figure 8-1. Segregation Coefficient Versus Atom Fraction Ge in the Melt for Equilibrium and CBCR Si-Ge Alloys

If only these two regions are present, the ribbon surface would be expected to show

77.8 volume % of Region 1
22.2 volume % of Region 2

A cross-section of the solidified ribbon 25 microns thick and 3000 microns wide studied by a scanning electron microscope revealed two distinct regions of high Si and low Si content with about the same area ratio as given above. The Si-rich regions were about 3 microns in diameter separated by 1 micron thick Ge-rich regions.

From this type of picture the following calculation can be made. The diffusion coefficient of Ge in liquid Ge (or Si in liquid Si) is about:

$$D = 1 \times 10^{-4} \text{ cm}^2/\text{sec}$$

just above the melting point. In order for the excess Ge atoms to move 1 micron in the cooling time of the melt from liquid to solid, the cooling time, τ_c, must have been about:

$$\tau_c = \frac{\ell^2}{D} = \frac{10^{-8}\text{cm}^2}{1\times10^{-4}\text{cm}^2/\text{sec}} = 10^{-4} \text{ sec}$$

The melt in the fused-quartz syringe was about 100°C above the melting point of the alloy. Thus, the cooling rate was about 10^6 degrees/sec., which is typical of the CBCR technique.

8.1.5 OSMIUM-DOPED SILICON

A silicon melt was doped with 2 atom % osmium. The initial Si-Os charge was melted in a CVD boron nitride crucible. This melt was cast into a cold copper mold. Sections of this first casting were placed in the quartz tube of the CBCR furnace, and a ribbon was formed. The ribbon so produced was analyzed by metallographic techniques with an optical microscope and an electron-beam microprobe. These results showed that Os-rich regions about 5×10^{-5} cm wide were present as long filaments and that the phase was $OsSi_2$. The Os

content of the silicon matrix was $\leq$0.3 atom % Os. An X-ray diffraction study of the ribbon revealed that it was crystalline (not amorphous), and that the lattice parameter of the cubic Si phase was 5.4287(4) angstroms. This value is to be compared with:

Pure starting silicon	a_o = 5.4308(2) angstroms
Silicon after melting in BN (boron contamination)	a_o = 5.4299(4) angstroms

Thus there was little if any effect of the Os on the lattice parameter of the Si, even after rapid quenching. Hence, it was concluded that very little if any Os was trapped in solid solution by the CBCR technique and further studies on the Os-doping approach were halted.

8.1.6 B-DOPED SAMPLES

It is known from annealing studies[4] that the maximum equilibrium solid solubility of boron in silicon is about 1.0 atom% at 1385°C. However it was found that by using the CBCR technique it is possible to produce ribbon samples of Si with 2.5 atom% boron in solid solution. For these samples the lattice parameter (Figure 8-2) had decreased from:

$$a_o \text{ (undoped Si)} = 5.43083(4)\text{Å}$$

to

$$a_o \text{ (max. boron)} = 5.402(2)\text{Å}$$

At this concentration the misfit strain in the lattice prevents further boron uptake. It is to be noted that boron is a substitutional impurity, and the boron atom radius is less than that of silicon.

$$r(B) = 0.90\text{Å}$$
$$r(Si) = 1.176\text{Å}$$

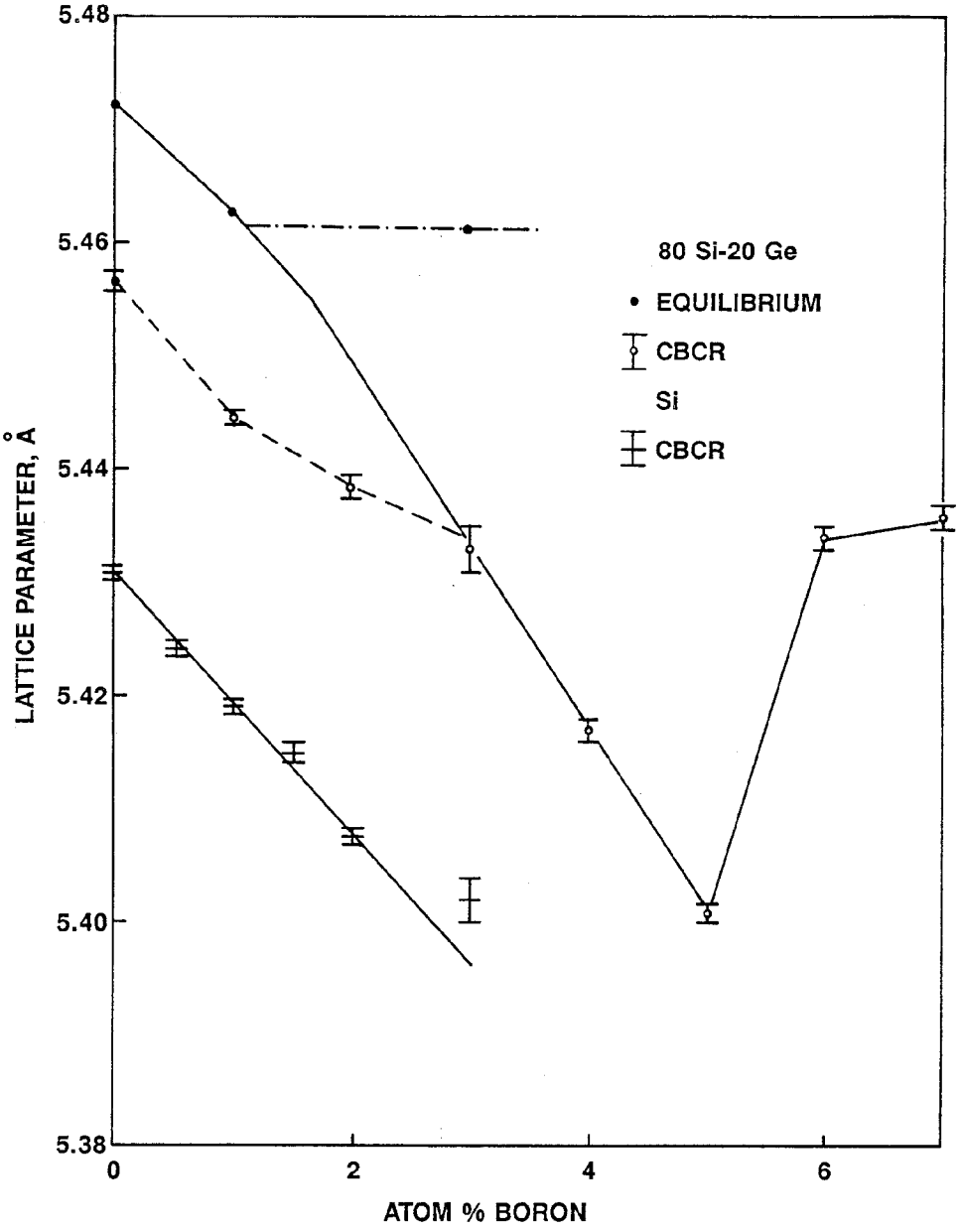

Figure 8-2. Lattice Parameter Versus Atom% Boron in Equilibrium and CBCR Si-Ge Alloys

Since Ge atoms have a radius of

$$r(Ge) = 1.225\text{Å}$$

one can help to compensate the boron strain by counterdoping with Ge. This indeed has proved to be the case. An undoped 80 atom% Si + 20 atom% Ge alloy has:

$$a_o\ (80/20) = 5.472(1)\text{Å}$$

By the CBCR technique a ribbon containing 5 atom% B in solid solution in an 80/20 alloy has been produced. For this sample:

$$a_o\ (\text{B-doped}) = 5.401(1)\text{Å}$$

Note that this a_o is very close to that of the Si with 2.5 atom% B. Hence the lattice strain limit is about the same. Thus it can be hypothesized that 8 to 10 atom% B in solid solution could be achieved in a 50/50 Si-Ge alloy by the CBCR technique.

8.1.7 B_3Si PRECIPITATES

It is known that the boron which is in solid solution in Si at high temperatures will precipitate out as internal B_3Si clusters after annealing at 900°C for 1 hour. The precipitate particle diameter by transmission electron microscopy has been measured and found to be about 150 angstroms. After a 10 hour anneal the particle diameters are expected to be about 400 angstroms.

Studies of 80 atom% Si - 20 atom% Ge alloys containing boron show that the equilibrium boron concentration in these is somewhat (approximately 50%) higher than in Si itself. The precipitates that form are still B_3Si; there are no known B-Ge compounds. A sample containing 1.2 atom% boron in solid solution was annealed at 900°C for 10 hours. The transmission electron microscopy study found 150 angstrom diameter precipitates at a concentration of about $1.6 \times 10^{14}/cm^3$.

8.2 SUMMARY

The feasibility of producing samples containing small diameter B_3Si precipitates has been demonstrated. These should be useful for studying the thermal conductivity and phonon scattering by precipitates. It is believed from theoretical calculations that such precipitates could reduce the lattice thermal conductivity of 80/20 alloys by a factor of at least 2 below presently found values of approximately 30 mW/cm K. Whether this approach has high potential for improving 'p' type alloys needs to be determined.

8.3 REFERENCES

(1) J.L. Walter, Proc. Third Intern. Conf. on Rapidly Quenched Metals, Brighton, 1978, Vol. 1, p. 30, pub. by Metals Society, London (78CRD172).

(2) J.L. Walter, J. Non-Crystalline Solids, 44, 195 (1981).

(3) N. Stohr and W. Klemm, Z. Anorg. Allgem. Chem. 241, 305 (1939).

(4) A. Armigliato, D. Nobili, P. Ostoja, M. Servidori and S. Solmi, Proc. Third Intern. Symp. Silicon Mater. Sci. Tech., 77-2, Ed. H.R. Huff and E. Sirtl, p. 638 (1977).

SECTION 9
GENERAL SUMMARY, DISCUSSION AND PERTINENT OBSERVATIONS

9.1 GENERAL SUMMARY

Reliable, reproducible fabrication of n-type SiGe-Gap compacts with improvements in average high temperature thermoelectric properties of 30 to 40 percent or more were achieved. Comparison of data obtained at GE-ASD, Ames and Battelle-Columbus Laboratories indicate that the improvement may be even higher for measurements made under simulated service in-gradient test conditions and/or when the alloys are subjected to additional heat treatments after hot pressing.

The fabrication procedures selected appear to have accomplished the improvements by retaining the good electrical property characteristics of highly doped, conventional coarse grained Si-Ge alloys under conditions in which the lattice thermal conductivities are reduced. The thermal conductivity reduction was achieved in hot pressed compacts made from powder blends with enhanced phonon scattering due to their small median grain sizes (5 microns or less) and/or the controlled precipitation of very small diameter GaP particles.

The following subsections review the progress made in each phase of the program and the conclusions which can be drawn for each phase.

9.2 Si-Ge ALLOYS PREPARED WITH TAILORED PARTICLE SIZES

A variety of process methods was used to prepare hot pressed compacts of silicon-germanium alloys with median powder particle sizes ranging from over 100 microns to less than 2 microns and oxygen contents ranging from about 5 weight percent to less than 0.1 weight percent. While no clear correlation of figure-of-merit with oxygen content was noted, compacts prepared from 5 micron or smaller powder exhibited high temperature figure-of-merit values up to 13.4 $\pm$4.6% higher than the figure-of-merit values of compacts prepared from powders larger than about 12 microns. This effect is attributed to the greater homogeneity of the smaller particle size samples compared to those with larger particle sizes. Further, these figure-of-merit value improvements were only

slightly greater than those observed by RCA in zone leveled materials of similar carrier concentrations.

The above result was very surprising since the thermal conductivities were found to decrease by as much as 50 percent for the smallest particle sizes without a corresponding sharp increase in figure-of-merit. This trend resulted from a compensating reduction in the electrical conductivity. However, the thermoelectric figures-of-merit are in good agreement with the results of Dismukes on similarly doped alloys prepared by zone leveling techniques. The electrical and thermal conductivities were found to be sensitive to preparation procedure while the Seebeck coefficient and figure-of-merit were much less sensitive. The high temperature electrical properties were consistent with charge carrier scattering by acoustic or optical phonons.

The actual degradation in electrical properties was hypothesized as being due to such factors as voids, dangling bonds at grain boundaries, SiO_2 insulating layers around the particles, and/or built in strains (piezoresistive effects). Approaches suggested for minimizing these effects were to produce denser compacts, remove oxygen impurities, minimize Fe contamination from milling and/or add GaP for better control of charge carrier concentration and mobility and possible "fluxing" action on oxygen films at the grain boundaries.

A simple theory of samples with fine porosity in the body of the material would show K and σ both decreasing at the same rate with increasing porosity. The effect on Z would be small.

9.3 GaP DOPED ALLOYS PREPARED BY VACUUM MELTING/GRINDING/HOT PRESSING

The solution of GaP up to about 2 Mol percent in 80/20 Si-Ge alloys resulted in improvements in high temperature thermoelectric properties of 30 to 40 percent or more. The improvement appears to be due to a possible small but significant improvement in electrical properties and reduced lattice thermal conductivity. Possible explanations for these improvements include:

A. Increased carrier concentrations

B. Structure modification

C. Passivation of scattering sites

D. Increased homogeneity

E. Grain boundary effects (minimization of potential barrier heights)

F. Second phase inclusions

A brief discussion of these possibilities follows:

A. Increased Carrier Concentration

P, in solution, is an electron donor and, as such, is expected to have a small ionic radius. Ga, in solution, is an acceptor and is expected to have much larger (and negatively charged) ions. It is not uncommon for the compensation of strains to raise the solubility limit of dopants in the presence of the compensating elements. Thus, this may occur in SiGe-GaP alloys under proper preparation conditions, resulting in higher carrier concentrations and increased electrical power factors. This increased concentration was indeed found in some of the alloys produced here. The increased carrier concentration hypothesis has been recognized for some time. The electrical power factors of zone leveled n-type Si-Ge alloys increase with increasing carrier concentrations up to the solubility limit of phosphorus. Higher carrier concentrations can therefore be expected to possibly result in higher electrical power factors and increased figure-of-merit values. Estimates suggest a maximum electrical power factor of about 40 $\mu W/cm\text{-}K^2$ at S=171μV/K and rho=0.74x10^{-3} ohm-cm. If the carrier concentration was less than the optimum value by a factor of two, doubling the electrical resistivity from the optimum value, the electrical power factor would only be 10% lower than the optimum value. This relative insensitivity of the power factor to carrier concentration is characteristic of the relationship between the Seebeck coefficient and the electrical resistivity.

B. Structure Modification

It is possible that under specific preparation conditions, such as extended annealing or vacuum melting, GaP can form solid solutions with Si-Ge alloys and thus alter their bulk properties, perhaps in a beneficial way. GaP has a bandgap of about 2.24 eV; more than double the value for Si-Ge. Thus, a solid solution of GaP in Si-Ge should result in a larger bandgap and perhaps a larger Seebeck coefficient.

C. Activation/Passivation of Scattering Sites

The bonding state of the GaP can, in principle, affect the scattering mechanism. "Clusters" of GaP could have a very different local electrostatic field in the lattice than either Ga or P alone. Such clusters could scatter either more effectively, less effectively,

alter the energy dependence, or otherwise change the scattering process. A stronger energy dependence to the scattering (possibly as a result of introducing or activating a new scattering process) could increase the Seebeck coefficient, while affecting the resistivity in only a minor way. Alternatively, the effectiveness of some existing scattering mechanism could be reduced (pacified) by, for example, compensation of the localized strain field around donor impurities.

D. Increased Homogeneity

An obvious benefit of either modified hot pressing procedures or annealing is increased homogeneity of the Si-Ge alloys. While it is not obvious how this alone could result in higher thermoelectric performance than observed in zone leveled material, greater homogeneity is certainly desired in general.

E. Grain Boundary Effects

Grain boundaries clearly play an important role in Si-Ge alloys. GaP doping with or without long term annealing might remove defects from the grain boundaries allowing the properties of the material to approach the properties of single crystal materials. Results in this Program have suggested that grain boundary effects in heavily doped, hot pressed Si-Ge and SiGe-GaP alloys (prepared by many different methods) have essentially the same effect on the electrical mobility as on the thermal conductivity and that such materials, properly prepared, have the same figure-of-merit as their zone leveled counterparts. "Cleaning up" of grain boundaries can be expected to result in somewhat higher mobilities (and power factors).

F. Second Phase Inclusions

Changes in the solubility of GaP with Si to Ge ratio suggest that the reduced lattice thermal conductivity of the improved SiGe-Gap alloys such as ITM compacts 197, 232 and 234 might be due to precipitation of fine particles of GaP. These alloys were made by blending Si-Ge alloy powders (50/50), in which all of the GaP is soluble, with P doped Si powder in which the GaP is essentially insoluble. The resulting 80/20 SiGe-Gap alloys do show evidence of the presence of separate and discrete GaP phases (fine particles) by both SEM and electron probe analyses.

9.4 GENERAL OBSERVATIONS

In addition to significant improvements in thermoelectric properties resulting from GaP additions, a series of observations and conclusions can be drawn from the test results which are extremely significant. These include:

1. GaP appears to be highly soluble in 50/50 Si-Ge alloys at concentrations up to at least 16 Mol percent. High bandgap additives, such as GaP to these alloys, do significantly increase their high temperature Seebeck coefficients. However, this was accomplished by sharply increased electrical resistivity values. The resistivity increases appear to result from a combination of lower concentrations of electrically active phosphorus charge carriers and lower charge carrier mobilities.

   GE-CR&D demonstrated that it was feasible to heat treat the alloy powders in a phosphorus containing atmosphere. This should produce more effective compensation of the excess gallium atoms and increase the number of electrically active phosphorus atoms in solution.

   The preparation methods employed in producing the 50/50 SiGe-GaP alloys led to the production of very homogeneous materials. The homogeneity of these materials was found to be superior to standard Si-Ge alloys. The alloys were found to contain some porosity and oxide particles of the type SiO_y. The oxide particles were primarily concentrated in the grain boundaries. Based on the analysis done here, the hot pressing and thermal processing methods employed appear to result in some loss of germanium and gallium.

2. The vacuum melting/grinding/hot pressing approach for fabricating 80/20 SiGe-Gap alloys appears to be very effective in reproducibly making homogeneous alloys. There is, however, some loss of Ge. Also, the presence of discrete SiO_y particles in the GaP doped alloys suggests that Ga (or GaP) may help improve properties by effecting the chemistry or surface energies at particle boundaries. As an example, the Ga may be "scavenging" the oxygen and minimizing its effect in promoting high electrical resistivities. Also, the data tend to confirm the limited solubility of GaP in the 80/20 Si-Ge composition since free GaP was found in the compacts. Estimated maximum solubility at this Si-Ge alloy ratio is about 1 to 2 Mol percent.

   Samples of these materials subjected to thermal treatments indicate that an additional 20 percent improvement in thermoelectric properties can be achieved. Whether this was due to charge carrier concentration control, modification of carrier mobility and/or heat treating effects was not established.

3. The thermoelectric property data for ITM 197 and ITM 232 demonstrate that a high degree of reproducibility in property improvement for n-type SiGe-GaP alloys is achievable with appropriate fabrication process control. Also, the data show that further improvement can be made by increasing the carrier concentration (ITM 234). Details of the fabrication procedures used for ITM 234 are summarized in Appendix D.

Preliminary long term aging tests and thermal treatment studies at Ames and Battelle Laboratories show that the 80/20 SiGe-GaP alloys are (a) remarkably stable and (b) may be amenable to substantial property improvements by thermal treatments. However, much additional effort will be required to quantify the trends.

4. Techniques such as NMR show promise as both a research and possibly quality assurance tool to monitor the quality and reproducibility of compact fabrication. However, much more extensive research would have to be done to assess its potential.

5. Useful methods for the preparation of SiP powder for use as a controlled source of charge carriers in compact fabrication were demonstrated. Alloying with this compound may permit even further improvement in thermoelectric properties.

APPENDIX A

DESCRIPTIVE SUMMARY OF Si-Ge ALLOY SAMPLES/COMPACTS PREPARED ON THE ITM PROGRAM

PROPERTIES RELATIONSSi/Ge = 4

TASK 1.1

January 11, 1989

Sub-Task	Cast #	Sample #	Particle Size -	50%	Feed Method	GaP Addition Si	Ge	Mole Fraction B	Ga	P	Type	Thermal Conduct. W/m-K	Abs. See Coef.	Elect. Feeds. (muV/C)	Hall Mobility (ohm-cm	Carrier Conc. cm2/V-sec	Density @1000 1/K 1E20/cm3	(g/cc)	S*S2	Elect. Conduct.	k/k2	Z/Z2	ZT Ratio	Maximum IRT weight %	Oxygen Anal.
Vary Particle Size, Undoped																									
1	2	2	80 #	124 #		80.0	20.0			P		7.03						2.88							
1	2	8	325 #	16 #		80.0	20.0			P		6.65	IIND	2240	0.038	0.741		2.995							
1	3A	1	A.J.#	2.5 #		80.0	20.0			N		3.75	IIND					2.88						SRDa	
Production-Style Preparation, without GaP																									
1		54	325		PR 1st pr	79.8	20.0	0.25		P		4.53	# 117.8					2.99			0.900	1.000			
1		54A	325		PR 2nd pr	79.8	20.0	0.25		P		4.46	# 121.1	1.34	30.7	1.52		2.99	0.245	# 0.967	#0.760	#0.782	0.91	SRDa	1.990
1		55	325		PR 1st pr	79.5	19.9		0.59	N		5.03	# -107.2					2.94							
1		55A	325		PR 2nd pr	79.5	19.9		0.59	N		3.97	# -123.2	1.42	43.2	1.02		2.99	0.269	#-1.008	#0.660	#0.752	0.89	0.789	2.440
Vary Particle Size, Fixed GaP content, Melt added																									
2	4A	4A	80 #	124	#MEUse	78.4	19.6		1	1	N		5.22 # -120.8	1.17	46.9	1.14		3	0.239	#-1.045	#0.740	#0.999	0.81		0.166
2	4A	19	325 #	12	#MEDiff.	78.4	19.6		1	1	N		5.09 # -130.6	2.01	34.2	0.908		3.06	0.167	#-1.008	#0.504	#0.955	0.54		1
2	4A	20	A.J.#	2.8	#MEfor k	78.4	19.6		1	1	N		4.49 # -148.9	3.45	25.3	0.718		3	0.143	#-1.021	#0.348	#0.826	0.44		0.716
Vary GaP content, Blend-add GaP																									
3	3A	15	325 #	6.4	#BLEND	79.2	19.8		0.5	0.5	N		5.21 # -135.7					2.98				0.970			
3	3A	16	325 #	6.4	#BLEND	78.4	19.6		1	1	N		5.51 # -116.4	2.06	33.1	0.916		3.01	0.119	#-0.902	#0.489	#1.035	0.38	SRDa	0.613
		annealed at 1165 C-100 hours, and at 1225 C-8 hours in air											# -101.9	0.8458	53.46	1.38		3.031		#-0.970	#0.894	#		SRDa	0.561
3	3A	17	325 #	6.4	#BLFractur	76.8	19.2		2	2															
3	3A	18	325 #	6.4	#BLEND	73.6	18.4		4	4	N		5.65 # -82.2	0.569	48.8	2.25		2.84	0.210	#-1.001	#0.945	#1.145	0.83	SRDa	1.050
		annealed at 1165 C-100 hours, and at 1225 C-8 hours in air											# -88.1	0.6086	53.88	1.91		2.848		#-0.987	#0.993	#		0.687	
Vary Particle Size and GaP content, Melt-added GaP																									
4	5	5	80 #	124	#MELT	79.2	19.8		0.5	0.5	N		5.60 # -178.5	2.51	52.2	0.477		2.98	0.227	#-0.871	#0.644	#1.007	0.49		0.318
4	6	6	80 #	124	#MELT	76.8	19.2		2	2	N		5.10 # -92.2	0.681	48.6	1.89		3.03	0.245	#-1.027	#0.893	#1.019	0.93		0.178
4	7	7	80 #	124	#MELT	73.6	18.4		4	4	N		4.72 # -81.8	0.596	46	2.28		3.04	0.238	#-1.003	#0.894	#0.958	0.94		0.193
4	5	9	325 #	16	#MELT	79.2	19.8		0.5	0.5	N		5.42 # -185.1	8.17	21.3	0.359		3.035	0.077	#-0.819	#0.254	#0.933	0.18		0.512
4	6	10	325		MELT	76.8	19.2		2	2	N		4.81 # -95.0	0.917	41.1	1.66		3.08	0.205	#-0.993	#0.726	#0.950	0.75		0.561
4	7	21	325		MELT	73.6	18.4		4	4	N		4.26 # -93.7	0.864	38.5	1.88		3.07	0.239	#-1.042	#0.706	#0.850	0.90		0.450
P-Type Factorial Experiment																									
5	22	22	-200		MELT	79.0	19.8	0.2	0.5	0.5	N		5.07 # -204.1	21.3	10	0.293		2.96	0.039	#-0.843	#0.112	#0.868	0.09		
5	23	23	-200		MELT	76.6	19.2	0.2	2	2	N		4.49 # -108.3	1.29	36.2	1.34		3.06	0.203	#-1.016	#0.600	#0.871	0.71		
5	24	24	-200		MELT	78.4	19.6	1	0.5	0.5	P		4.73 # 113.3	1.77	18.9	1.92		2.93	0.153	# 1.005	#0.481	#0.846	0.57		
5	25	25	-200		MELT	76.0	19.0	1	2	2	N		4.97 # -184.6	10.1	18.6	0.333		3.04	0.068	#-0.802	#0.214	#0.855	0.16		
5	22	38	A.J.#	3.1	#MELT	79.0	19.8	0.2	0.5	0.5	N		4.84 # -233.6	27.2	6.84	0.336		3.016	0.041	#-1.016	#0.079	#0.833	0.10		
5	23	39	A.J.#	2.5	#MELT	76.6	19.2	0.2	2	2	N		4.49 # -119.7	2.09	26.9	1.11		3.05	0.153	#-1.022	#0.421	#0.857	0.51		
5	28	48	A.J.#	4	#MELT	78.4	19.6	1	0.5	0.5	P		4.57 # 125.1	2.37	16.8	1.57		3.18	0.144	# 1.014	#0.418	#0.803	0.53		
5	25	41	A.J.#	4.3	#MELT	76.0	19.0	1	2	2	N		4.93 # -165.7	51	5.42	0.226		3.06	0.011	#-0.609	#0.057	#0.808	0.03		
Excess Boron																									
6	11	11	325			79.2	19.8	1		P		5.32 # 79.2		0.55	33.2	3.45		2.998	0.214	# 0.915	#0.904	#1.003	0.75		
6	12	12	325			78.4	19.6	2		P		5.31 # 80.2		0.545	33.2	3.45		2.997	0.222	# 0.927	#0.904	#1.001	0.78		
6	13	13	325			76.8	19.2	4		P		5.44 # 78.8		0.54	32.1	3.61		2.993	0.211	# 0.939	#0.879	#1.030	0.74		
6	14	14	325	To 1100 C before		73.6	18.4	8		P		5.42 # 90.9		0.7073	32.13	2.75		2.98	0.215	# 0.948	#0.852	#1.001	0.77	0.551	

January 11, 1989

Sub-Task #	Cast #	Sample #	Ranqsize 50%	Addition Method	Mole Fraction Si	Ge	P	Type	Conduct. W/P	Coef.	Resis.	Mobility	Conc.	Density	Conduct. Ratio	Maximum Wt. %
				Alternative Additions												
8		56	W.M.# 1.9	#Al2O3	79.8	20.0	0.23	P	4.47 #	122.5	1.34	32.2	1.44	3.01	0.230 # 0.955 #0.792 #0.780	0.93
8		60A	W.M.# 2.3	#control	79.8	20.0	0.23	P	4.36 #	123.3	1.36	31.1	1.48	3	0.260 # 0.973 #0.768 #0.752	0.97
8		57	W.M.# 3.2	#Y2O3	79.8	20.0	0.23	P	4.22 #	128.6	1.4	31.1	1.36	3.04	0.280 # 0.977 #0.760 #0.732	0.99
8		59	W.M.# 1.6	#Graphite	79.8	20.0	0.23	P	3.98 #	129.6	2.01	25.9	1.2	2.91	0.210 # 0.931 #0.624 #0.683	0.79 P
8		58	W.M.# 1.8	#V2O5	79.8	20.0	0.23	P	3.55 #	201.5	6.57	16.3	0.564	3.07	0.174 # 1.045 #0.361 #0.571	0.67
8	69a	79	# 2.4	#control	79.5	19.9	0.59 N		3.81 #	-119.5	1.3	41.4	1.16	2.98	0.288 #-1.043 #0.657 #0.730	0.98
8	69a	80	# 2.3	#2w/oBe	79.5	19.9	0.59 N		3.75 #	-118.6	1.27	41	1.2	3.01	0.296 #-1.053 #0.657 #0.721	1.01
8		85	W.M.# 1.8	#1% Ti	79.5	19.9	0.59 N		4.05 #	-202.9	3.8	43.6	0.377	2.99	0.268 #-0.898 #0.501 #0.728	0.55
8		98	L.M # 1.9	#layered m	79.9	20.0	0.11	P	3.70 #	160.9	2.55	34.91	0.704	2.98	0.274 # 0.908 #0.791 #0.605	1.08 0.446
				Pressure Assisted Reaction Sintering of Si, Ge and Boron												
8		66	insit# 4.2 #		79.8	20.0	0.23	P	4.18 #	149.5	2.39	29.3	0.892	2.97	0.224 # 0.938 #0.682 #0.698	0.86
8		66A	insit# 4.6 #		79.8	20.0	0.23	P	3.77 #	150.6	2.65	28.7	0.823	2.96	0.227 # 0.912 #0.662 #0.625	0.88 0.523
8		67	insit# 1.7 #		79.8	20.0	0.23	P	96.50 #	177.2	2.41	30	0.864	2.34	0.014 # 1.097 #0.696 #######	0.05
				ADVANCED PROCESSING STUDY												
TASK 1.2																
				Rapid Solidification												
1		61	G.A. #	13 #72% Silic?	?		0.23	P	5.00 #	221.1	5.15	42.6	0.285	3.27	0.190 # 0.885 #0.804 #0.755	0.83
1		110	G.A. #	15 #RS-154				N	4.51 #	-97.7	0.727	51.1	1.68	3.01	0.291 #-1.026 #0.906 #0.892	1.07 0.972
1		111	G.A. #	16 #RS-156				N	4.47 #	-402.3	0.781	51.86	1.54	2.99	0.366 #-1.029 #0.896 #0.877	1.08
1		112	G.A. #	15 #RS-157				P	4.96 #	117.8	1.07	33.74	1.73	2.983	0.262 # 0.998 #0.848 #0.879	0.96 SRDa
1		113	S.E													
1		114	S.E.													
1		115	M.S., 78%Si-22;runs 2175 and 2176, 78%Si-22%Ge, pistons cracked.													
1		71	Ospre# 20	#Run #2	?	?		P	5.02 #	125.5	1.32	32.9	1.44	2.96	0.238 # 0.978 #0.810 #0.875	0.88
2		76	Prod. Spec		79.5	19.9	0.59 N									
2		77	Prod. Spec		79.8	20.0	0.23	P								
				COMPOSITION/PROCESSING OPTIMIZATION												
TASK 1.3																
				Effect of Particle Size: N-type SiGe												
1		68	S.B. # 124 #		79.5	19.9	0.59 N		5.03 #	-121.6	1.06	55.1	1.07	2.87	0.277 #-1.019 #0.853 #0.957	0.93 0.832 0.168
1	69a	69	S.B. #13.5 #		79.5	19.9	0.59 N		4.82 #	-116.4	0.926	52.7	1.28	3.04	0.303 #-1.067 #0.861 #0.931	1.05 0.762 0.244
1	69a	70	DM # 3.9 #		79.5	19.9	0.59 N		4.17 #	-114.3	1.07	46.4	1.26	3.02	0.293 #-1.039 #0.755 #0.805	1.01 0.967 0.905
1		63	W.M # 3.3 #		79.5	19.9	0.59 N		4.11 #	-117.3	1.09	44.8	1.28	2.99	0.281 #-1.029 #0.732 #0.794	0.98 0.969 0.996
1		93	Hexan#1.75	#No exposu	79.5	19.9	0.59 N		3.97 #	-115.9	1.15	43.8	1.25	2.96	0.294 #-1.050 #0.711 #0.765	1.02 1.040 0.917
1		84	H2O # 1.3 #		79.5	19.9	0.59 N		3.74 #	-117.2	1.14	46.5	1.18	2.96	0.322 #-1.032 #0.742 #0.718	1.10 0.952 2.930
1		81	Attri# 3.3	#Butanol	79.5	19.9	0.59 N		3.54 #	-121.4	1.3	42.97	1.12	3.01	0.320 #-1.041 #0.675 #0.676	1.08 0.971 1.310
1		116	AJP # 2.8 #		79.5	19.9	0.59 N		4.43 #	-119.2	0.981	53.72	1.19	2.94	0.327 #-1.054 #0.859 #0.851	1.12 SRDa
				Effect of Particle Size: P-type SiGe												
2		73	S.B. # 124	#-80+200me	79.8	20.0	0.23 S	P	5.02 #	114.6	1.16	32.5	1.66	2.87	0.225 # 0.952 #0.813 #0.887	0.83 0.508 0.148
2		74	S.B. # 11	#-325mesh	79.8	20.0	0.23 S	P	5.25 #	117.0	1.14	32.8	1.67	2.94	0.229 # 0.975 #0.821 #0.928	0.84 0.501 0.278
2		78	S.B. # 4.5	#1 hr. S.B	79.8	20.0	0.23 S	P	4.37 #	119.5	1.28	31.5	1.55	2.98	0.255 # 0.963 #0.782 #0.767	0.94 0.619 0.991
2		62	W.M # 4.1 #		79.8	20.0	0.23 S	P	4.25 #	124.2	1.34	31.1	1.5	2.99	0.270 # 0.986 #0.769 #0.746	1.00 0.584 1.000
2	75o	75	shatt# 2.6 #		79.8	20.0	0.23 S	P	3.88 #	120.9	1.39	29.2	1.34	2.96	0.271 # 0.971 #0.724 #0.631	1.00 0.615 1.530
2		83	H2O # 1.3 #		79.8	20.0	0.23 S	P	3.63 #	124.2	1.7	27.6	1.33	2.95	0.250 # 0.934 #0.673 #0.629	0.93 0.535 2.840
2		72	Attri# 2.95	#Ethanol	79.8	20.0	0.23 A	P	3.32 #	131.3	2.06	25.1	1.21	2.98	0.252 # 0.946 #0.605 #0.570	0.95 0.537 2.200
2		82	Attri# 2.3	#Butanol	79.8	20.0	0.23 A	P	3.12 #	133.3	1.78	27.91	1.26	2.97	0.305 # 0.971 #0.676 #0.555	1.15 0.564 1.730
		117	AJP # 2.8 #		79.8	20.0	0.23	P	4.55 #	123.9	1.245	34.57	1.46	2.96	0.252 # 0.968 #0.852 #0.849	0.94 SRDa

January 11, 1989

Sub- Task	Cast #	Sample #	Parti Rang -	Feed size 50%	PaGa Addition Method	Mole Fraction Si	Ge	B	Ga	F	Type N/P	Thermal Conduct W/m-K	Abs. Seebeck Coef. mV/C	Elect. Resis. mohm-cm	Hall Mobility cm2/V-se	Carrier Conc. 1E20/cm3	Density (g/cc)	Z... 1/K	S/S1	Elect. Conduct. Ratio	K/K1	Z/Z1	Z1	Oxygen Max. Anal. IRT weight %
Effect of Oxygen																								
		99	S.M.	2.7	Acetone	79.8	20.0	0.23		LD	P	3.99	133.5	1.583	29.75	1.25	2.99	0.265	0.976	0.720	0.687	1.00		1.490
poor seal		100	SM(1)	3.5	Hexane,1"	79.8	20.0	0.23			P		129.4	1.42	31.99	1.38	2.99	ERR	0.990	0.783	0.000	ERR		0.67
		101	S.M.	1.6	Hexane	79.8	20.0	0.23	LD		P	4.1	131.7	1.62	31.32	1.23	3.02	0.261	0.956	0.757	0.705	0.98		0.37
		102	S.M.	1.5	Sealed	79.8	20.0	0.23	LD		P	3.9	139.0	2.109	30.15	0.983	3.03	0.235	0.912	0.710	0.657	0.90	0.519	0.23
		103		2.2	Control	79.8	20.0	0.23	MD		P	3.93	131.4	1.863	29.73	1.13	3	0.236	0.918	0.711	0.671	0.89		0.91
		104		2.2	Air Roast	79.8	20.0	0.23	HD		P	3.24	133.4	2.244	26.82	1.04	3	0.245	0.898	0.636	0.549	0.93		4.68
		105	TBD																					
		106	TBD																					
		107	TBD																					
Effect of Hot Pressing Parameters																								
4	86c	86		2	Short Soa	79.8	20.0	0.23		D	P	3.62	127.4	1.67	28.4	1.32	2.93	0.269	0.955	0.652	0.626	1.01		1.520
4	86c	88		2	Nor. Soak	79.8	20.0	0.23		D	P	3.78	127.5	1.63	28.2	1.36	2.96	0.264	0.969	0.689	0.656	0.99		
4	86c	87		2	Long Soak	79.8	20.0	0.23		D	P	4.03	127.1	1.5	29.1	1.43	2.98	0.267	0.987	0.715	0.702	0.99		
4	89d	89		2.2	T=1240(Co	79.8	20.0	0.23		1240	P	3.68	129.6	1.69	27	1.37	2.94	0.270	0.988	0.661	0.639	1.01		
4	89d	90		2.2	T=1255	79.8	20.0	0.23		1255	P	3.91	126.5	1.54	29.27	1.38	2.96	0.266	0.967	0.717	0.679	0.99		
4	89d	91		2.2	T=1270	79.8	20.0	0.23		1270	P	4.05	124.2	1.4	30.94	1.44	2.99	0.272	0.968	0.761	0.706	1.01		
4	89d	92		2.2	T=1285	79.8	20.0	0.23		1285	P	4.49	124.7	1.39	30.8	1.46	3-	0.249	0.978	0.759	0.784	0.93		1.500
4	94	94		1.9	T=1300	79.8	20.0	0.23	1300		P	4.18	122.7	1.3	33.04	1.45	3	0.277	0.959	0.814	0.729	1.03		
4	94	95		1.9	T=1315	79.8	20.0	0.23	1315		P	4.35	123.4	1.2	24.79	2.1	2.96	0.292	1.140	0.637	0.785	1.06		
4	94	96		1.9	T=1330	79.8	20.0	0.23	1330		P	4.54	123.1	1.22	28.17	1.82	2.94	0.274	1.066	0.712	0.808	1.00		1.750
4	94	97		1.9	T=1240(1o	79.8	20.0	0.23	LD		P	3.90	124.7	1.31	32.63	1.46	2.98	0.304	0.978	0.804	0.681	1.13	0.565	1.600
P-type SiGe/GaP																								
3	MHPG- 8P	Product.			BLEND	71.7	17.9	8.4	0.98	0.98	P	3.73	130.7	1.84	23.1	1.47	3.004	0.249	1.028	0.570	0.652	0.92		
Effect of Particle Size: N-type SiGe/GaP																								
3	MHPG- 16N	Produ		3.9	BLEND	76.4	19.1		1.96	2.53	N	4.25	-94.3	0.85	47	1.71	3.034	0.246	-1.000	0.838	0.842	1.00		
3	MHPG- 19N	Produ		4.2	BLEND	76.4	19.1		1.96	2.53	N	3.70	-95.5	0.954	36.79	1.78	3.031	0.259	-1.033	0.664	0.735	0.96	0.821	1.201
		Annealed 100 hours, 1220 C in air																					0.830	
		Annealed 100 hours, 1240 C in vacuum																					0.667	
3	MHPG- 20N	Produ		2.75	BLEND	76.4	19.1		1.96	2.53	N	4.13	-96.3	0.953	37.33	1.76	2.971	0.236	-1.036	0.671	0.820	0.88	0.797	1.420
		annealed at 1165 C-100 hours, and at 1225 C-8 hours in ai											-91.8	0.715	50.25	1.74	3.03		-0.981	0.900			0.814	
3	MHPG- 21N	Produ		2.75	BLEND	76.4	19.1		1.96	2.53	N	3.94	-99.1	0.984	36.34	1.75	3.033	0.253	-1.063	0.652	0.782	0.94	0.802	1.520
3	MHPG- 23N	Extra		1.9	BLEND	76.4	19.1		1.96	2.53	N	3.76	-100.8	1.23	34	1.50	3.03	0.220	-1.000	0.581	0.736	0.79		
3	MHPG- 22N	AJP		1.2	BLEND	76.4	19.1		1.96	2.53	N	3.50	-106.0	1.389	31.08	1.45	3.013	0.231	-1.035	0.527	0.683	0.83	0.954	1.710
3	MHPG- 7N	Produ		2	BL10hr at	76.4	19.1		1.96	2.53	N	3.28	-119.2	1.54	40.13	1.01	3.024	0.281	-0.970	0.611	0.621	0.93	0.826	1.590
		After 100 hrs at 1240 C in Vacuum																					0.731	
3	MHPG-24N	Slice			BLEND	76.4	19.1		1.96	2.53	N	3.66	-103.5	1.517	28.91	1.43	3.035	0.193	-1.001	0.488	0.714	0.68		
MOD-RTG Specifications																								
		130			First Pre	79.6	19.8			0.59	N	5.09	-104.2	0.8475	53.19	1.39	2.915	0.251	-0.995	0.891	0.990	0.89	0.942	
		131		6.1				0.25			P	4.75	117.7	1.112	34.21	1.64	2.992	0.262	0.973	0.855	0.838	0.97	0.506	
GPHS Material																								
3		A-3334				77.8	21.9	0.25			P	5	112.5	1.065	34.15	1.72	3.006	0.238	0.950	0.858	0.886	0.87	0.522	0.21
3		A-3332				77.5	21.9			0.59	N	4.65	-108.9	0.869	55.75	1.29		0.293	-1.002	0.913	0.901	1.02	0.917	0.137

January 11, 1989

Sub-Task	Cast #	Sample #	Partifeed Rangsize - 50%	FaHot Pressing Temperatu	Mole Fraction Si Ge B Ga P	Type N/F	Conduct (W/m-K)	S Coef. (muV/C)	Resis. (ohm-cm)	Mobility (cm2/V-se)	Conc. (1E20/cm3)	Density (g/cc)	1/A, Seebeck, Elect. Conduct. Ratio	MaximuAral. IRT weight %
		SYNCAL SAMPLES												
N-1	120			as received		N						3.06		0.784
N-2	121			as received		N								
P-3	122			as received		F						3.52		
P-4	123			as received		P								
		TECO SAMPLES												
		T257				P	#	91.2	0.784	24.05	2.54	2.949	ERR # 0.934 #0.635 #0.000	ERR 0.458
		T255				N	#	-71.0	0.884	38.05	1.86	3.037	ERR #-1.006 #0.696 #0.000	ERR 0.727
		Si/Ge RATIO VARIATIONS												
		153	# 1.9	# 80% Si	Si78.4 19.6	2 N	3.9 #	-105.0	0.9122	49.35	1.39	3.01	0.310 #-1.003 #0.827 #0.759	1.10 0.919
		annealed at 1165 C-100 hours, and at 1225 C-8 hours in air						-115.0	1.004	54.5	1.14	3.029	#-0.994 #0.860	0.91
		154	# 2.1	# 85% Si	Si83.3 14.7	2 N	4.25 #	-95.9	0.76	47.94	1.7	2.64	0.285 #-1.014 #0.853 #0.841	1.04 0.968
		155	# 2	# 90% Si	Si88.2 9.8	2 N	4.75 #	-90.2	0.7346	43.11	1.97	2.58	0.233 #-1.027 #0.802 #0.952	0.89 0.870
		156	# 1.8	# 95% Si	Si93.1 4.9	2 N	6.53 #	-82.7	0.6218	41.8	2.4	2.494	0.169 #-1.040 #0.825 #1.331	0.67 0.733
		157	# 1.7	#100% Si	Si98.0 0.0	2 N	20.32 #	-79.8	0.5569	38.71	2.9	2.349	0.056 #-1.103 #0.809 #4.209	0.23 0.395
		Doping Level Variations												
		153	# 1.9 #		78.4 19.6	2.00 N	3.9 #	-105.0	0.9122	49.35	1.39	3.01	0.310 #-1.003 #0.827 #0.759	1.10 0.919
		151	# 2.4 #		79.3 19.8	0.90 N	3.83 #	-110.6	1.037	46.28	1.3	2.99	0.308 #-1.022 #0.760 #0.741	1.07 0.918
		152	# 2.1 #		79.4 19.8	0.77 N	3.81 #	-110.8	1.03	47.22	1.29	3.02	0.313 #-1.020 #0.774 #0.737	1.09 0.926
		63 W.M	# 3.3 #		79.5 19.9	0.59 N	4.11 #	-112.3	1.09	44.8	1.28	2.99	0.281 #-1.029 #0.732 #0.794	0.98 0.969 0.996
		158	# 2.5 #		79.8 19.9	0.30 N	3.98 #	-128.6	1.254	52.74	0.945	3.035	0.332 #-1.013 #0.787 #0.749	1.08 SRDa
		159	# 2.8 #		79.9 20.0	0.15 N	4.04 #	-177.8	2.273	53.21	0.517	2.996	0.344 #-1.034 #0.663 #0.723	0.98 SRDa
		160	# 2.5 #		79.9 20.0	0.07 N	4.11 #	-228.9	4.209	45.56	0.326	2.968	0.303 #-1.056 #0.494 #0.707	0.78 SRDa
6	14	14	-325	To 1100 C before	73.6 18.4 8	P	5.42 #	90.9	0.7072	32.13	2.75	2.98	0.215 # 0.948 #0.852 #1.001	0.77 0.551
		89	# 2.2 #		79.8 20.0 0.23	P	3.68 #	129.6	1.69	27	1.37	2.94	0.270 # 0.988 #0.661 #0.639	1.01
		161	# 2.2 #		79.9 20.0 0.12	P	#	160.6	2.018	38.9	0.796	2.971	ERR # 0.958 #0.894 #0.000	ERR
		162	# 2.2 #		80.0 20.0 0.06	P	#	205.0	3.937	36.24	0.438	2.994	ERR # 0.934 #0.777 #0.000	ERR
		124	# 8.1 #		80.0 20.0 0.03	P	5.73 #	278.4				2.982	ERR # ERR # ERR # ERR	ERR 0.184
		Hydride Additions												
		These three compacts prepared from a single batch of powder of SiGe												
		163	# 2	#Control	79.5 19.9	0.59 N	3.87 #	-114.5	1.119	46.72	1.2	2.991	0.303 #-1.016 #0.749 #0.744	1.04 SRaDp
		164	# 2	#+2w/o ZrH	79.5 19.9	0.59 N	4.1 #	-247.2	Hall Data Unreliable			3.031		SRaDp
		165	# 4.2	#+2w/o TiH	79.5 19.9	0.59 N	4.3 #	-204.0	3.703	50.41	0.335	3.043	0.261 #-0.954 #0.551 #0.741	0.68 SRDa
		Single Crystal-based materials												
		170 p-type Single Crystal				P		1.8	4.085	44.03	0.347			SRa,Dp
		171 sinter 2.5				P	#	110.4	4.647	70	0.192	2.335	S,u,n UNRELIABLE	SRDp
		172 n-type Single Crystal				N		1.8	2.654	32.38	0.255			SRDp
		173 sinter 4.8				N	#	-201.0	3.436	76.87	0.237	2.33	S,u,n UNRELIABLE	SRDp
		ET-820SiMo					#	-53.3	0.3255	32	6	2.752		SRDp

January 11, 1989

Sub-Task #	Cast #	Sample #	Partisize - 50%	Feed Temperature	Pa Pressing	Si	Ge	Mole Fraction B	Ga	P	Type	Conductivity N/P	Seebeck Coef. (W/K-K	Resis. (muV/C	Mobility (muna-cm	Conc. cm2/V-se	1E20/cm3	Density (g/cc)	Band Gap 1/k	Electrical Conduct. Ratio	Maximum Mat. IRT weight %
	Boron precipitate Study, CR&D													1.8							
	180		6.1		98		2			P		127.8					2.315				
	181		3.9		98.5		1.5			P		128.7					2.289				
	182		4.7		99		1			P		133.5					2.293				
	183		4		99.7		0.3			P		146.4					2.263				
	184		3.3		79.2	19.8	1			P		87.3					2.993				
	185		9.7		80	20				P		498.5					2.923				
	186		6		77.6	19.4	3			P		84.5					2.983				
	GaP solubility in 50% Si-50% Ge																				
	191	325	4.6	MELT	46	46		4	4	N	3.982	-156.8	6.82	19.03	0.48	3.86	0.091	-0.879	0.232	0.708	0.25
	192	325	5.6	MELT	48	48		2	2	N	3.441	-166.7	5.01	26.36	0.47	3.923	0.161	-0.924	0.319	0.610	0.45
	193	325	5	MELT	49	49		1	1	N	4.074	-171.7	5.5	27.54	0.41	3.895	0.132	-0.889	0.320	0.714	0.35
	GaP solubility in 80% Si-20% Ge																				
	196	325	3.4	MELT	73.1	18.3		3.5	5.2	N	3.843	-81.5	0.824	34.29	2.21	2.954	0.210	-0.982	0.660	0.778	0.82	1.18
	197	325	5.6	MELT	76	19		1.6	3.4	N	4.045	-80.5	0.675	37.45	2.47	3	0.237	-1.026	0.745	0.827	0.95	1.19
	198	325	4.8	MELT	77.3	19.3		0.8	2.6	N	4.127	-82.4	0.684	39.36	2.32	3.006	0.241	-1.019	0.769	0.839	0.95	1.06
	199	325	4.6	MELT	77.9	19.5		0.4	2.2	N	4.127	-86.4	0.724	40.92	2.11	2.999	0.250	-1.018	0.777	0.832	0.97	1.18
	Pressure Assisted Rxn Sintering Si,Ge,GaP,Ga2O3 elem method																				
	212	325	3.8	POWD	78.4	19.6		2	2	N	4.658	-127.1	2.083	25.78	1.16	2.953	0.166	-1.109	0.409	0.892	0.56	
	213	325	3.8	POWD	76.5	19.1		1.9	1	N	5.14	-166.7	15.22	9.49	0.44	2.946	0.036	-0.894	0.113	0.907	0.10	
	Demonstrate reproducibility of ITM-197																				
	232	325	5	MELT	76	19		1.6	3.4	N		-82.4	0.677	36.22	2.43	3.019	ERR	-1.043	0.757	0.000	ERR	0.923
	234	325	4.2	MELT	74.7	18.7		1.6	5	N		-79.5	0.603	40.62	2.55	2.984	ERR	-1.030	0.816	0.000	ERR	1.14
	237	325	5.2	MELT	76.9	19.2		1.6	2.2	N		-97.3	0.834	41.31	1.82	3.024	ERR	-1.065	0.750	0.000	ERR	0.944

::
January 11, 1989

Sub-Task	Cast #	Sample #	PartiFeed Rangsize - 50%	PaHot (#Pressing Temperatu	Si	Ge	Mole Fraction B	Ga	P	Type N/P	Conduct (W/m-K	SCoef. (muV/C,	Resis. muhm-cm	Mobilit cm2/V-se	Conc. 1E20/cm3	2.515 0	0.25149 0.25241	-0.595	0.891 0.854 0	0.990	0.891	0.942 0.506 Anal. IRT weight %
CONTROLED POROSITY																						

Note: for slices k is calculated from diffusivity measurements at 400 C using Cp=0.6677 J/g-k

Sample		Si	Ge	P	N/P	Conduct	SCoef.	Resis.	Conc.						
201	##	79.5	19.9	0.59	N	#	-115.4	1.172	1.15	2.934	ERR #	-1.002 #	0.000 #	0.000	ERR
202	##	79.5	19.9	0.59	N	#	-132.8	9.716		2.361	ERR #	ERR #	ERR #	ERR	ERR
203 Compact	##	79.5	19.9	0.59	N	1.56 #	-144.0			2.239	ERR #	ERR #	ERR #	ERR	ERR
203-T Slice	##	79.5	19.9	0.59	N	#	-141.5	29.68		2.059					
203-1 Slice	##	79.5	19.9	0.59	N	1.92 #	-138.2	30.56		2.025					
203-2 Slice	##	79.5	19.9	0.59	N	1.75 #	-135.5	30.22		2.18					
203-3 Slice	##	79.5	19.9	0.59	N	1.67 #	-138.8	33.27		2.198					
203-4 Slice	##	79.5	19.9	0.59	N	1.66 #	-138.9	37.08		2.205					
203-5 Slice	##	79.5	19.9	0.59	N	1.63 #	-140.4	41.58		2.204					
203-6 Slice	##	79.5	19.9	0.59	N	1.85 #	-141.2	50.51		2.203					
203-B Slice	##	79.5	19.9	0.59	N	#	-145.5	52.65		2.126	ERR #	ERR #	ERR #	ERR	ERR
204 Compact	##	79.5	19.9	0.59	N	1.27 #	-152.3			2.096	ERR #	ERR #	ERR #	ERR	ERR
204-T Slice	##	79.5	19.9	0.59	N	1.16 #	-152.3	192.1		2.073	0.010 #	ERR #	ERR #	ERR	ERR
204-1 Slice	##	79.5	19.9	0.59	N	1.24 #	-151.8	176.7		2.079	0.011 #	ERR #	ERR #	ERR	ERR
204-2 Slice	##	79.5	19.9	0.59	N	1.24 #	-152.1	156.5		2.084	0.012 #	ERR #	ERR #	ERR	ERR
204-3 Slice	##	79.5	19.9	0.59	N	1.31 #	-151.5	121.3		2.091	0.014 #	ERR #	ERR #	ERR	ERR
204-4 Slice	##	79.5	19.9	0.59	N	1.38 #	-151.0			2.036	ERR #	ERR #	ERR #	ERR	ERR
204-5 Slice	##	79.5	19.9	0.59	N	1.33 #	-150.9	109.8		2.122	0.016 #	ERR #	ERR #	ERR	ERR
204-6 Slice	##	79.5	19.9	0.59	N	1.39 #	-150.3	105.3		2.145	0.015 #	ERR #	ERR #	ERR	ERR
204-B Slice	##	79.5	19.9	0.59	N	1.37 #	-149.9	98.72		2.114	0.017 #	ERR #	ERR #	ERR	ERR
205	##	79.5	19.9	0.59	N	3.86 #				2.986					
206	##	79.5	19.9	0.59	N										
207	##	79.5	19.9	0.59	N										
208	##	79.5	19.9	0.59	N										
209	##	79.5	19.9	0.59	N										

COMMENTS

64,65 NO COMPACTS PREPARED

69a, three castings combined into one batch of powder. See W.L. 06155-384-4,5,6

75b, three castings combined into one batch of powder. See W.L. 061785-384-4,5,6

Insitu=Elements reacted in Hot Press: Pressure Assisted Reaction Sintered

Blend=GaP mechanically blended with SiGe feed powder to hot press

Melt=GaP added directly to the SiGe melt, during vacuum casting

G.A.=Gas Atomized (GE-CRD) W.M=Wet Milled, Acetone SM(1)=Steel ball milled in a Nylon Bag.

Osprey=Rapid quenched S.H.=Shatter Boxed Only Mill emptied in air, Nylon bag seal imperfect

DM=Shatter Box + 4 hours Dry Milling AJP=Air Jet Pulverized

Attrit=Attrition Milled M.S.=Melt Spinning

L.M.=Mixed Doped and Undoped Powder S.M.=Steel Ball Milled

S.E.=Spark Erosion Method

January 11, 1989
PartiFeed PaGaP

Sub- Task	Cast #	Sample #	Rangsize - 50%	Addition Method	Si	Ge	B	Ga	P	Type	Thermal Conduct (W/m-K)	SeeCoef. (muV/C)	Elect. Resis. (mohm-cm)	Hall Mobility (cm2/V-sec)	Carrier Conc. (E20/cm3)	Density @ 100K (g/cc)	S/Si	Elect. Conduct.	k/xzl Z/Izl Ratio	Oxygen Anal. IRT weight I
Zone Leveled Material, RCA data										P	6.20	190.49	2.316	44.98	0.600					
For n,p between 0.6 E20/cm3 and 2.0 E20/cm3 the following re										P	6.12	177.68	2.021	44.18	0.700					
are good to better than 2% for zone leveled material.										P	6.04	167.29	1.796	43.50	0.800					
										P	5.98	158.63	1.618	42.91	0.900					
				ln(QP)##ln(p)+			5.01			P	5.92	151.26	1.474	42.39	1.000					
				ln(uP)##ln(p)+			3.74			P	5.87	144.89	1.355	41.93	1.100					
				ln(kP)##ln(p)+			1.77			P	5.83	139.31	1.255	41.51	1.200					
										P	5.79	134.37	1.169	41.13	1.300					
										P	5.75	129.95	1.095	40.77	1.400					
										P	5.71	125.96	1.030	40.45	1.500					
										P	5.68	122.34	0.973	40.15	1.600					
										P	5.65	119.04	0.922	39.87	1.700					
										P	5.62	116.01	0.877	39.60	1.800					
										P	5.59	113.21	0.836	39.36	1.900					
										P	5.57	110.62	0.799	39.12	2.000					
				ln(QN)##ln(n)+			#####			N	5.52	-159.56	1.356	76.80	0.600					
				ln(uN)##ln(n)+			4.18			N	5.45	-147.68	1.218	73.33	0.700					
				ln(kN)##ln(n)+			1.66			N	5.39	-138.11	1.109	70.45	0.800					
										N	5.33	-130.18	1.021	68.01	0.900					
										N	5.29	-123.47	0.949	65.89	1.000					
										N	5.24	-117.70	0.887	64.03	1.100					
										N	5.20	-112.67	0.835	62.38	1.200					
										N	5.17	-108.23	0.789	60.90	1.300					
										N	5.14	-104.28	0.749	59.56	1.400					
										N	5.11	-100.73	0.714	58.34	1.500					
										N	5.08	-97.52	0.683	57.23	1.600					
										N	5.05	-94.60	0.654	56.19	1.700					
										N	5.03	-91.92	0.629	55.24	1.800					
										N	5.00	-89.46	0.605	54.35	1.900					
										N	4.98	-87.19	0.584	53.52	2.000					

Sub-Task #	Cast #	Sample #	Rangsize - 50%	ERR Partifeed Method	Addition B	Addition Ga	Addition P	Type N/P	Thermal Conduct (W/m-K)	Abs. See Coef. (mcV/C)	Elect. Resis. (ohm-cm)	Hall Mobility (cm2/V-se)	Carrier Conc. (1E20/cm3)	Density (g/cc)	Z@1000 1/K	S/Sz	Elect. k/kz Conduct. Ratio	I/Iz	Oxygen Anal. IRT weight %
Commonly Refered to Data Set: Room Temperature Values																			
JPL 50 hour data (1500 hr data identicle)								N	5.08	-101.40	0.83	50.87	1.48		0.244	#-1.000	#0.868	#0.994	0.874
JPL 50 hour data (1500 hr data identicle)								P	5.78	121.00	0.93	40.99	1.64		0.272	# 1.000	#1.024	#1.020	1.004
ET-285-2N Battelle Diffusivity Data, Ames S and rho Extrapolat								N	5.55	-125.91	0.72	90.06	0.96		0.396	#-1.000	#1.351	#1.047	1.290
ET-285-4P Used in Bicouple Predictions				To RT				P	4.39	99.18	1.01	24.33	2.55		0.222	# 1.000	#0.639	#0.805	0.794
SiGe/GaP Syncal data and samples Sept.-Oct. 1981								N	3.07	-72.89	0.84	26.16	2.86		0.207	#-1.000	#0.544	#0.636	0.856
SiGe/GaP Used in Bicouple Predictions								P	3.06	103.88	1.52	17.93	2.30		0.233	# 1.000	#0.466	#0.556	0.837
SiGe Syncal Memorandum #6, March 3, 1970								N	5.1033	-121.64	0.9466	64	1.03		0.306	#-1.000	#0.979	#0.968	1.01
SiGe Syncal Memorandum #6, March 3, 1970								P	6.3044	130.45	1.2251	37	1.39		0.220	# 1.000	#0.901	#1.096	0.82
SiGe/GaP 8311 Data Se8311-1N								N	3.28	-106.49	0.9345	50	1.34		0.370	#-1.000	#0.826	#0.636	1.30
SiGe/GaP 8311 Data Se8311-4P								P	3.2968	117.388	1.23722	29	1.75		0.338	# 1.000	#0.725	#0.585	1.24
This Data set represents the average electrical properties determined by Ames, Battelle and TECO on samples from batch numbers 8311-4P and 8311-1N. These materials were made by TECO from GE material in November 1983. Thermal Conductivity Are From the 1981 Purdue Measurements on Syncal Made Materials. The P resistivity was taken from the battelle and TECO data, Since there was obviously a problem with the Ames Test.																			
Theortical Minimum, G. 0.1								N	3.41	-123.47	0.949	65.89	1	3.0098	0.472	#-1.000	#1.000	#0.645	1.55

APPENDIX B

ADVANCED TECHNOLOGY THERMOELECTRIC MATERIALS

APPENDIX B
ADVANCED TECHNOLOGY THERMOELECTRIC MATERIALS

B.1 OBJECTIVES

The objectives of this part of the Program were to identify new n- and p-type thermoelectric materials that have an average figure-of-merit over the temperature range from 300°C to 1000°C of at least 1.3×10^{-3} $°K^{-1}$. These materials were also to be stable for at least 40,000 hours of operation, have low vapor pressures (less than 10^{-6} torr at 1100°C), have good mechanical strengths, and have an operating temperature range between 150°C and 1100°C. Electrical contacting system(s) compatible with these materials were also to be identified.

A Program of search for materials that will meet the above objectives was divided into the following areas of effort:

1. From a consideration of data in the literature and the physics of material behavior, the materials, or classes of materials, that appear to have the potential to meet the Program objectives were identified or selected. Also a priority list for the selected materials was established.

2. Test samples were to be made and tested with varying sample compositions to identify trends of physical property changes and to establish a basis for a judgement about the possibility of the materials meeting the Program objectives.

3. The most promising candidates were to be selected for optimization of properties and development of an electrical contacting system.

4. In-gradient life tests on selected materials were to be conducted to determine the system viability of the materials.

The following sections of this Appendix contain a discussion of Item 1 based on present day information, and a description of the methods that can be used to accomplish the other objectives of the proposed effort. Only limited progress was made on these tasks as much of the Program was directed by the Department of Energy to emphasize Si-Ge alloys.

B.2 CANDIDATE THERMOELECTRIC MATERIALS

B.2.1 SILICON GERMANIUM ALLOYS

Present day Radioisotope Thermoelectric Generators[1] (RTGs) characteristically use silicon-germanium alloys as the active thermoelectric materials. The hot-junction operating temperature of these thermoelements is about 1273 K (1000°C). The alloys typically have nominal compositions of 78 a/o Si plus 22 a/o Ge and 64 a/o Si plus 36 a/o Ge. The 78 percent Si alloy begins melting at 1540 K (1267°C), which sets the upper limit on the operating hot-junction temperature. Lower operating limits are set by the metal-to-semiconductor bond interface materials and by the decrease in efficiency as the cold junction temperature is increased. In Figure B-1 the thermoelectric figure-of-merit, Z, is shown as a function of temperature for the n-type and p-type alloys.[2] Note that Z starts to decrease at about 1100 K. The drop is caused by the onset of the intrinsic behavior of the Si-Ge materials at these high temperatures. The thermal band-gap[3] of the material is 0.94 eV at 300 K and drops to 0.51 eV at 1300 K. Theoretical considerations[4] suggest that the semiconductor band-gap should be about $10k_BT_{MAX}$, where T_{MAX} is the maximum operating temperature and k_B is Boltzmann's constant. Thus, for T_{MAX} equal to 1323 K, one would like to use a material with a band-gap grater than or equal to 1.14 eV. This means Si-Ge has a less than optimum band-gap. This is reflected in the downward curvature of Z at the highest temperatures in Figure B-1. So, for operation at or above 1323 K, one is looking for materials with a higher band-gap than Si-Ge alloys.

B.2.2 OTHER MATERIALS

The operating efficiency of thermoelectric generators can be calculated[5] from a knowledge of Z. Since, in general, Z is temperature dependent, an average value over the operating temperature interval can be computed.[6] The value of Z at any particular temperature is given by

$$Z = S^2 \sigma / K$$

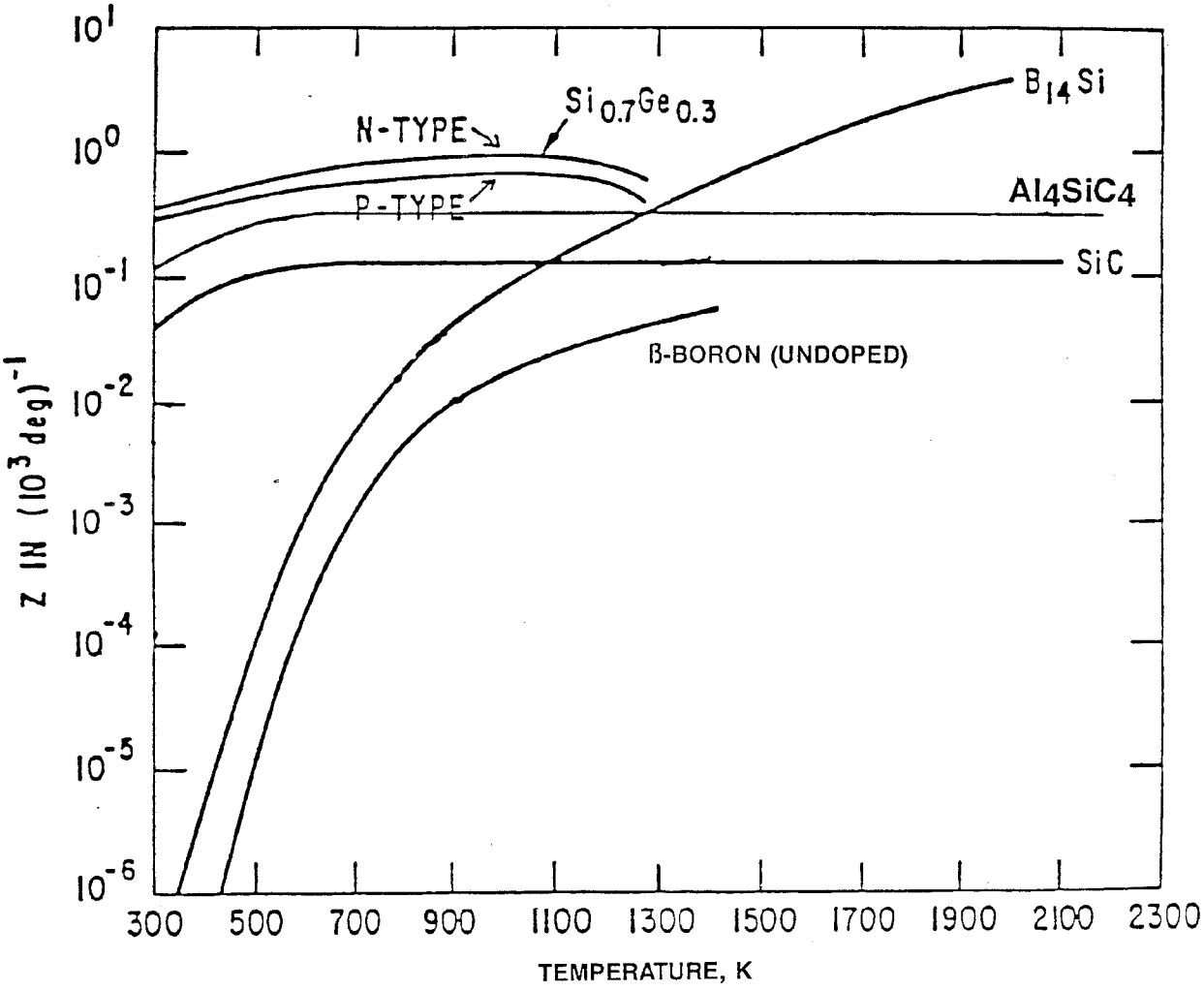

Figure B-1. The Thermoelectric Figure-of-Merit (Z) as a Function of Temperature as Estimated for a Number of Compounds

where S is the Seebeck coefficient, σ the electrical conductivity, and K the thermal conductivity at that temperature. Following the analysis of Goff and Lowney,[7] the total K can be written as the sum of a lattice part, K_g, and an electronic part, K_e. Thus:

$$K = K_e + K_g.$$

The electronic part is related to the electrical conductivity by

$$K_e = L_o \sigma T$$

where L_o is the Weidemann-Franz, Lorentz ratio.

Thus, if K_g equals 0, one obtains

$$ZT = S^2/L_o$$

The value of L_o for free electrons is 2.45×10^{-8} $volt^2/deg^2$ which is also approximately the value for semiconductors. Thus if

$$S \geq 157 \text{ microvolt/K}$$

one obtains

$$ZT \geq 1.$$

For Si-Ge alloys at 1000 K, the measured value of ZT is 0.75. Note that ZT values of the order of 1 or larger are needed to obtain usable efficiencies. The problem then of finding new thermoelectric materials is to find ones with large S values and K_g values approaching zero. Most metals have S values of 20 microvolt/K or less, hence are not useful. Most large band-gap semiconductors have S values of 100 to 1000 microvolts/K, and are therefore possible candidates. The salient problems are to find low K_g values, and high σ values.

Since σ is directly related to the carrier mobility, μ, by:

$$\sigma = \eta e \mu,$$

one needs high μ values. η is the carrier concentration and e is the electron charge. To obtain appropriate values of S the value of η is of the order of $2 \times 10^{20}/cm^3$. For band-type rather than hopping-type conductivity the mobility needs[8] to be:

$$\mu \geq 0.5 \text{ cm}^2/\text{volt sec.}$$

This sets a lower limit on σ of

$$\sigma \geq 16 \text{ ohm}^{-1}\text{cm}^{-1}$$

The currently used Si-Ge alloys have values of σ of approximately 1000 $\text{ohm}^{-1}\text{cm}^{-1}$.

The theory of the lattice thermal conductivity of nonmetallic solids has been developed recently by Slack.[9] One new concept is that any crystal possesses a minimum K_g. Thus, as long as the basic crystal structure is maintained, the phonon conductivity K_g cannot be reduced below this value no matter how many different varieties of phonon scattering are introduced. In Figure B-2 the K_g for Si, Ge and $Si_{0.7}Ge_{0.3}$ alloy are plotted. The dashed line gives the minimum K_g calculated from

$$K_{min}(\text{Si-Ge}) = 0.7\ K_{min}(\text{Si}) + 0.3\ K_{min}(\text{Ge})$$

The values for Si and Ge are taken from Table XVII of Slack.[9] The values of K_{min} are calculated for $T > \Theta$. However, K_{min} is rather independent of temperature for T greater than 300 K, so the temperature dependence may be initially ignored. Figure B-2 also shows the effect of alloying on K_g in the curve labeled "undoped alloy". Here the phonons are scattered by the mass fluctuations between Si and Ge atoms located on the lattice sites. If the large-grain size or single crystal $Si_{0.7}Ge_{0.3}$ alloy is further doped with $1.8 \times 10^{20}/cm^3$ of B or P, the K_g curve drops even further to that

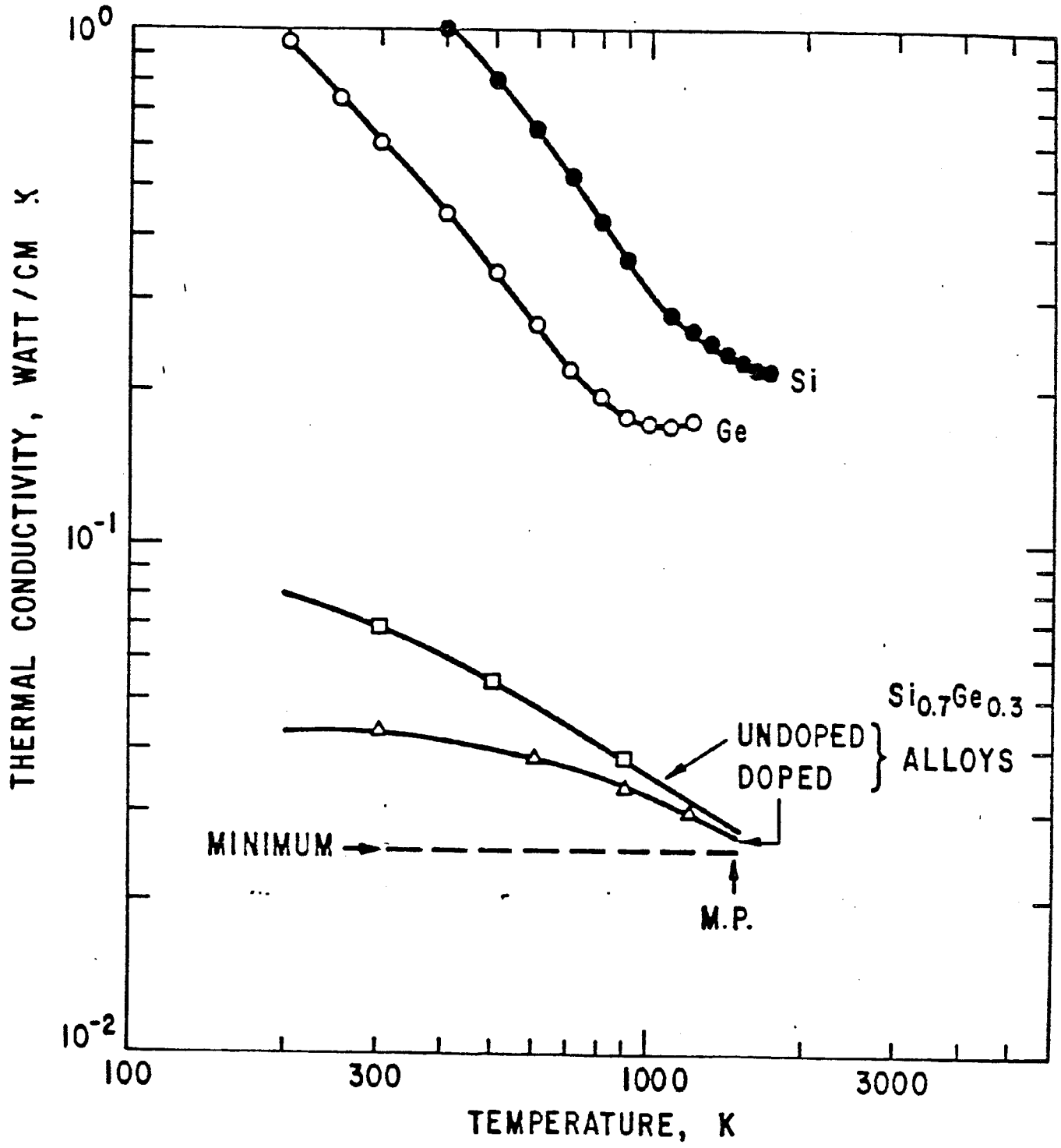

Figure B-2. Thermal Conductivity Versus Temperature for Undoped Si and Ge and for a Doped and Undoped Si-Ge Alloy. The Dashed Line is the Calculated Minimum Thermal Conductivity for a $Si_{0.7}Ge_{0.3}$ Alloy.

labeled "doped". From Figure B-2 one can see that the very "best" $Si_{0.7}Ge_{0.3}$ can only be improved at most to a 70 percent increase in Z at 300 K and a 30 percent increase in Z at 1000 K. It may be that by decreasing the grain size of a polycrystalline $Si_{0.7}Ge_{0.3}$, or by adding GaP to the lattice, one may affect this possible improvement in Si-Ge alloys.

The next method of reducing K_g is to use materials with a large average atomic mass, M. This technique was pioneered by Ioffe, and resulted in PbTe and Bi_2Te_3 based thermoelectrics. However, large M means, in general, low melting points, high vapor pressures, high thermal-expansion coefficients, low strengths, and poor mechanical properties. Thus, searching for large M materials is not the best approach.

A third method of reducing K_g is to look for crystals with a large number of atoms, n, in the primitive crystallographic unit cell. According to Slack[9] the value of K_g is given by:

$$K_g = \left(\frac{B \bar{M} \delta \Theta^3}{n^{2/3} \gamma^2} \right) \frac{1}{T}$$

Here B is a constant, δ^3 the average volume per atom, Θ the Debye temperature, and γ the Gruneisen constant. It can also be shown that γ becomes larger as the internal free volume of the lattice decreases. For 4-coordinated lattices such as Si or Ge, γ is approximately 0.7; for 12-coordinated lattices $\gamma \simeq 2.7$. Thus if we choose a 10-coordinated lattice with γ approximately 2.5 and n equal to 20, the K_g will be lower than that in pure Si or Ge by a factor of about 50. This analysis illustrates the leverage one has on choosing K_g by choosing the right alloy structure. The Si-Ge alloys have a lattice with about as high a thermal conductivity as one could anticipate ever using. Such crystals work only because K_g has been reduced to values near K_{min}.

When considering materials other than Si-Ge alloys it may be noted that there are semiconducting compounds which are still semiconducting solids at temperatures far above the melting point of Si (1681 K). These hold out the

promise of obtaining higher Carnot efficiencies than available with Si-Ge when higher temperature heat sources become available.

B.2.3 SiC AND Al_4SiC_4

Using elements from the fourth column of the periodic table, the next most refractory material above Si is SiC. It is the obvious choice[10] for higher Carnot efficiencies if everything else is satisfactory. Its melting point is 3100 K. It can be made both n- and p-type, and both have good carrier mobilities. Its Z values have been estimated by Lowney and Goff[10] assuming that K_g equals 10^{-2} watt/cm K. However, from the values in Slack[9] the calculated K_{min} is

$$K_{min}(SiC) = 7.5 \times 10^{-2} \text{ watt/cm K}$$

Thus, the ZT values in Figure 4 of Lowney and Goff[10] are reduced by a factor of 5 to 7 times. The resultant Z versus T curve for cubic SiC, n-type doped at $2 \times 10^{20}/cm^3$ is shown in Figure B-2. These Z values are calculated assuming that the K_g of SiC can be reduced to its minimum value by some procedure such as making mixed crystals of SiC with AlN or BP and then using free carrier scattering and grain boundary scattering in addition. Such approaches have not tried for SiC. It is concluded that a material other than SiC is needed for temperatures above 1000°C.

The high K_{min} of SiC is caused by its high Debye temperature and simple crystal structure with only 2 atoms per unit cell in the cubic polytype. By choosing a ternary compound such as Al_4SiC_4 with n equal to 18 atoms in a unit cell, we can reduce K_{min}. If it is reduced by a factor of $n^{2/3}$ from that of SiC, we would expect a K_{min} of

$$K_{min} = (7.5 \times 10^{-2}/9)^{(2/3)} = 1.7 \times 10^{-2} \text{ watt/cm K}$$

This would be a very useful value, however, a more likely value would be somewhat higher than that of Si-Ge, say about 3.5×10^{-2} watt/cm K.

The compound Al_4SiC_4 can be thought of as Al_4C_3 plus SiC. Its structure has been worked out,[11-13] it is stable[12] to at least 1900°C, and is yellow to transparent in color, which means a band-gap of 2 to 3 eV. Furthermore, it is stable to degradation by moisture in air,[14] which Al_4C_3 is not. If it has doping and mobility characteristics similar to SiC, it would be worth investigating. Dopant elements might be beryllium, boron, phosphorus, or nitrogen. Some preliminary studies of this material would appear to be worthwhile.

B.2.4 OTHER CHOICES

There are other binary, semiconducting carbides such as Be_2C, B_4C, and Al_4C_3. Of these only B_4C is stable in the presence of moisture, and will be discussed later. Ternary carbides such as[15,16] $Al_8B_4C_7$, $Ce_5B_2C_6$ may be interesting. Further studies are needed to ascertain more of their physical properties.

B.2.5 SILICIDES

There are a number of silicide semiconductors as shown in Table B-1. Their band-gaps vary from 0.2 to 1.8 eV. They are mainly disilicides. It is not known whether $IrSi_3$ is a semiconductor or not. They can all be considered to be cases of metal atoms inserted into an otherwise pure silicon lattice. From the point of view of the minimum required band-gap of 1.14 eV, the choice is $OsSi_2$. Some of its properties have been reported by Mason et al.[17] Angstrom[18] established the crystal structure of $OsSi_2$ to be orthorhombic using arc-melted samples. It is a slight distortion of the CaF_2 structure, and is identical to that[19] of a ß-$FeSi_2$. The equivalent lattice parameter of the cubic, pseudo-CaF_2 structure for $OsSi_2$ is:

$$a_1 = \left(\frac{a_o b_o c_o}{4}\right)^{1/3} = 5.553\text{Å}$$

Thus it compares closely to ThO_2 which has a_o equal to 5.5997Å. The average atomic mass of $OsSi_2$ is 82.11 gm, while that of ThO_2 is 88.04 gm, so some of the properties of the two may be similar. The measured room

Table B-1. Properties of Silicide Semiconductors at 300K

Material	Eg eV	M.P. K	N	Type n	Type p	K W/cm K	S μ V/K	α, 10^{-6}/K
Si	1.21	1681	2	Yes	Yes	1.56		2.6
$BaSi_2$	1.3	2120	24	?	Yes	0.10	+600	8.2
$CrSi_2$	0.90	1760	6	No	Yes	0.06	+160	
$(Cr-Mn)Si_2$		1760	6	Yes	Yes		-200	
β-$FeSi_2$	0.88	1220 (P.C.)	48	Yes	Yes	0.11	+ or -	6.7
$ReSi_2$	0.2	2250	6	Yes	Yes	0.19	+ 80	
$OsSi_2$	1.8	2330	48	?	Yes	0.15	+380	7
$IrSi_2$								
$IrSi_3$			8					

Eg = Band-gap
N = Number of atoms in a primitive unit cell
K = Thermal conductivity (also degrees Kelvin)
S = Seebeck coefficient
α = Linear thermal expansion coefficient
P.C. = Phase change

temperature thermal conductivity[9] of ThO_2 is 0.15 watt/cm K, while its minimum thermal conductivity[9] is about 0.025 watt/cm K. We expect $OsSi_2$ to be similar. Its minimum lattice thermal conductivity will thus be similar to Si-Ge alloys.

The average linear thermal expansion coefficient, α, near room temperature of β-$FeSi_2$ is[20] 6.7×10^{-6}/K. We expect $OsSi_2$ to be about the same. For ThO_2 the value[21] of the expansion coefficient is 8.44×10^{-6}/K.

Thus the thermal expansion coefficient is sufficiently low to be useful as a thermoelectric generator material.

We can also obtain an estimate of the likely carrier mobility. In ß-$FeSi_2$ made by powder metallurgy, the mobilities[21] at room temperature are:

$\mu(n) = 2.0\ cm^2/volt\ sec,$
$\mu(p) = 7.5\ cm^2/volt\ sec.$

The n-type material is Co doped. If we proceed with Co substitution all the way to $CoSi_2$, the material has a true, not distorted, CaF_2 structure. In $CoSi_2$ Nikitin[23] has found that it is still n-type and the electrical conductivity, σ, depends on the purity.

Hall effect studies[24] show that each Co contributes one electron to the conduction process. Matthias and Hulm[25] measured the electrical conductivity of $CoSi_2$ at 300 K and found $5.56 \times 10^4\ ohm^{-1}cm^{-1}$. This corresponds to a mobility of $\mu(n) = 13.5\ cm^2/volt\ sec$ for melt-grown samples. Thus we conclude that $OsSi_2$ will have a room temperature mobility of the order of approximatey $10\ cm^2/volt\ sec$, and will be a band-type conductor. The utility of this will be discussed later.

We conclude that $OsSi_2$ should be a useful thermoelectric up to 1500 K while the companion ß-$FeSi_2$ is only good to about 1/2 this temperature because of its smaller band-gap.

We note that the highest valence of Os is Os^{+8}. The nominal valence of Si is Si^{-4}. Thus each Os has just the correct number of electrons to share with two Si atoms. In the crystal structure each Si is surrounded tetrahendrally by four Os atoms and each Os by a cube of eight Si atoms. All of the available electrons are nicely shared, and the material is a good semiconductor. In $ReSi_2$ the Re has only seven electrons available, the structure is different, and the material is a very small band-gap semiconductor. The extra electron in Os makes a large difference.

As to the available dopants in $OsSi_2$, we know[7] that Al makes it p-type. Probably B would also since OsB_2 exists. Also Re could be useful. For n-type $OsSi_2$ we can think of doping with P or As. However, Ir doping might

also work. The lattice thermal conductivity could probably be reduced by alloying the Si with Ge or the Os with Ru or Fe.

At high temperatures we are concerned with evaporation of both Os and Si from $OsSi_2$. The boiling points of Si and Os are 3100°C and 5000°C, respectively. These will be somewhat increased in $OsSi_2$ because of the atomic binding in the compound. The osmium volatility in OsO_4 will have to be watched, but the thermoelectrics are to be operated in vacuum, not in air. A protective coating of SiO_2 should also form on the surface. Note that it is the Os^{+8} nature of Os that produces volatile OsO_4. It is also this feature that makes its bonding with Si so special.

B.2.6 NITRIDES

The classes of materials that seem to offer the most promising candidates are the borides and the silicides. However, there are also nitride semiconductors. Among these are cubic BN, AlN, Si_3N_4, $BeSiN_2$ and $MgSiN_2$. These have band-gaps that are too large to be useful. Other nitrides such as Mg_3N_2, Ca_3N_2, Li_3N_2 and LiMgN react very readily with moisture, and thus are also not useful. The GaN, $ZnGeN_2$, Ge_3N_4, InN, and CrN compounds decompose into metal and nitrogen gas below 1300 K. One possible remaining binary candidate is ScN. The band-gap of ScN is 2.1 eV, it is stable in moist air and in water, has a low thermal conductivity, a high melting point and a low dissociation pressure. Its main problem is that the carrier concentration of the n-type material has not yet been reduced below $10^{20}/cm^3$. Work to reduce the carrier concentration and the thermal conductivity are needed to make this a useful candidate. There may be possibilities in some new[26] ternary nitride phases such as $Sm_3Si_6N_{11}$ or $3SmN\text{-}2Si_3N_4$. However, much more information is needed on such ternaries before useful predictions can be made.

B.2.7 BORON AND BORIDES

Several years ago GE-CR&D undertook to study the thermoelectric properties of elemental boron and boride compounds. Some of this information is shown in Table B-2. There are at least 16 different materials that one might work on. The problem is to decide on which one to try first and why.

Table B-2. Properties of Boron and Boride Semiconductors at 300 K

MATERIAL	CRYSTAL STRUCTURE	M.p. K	Eg eV	N	TYPE	K W/cm K	μ cm^2/Vsec	S 10^{-6}V/K	α,10^{-6}/K
α - B	RHOMB.	1470	2.0	12	p	1.5	100		6.0
ß - B	RHOMB.	2350	1.5	105	n + p	0.26	55	±400	6.5
B_6Ca	CUBIC	2505	0.4	7					
$B_{13}C_2$	RHOMB.	2650	0.7	15	p	0.38	≥1.5	+200	3.0
$B_{12}Be$	RHOMB.	2300		13					
$B_{12}C_2Be$	RHOMB.	2600		15					
$B_{12}P_2$	RHOMB.	2390	3.35	14	n + p	0.4	20		
$B_{12}As_2$	RHOMB.	1300	3.47	14		1.2			
α-$B_{12}Al$	TETRG. II	2430	2.2	189	p			+200	
ß-$B_{12}Be$	TETRG. II	2570		189		0.25			
B_6Si	ORTHORH.	2120	1.2	292	p	0.12	30	+300	5.1
$B_{68}Y$	CUBIC	2370	0.8	414	p	0.02	15	+560	
$B_{68}Gd$	CUBIC	2370		414	p	0.02	15	+645	
$B_{14}LiAl$	ORTHORH.	1500		64					
$B_{14}MgAl$	ORTHORH.	2200	1.0	65	p			+360	
$B_{48}Al_3C_2$	TETRAG. I	2490	2.5	53	p			+200	
$B_{12}Be$	TETRAG. I	1500		52					

Eg = ENERGY GAP
N = NUMBER OF ATOMS IN A PRIMITIVE UNIT CELL
K = THERMAL CONDUCTIVITY; ALSO DEGREES KELVIN
μ = CARRIER MOBILITY
S = SEEBECK COEFFICIENT
α = LINEAR THERMAL EXPANSION COEFFICIENT

The general reason for choosing boron and/or boron compounds is that they have high melting points and are semiconductors. They are mechanically rugged, have low thermal expansion coefficients and low vapor pressures. Some of them have very low thermal conductivities (e.g., $B_{68}Y$) caused, in part, by the large number of atoms in a unit cell, N. Their band-gaps are in the correct range to be useful and the Seebeck coefficients are acceptably large, at least for p-type materials. The most severe limitations are the low carrier mobility values and the effects of the dopant atoms on the mobility. The intrinsic mobilities of α-boron, ß-boron, and B_6Si may be high enough to be useful according to our criterion of $\mu \geq 0.5$ cm^2/volt sec, i.e., they are hopping conductors. Thus we digress here to a discussion of mobilities.

B.2.7.1 Carrier Mobility in ß-Boron

Dopant Effects

The main problem that limits the performance of ß-boron as a thermoelectric generator material is its low carrier mobility. The measured mobilities of Cu- or V-doped ß-boron at room temperature are 0.10 to 0.26 cm^2/volt sec for doping levels of approximately 1×10^{21}/cm^3. The intrinsic lattice mobility of p-type ß-boron has been measured by A.K. Hagenlocher[27,28] as 50 cm^2/volt sec at 300 K. His samples were doped with Be at concentrations of 1.8×10^{18} to 4×10^{19}/cm^3. It is essential to know how the mobility is influenced by the doping element and its concentration.

In Figure B-3 we show the mobility versus carrier concentration for p-type ß-boron,[28] silicon,[29-31] germanium[32-33] and a silicon-germanium alloy[34-35] containing 80 a/o Si plus 20 a/o Ge. From Figure B-3 we see that Be doped ß-boron behaves in a fashion similar to boron-doped Si and Ga-doped Ge. The mobility at 10^{20}/cm^3 of ß-boron is about 1/2 that of $Si_{0.8}Ge_{0.2}$. We have chosen $Si_{0.8}Ge_{0.2}$ for comparison because this is close to the composition of the standard thermoelectric-generator alloy. It is not known whether Be is a substitutional or interstitial impurity in ß-boron. However, the Be atom is just slightly (20 percent) larger in size than the B atom and it readily forms Be icosahedra in compounds such as $CeBe_{13}$. Furthermore, Be appears to substitute for B in the compound[35] BeB_3 and in tetragonal boron.[36] Thus we speculate here that Be, at low

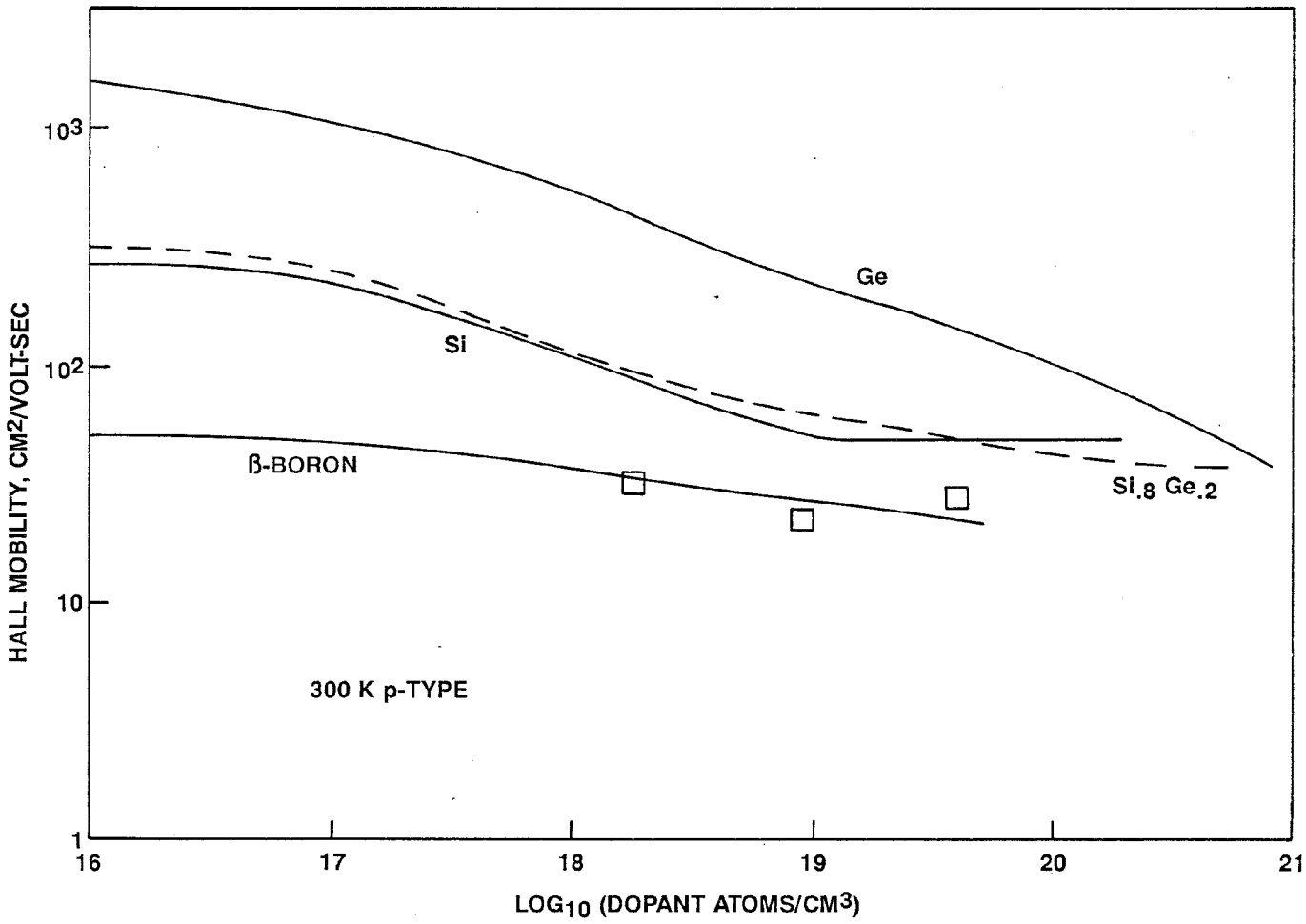

Figure B-3. Measured Hall Mobility at Room Temperature for p-Type Si, Ge, Si-Ge and ß-Boron as a Function of Dopant Concentrations

concentrations (i.e., $\leq$1 atom percent) is a substitutional impurity in ß-boron.

In contrast to Be we consider C as an impurity in ß-boron. Carbon produces[27,28] n-type ß-boron at low temperatures. The mobility at 300 K is equal to 1.5 cm^2/volt sec for the lowest doping and decreases rapidly with increasing carbon content, dropping to 0.2 cm^2/volt sec at about $2 \times 10^{18}/cm^3$. We speculate that carbon enters ß-boron as a substitutional impurity. It is known that carbon is a smaller (16 percent smaller) atom than boron, yet carbon expands[27] the lattice of ß-boron. This effect is not understood.

The interstitial atoms locally distort the ß-boron lattice. It may be this distortion, producing a local alteration of the lattice vibrations around an impurity that causes the lower charge carrier mobility. Thus V and Cu impurities also produce low mobility ß-boron. The direction to high Z thermoelectrics based on boron may be the substitutional-versus-interstitial nature of the impurities.

The mobility of $Si_{0.8}Ge_{0.20}$ in Figure B-3 is close to that of Si instead of a weighted arithmetic average of Si and Ge. The randomness of the Si and Ge positions in the lattice produces additional carrier scattering which reduces the mobility below that of the expected average. Apparently ß-boron is much more sensitive to the effects of randomness in the structure, and its mobility drops much more rapidly with increasing disorder than that of silicon. The Si-Ge randomness is needed to reduce the thermal conductivity to usable levels. In boron compounds the thermal conductivity will also be reduced by such randomness, but it remains to be discovered if the reduction in carrier mobility caused by randomness is of a magnitude that will make these materials poor prospects for thermoelectrics.

Temperature Effects

Figure B-4 shows the temperature dependence of the mobility of nearly-intrinsic, p-type ß-boron. For comparison the mobilities of high-purity, p-type Ge, Si, SiC, and Mg_2Si are also shown. The ß-boron data are from Hagenlocher.[27,28] The other data are from various

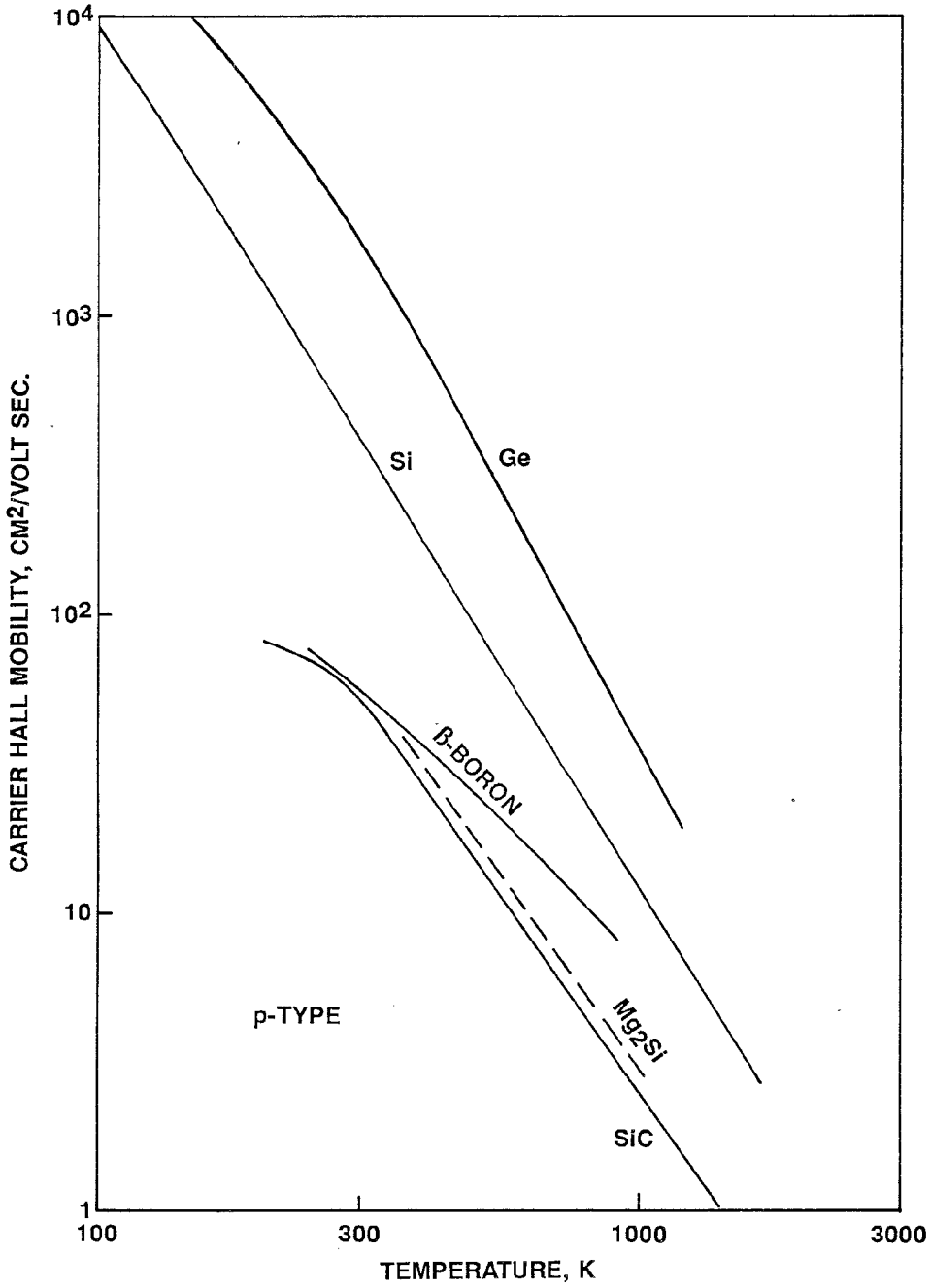

Figure B-4. The Measured Hall Mobility Versus Temperature for a Number of Lightly Doped p-Type Semiconductors

literature sources: Ge,[33,38,39] Si,[29,40-42] SiC,[43,44] and Mg_2Si.[45] For SiC the cubic and 6H hexagonal polytypes have very nearly the same p-type mobility. From Figure B-4 we note that ß-boron has a lower mobility than Si or Ge, but equal to or higher than SiC or Mg_2Si. The magnitude and temperature dependence of the mobility of ß-boron is approximately:

$$\mu(\text{p-type}) = \frac{1.2 \times 10^6 \text{cm}^2\text{deg}^{1.77}}{T^{1.77}\text{volt sec}}$$

It is possible that natural ß-boron made from the natural abundance boron isotopes of 80 percent B^{11} and 20 percent B^{10} may have a lower intrinsic mobility than either pure B^{10} or B^{11} alone. Since Be^9 appears to be the best p-type dopant, consideration should be given to use B^{11} doped with Be^9 as a possible higher-mobility material. The mass difference between Be^9 and B^{10} is less than that between Be^9 and B^{11}. Thus the lattice-vibration distortion around a Be impurity might be lower in B^{10}.

B.2.7.2 Mobilities in Other Boron Compounds

It is claimed by Golikova and Samatov[46] that α-boron has a high mobility of approximately 100 cm^2/volt sec at 300 K. They also state that ß-boron has a mobility of 0.01 cm^2/volt sec. In neither case is the donor or acceptor impurity stated. In other references, other α-boron-like structures are reported to have reasonable mobilities. Burmeister and Greene[47] report data from n-type B_6P which can be converted to:

$$\mu(n) = 20 \text{ cm}^2/\text{volt sec at room temperature.}$$

This value is good to within a factor of 3. Data of Neshpor et al.[48] on CVD boron carbide give calculated room temperature mobilities of up to:

$$\mu = 60 \text{ cm}^2/\text{volt sec.}$$

Thus the intrinsic mobility of α-boron-like structures may be as high as or higher than those in n-type ß-boron.

The carrier mobilities in LuB_{12} and YB_{12} at 300 K can be calculated from the electrical conductivity data of Zhurakovskii et al.[49] Each rare-earth atom donates one electron to the conduction process (and two electrons to fill the B_{12} bonding). The calculated mobilities at 300 K of these compounds with B_{12} groups in them is:

$$\mu(LuB_{12}) = 65 \text{ cm}^2/\text{volt sec}$$
$$\mu(YB_{12}) = 44 \text{ cm}^2/\text{volt sec}$$

These are similar to those of the α-boron-like compounds. It is noted that LuB_{12} and YB_{12} are metallic. It may be possible to make them into semiconductors by substituting one Be atom for a boron in each of the B_{12} groups. This would subtract the one electron from the conduction band and lead to a semiconductor. Thus compounds close to $LuB_{11}Be$ or $YB_{11}Be$ might well be useful semiconductors.

Similar arguments can be applied to compounds such as LaB_6 which have one excess electron per formula unit. Perhaps LaB_5Be would be a semiconductor.

B.2.7.3 Some Predicted Mobilities

A highly useful thermoelectric material is likely to require a mobility $\geq$10 cm^2/volt sec. This means a band-type electrical conduction, not a hopping process. The boron compounds that might exhibit band-type conduction would be ones which have no disorder in their atomic positions, and would be susceptible to substitutional doping. Good candidates might be:

Host	Dopant
α-boron	Be
ß-boron	Be
$B_{13}C_2$ (Ordered)	Be,Al,Si
$LuB_{11}Be$,$YB_{11}Be$,B_6P	Be,C,S,Si
CaB_6,SrB_6,BaB_6	Be,Sc,La
$LiAlB_{14}$	Be,Si
$MgAlB_{14}$	Be,Si
BeB_{12}	C3
$Al_8B_4C_7$	Be,Si,N

Poor candidates might be:

Host	Problem
β-boron	Transition metals, random
β-AlB_{12}	Al sites randomly occupied
B_6Si, B_3Si	Si sites randomly occupied
$B_{68}Y$	Y sites randomly occupied
High Temp. $B_{10}C$ to B_4C	B and C sites mixed

Amplifying on boron carbide, it is believed that the well-ordered $B_{13}C_2$ made[48,50] at 1000°C has a high (approximately 50 cm^2/volt sec) intrinsic mobility. However, boron carbide made at high temperatures like 1200°C may well have B and C exchanged on the lattice sites and have low mobility. Also it is suspected that at B to C ratios different from 13:2, additional randomness and disorder occurs in the structure, as shown in the X-ray studies of Yakel[51] on B to C ratios of 10:1 to 4:1. Emin and Wood[52] have found room temperature mobilities over this whole range of compositions of about $\mu(p)$ equal to 0.7 cm^2/volt sec in various boron carbides made at 1200°C.

B.2.7.4 Mobility, Randomness, and Doping

In order to produce a useful thermoelectric material from boron or a boride it should have a high mobility. This would probably mean a well-ordered crystal structure. In a semiconductor there is a relationship[53] between the carrier mean-free-path, ℓ, and the mobility, μ. At room temperature for free electrons: ℓ/μ equals 0.7207×10^{-8} volt sec/cm. For β-boron the average size of the unit cell is 9.365 angstroms. So, for a greater than or equal to 9.365 angstroms, the needed value of μ is greater than or equal to 13 cm^2/volt sec. It is seen that one distorted unit cell can cause difficulty in intrinsic, p-type, β-boron; the intrinsic carrier mean-free-path is only four unit cells in length. In simpler semiconductors, such as silicon, the intrinsic mean-free-path is longer and the unit cells are much smaller. Thus one damaged unit cell does not produce as large an effect.

In selecting a candidate dopant for ß-boron, it is observed that Be is most likely the best, since it probably substitutes for a boron atom. It is also observed that heavy interstitial impurities such as Cu, V or Hf could produce low mobilities when they distort the unit cells. At 1 atom percent V there is one dopant atom for every unit cell. The mobility of 0.26 cm^2/volt sec. The value of "ℓ" is then 0.4 angstrom.

In order to choose a high mobility candidate, it is essential to select a crystal structure and dopant element together. Any structure such as α-AlB_{12} which has many partially occupied and also many vacant cavities in the lattice[54,55] would probably not be a good candidate.

Another feature of these complex boron and boride structures requires further explanation. Consider a compound $A_x B_y$ as a host and an atom D as the possible dopant. If D is some small atom of a light element with a different number of electrons from A or B, it usually happens that D is not an effective dopant. It seems that the lattice rearranges itself easily around D to use all of the electrons of D in bonding and none are left over to donate to the conduction band (or holes to the valence band). It is this "plasticity" of these complex lattices that makes doping with light elements very difficult. We have noted that heavy elements ruin the mobility. By way of contrast, in silicon a phosphorus dopant atom must go into a silicon site. There is no room for much bond rearrangement and the extra electron escapes. It is therefore concluded that tightly bound crystal structures with very little space for rearrangement around the dopant atoms are needed. These seem to be limited in number. ß-boron thus appears, based on the work performed to date, to be a marginal candidate. It may, however, still be useful with Be as a dopant.

B.2.8 REVIEW OF BORON-BASED CANDIDATES

B.2.8.1 ß-Boron

One may be able to obtain high mobility ß-boron by doping with Be, as mentioned previously. It must be determined how the Be atoms enter into the ß-boron lattice, and whether the mobility is really as high as Hagenlocher[27,28] reports. It must also be determined if such mobility

values can be obtained with polycrystalline, hot-pressed samples, or melt-grown single crystals. The next step is to measure mobilities in carbon-doped ß-boron in order to check on Hagenlocher. The lattice positions of the carbon should be examined using X-ray single crystal studies. It must be determined if carbon produced n-type samples of ß-boron as Hagenlocher reports.

The next step is to look at the effects of double-doping in ß-boron. It may be possible to make high-mobility p-type material with Be doping, but reduction of the thermal conductivity must be obtained without destroying the mobility. The addition of 1 atom percent Zr or Hf is known to drastically lower K almost to K_{min}. If Be plus Zr or Be plus Hf doping does not destroy the mobility, a useful thermoelectric material results. Use of somewhat lighter atoms than Zr or Hf may be necessary if mobility is adversely effected. A possible combination may be Be plus Ti. Note Ti, Zr, and Hf are all p-type dopants. Similar double-doping combinations can be suggested for C doping. Here, however, it may be better to use n-type heavy metals such as V, Cr, Ni, or W. Again the balance between reducing the thermal conductivity and the mobility will have to be carefully studied. Furthermore it may not be possible to maintain ß-boron as an n-type material up to 1000°C or above because it is intrinsically p-type. It is believed that further work on purely interstitial dopants will not yield high mobility samples. Even samples double-doped with two transition elements such as V plus Cr, V plus Ni, or V plus Cu have yielded poorer performance than the same total concentration of V itself. So the mode of providing different hopping sites by using two different elements to increase the electrical conductivity has not been useful, possible because ß-boron does not really operate according to this model.

B.2.8.2 Beryllium Boride

The beryllium boride with the highest boron concentration is $B_{12}Be$. It is thought to possess at least three[56,57] different structures. The lowest temperature[58] tetragonal-I structure, termed γ-$B_{12}Be$, consists of four B_{12} units held together by various interstitial atoms. For Be atoms the same lattice can accommodate[58] Be from $B_{12}Be$ to $B_{12}Be_2$. Even less Be can also be used.[56] The structure is very open and has sites of

variable occupancy.[59] It does not appear to be a useful candidate. This tetragonal-I structure is found between 850°C and 1350°C.

At about 1600°C the tetragonal-II phase of β-$B_{12}Be$ is stable. It has nearly the same tetragonal-II structure[54] as an α-$B_{12}Al$ or as tetragonal-II boron itself.[60] It is not a useful thermoelectric, as stated previously.

Above 1700°C, and presumably to the melting point, $B_{12}Be$ apparently forms[56,57] an α-boron type simple rhombohedral structure with N equal to 13. In Table B-2 this is called α-$Be_{12}Be$. Just where the Be atom in this structure occurs is uncertain. Perhaps it is in the center of the icosahedra as it is in $CeBe_{13}$. If so, this is a particularly simple structure and should have a high mobility. It would be worth investigating for this reason. Maybe Li or C would act as useful dopants. This structure should have a very high thermal conductivity at room temperature of about 1 watt/cm K. Whether it could be made into a useful thermoelectric is, at present, doubtful because of its high thermal conductivity. Its K_{min} would probably be about 0.1 watt/cm K.

B.2.8.3 Boron Carbide

The well ordered, stoichiometric composition of boron carbide is $B_{13}C_2$. The intrinsic room temperature thermal conductivity of this composition is about 1 watt/cm K. The K_{min} appears[61] to be about 0.056 watt/cm K for material badly disordered by neutron irradiation. The well ordered $B_{13}C_2$ appears[48] to have a carrier mobility equal to 60 cm^2/volt sec. Badly disordered material[52] has a mobility of 0.7 cm^2/volt sec. The figure-of-merit, Z, is:

$$Z = \frac{S^2\sigma}{K} = \frac{S^2 ne\mu}{K}$$

Thus the ratio μ/K is proportional to Z. Comparing well-ordered boron carbide with μ/K approximately 60, to badly-disordered boron carbide with μ/K approximately 13, it is observed that the current approach of trying to make thermoelectric devices from badly disordered boron carbide (e.g., B_9C)

may be headed in the wrong direction. Well-ordered material might provide higher Z values, however, they might still not be high enough for useful devices.

A compound closely related to $B_{13}C_2$ is $B_{12}C_2Be$. Presumably the Be atom here goes into the central chain position, but there is no X-ray evidence to support this. The unit cell volume is slightly larger than that for $B_{13}C_2$. Even though there has been a "nominal" substitution of one Be for one B, the material is not a better p-type conductor than $B_{13}C_2$. If anything it has a much higher electrical resistivity (10^6 ohm cm) at room temperature than $B_{13}C_2$ (0.04 ohm cm) according to recent findings at GA Technologies Laboratories. The incorporation of Be may help to produce an ordered structure in "boron carbide". However, as a thermoelectric material, its properties seem to be close to those of ordered $B_{13}C_2$.

B.2.8.4 Boron Subphosphide

The boron subphosphide,[62] B_6P, was suggested as a thermoelectric generator material many years ago.[63] It can be made n-type (S doped) and p-type (Cd doped). Its intrinsic room-temperature thermal conductivity[64] is probably very close to that of B_6As, i.e., K equal to 1.2 watt/cm deg. Actual measurements[64] on a less-than-perfect sample gave values about 1/3 of this. Its estimated room temperature mobility[47] is 20 cm^2/volt sec. Thus its values of μ/K fall within approximately 17 to 50, very similar to boron carbide. Hill and Epstein[63] give a device value at 1473 K of ZT equal to 0.81 which is respectable. It may be that B_6P would be a very useful n-type element for high temperature thermoelectric generators. It seems that Be-doped ß-boron may be better as a p-type material.

Another useful property of B_6P is its high microhardness[65] of 5900 kg/mm^2. It can be hot-pressed[66] to high density at 2050°C. It can also be melted under inert gas pressure[62] and the cooled material maintains the B_6P crystal structure without noticeable loss of phosphorus. It has been found[67] possible to partially substitute B for P in the chain

positions to give a chemical composition of $B_{9.3}P$. It is not known what this would do to the μ and K values. These effects might be similar to those in B_9C. However, C might enter the icosahedra, P probably is too large to do so. Thus the disorder in $B_{9.3}P$ might be rather different than that in B_9C.

One of the unanswered problems in B_6P is the phosphorus dissociation pressure at the proposed operating temperature of 1000°C (1373 K). From Slack et al.[62] the estimate is 10^{-8} atmospheres. The equilibrium phosphorus pressure[68] over n-type Si-Ge thermoelectric alloys at 1050°C is about 10^{-1} atmospheres. Thus if Si-Ge alloys can be used with 10^7 times as high a dissociation pressure at its maximum use temperature, there should be very little problem with B_6P. Its chemical stability is very high.

The lack of chemical stability of B_6As is the real limitation of this compound. It readily loses As above 1000°C.

B.2.8.5 Boron Silicide

The highest melting point (peritectic decomposition) boride of silicon is B_6Si. Some work was done on this compound under DOE contract at GE-CR&D and, in particular, its crystal structure was determined.[69] It is a densely packed structure with very little room for interstitial impurities. All attempts to dope it with interstitials failed. It may have[70] a room temperature carrier mobility of 15 to 70 cm^2/volt sec. Its measured room temperature thermal conductivity is 0.12 watt/cm deg. Thus for well-ordered B_6Si the ratio μ/K has an approximate range of 125 to 580.

If these values are correct, B_6Si looks like a good candidate. So far only p-type material has been made with room temperature values of σ from 0.04 to 0.3 $ohm^{-1}cm^{-1}$.

More work on finding suitable dopants for B_6Si should be pursued; perhaps Be would be useful. This material has the correct kind of structure for a possibly high mobility material. There are 292 atoms in a unit cell. Careful

measurements should be made of its mobility in order to check Dzhafarov et al.[70] These should be made as a function of the boron to silicon ratio. It appears[69] that the most well-ordered material may have a chemical composition of $B_{6.2}Si$.

B.2.8.6 Dodecaborides

There are a number of boron compounds with the chemical formula $B_{12}Me$, where Me is some metal. These exist as a cubic material for the rare-earth metals from Tb to Lu and for Y, Zr, and U. Note that $B_{12}Me$ compounds also exist for Be, Al, and Sc. For Sc and the heavier metals these compounds are metallic. They consist of Me atoms, each surrounded by 12 B atoms. The Me atoms are on a FCC lattice. The boron atoms all have well-defined positions, and there is very little room for interstitial impurities. The metallic nature of these compounds is governed by the fact that the Me atoms supply too many electrons; one for each of the trivalent Me atoms.[71] The compound YbB_{12} has some Yb^{2+} and some Yb^{3+} ions. It is a semiconductor[72] with a very small activation energy and a much higher electrical resistivity than the other MeB_{12} compounds.

It has been suggested earlier in this review that $YB_{11}Be$ may be a semiconductor. This partial replacement of B by Be has been carried out[73] in LaB_6 with up to 30 atom percent replacement of the boron. It has been done[74] in HfB_2 with 15 atom percent of the boron replaced by Be. In both cases the lattice expands slightly as the Be content increases. It should also be possible to replace some Y^{3+} with a divalent ion such as Ca^{2+} or Sr^{2+} to help reduce the electron concentration and maybe decrease the thermal conductivity. One might also be able to use phonon scattering from Dy^{3+} or Tb^{3+} ions to also reduce the thermal conductivity as is done[75] in some rare-earth garnets.

The intrinsic lattice thermal conductivity of YB_{12} at room temperature is probably similar to that[76] of EuB_6, which is a semiconductor. This is K_g= 0.16 watt/cm deg. Combined with a mobility of μ = 44 cm^2/volt sec, a μ/K equal to approximately 275 is obtained, which is promising. These materials, as metals, are all n-type conductors. Thus they should be n-type semiconductors if not too much Be or Ca is added.

B.2.8.7 Tetradecaborides

There are three such boron compounds known, having the chemical formulas $B_{14}MgAl$, $B_{14}Mg_2$, and $B_{14}LiAl$. Their structure is given by Matkovich and Economy.[77] The orthorhombic unit cell has four formula units per crystallographic unit cell for $B_{14}MgAl$. All of the sites are filled and the structure is well-ordered with this stoichiometry. It is possible[78] to make them with the metal sites only partially filled. Polycrystalline samples can be made by hot-pressing[79] at 1800°C. They appear to have ionic[80] rather than covalent bonding of metal atoms and B_{12} units. They are p-type.

In view of the possible high volatility of Li and Mg at high temperatures, they do not appear to be especially interesting.

B.2.8.8 High-Boron Borides

These high-boron borides are typified by $B_{68}Y$. Many rare-earth and actinide elements form these cubic borides with N approximately equal to 414. A few studies of their properties have been reported.[81-83] Mobility measurements[81] gave μ = 15 cm^2/volt sec for $B_{66}Gd$, while thermal conductivity measurements in this laboratory gave K = 0.022 watt/cm deg at 300 K. The resultant μ/K = 680 looks quite impressive.

The E_g = 0.8 eV is the measured activation energy of the Y donor in this p-type material at 300 K. The real problem is to find some method of doping $B_{68}Y$ to increase the electrical conductivity. It has been possible to increase σ from 3×10^{-3} to 0.14 $ohm^{-1}cm^{-1}$ at 300 K, while simultaneously decreasing S from +560 microvolt/K to S = +23 microvolt K, by doping with 1 atom percent of Cr. Thus some transition metals are probably soluble interstitially, but the mobility after such doping appears to be low. Some other doping scheme, maybe Be doping, is needed to make a useful thermoelectric. However, with the very open structure, the Be added at the 1 percent level may drastically alter the crystal structure. The Cr addition only expanded the unit cell volume by +0.6 percent without altering the structure. More work should be done on these materials.

B.2.8.9 Ternary Al-B-C Borides

There are a number of different ternary Al-B-C borides. $Al_8C_7B_4$ has already been mentioned.[15] This compound was first discussed by Matkovich et al.[84] It has a hexagonal structure: a_o = 5.906 angstrom, c_o = 15.901 angstrom. The atomic positions are not known. It melts,[85] almost congruently, at 1836°C. It is yellow in color, which means a band-gap greater than or equal to 2.3 eV, and has a very narrow composition range. It has an N of approximately 48. Thus the intrinsic thermal conductivity at room temperature should be about 0.2 watt/cm deg. It appears to have no phase changes between room temperature and the melting point. Polycrystalline compacts have been obtained by hot pressing. It seems that Be or N or Si doping might be useful.

Other ternaries[84] in the system are AlC_4B_{24} and $Al_3C_2B_{48}$. The latter compound is amber in color and is sometimes called "diamond-like" boron or ß-AlB_{12}. It was discovered in 1857 by Woehler and DeVille. Above 850°C it has[86] the tetragonal-I structure with one formula unit per unit cell; below this temperature the cell becomes larger due to distortion and it is orthorhombic with four formula units per unit cell. This phase change and twinning make it unsuitable for use. The first compound is better written as $B_{48}C_8Al_x$ with $1/2 < x < 2$. It is black in color. At temperatures below 2000°C its cell contains four B_{12} units and has an orthorhombic structure;[87,88] but above 2000°C it converts to the simpler rhombohedral boron carbide structure[89] of $B_{12}C_2Al_{x/4}$, with the Al probably in the central chain position. The electrical properties are unknown, but it is probably similar to boron carbide. Its main advantage over boron carbide might be the larger unit cell (below 2000°C) with an N of (approximately) 58 and a lower thermal conductivity. Its minimum thermal conductivity might also be lower than that of boron carbide. Its advantage over α-$B_{12}Al$ is that the Al sites at x = 2 appear to be fully occupied. Thus the mobility may be greater than or equal to 10 cm^2/volt sec. Investigation of it might be a logical extension of work on boron carbide thermoelectrics.

B.2.9 OXIDES

There are a large number of oxide semiconductors, but none appear to have high enough mobilities to be interesting. Many of them are ionic or partially ionic conductors which causes severe troubles at long operating times and large current through-put.

B.2.10 SULFIDES, SELENIDES, TELLURIDES

These materials tend to have high vapor pressures at high temperatures, large thermal expansion coefficients, and to be mechanically weak. The sulfides, which are more thermally stable than the selenides or tellurides, tend to lose sulfur by evaporation and turn metallic. Data on Sc_2S_3, Y_2S_3, and La_2S_3 are sufficient to make these materials seem rather unattractive by comparison with Si-Ge, or the borides, carbides, or silicides.

B.3 CANDIDATE SELECTION

In the preceding sections a review of the information available about, and the pros and cons concerning, the various candidates has been given. Now we wish to rank these and select the most promising for further work. A method of attacking this problem is to look at the ratio μ/K_g, where μ is the carrier mobility, and K_g is the lattice thermal conductivity. For the case where the semiconductor can be considered a band conductor instead of a hopping conductor, then μ/K_g should be as large as possible. If the effective mass is equal to the free electron mass, then the optimum doping level is about $3 \times 10^{19}/cm^3$. For present purposes we shall call μ/K_g equal to F, the "figure of promise". A considerable amount of work will be required to ascertain the value of Z, i.e., the "figure-of-merit" for these promising materials.

Since any new material will be compared to Si-Ge alloys, let us calculate F for them at room temperature. For intrinsic, undoped, p-type Si at 300K, we have:

$\mu(p) = 260\ cm^2/volt\ sec$

$K_g = 1.56\ watt/cm\ deg$

$F = \mu/K_g = 167\ amp\ cm\ deg/volt^2 sec$

If we reduce K_g by alloying the Si with 20 mole percent Ge, we also increase μ slightly, and the result is:

$F = 4560.$

See Table B-3 for the μ and K_g values.

If we now dope the Si-Ge with boron up to the useful range (about $10^{20}/cm^3$), we obtain (See Figures B-1 and B-3)

$\mu = 4.0\ cm^2/volt\ sec,$
$K_g = 0.043\ watt/cm\ deg,$
$F = 930.$

Thus, in order to improve Si-Ge, we are looking for F values in excess of 900 in a heavily doped material.

All the requisite data are not available for the candidate materials listed in Table B-3 to permit calculation of F-values at high doping levels and/or high material impurity alloying levels. However, it was assumed that those materials with intrinsic characteristics similar to or greater than Si (F equal to 167) have the potential for meeting the figure-of-merit goals of the Program for new technology material. This is based on the fact that the F values of Si have been increased by nearly an order of magnitude as a result of extensive theoretical considerations and experimentation. It is thus believed that these other materials have the potential of equal to greater improvement with a similar degree of emphasis.

B.4 REFERENCES

(1) W.R. Corliss and D.G. Harvey, "Radioisotope Power Generation," Prentice-Hall, Englewood Cliffs, NJ (1964).

(2) J.P. Dismukes, L. Ekstrom, E.F. Steigmeier, I. Kudman and D.S. Beers, J. Appl. Phys. 35, 2899 (1964).

(3) E.J. Steigmeier and B. Abeles, Phys. Rev. 136A, 1149 (1964).

Table B-3. Figure of Promise Values for Various Semiconductors in Intrinsic, Undoped State of 300 K

Material	μ $cm^2/volt\ sec$	K_g watt/cm deg	$F = \mu/K_g$ amp cm deg/$volt^2$sec	Type
Si	260	1.56	167	p
$Si_{0.8}Ge_{0.2}$	310	0.068	4560	p
Doped Si-Ge	40	0.043	930	p
α-Boron	100	1.5	67	p
β-Boron	55	0.26	210	p
α-$B_{12}Be$	50	1.2	40	p
$B_{13}C_2$	60	1	60	p
B_6P	20	0.4	50	n,p
B_6Si	15 to 70	0.12	125 to 580	p
$YB_{11}Be$	44	0.16	275	n
$B_{68}Y$	15	0.022	680	p
$OsSi_2$	~15	0.15	100	n,p
Al_4SiC_4	~30	0.50?	60?	n,p

(4) R.P. Chasmar and R. Stratton, J. Electronics and Control 7, 52-72 (1959).

(5) F.D. Rosi, E.E. Hockings, and N.E. Lindenblad, RCA Review 22, 82 (1961).

(6) R.W. Cohen and B. Abeles, J. Appl. Phys. 34, 1687 (1963).

(7) J.F. Goff and J.R. Lowney, Trans. Am. Nuc. Soc. 23, 121 (1976).

(8) N.F. Mott and W.D. Twose, Adv. Phys. 10, 107 (1961).

(9) G.A. Slack, Solid State Phys. 34, 1 (1979).

(10) J.R. Lowney and J.F. Goff, Proc. Fourteenth Intersociety Energy Eng. Conf., p. 1816 (1979); pub. by Am. Chem. Soc.

(11) V.J. Barczak, J. Am. Ceram. Soc. 44, 299 (1961).

(12) G. Schneider, L.J. Gauckler, G. Petzow, and A. Zangvil, J. Am. Ceram. Soc. 62, 574 (1979).

(13) Z. Inoue, Y. Inomata, H. Tanaka, and H. Kawabata, J. Mater. Sci. 15, 575 (1980).

(14) S. Prochazka, private communication.

(15) Z. Inoue, H. Tanaka, and Y. Inomata, J. Mater. Sci. 15, 3036 (1970).

(16) J. Bauer and O. Bars, J. Less-Comm. Met. 83, 17 (1982).

(17) K. Mason and G. Muller-Vogt, J. Crystal Growth 63, 34 (1983).

(18) I. Engstrom, Acta Chem. Scand. 24, 2117 (1970).

(19) R. Wandji, Y. Dusausoy, J. Protas, and B. Rogues, Comptes Rendus C269, 907 (1969).

(20) V.S. Neshpor and M.I. Reznichenko, Ogneupory 28, 134 (1963).

(21) M. Hock and A.C. Momin, High Temp.-High Press. 1, 401 (1969).

(22) J. Hesse, Zeit. Metallkunde 60, 652 (1969).

(23) E.N. Nikitin, Zhurn. Tekn. Fiz. 28-26 (1958) [Sov. Phys.-Tech. Phys. 3, 23 (1958)].

(24) V.S. Neshpor and G.V. Samsonov, Doklad. Akad. Nauk SSSR 134, 1337 (1980).

(25) B.T. Matthias and J.K. Hulm, Phys. Rev. 89, 439 (1953).

(26) J. Gaude, J. Lange and D. Louer, Rev. Chim. Miner. 20, 523 (1983).

(27) A.K. Hagenlocher, "Semiconducting Properties of Boron," Thesis, Tech. Hochsch. Stuttgart, 1958.

(28) A.K. Hagenlocher, "Boron, Synthesis, Structure, and Properties," ed. by J.A. Kohn et al., Plenum, New York, 1960, p. 128.

(29) F.J. Morin and J.P. Maita, Phys. Rev. 96, 28 (1954).

(30) R.O. Carlson, Phys. Rev. 100, 1075 (1955).

(31) J.C. Irvin, Bell Sys. Tech. Jour. 41, 387 (1962).

(32) F.A. Trumbore and A.A. Tartaglia, J. Appl. Phys. 29, 1511 (1958).

(33) O.A. Golikova, B. Ya. Moizhes, and A.G. Orlow, Fiz. Tverd. Tela 4, 3482 (1962) [Sov. Phys.-Solid State 4, 2550 (1963)].

(34) A. Levitas, Phys. Rev. 99, 1810 (1955).

(35) J.P. Dismukes, L. Ekstrom, E.F. Steigmeier, I. Kudman, and D.S. Beers, J. Appl. Phys. 35, 2899 (1964).

(36) E. Laube and H. Nowotny, Monatsh. Chem. 93, 681 (1962).

(37) R. Mattes, K.F. Tebbe, H. Neidhard and H. Rethfeld, J. Less-Comm. Metals 47, 29 (1976).

(38) F.J. Morin and J.P. Maita, Phys. Rev. 94, 1525 (1954).

(39) D.M. Brown and R. Bray, Phys. Rev. 127, 1593 (1962).

(40) G.L. Pearson and J. Bardeen, Phys. Rev. 75, 865 (1949).

(41) J. Messier and J.M. Flores, J. Phys. Chem. Solids 24, 1539 (1963).

(42) S.S. Li, Solid State Electronics 21, 1109 (1978).

(43) H.J. Van Daal, J. Phys. Chem. Solids 24, 109 (1963).

(44) H.J. Van Daal, Philips Res. Repts.-Supple No. 3 (1965), pp. 1-92.

(45) V. Winkler, Helv. Phys. Acta 28, 633 (1955).

(46) O.A. Golikova and S. Samatov, Phys. Status Solidi 77, 449 (1983).

(47) R.A. Burmeister and P.E. Greene, Trans. Met. Soc. AIME 239, 408 (1967).

(48) V.S. Neshpor, V.P. Nikitin, and V.V. Rabotnov, Porosh. Met. 7 (#11), p. 62 (1968) [Sov. Powd. Met. Met. Ceram. 7, 889 (1968)].

(49) E.A. Zhurakovskii, Yu. B. Paderno and V.V. Odintsov, Metallofizika 73, 1 (1978)]Chem. Abstr. 89, 221271d (1978)].

(50) G. Will and K.H. Kossobutski, J. Less-Common Metals 47, 43 (1976).

(51) H.L. Yakel, Acta Cryst. B31, 1797 (1975).

(52) D. Emin and C. Wood, Proc. 18th Intersociety Energy Conversion Engineering Conference, p. 222 (1983).

(53) F. Seitz, "Modern Theory of Solids," McGraw-Hill, New York, 1940, p. 190.

(54) I. Higashi, T. Sakurai, and T. Atoda, J. Solid State Chem. 20, 67 (1977).

(55) I. Higashi, J. Less-Comm. Metals 67, 7 (1979).

(56) Yu. D. Kondrashev, G.S. Markevich and L. Ya Markovskii, Zhurn. Neorg. Khim. 11, 1461 (1966) [Russ. J. Inorg. Chem. 11, 780 (1966)].

(57) N.V. Vekshina, L. Ya Markovskii, Yu. D. Kondrashev and I.M. Stroganova, Zhur. Prikl. Khim. 42, 1229 (1969) [J. Appl. Chem. USSR 42, 1168 (1969)].

(58) H.J. Becker, Zeit. anorg. allgem. Chem. 306, 266 (1960).

(59) V.I. Matkovich and J. Economy, in "Boron and Refractory Borides," ed. by V.I. Matkovich, Springer, Berlin (1977), p. 78.

(60) M. Vlasse, R. Naslain, J.S. Kasper and K. Ploog, J. Less-Comm. Met. 67, 1 (1979).

(61) K.E. Gilchrist and S.D. Preston, High Temp.-High Press. 11, 643 (1979).

(62) G.A. Slack, T.F. McNelly, and E.A. Taft, J. Phys. Chem. Solids 44, 1009 (1983).

(63) D.E. Hill and A.S. Epstein, U.S. Pat. 3,077,506, Feb. 12, 1963 [Chem. Abstr. 59, 2275g (1963)].

(64) G.A. Slack, D.W. Oliver, and F.J. Horn, Phys. Rev. B4, 1714 (1971).

(65) M. Takigawa and K. Shohno, Jap. J. Appl. Phys. 16, 637 (1977).

(66) J.L. Peret, J. Am. Ceram. Soc. 47, 44 (1964).

(67) E. Amberger and P.A. Rauh, Acta Cryst. B30, 2549 (1974).

(68) G.A. Slack, General Electric Company Report 80CRD201, August, 1981.

(69) J.H. Rosolowski, et al., Monthly Technical Progress Report #20, Contract No. DE-AC01-81NE32084, May 11, 1983.

(70) E.A. Dzhafarov, O.A. Golikova and M.I. Aliev, Dokl. Akad. Nauk Az. S.S.R. 36 (#5), p. 23 (1980).

(71) R. Johnson and A. Daane, J. Chem. Phys. 38, 425 (1963).

(72) M. Kasaya, F. Iga, K. Negishi, S. Nakai, and T. Kasuya, J. Magn. Magn. Mater. 31-34, 437 (1983).

(73) K. Hiebl and M.J. Sienko, Inorg. Chem. 19, 2179 (1980).

(74) E. Rudy, F. Benesovsky, H. Nowotny, and L.E. Toth, Monatsh. Chem. 92, 692 (1961).

(75) G.A. Slack and D.W. Oliver, Phys. Rev. B4, 592 (1971).

(76) M.I. Aivazov, T.I. Brushkova, V.S. Mkrtchyan, and V.A. Rubanov, Teplofiz. Vys. Temp. 17, 330 (1979) [High Temp. 17, 277 (1979)].

(77) V.I. Matkovich and J. Economy, Ref. 59, p. 104.

(78) V.I. Matkovich and J. Economy, Acta Crystallogr. B26, 616 (1970).

(79) I.A. Bairamashvili, L.I. Kekelidze, O.A. Golikova, and V.M. Orlov. J. Less-Comm. Met. 67, 461 (1979).

(80) T. Ito and I. Higashi, Acta Cryst. B39, 239 (1983).

(81) O.A. Golikova and A. Tadzhiev, J. Less-Comm. Met. 82, 169 (1981).

(82) O.A. Golikova, V.M. Orlov, G.V. Panteleeva, A.A. Tadzhiev, and E.O. Dzhafarov, Fiz. Tekh. Poluprovodn. 14, 1405 (1980) [Sov. Phys.-Semic. 14, 833 (1980)].

(83) G.A. Slack, D.W. Oliver, G.D. Brower, and J.D. Young, J. Phys. Chem. Solids 38, 45 (1977).

(84) V.I. Matkovich, J. Economy, and R.F. Giese, Jr., J. Am. Chem. Soc. 86, 2337 (1964).

(85) P. Dorner, "Phase Studies of High Temperature Ceramics in the Systems B-Al-C-Si-N-O with the Aid of Thermodynamic Calculations," Ph.D. Thesis, University of Stuttgart, West Germany, 1982.

(86) V.I. Matkovich, R. Giese, and J. Economy, Zeit. f. Kristallogr. 122, 108 (1965).

(87) G. Will, Acta Cryst. B25, 1219 (1965).

(88) A.J. Perrotta, W.D. Townes, and J.A. Potenza, Acta Cryst. B25, 1223 (1969).

(89) E. Born and W. Borchert, Neues Jahrb. Mineral. Monatsh. (#3), 135 (1970).

APPENDIX C

HIGH TEMPERATURE THERMOELECTRIC PROPERTY DATA FOR 12 OF THE Si-Ge ALLOY COMPACTS EVALUATED IN SECTION 4

SAMPLE: ITM-68
DESCRIPTION: 80%Si-20%Ge
Molecular Weight 36.96

TEMPERATURE	SEEBECK COEFFICIENT	ELECTRICAL RESISTIVITY	THERMAL DIFFUSIVITY	HEAT CAPACITY	DENSITY	THERMAL CONDUCTIVITY	ELECTRICAL POWER FACTOR	FIGURE OF MERIT	DIMENSIONLESS FIGURE OF MERIT
	Seebeck and Resistivity Measured Simultaneously GE-SCD		Laser Flash Diffusivity GE-RSD	Drop Calorimetry Ames Lab. MHPS-077P	Immersion Density Thermal Expansion GE-RSD	Calculated	Calculated	Calculated	Calculated
# Points in Fit	96	96	11	11					
Temp. Range of D	19 C	37 C	107 C	375 K					
	956 C	963 C	1111 C	1375 K					
RMSD (%)	1.07	0.69	0.95	0.93	0.33	2.22	2.83	5.04	5.04
A	-1.17652E+02	9.44210E-01	2.96032E-02	4.66300E+00	2.87			Z	ZT
B	-3.29771E-01	1.30897E-03	-1.49819E-05	1.62220E-03	4.300E-06				
C	4.71709E-05	9.56441E-06	-1.20906E-08	6.31000E+04					
D	1.31163E-07	-5.01901E-08	1.95257E-11	0.113					
E		1.31974E-10							
F		-1.54104E-13							
G		6.33889E-17							
H									
Units for Temp:	C	C	C	K	C				K
Equation	A+BT+CT^2+DT^3	A+BT+...HT^7	A+BT+...ET^4	D*(A+BT+C/T^2)	A/(1+B(T-27))^3 a*Cp*d		S^2/r	S^2/rk	ZT
(K)	(C)	(microV/K)	(milliohm-cm)	(cm2/sec)	(J/g-K)	(g/cm3)	(W/cm-K)	(microW/cm-K2	(1000/K)	
275	2	-118.26	0.947	0.0296	0.6729	2.871	0.0571	14.77	0.2586	0.0711
300	27	-125.47	0.985	0.0292	0.6824	2.870	0.0555	16.23	0.2925	0.0877
325	52	-134.61	1.032	0.0288	0.6552	2.869	0.0541	17.56	0.3244	0.1054
350	77	-142.66	1.083	0.0284	0.6505	2.868	0.0530	18.80	0.3549	0.1242
375	102	-150.61	1.136	0.0280	0.6476	2.867	0.0519	19.96	0.3844	0.1441
400	127	-158.46	1.191	0.0275	0.6460	2.866	0.0510	21.08	0.4133	0.1653
425	152	-166.18	1.246	0.0271	0.6455	2.865	0.0502	22.16	0.4418	0.1878
450	177	-173.77	1.302	0.0267	0.6458	2.864	0.0494	23.20	0.4700	0.2115
475	202	-181.22	1.357	0.0262	0.6468	2.864	0.0486	24.20	0.4978	0.2364
500	227	-188.50	1.413	0.0258	0.6483	2.863	0.0479	25.15	0.5250	0.2625
525	252	-195.62	1.470	0.0254	0.6503	2.862	0.0472	26.04	0.5514	0.2895
550	277	-202.55	1.528	0.0249	0.6525	2.861	0.0466	26.85	0.5767	0.3173
575	302	-209.29	1.588	0.0245	0.6551	2.860	0.0459	27.59	0.6006	0.3459
600	327	-215.82	1.650	0.0241	0.6580	2.859	0.0453	28.23	0.6229	0.3737
625	352	-222.13	1.715	0.0237	0.6610	2.858	0.0447	28.78	0.6432	0.4020
650	377	-228.21	1.782	0.0233	0.6642	2.857	0.0442	29.23	0.6615	0.4300
675	402	-234.04	1.851	0.0229	0.6676	2.856	0.0437	29.59	0.6777	0.4574
700	427	-239.62	1.923	0.0225	0.6711	2.855	0.0432	29.86	0.6918	0.4843
725	452	-244.93	1.997	0.0222	0.6747	2.854	0.0427	30.05	0.7039	0.5103
750	477	-249.96	2.071	0.0218	0.6784	2.853	0.0422	30.17	0.7142	0.5356
775	502	-254.69	2.145	0.0215	0.6821	2.852	0.0418	30.24	0.7227	0.5601
800	527	-259.12	2.217	0.0212	0.6860	2.852	0.0415	30.28	0.7296	0.5838
825	552	-263.23	2.288	0.0209	0.6899	2.851	0.0412	30.29	0.7356	0.6069
850	577	-267.01	2.354	0.0207	0.6939	2.850	0.0408	30.29	0.7404	0.6294
875	602	-270.44	2.415	0.0205	0.6979	2.849	0.0407	30.29	0.7444	0.6514
900	627	-273.53	2.469	0.0203	0.7020	2.848	0.0405	30.31	0.7478	0.6730
925	652	-276.24	2.515	0.0201	0.7061	2.847	0.0404	30.34	0.7506	0.6943
950	677	-278.58	2.552	0.0200	0.7103	2.846	0.0404	30.41	0.7530	0.7153
975	702	-280.52	2.579	0.0199	0.7145	2.845	0.0404	30.51	0.7549	0.7360
1000	727	-282.06	2.596	0.0198	0.7187	2.844	0.0405	30.64	0.7562	0.7562
1025	752	-283.18	2.604	0.0198	0.7230	2.843	0.0407	30.80	0.7568	0.7755
1050	777	-283.88	2.602	0.0198	0.7272	2.842	0.0410	30.97	0.7568	0.7939
1075	802	-284.13	2.594	0.0199	0.7315	2.842	0.0413	31.12	0.7560	0.8095
1100	827	-283.93	2.581	0.0200	0.7358	2.841	0.0418	31.23	0.7475	0.8223
1125	852	-283.26	2.569	0.0201	0.7402	2.840	0.0423	31.24	0.7380	0.8303
1150	877	-282.12	2.561	0.0203	0.7445	2.839	0.0430	31.07	0.7231	0.8315
1175	902	-280.48	2.566	0.0206	0.7489	2.838	0.0437	30.66	0.7010	0.8236
1200	927	-278.35	2.592	0.0209	0.7533	2.837	0.0446	29.90	0.6701	0.8041
1225	952	-275.69	2.649	0.0212	0.7577	2.836	0.0456	28.70	0.6292	0.7709
1250	977			0.0216	0.7621	2.835	0.0467			
1275	1002			0.0221	0.7665	2.834	0.0480			
1300	1027			0.0226	0.7709	2.833	0.0494			
INTEGRATED AVERAGE 302 C TO 952 C		-283.15	2.304	0.0211	0.7034	2.85	0.0423	30.18	0.7158	0.6480

SAMPLE: ITM-698
DESCRIPTION: 80%Si-20%Ge
Molecular Weight 36.86

TEMPERATURE	SEEBECK COEFFICIENT	ELECTRICAL RESISTIVITY	THERMAL DIFFUSIVITY	HEAT CAPACITY	DENSITY	THERMAL CONDUCTIVITY	ELECTRICAL POWER FACTOR	FIGURE OF MERIT	DIMENSIONLESS FIGURE OF MERIT
	Seebeck and Resistivity Measured Simultaneously GE-SCO		Laser Flash Diffusivity GE-RSO	Drop Calorimetry Ames Lab. MHPS-077P	Immersion Density Thermal Expansion GE-RSO	Calculated	Calculated	Calculated	Calculated
# Points in Fit	30	29	11	11					
Temp. Range of D	17 C	17 C	105 C	375 K					
	1006 C	1006 C	1100 C	1375 K					
RMSD (%)	1.06	1.09	0.99	0.93	0.33	2.25	3.21	5.46	5.46
								Z	ZT
A	-1.49991E-02	1.06478E+00	3.00494E-02	4.66900E+00	3.040				
B	-3.56089E-01	-1.62041E-04	-3.66713E-05	1.62220E-03	4.300E-06				
C	5.14053E-04	2.92107E-05	6.11495E-08	6.31000E+04					
D	-1.58216E-06	-1.64772E-07	-6.41265E-11	0.113					
E	2.38851E-09	4.66171E-10	3.09485E-14						
F	-1.07745E-12	-6.59742E-13							
G		4.38245E-16							
H		-1.08928E-19							
Units for Temp:	C	C	C	K	C				K
Equation	A+BT+...FT^5	A+BT+...HT^7	A+BT+...ET^4	D*(A+BT+C/T^2)	A/(1+B(T-ZT))^3 a*Cp*d		S^2/r	S^2/rk	ZT
(K)	(C)	(microV/K)	(milliohm-cm)	(cm2/sec)	(J/g-K)	(g/cm3)	(W/cm-K)	(microW/cm-K2	(1000/K)
275	2	-214.05	1.985	0.0300	0.6729	3.041	0.0613	11.89	0.1955	0.0538
300	27	-222.61	1.998	0.0291	0.6824	3.040	0.0598	13.69	0.2336	0.0701
325	52	-230.68	1.134	0.0283	0.6552	3.039	0.0584	15.06	0.2672	0.0859
350	77	-238.26	1.169	0.0276	0.6505	3.038	0.0545	16.18	0.2970	0.1040
375	102	-245.76	1.239	0.0269	0.6476	3.037	0.0529	17.15	0.3244	0.1217
400	127	-252.96	1.296	0.0263	0.6460	3.036	0.0515	18.05	0.3505	0.1402
425	152	-260.00	1.354	0.0257	0.6455	3.035	0.0503	18.91	0.3758	0.1598
450	177	-266.95	1.410	0.0252	0.6458	3.034	0.0493	19.77	0.4012	0.1805
475	202	-273.82	1.464	0.0247	0.6468	3.033	0.0484	20.64	0.4265	0.2026
500	227	-280.63	1.518	0.0242	0.6483	3.032	0.0476	21.50	0.4516	0.2259
525	252	-287.39	1.572	0.0238	0.6503	3.031	0.0469	22.34	0.4764	0.2501
550	277	-294.08	1.627	0.0234	0.6525	3.030	0.0463	23.16	0.5004	0.2752
575	302	-300.70	1.684	0.0230	0.6551	3.029	0.0457	23.92	0.5231	0.3009
600	327	-307.22	1.744	0.0227	0.6580	3.028	0.0452	24.62	0.5442	0.3265
625	352	-313.60	1.807	0.0224	0.6610	3.027	0.0448	25.24	0.5633	0.3520
650	377	-319.81	1.874	0.0221	0.6642	3.026	0.0444	25.78	0.5801	0.3771
675	402	-325.90	1.944	0.0218	0.6676	3.025	0.0441	26.22	0.5947	0.4014
700	427	-331.53	2.017	0.0216	0.6711	3.024	0.0438	26.58	0.6069	0.4249
725	452	-336.95	2.091	0.0213	0.6747	3.023	0.0435	26.85	0.6170	0.4473
750	477	-342.01	2.164	0.0211	0.6784	3.022	0.0433	27.06	0.6251	0.4688
775	502	-346.67	2.236	0.0209	0.6821	3.021	0.0431	27.21	0.6316	0.4895
800	527	-350.88	2.304	0.0207	0.6860	3.020	0.0429	27.32	0.6366	0.5093
825	552	-354.56	2.365	0.0205	0.6899	3.020	0.0428	27.40	0.6407	0.5285
850	577	-357.72	2.419	0.0204	0.6939	3.019	0.0426	27.46	0.6439	0.5473
875	602	-360.30	2.462	0.0202	0.6979	3.018	0.0426	27.52	0.6467	0.5656
900	627	-362.28	2.493	0.0201	0.7020	3.017	0.0425	27.58	0.6491	0.5841
925	652	-363.65	2.511	0.0200	0.7061	3.016	0.0425	27.68	0.6515	0.6026
950	677	-364.38	2.514	0.0199	0.7103	3.015	0.0425	27.80	0.6539	0.6212
975	702	-364.48	2.503	0.0198	0.7145	3.014	0.0426	27.94	0.6563	0.6398
1000	727	-363.96	2.478	0.0197	0.7187	3.013	0.0427	28.12	0.6588	0.6586
1025	752	-362.85	2.438	0.0197	0.7230	3.012	0.0429	28.34	0.6613	0.6778
1050	777	-361.18	2.387	0.0197	0.7272	3.011	0.0431	28.58	0.6639	0.6969
1075	802	-358.01	2.327	0.0197	0.7315	3.010	0.0434	28.83	0.6649	0.7147
1100	827	-356.42	2.261	0.0197	0.7358	3.009	0.0437	29.08	0.6651	0.7316
1125	852	-353.49	2.194	0.0198	0.7402	3.008	0.0442	29.29	0.6631	0.7480
1150	877	-350.32	2.130	0.0200	0.7445	3.007	0.0447	29.42	0.6590	0.7647
1175	902	-347.06	2.076	0.0201	0.7489	3.006	0.0454	29.40	0.6493	0.7819
1200	927	-343.86	2.038	0.0204	0.7533	3.005	0.0461	29.18	0.6327	0.7999
1225	952	-340.93	2.023	0.0206	0.7577	3.004	0.0470	28.67	0.6101	0.7474
1250	977	-338.33	2.033	0.0210	0.7621	3.003	0.0480	27.85	0.5800	0.7250
1275	1002	-336.13	2.068	0.0214	0.7665	3.002	0.0492	26.71	0.5428	0.6921
1300	1027			0.0218	0.7709	3.001	0.0505			
INTEGRATED AVERAGE 302 C TO 1002 C		-246.35	2.205	0.0206	0.7075	3.02	0.0440	27.58	0.6279	0.5842

SAMPLE: ITM-70
DESCRIPTION: 80%Si-20%Ge
Molecular Weight 36.86

TEMPERATURE	SEEBECK COEFFICIENT	ELECTRICAL RESISTIVITY	THERMAL DIFFUSIVITY	HEAT CAPACITY	DENSITY	THERMAL CONDUCTIVITY	ELECTRICAL POWER FACTOR	FIGURE OF MERIT	DIMENSIONLESS FIGURE OF MERIT
	Seebeck and Resistivity Measured Simultaneously GE-SCO		Laser Flash Diffusivity GE-RSO	Drop Calorimetry Ames Lab. MHPS-077P	Immersion Density Thermal Expansion GE-RSO	Calculated	Calculated	Calculated	Calculated
# Points in Fit	19	19	11	11					
Temp. Range of D	37 C	37 C	111 C	375 K					
	901 C	901 C	1118 C	1375 K					
RMSD (%)	3.64	1.51	0.51	0.93	0.33	1.77	8.79	10.56	10.56
A	-1.07544E+02	9.51961E-01	2.44287E-02	4.66300E+00	3.020			Z	ZT
B	-3.12763E-01	6.10650E-04	-1.18837E-05	1.62220E-03	4.300E-06				
C	-6.81434E-05	1.21890E-05	-3.73680E-09	6.31000E+04					
D	2.76356E-07	-5.53692E-08	1.11433E-11	0.113					
E		1.32043E-10							
F		-1.47091E-13							
G		5.81953E-17							
H									
Units for Temp:	C	C	C	K	C				K
Equation	A+BT+CT^2+DT^3	A+BT+...GT^6	A+BT+...DT^3	D*(A+BT+C/T^2)	A/(1+B(T-27))^3 a*Cp*d		S^2/r	S^2/rk	ZT

(K)	(C)	(microV/K)	(milliohm-cm)	(cm2/sec)	(J/g-K)	(g/cm3)	(W/cm-K)	(microW/cm-K2	(1000/K)	
275	2	-108.12	0.953	0.0244	0.6729	3.021	0.0496	12.27	0.2472	0.0630
300	27	-115.89	0.976	0.0241	0.6624	3.020	0.0482	13.78	0.2858	0.0857
325	52	-123.91	1.010	0.0238	0.6552	3.019	0.0471	15.21	0.3230	0.1050
350	77	-131.86	1.050	0.0235	0.6505	3.018	0.0461	16.56	0.3590	0.1256
375	102	-139.81	1.095	0.0232	0.6476	3.017	0.0453	17.86	0.3941	0.1478
400	127	-147.75	1.142	0.0229	0.6460	3.016	0.0446	19.12	0.4288	0.1715
425	152	-155.64	1.190	0.0226	0.6455	3.015	0.0439	20.35	0.4631	0.1968
450	177	-163.46	1.240	0.0223	0.6458	3.014	0.0434	21.55	0.4971	0.2237
475	202	-171.18	1.290	0.0220	0.6468	3.013	0.0428	22.72	0.5307	0.2521
500	227	-178.78	1.340	0.0217	0.6483	3.012	0.0423	23.86	0.5639	0.2819
525	252	-186.22	1.390	0.0214	0.6503	3.011	0.0419	24.96	0.5960	0.3129
550	277	-193.49	1.441	0.0211	0.6525	3.010	0.0414	25.97	0.6270	0.3448
575	302	-200.56	1.494	0.0208	0.6551	3.009	0.0410	26.93	0.6564	0.3774
600	327	-207.40	1.547	0.0205	0.6580	3.008	0.0406	27.80	0.6839	0.4103
625	352	-213.99	1.602	0.0203	0.6610	3.007	0.0403	28.58	0.7092	0.4432
650	377	-220.30	1.659	0.0200	0.6642	3.006	0.0400	29.26	0.7320	0.4758
675	402	-226.30	1.716	0.0198	0.6676	3.005	0.0397	29.84	0.7521	0.5077
700	427	-231.97	1.775	0.0195	0.6711	3.004	0.0394	30.32	0.7695	0.5387
725	452	-237.28	1.833	0.0193	0.6747	3.004	0.0392	30.71	0.7843	0.5686
750	477	-242.22	1.891	0.0191	0.6784	3.003	0.0389	31.02	0.7965	0.5973
775	502	-246.74	1.948	0.0189	0.6821	3.002	0.0388	31.25	0.8063	0.6249
800	527	-250.82	2.002	0.0188	0.6860	3.001	0.0386	31.43	0.8139	0.6512
825	552	-254.45	2.051	0.0186	0.6899	3.000	0.0385	31.56	0.8198	0.6763
850	577	-257.59	2.095	0.0185	0.6939	2.999	0.0384	31.67	0.8241	0.7004
875	602	-260.22	2.132	0.0184	0.6979	2.998	0.0384	31.76	0.8271	0.7237
900	627	-262.31	2.160	0.0183	0.7020	2.997	0.0384	31.85	0.8293	0.7464
925	652	-263.83	2.178	0.0182	0.7061	2.996	0.0385	31.96	0.8309	0.7686
950	677	-264.76	2.185	0.0181	0.7103	2.995	0.0386	32.09	0.8321	0.7905
975	702	-265.08	2.178	0.0181	0.7145	2.994	0.0387	32.26	0.8332	0.8124
1000	727	-264.76	2.156	0.0181	0.7187	2.993	0.0389	32.48	0.8343	0.8343
1025	752	-263.76	2.125	0.0181	0.7230	2.992	0.0392	32.75	0.8356	0.8565
1050	777	-262.08	2.077	0.0182	0.7272	2.991	0.0395	33.07	0.8369	0.8788
1075	802	-259.67	2.016	0.0182	0.7315	2.990	0.0399	33.44	0.8381	0.9010
1100	827	-256.52	1.944	0.0183	0.7358	2.989	0.0404	33.84	0.8396	0.9225
1125	852	-252.59	1.864	0.0185	0.7402	2.988	0.0409	34.23	0.8374	0.9421
1150	877	-247.87	1.778	0.0186	0.7445	2.987	0.0415	34.55	0.9230	0.9580
1175	902	-242.32	1.693	0.0188	0.7489	2.986	0.0421	34.68	0.8229	0.9670
1200	927			0.0191	0.7533	2.985	0.0429			
1225	952			0.0193	0.7577	2.984	0.0437			
1250	977			0.0196	0.7621	2.983	0.0447			
1275	1002			0.0200	0.7665	2.982	0.0457			
1300	1027			0.0204	0.7709	2.981	0.0468			
INTEGRATED AVERAGE 302 C TO 900 C		-247.25	1.938	0.0198	0.6992	2.998	0.0394	31.60	0.9016	0.7084

SAMPLE: ITM-81
DESCRIPTION: N-TYPE, ATTRITION MILLED
Molecular Weight 36.93

TEMPERATURE	SEEBECK COEFFICIENT	ELECTRICAL RESISTIVITY	THERMAL DIFFUSIVITY	HEAT CAPACITY	DENSITY	THERMAL CONDUCTIVITY	ELECTRICAL POWER FACTOR	FIGURE OF MERIT	DIMENSIONLE FIGURE OF MERIT
	Seebeck and Resistivity Measured Simultaneously GE-SCO		Laser Flash Diffusivity GE-RSO	Drop Calorimetry Ames Lab. MHPS-077P	Immersion Density Thermal Expansion GE-RSO	Calculated	Calculated	Calculated	Calculate
# Points in Fit	106	106	11	11					
Temp. Range of D	31 C	31 C	92 C	375 K					
	1003 C	1003 C	1117 C	1375 K					
RMSD (%)	0.67	1.62	1.13	0.93	0.33	2.39	2.96	5.35	5.3
								Z	ZT
A	-1.23315E+02	1.33864E+00	2.06656E-02	4.66300E+00	3.01				
B	-1.72465E-02	7.80300E-04	-8.23967E-07	1.62220E-03	4.300E-06				
C	-3.74905E-03	1.24522E-05	-2.24615E-08	6.31000E+04					
D	1.95344E-05	-6.54974E-08	2.11850E-11	0.113					
E	-4.91480E-08	1.70098E-10							
F	6.48625E-11	-1.98097E-13							
G	-4.24638E-14	8.11230E-17							
H	1.08494E-17								
Units for Temp:	C	C	C	K	C				K
Equation	A+BT+...HT^7	A+BT+...HT^7	A+BT+...ET^4	D=(A+BT+C/T^2)	A/(1+B(T-27))^3	a*Cp*d	S^2/r	S^2/rk	ZT

(K)	(C)	(microV/K)	(milliohm-cm)	(cm2/sec)	(J/g-K)	(g/cm3)	(W/cm-K)	(microW/cm-K	(1000/K)	
275	2				0.6734	3.011				
300	27	-126.13	1.3674		0.6629	3.010				
325	52	-131.90	1.4046		0.6557	3.009				
350	77	-139.46	1.4478		0.6510	3.008				
375	102	-147.95	1.4943	0.0204	0.6481	3.007	0.0397	14.65	0.3690	0.138
400	127	-156.72	1.5422	0.0202	0.6465	3.006	0.0393	15.93	0.4048	0.161
425	152	-165.38	1.5904	0.0201	0.6460	3.005	0.0390	17.20	0.4408	0.187
450	177	-173.67	1.6384	0.0199	0.6463	3.004	0.0387	18.41	0.4756	0.214
475	202	-181.47	1.6863	0.0198	0.6473	3.003	0.0384	19.53	0.5084	0.241
500	227	-188.75	1.7343	0.0196	0.6488	3.002	0.0381	20.54	0.5389	0.269
525	252	-195.55	1.7830	0.0194	0.6507	3.001	0.0378	21.45	0.5669	0.297
550	277	-201.93	1.8329	0.0192	0.6530	3.000	0.0375	22.25	0.5925	0.325
575	302	-207.98	1.8844	0.0190	0.6556	2.999	0.0373	22.95	0.6159	0.354
600	327	-213.78	1.9382	0.0187	0.6584	2.998	0.0370	23.58	0.6375	0.382
625	352	-219.42	1.9944	0.0185	0.6615	2.997	0.0367	24.14	0.6575	0.410
650	377	-224.95	2.0531	0.0183	0.6647	2.996	0.0364	24.65	0.6763	0.439
675	402	-230.41	2.1141	0.0181	0.6680	2.995	0.0362	25.11	0.6940	0.468
700	427	-235.81	2.1770	0.0179	0.6715	2.995	0.0359	25.54	0.7108	0.497
725	452	-241.12	2.2409	0.0177	0.6751	2.994	0.0357	25.94	0.7268	0.527
750	477	-246.31	2.3048	0.0175	0.6788	2.993	0.0355	26.32	0.7420	0.556
775	502	-251.29	2.3674	0.0173	0.6826	2.992	0.0353	26.67	0.7562	0.586
800	527	-256.00	2.4270	0.0171	0.6865	2.991	0.0351	27.00	0.7694	0.615
825	552	-260.33	2.4820	0.0169	0.6904	2.990	0.0349	27.30	0.7813	0.644
850	577	-264.18	2.5305	0.0168	0.6944	2.989	0.0348	27.58	0.7918	0.673
875	602	-267.46	2.5704	0.0167	0.6984	2.988	0.0347	27.83	0.8009	0.700
900	627	-270.08	2.5999	0.0165	0.7025	2.987	0.0347	28.06	0.8083	0.727
925	652	-271.98	2.6173	0.0165	0.7067	2.986	0.0347	28.26	0.8142	0.753
950	677	-273.11	2.6211	0.0164	0.7108	2.985	0.0348	28.46	0.8185	0.777
975	702	-273.45	2.6100	0.0163	0.7150	2.984	0.0349	28.65	0.8214	0.800
1000	727	-273.03	2.5836	0.0163	0.7192	2.983	0.0350	28.85	0.8233	0.823
1025	752	-271.90	2.5420	0.0164	0.7235	2.982	0.0353	29.08	0.8243	0.845
1050	777	-270.16	2.4861	0.0164	0.7278	2.981	0.0356	29.36	0.8250	0.866
1075	802	-267.95	2.4181	0.0165	0.7321	2.980	0.0360	29.69	0.8256	0.887
1100	827	-265.42	2.3412	0.0166	0.7364	2.979	0.0364	30.09	0.8261	0.908
1125	852	-262.78	2.2604	0.0168	0.7407	2.978	0.0370	30.55	0.8263	0.929
1150	877	-260.22	2.1820	0.0170	0.7451	2.977	0.0376	31.03	0.8251	0.948
1175	902	-257.97	2.1147	0.0172	0.7494	2.976	0.0383	31.47	0.8206	0.964
1200	927	-256.22	2.0691	0.0175	0.7538	2.975	0.0392	31.73	0.8095	0.971
1225	952	-255.12	2.0586	0.0178	0.7582	2.974	0.0401	31.62	0.7876	0.964
1250	977	-254.78	2.0990	0.0182	0.7626	2.973	0.0412	30.93	0.7504	0.938
1275	1002	-255.20	2.2095	0.0186	0.7670	2.972	0.0424	29.48	0.6951	0.886
300	1027			0.0191	0.7715	2.972	0.0437			
INTEGRATED AVERAGE		-254.53	2.316	0.0172	0.7081	2.986	0.0364	28.06	0.7716	0.722
302 C TO 1002 C										

Carnot Efficiency from 300 C to 1000 C 54.9
Material Conversion Efficiency from 300 C to 1000 10.2

SAMPLE: [illegible]
DESCRIPTION: 80%Si-20%Ge
Molecular Weight 36.95

TEMPERATURE	SEEBECK COEFFICIENT	ELECTRICAL RESISTIVITY	THERMAL DIFFUSIVITY	HEAT CAPACITY	DENSITY	THERMAL CONDUCTIVITY	ELECTRICAL POWER FACTOR	FIGURE OF MERIT	DIMENSIONLESS FIGURE OF MERIT
	Seebeck and Resistivity Measured Simultaneously GE-SCO		Laser Flash Diffusivity GE-RSO	Drop Calorimetry Ames Lab. MHPS-077P	Immersion Density Thermal Expansion GE-RSO	Calculated	Calculated	Calculated	Calculated
# Points in Fit	98	91	11	11					
Temp. Range of D	24 C	24 C	107 C	375 K					
	994 C	994 C	1108 C	1375 K					
RMSD (%)	1.05	1.20	0.91	0.93	0.33	2.17	3.30	5.47	5.47
A	-1.14440E+02	1.20639E+00	2.25834E-02	4.66300E+00	2.96			Z	ZT
B	-3.08167E-01	-1.60488E-04	-8.73488E-06	1.62220E-03	4.300E-06				
C	-1.64407E-04	2.52077E-05	-1.01198E-08	6.31000E+04					
D	5.86021E-07	-1.13368E-07	1.49910E-11	0.113					
E	-2.63103E-10	2.53273E-10							
F		-2.85712E-13							
G		1.02068E-16							
H									
Units for Temp:	C	C	C	K	C				K
Equation	A+BT+...HT^7	A+BT+...HT^7	A+BT+...ET^4	D*(A+BT+C/T^2)	A/(1+B(T-27))^3 a*Cp*d		S^2/r	S^2/rk	ZT
(K)	(C)	(microV/K)	(milliohm-cm)	(cm2/sec)	(J/g-K)	(g/cm3)	(W/cm-K)	(microW/cm-K2	(1000/K)
275	2				0.6730	2.961				
300	27	-122.82	1.218		0.6825	2.960		12.38		
325	52	-130.78	1.252		0.6554	2.959		13.66		
350	77	-138.84	1.300		0.6506	2.958		14.83		
375	102	-146.94	1.356	0.0216	0.6477	2.957	0.0414	15.92	0.3847	0.1443
400	127	-155.05	1.418	0.0213	0.6461	2.956	0.0408	16.96	0.4160	0.1664
425	152	-163.11	1.481	0.0211	0.6456	2.955	0.0402	17.97	0.4468	0.1899
450	177	-171.10	1.544	0.0208	0.6460	2.954	0.0397	18.96	0.4775	0.2149
475	202	-178.96	1.607	0.0205	0.6469	2.953	0.0392	19.93	0.5080	0.2413
500	227	-186.66	1.669	0.0203	0.6484	2.952	0.0388	20.88	0.5384	0.2692
525	252	-194.18	1.730	0.0200	0.6504	2.951	0.0384	21.80	0.5684	0.2984
550	277	-201.47	1.790	0.0197	0.6527	2.950	0.0380	22.67	0.5975	0.3286
575	302	-208.51	1.851	0.0194	0.6552	2.950	0.0376	23.49	0.6253	0.3596
600	327	-215.27	1.912	0.0192	0.6581	2.949	0.0372	24.23	0.6515	0.3909
625	352	-221.73	1.975	0.0189	0.6611	2.948	0.0369	24.89	0.6755	0.4222
650	377	-227.86	2.040	0.0187	0.6643	2.947	0.0365	25.46	0.6971	0.4531
675	402	-233.66	2.106	0.0184	0.6677	2.946	0.0362	25.93	0.7159	0.4832
700	427	-239.09	2.174	0.0182	0.6712	2.945	0.0359	26.29	0.7319	0.5123
725	452	-244.16	2.244	0.0180	0.6748	2.944	0.0357	26.57	0.7450	0.5401
750	477	-248.84	2.314	0.0177	0.6785	2.943	0.0354	26.76	0.7554	0.5666
775	502	-253.12	2.383	0.0175	0.6823	2.942	0.0352	26.88	0.7633	0.5916
800	527	-257.01	2.451	0.0174	0.6861	2.941	0.0350	26.95	0.7690	0.6152
825	552	-260.49	2.516	0.0172	0.6901	2.940	0.0349	26.97	0.7730	0.6377
850	577	-263.56	2.575	0.0171	0.6940	2.939	0.0348	26.98	0.7755	0.6592
875	602	-266.23	2.626	0.0169	0.6981	2.938	0.0347	26.99	0.7772	0.6801
900	627	-268.50	2.669	0.0168	0.7022	2.937	0.0347	27.01	0.7784	0.7006
925	652	-270.37	2.701	0.0167	0.7063	2.936	0.0347	27.07	0.7796	0.7211
950	677	-271.85	2.719	0.0167	0.7104	2.935	0.0348	27.18	0.7812	0.7421
975	702	-272.95	2.724	0.0167	0.7146	2.934	0.0349	27.35	0.7834	0.7638
1000	727	-273.69	2.713	0.0166	0.7188	2.933	0.0351	27.61	0.7865	0.7865
1025	752	-274.08	2.688	0.0167	0.7231	2.932	0.0353	27.95	0.7908	0.8105
1050	777	-274.14	2.648	0.0167	0.7274	2.932	0.0356	28.38	0.7960	0.8358
1075	802	-273.89	2.597	0.0168	0.7317	2.931	0.0360	28.89	0.8019	0.8621
1100	827	-273.35	2.536	0.0169	0.7360	2.930	0.0365	29.47	0.8079	0.8897
1125	852	-272.55	2.471	0.0171	0.7403	2.929	0.0370	30.06	0.8125	0.9141
1150	877	-271.51	2.408	0.0173	0.7447	2.928	0.0376	30.61	0.8138	0.9359
1175	902	-270.27	2.358	0.0175	0.7490	2.927	0.0383	30.97	0.8087	0.9502
1200	927	-268.86	2.331	0.0177	0.7534	2.926	0.0391	31.01	0.7934	0.9520
1225	952	-267.32	2.342	0.0180	0.7578	2.925	0.0400	30.51	0.7636	0.9354
1250	977	-265.67	2.408	0.0184	0.7622	2.924	0.0409	29.32	0.7162	0.8963
1275	1002	-263.97	2.549	0.0187	0.7666	2.923	0.0420	27.33	0.6505	0.8294
1300	1027			0.0192	0.7710	2.922	0.0432			
INTEGRATED AVERAGE 302 C TO 952 C		-257.88	2.422	0.0175	0.7035	2.94	0.0360	27.52	0.7638	0.8947

Carnot Efficiency from 300 C to 1000 C 54.9
Material Conversion Efficiency from 300 C to 1000 C 9.94

SAMPLE: ITM-93
DESCRIPTION: 80%Si-20%Ge
Molecular Weight 36.95

TEMPERATURE	SEEBECK COEFFICIENT	ELECTRICAL RESISTIVITY	THERMAL DIFFUSIVITY	HEAT CAPACITY	DENSITY	THERMAL CONDUCTIVITY	ELECTRICAL POWER FACTOR	FIGURE OF MERIT	DIMENSIONLESS FIGURE OF MERIT
	Seebeck and Resistivity Measured Simultaneously GE-SCO		Laser Flash Diffusivity GE-RSD	Drop Calorimetry Ames Lab. MHPS-077P	Immersion Density Thermal Expansion GE-RSD	Calculated	Calculated	Calculated	Calculated
# Points in Fit	102	95	11	11					
Temp. Range of D	32 C 1036 C	32 C 1025 C	105 C 1103 C	375 K 1375 K					
RMSD (%)	1.19	1.65	1.23	0.93	0.33	2.49	4.03	6.52	6.52
								Z	ZT
A	-1.11831E+02	1.28552E+00	2.35678E-02	4.66300E+00	2.96				
B	-2.89072E-01	-4.98528E-03	-1.00688E-05	1.62220E-03	4.300E-06				
C	-7.89604E-05	7.84295E-05	-8.72852E-09	6.31000E+04					
D	2.27570E-07	-4.08399E-07	1.50201E-11	0.113					
E		1.07479E-09							
F		-1.46076E-12							
G		9.71947E-16							
H		-2.50256E-19							
Units for Temp:	C	C	C	K	C				K
Equation	A+BT+...HT^7	A+BT+...HT^7	A+BT+...ET^4	D*(A+BT+C/T^2)	A/(1+B(T-27))^3 a*Cp*d		S^2/r	S^2/rk	ZT

(K)	(C)	(microV/K)	(milliohm-cm)	(cm2/sec)	(J/g-K)	(g/cm3)	(W/cm-K)	(microW/cm-K2	(1000/K)	
275	2				0.6730	2.961	0.0000	ERR	ERR	ERR
300	27				0.6625	2.960	0.0000	ERR	ERR	ERR
325	52	-127.00	1.188		0.6554	2.959	0.0000	13.57	ERR	ERR
350	77	-134.41	1.214		0.6506	2.958	0.0000	14.88	ERR	ERR
375	102	-141.85	1.261	0.0225	0.6477	2.957	0.0430	15.96	0.3709	0.1351
400	127	-149.31	1.316	0.0222	0.6461	2.956	0.0424	16.94	0.3999	0.1600
425	152	-156.75	1.372	0.0219	0.6456	2.955	0.0418	17.91	0.4288	0.1822
450	177	-164.16	1.425	0.0216	0.6460	2.954	0.0412	18.91	0.4589	0.2065
475	202	-171.53	1.473	0.0213	0.6469	2.953	0.0407	19.97	0.4907	0.2331
500	227	-178.81	1.517	0.0210	0.6484	2.952	0.0402	21.08	0.5242	0.2621
525	252	-186.01	1.557	0.0207	0.6504	2.951	0.0398	22.23	0.5589	0.2934
550	277	-193.08	1.595	0.0204	0.6527	2.950	0.0393	23.37	0.5940	0.3267
575	302	-200.02	1.635	0.0201	0.6552	2.950	0.0389	24.47	0.6286	0.3614
600	327	-206.80	1.677	0.0199	0.6581	2.949	0.0386	25.50	0.6615	0.3969
625	352	-213.40	1.724	0.0196	0.6611	2.948	0.0382	26.42	0.6917	0.4323
650	377	-219.80	1.776	0.0193	0.6643	2.947	0.0379	27.20	0.7185	0.4671
675	402	-225.98	1.835	0.0191	0.6677	2.946	0.0375	27.84	0.7415	0.5005
700	427	-231.91	1.899	0.0188	0.6712	2.945	0.0373	28.33	0.7604	0.5323
725	452	-237.58	1.968	0.0186	0.6748	2.944	0.0370	28.69	0.7755	0.5622
750	477	-242.95	2.040	0.0184	0.6785	2.943	0.0368	28.94	0.7873	0.5905
775	502	-248.02	2.113	0.0182	0.6823	2.942	0.0366	29.12	0.7964	0.6172
800	527	-252.77	2.184	0.0180	0.6861	2.941	0.0364	29.25	0.8036	0.6425
825	552	-257.16	2.252	0.0179	0.6901	2.940	0.0363	29.36	0.8096	0.6669
850	577	-261.17	2.313	0.0177	0.6940	2.939	0.0362	29.50	0.8152	0.6909
875	602	-264.80	2.363	0.0176	0.6981	2.938	0.0361	29.67	0.8209	0.7149
900	627	-268.01	2.402	0.0175	0.7022	2.937	0.0361	29.90	0.8273	0.7446
925	652	-270.78	2.427	0.0175	0.7063	2.936	0.0362	30.21	0.8347	0.7721
950	677	-273.10	2.436	0.0174	0.7104	2.935	0.0363	30.62	0.8432	0.8011
975	702	-274.93	2.429	0.0174	0.7146	2.934	0.0365	31.11	0.8530	0.8317
1000	727	-276.27	2.407	0.0174	0.7188	2.933	0.0367	31.71	0.8639	0.8639
1025	752	-277.09	2.371	0.0174	0.7231	2.932	0.0370	32.38	0.8753	0.8971
1050	777	-277.36	2.322	0.0175	0.7274	2.932	0.0374	33.12	0.8867	0.9310
1075	802	-277.07	2.265	0.0176	0.7317	2.931	0.0378	33.89	0.8967	0.9649
1100	827	-276.19	2.203	0.0178	0.7360	2.930	0.0383	34.62	0.9038	0.9942
1125	852	-274.70	2.141	0.0179	0.7403	2.929	0.0389	35.24	0.9060	1.0192
1150	877	-272.59	2.085	0.0182	0.7447	2.928	0.0396	35.64	0.9006	1.0357
1175	902	-269.83	2.039	0.0184	0.7490	2.927	0.0403	35.71	0.8851	1.0400
1200	927	-266.39	2.009	0.0187	0.7534	2.926	0.0412	35.33	0.8573	1.0287
1225	952	-262.27	1.999	0.0190	0.7578	2.925	0.0422	34.42	0.8160	0.9995
1250	977	-257.43	2.012	0.0194	0.7622	2.924	0.0432	32.94	0.7616	0.9521
1275	1002	-251.86	2.049	0.0198	0.7666	2.923	0.0444	30.95	0.6967	0.8884
1300	1027	-245.52	2.109	0.0203	0.7710	2.922	0.0457	28.58	0.6253	0.8123
INTEGRATED AVERAGE 302 C TO 952 C		-255.68	2.134	0.0182	0.7035	2.94	0.0376	30.72	0.8168	0.7471
								302 to 1002	0.8075	
								502 to 1002	0.8349	
Carnot Efficiency from 300 C to 1000 C										54.98
Material Conversion Efficiency from 300 C to 1000 C										10.47

SAMPLE: ITN-72
DESCRIPTION: 80%Si-20%Ge
Molecular Weight 36.83

TEMPERATURE	SEEBECK COEFFICIENT	ELECTRICAL RESISTIVITY	THERMAL DIFFUSIVITY	HEAT CAPACITY	DENSITY	THERMAL CONDUCTIVITY	ELECTRICAL POWER FACTOR	FIGURE OF MERIT	DIMENSIONLESS FIGURE OF MERIT
	Seebeck and Resistivity Measured Simultaneously GE-SCD		Laser Flash Diffusivity GE-RSD	Drop Calorimetry Ames Lab. MMPS-077P	Immersion Density Thermal Expansion GE-RSD	Calculated	Calculated	Calculated	Calculated
# Points in Fit	102	86	11	11					
Temp. Range of D	22 C	22 C	101 C	375 K					
	1032 C	1032 C	1097 C	1375 K					
RMSD (%)	0.50	0.33	0.70	0.93	0.33	1.86	1.33	3.29	3.29
A	1.28625E+02	1.96806E+00	1.89539E-02	4.66300E+00	2.98			Z	ZT
B	2.35323E-01	4.25932E-03	7.58321E-07	1.62220E-03	4.300E-06				
C	3.47648E-04	-2.04987E-05	-2.88745E-08	6.31000E+04					
D	-1.74756E-06	9.20461E-08	2.76962E-11	0.113					
E	2.45894E-09	-1.85888E-10							
F	-1.17129E-12	1.76314E-13							
G		-6.35802E-17							
H									
Units for Temp:	C	C	C	K	C		S^2/r	S^2/rk	K
Equation	A+BT+...HT^7	A+BT+...HT^7	A+BT+...ET^4	D=(A+BT+C/T^2)	A/(1+B(T-27))^3	a*Cp+d			ZT
(K)	(C)	(microV/K)	(milliohm-cm)	(cm2/sec)	(J/g-K)	(g/cm3)	(W/cm-K)	(microW/cm-K2)	(1000/K)	
275	2				0.6734	2.981				
300	27	135.06	2.069		0.6629	2.980		8.82		
325	52	141.44	2.145		0.6557	2.979		9.32		
350	77	147.95	2.210		0.6510	2.978		9.90		
375	102	154.50	2.268	0.0188	0.6481	2.977	0.0362	10.52	0.2907	0.1090
400	127	161.00	2.324	0.0186	0.6465	2.976	0.0359	11.15	0.3110	0.1244
425	152	167.37	2.379	0.0185	0.6460	2.975	0.0356	11.77	0.3312	0.1407
450	177	173.55	2.436	0.0183	0.6463	2.974	0.0353	12.36	0.3508	0.1578
475	202	179.51	2.496	0.0182	0.6473	2.973	0.0349	12.91	0.3694	0.175
500	227	185.21	2.559	0.0180	0.6488	2.972	0.0346	13.40	0.3870	0.193
525	252	190.63	2.626	0.0178	0.6507	2.971	0.0343	13.84	0.4032	0.2117
550	277	195.78	2.696	0.0175	0.6530	2.970	0.0340	14.22	0.4180	0.229
575	302	200.65	2.768	0.0173	0.6556	2.969	0.0337	14.54	0.4315	0.2481
600	327	205.25	2.843	0.0171	0.6584	2.969	0.0334	14.82	0.4438	0.266
625	352	209.61	2.920	0.0169	0.6615	2.968	0.0331	15.05	0.4549	0.284
650	377	213.74	2.997	0.0166	0.6647	2.967	0.0328	15.24	0.4651	0.302
675	402	217.67	3.075	0.0164	0.6680	2.966	0.0325	15.41	0.4744	0.320
700	427	221.43	3.153	0.0162	0.6715	2.965	0.0322	15.55	0.4831	0.338
725	452	225.06	3.230	0.0160	0.6751	2.964	0.0319	15.68	0.4911	0.356
750	477	228.56	3.307	0.0158	0.6788	2.963	0.0317	15.80	0.4986	0.374
775	502	231.99	3.383	0.0156	0.6826	2.962	0.0315	15.91	0.5056	0.391
800	527	235.36	3.458	0.0154	0.6865	2.961	0.0313	16.02	0.5120	0.409
825	552	238.67	3.533	0.0152	0.6904	2.960	0.0311	16.12	0.5179	0.427
850	577	241.96	3.609	0.0151	0.6944	2.959	0.0310	16.22	0.5229	0.444
875	602	245.24	3.684	0.0150	0.6984	2.958	0.0310	16.32	0.5271	0.461
900	627	248.49	3.761	0.0149	0.7025	2.957	0.0310	16.42	0.5302	0.477
925	652	251.71	3.840	0.0149	0.7067	2.956	0.0310	16.50	0.5318	0.492
950	677	254.87	3.921	0.0148	0.7108	2.955	0.0311	16.57	0.5319	0.506
975	702	257.94	4.005	0.0148	0.7150	2.954	0.0313	16.61	0.5301	0.516
1000	727	260.87	4.090	0.0149	0.7192	2.953	0.0316	16.64	0.5262	0.526
1025	752	263.58	4.179	0.0150	0.7235	2.952	0.0320	16.63	0.5199	0.532
1050	777	266.01	4.268	0.0151	0.7278	2.951	0.0324	16.58	0.5111	0.53
1075	802	268.04	4.358	0.0153	0.7321	2.950	0.0330	16.48	0.4996	0.537
1100	827	269.55	4.446	0.0155	0.7364	2.949	0.0337	16.34	0.4855	0.534
1125	852	270.42	4.529	0.0158	0.7407	2.949	0.0344	16.14	0.4688	0.527
1150	877	270.47	4.604	0.0161	0.7451	2.948	0.0353	15.88	0.4497	0.517
1175	902	269.51	4.664	0.0165	0.7494	2.947	0.0364	15.57	0.4282	0.503
1200	927	267.33	4.705	0.0169	0.7538	2.946	0.0375	15.19	0.4047	0.485
1225	952	263.70	4.716	0.0174	0.7582	2.945	0.0388	14.74	0.3795	0.464
1250	977	258.34	4.690	0.0180	0.7626	2.944	0.0403	14.23	0.3530	0.441
1275	1002	250.97	4.613	0.0186	0.7670	2.943	0.0419	13.65	0.3255	0.415
1300	1027	241.25	4.472	0.0193	0.7715	2.942	0.0437	13.01	0.2975	0.388
INTEGRATED AVERAGE 302 C TO 1002 C		245.76	3.845	0.0159	0.7081	2.956	0.0333	15.81	0.4795	0.435

Carnot Efficiency from 300 C to 1000 C 54.5
Material Conversion Efficiency from 300 C to 1000 C 6.5

SAMPLE: ITH-73
DESCRIPTION: SiGe
Molecular Weight 36.93

TEMPERATURE	SEEBECK COEFFICIENT	ELECTRICAL RESISTIVITY	THERMAL DIFFUSIVITY	HEAT CAPACITY	DENSITY	THERMAL CONDUCTIVITY	ELECTRICAL POWER FACTOR	FIGURE OF MERIT	DIMENSIONLES FIGURE OF MERIT
	Seebeck and Resistivity Measured Simultaneously GE-SCD		Laser Flash Diffusivity GE-RSD	Drop Calorimetry Ames Lab. MHPS-077P	Immersion Density Thermal Expansion GE-RSD	Calculated	Calculated	Calculated	Calculate
# Points in Fit	100	101	11	11					
Temp. Range of D	31 C 971 C	31 C 971 C	103 C 1098 C	375 K 1375 K					
RMSD (%)	0.85	0.39	0.57	0.93	0.33	1.83	2.09	3.92	3.9
								Z	ZT
A	1.17204E+02	1.12750E+00	2.70068E-02	4.66300E+00	2.87				
B	2.45451E-01	1.63355E-03	7.56890E-06	1.62220E-03	4.300E-06				
C	-9.07395E-05	1.32010E-06	-4.99316E-08	6.31000E+04					
D		-4.76177E-10	3.71408E-11	0.113					
E									
F									
G									
H									
Units for Temp:	C	C	C	K	C				K
Equation	A+BT+...HT^7	A+BT+...HT^7	A+BT+...ET^4	D=(A+BT+C/T^2)	A/(1+B(T-ZT))^3	a+Cp+d	S^2/r	S^2/rk	ZT
(K)	(C)	(microV/K)	(milliohm-cm)	(cm2/sec)	(J/g-K)	(g/cm3)	(W/cm-K)	(microW/cm-K2	(1000/K)
275	2				0.6734	2.871			
300	27	123.73	1.1723		0.6629	2.870			
325	52	129.69	1.2157		0.6557	2.869			
350	77	135.53	1.2606		0.6510	2.868			
375	102	141.26	1.3071	0.0273	0.6481	2.867	0.0507		
400	127	146.88	1.3550	0.0272	0.6465	2.866	0.0505		
425	152	152.38	1.4043	0.0271	0.6460	2.865	0.0502		
450	177	157.77	1.4551	0.0270	0.6463	2.864	0.0500	17.11	0.3424 0.154
475	202	163.05	1.5071	0.0268	0.6473	2.864	0.0497	17.64	0.3550 0.168
500	227	168.22	1.5604	0.0266	0.6488	2.863	0.0494	18.13	0.3672 0.183
525	252	173.27	1.6150	0.0263	0.6507	2.862	0.0490	18.59	0.3790 0.199
550	277	178.20	1.6708	0.0261	0.6530	2.861	0.0487	19.01	0.3904 0.214
575	302	183.03	1.7278	0.0258	0.6556	2.860	0.0483	19.39	0.4014 0.230
600	327	187.74	1.7858	0.0254	0.6584	2.859	0.0479	19.74	0.4121 0.247
625	352	192.33	1.8450	0.0251	0.6615	2.858	0.0475	20.05	0.4224 0.264
650	377	196.82	1.9051	0.0248	0.6647	2.857	0.0470	20.33	0.4325 0.281
675	402	201.19	1.9662	0.0244	0.6680	2.856	0.0465	20.59	0.4422 0.298
700	427	205.44	2.0283	0.0240	0.6715	2.855	0.0461	20.81	0.4517 0.316
725	452	209.58	2.0912	0.0237	0.6751	2.854	0.0456	21.00	0.4607 0.334
750	477	213.61	2.1550	0.0233	0.6788	2.853	0.0451	21.17	0.4694 0.352
775	502	217.53	2.2196	0.0229	0.6826	2.852	0.0446	21.32	0.4776 0.370
800	527	221.33	2.2849	0.0226	0.6865	2.852	0.0442	21.44	0.4853 0.389
825	552	225.02	2.3510	0.0222	0.6904	2.851	0.0437	21.54	0.4925 0.406
850	577	228.60	2.4177	0.0219	0.6944	2.850	0.0433	21.61	0.4990 0.424
875	602	232.06	2.4850	0.0216	0.6984	2.849	0.0429	21.67	0.5049 0.441
900	627	235.41	2.5529	0.0213	0.7025	2.848	0.0426	21.71	0.5099 0.458
925	652	238.65	2.6214	0.0210	0.7067	2.847	0.0423	21.73	0.5140 0.475
950	677	241.77	2.6903	0.0208	0.7108	2.846	0.0420	21.73	0.5170 0.491
975	702	244.78	2.7597	0.0206	0.7150	2.845	0.0418	21.71	0.5190 0.506
1000	727	247.67	2.8294	0.0204	0.7192	2.844	0.0417	21.68	0.5197 0.519
1025	752	250.45	2.8995	0.0203	0.7235	2.843	0.0417	21.63	0.5191 0.532
1050	777	253.12	2.9700	0.0202	0.7278	2.842	0.0417	21.57	0.5172 0.543
1075	802	255.68	3.0406	0.0201	0.7321	2.842	0.0419	21.50	0.5137 0.552
1100	827	258.12	3.1116	0.0201	0.7364	2.841	0.0421	21.41	0.5087 0.559
1125	852	260.45	3.1826	0.0202	0.7407	2.840	0.0424	21.31	0.5021 0.564
1150	877	262.66	3.2538	0.0203	0.7451	2.839	0.0429	21.20	0.4940 0.568
1175	902	264.76	3.3251	0.0205	0.7494	2.838	0.0435	21.08	0.4844 0.569
1200	927	266.75	3.3965	0.0207	0.7538	2.837	0.0443	20.95	0.4733 0.567
1225	952	268.63	3.4678	0.0210	0.7582	2.836	0.0452	20.81	0.4608 0.564
1250	977	270.39	3.5391	0.0214	0.7626	2.835	0.0462	20.66	0.4470 0.558
1275	1002	272.03	3.6102	0.0218	0.7670	2.834	0.0474	20.50	0.4321 0.551
1300	1027			0.0223	0.7715	2.833	0.0488		
INTEGRATED AVERAGE 302 C TO 1002 C		234.93	2.637	0.0219	0.7081	2.847	0.0441	21.14	0.4810 0.448

Carnot Efficiency from 300 C to 1000 C 54.9
Material Conversion Efficiency from 300 C to 1000 C 7.1

SAMPLE: ITM-74
DESCRIPTION: 80%Si-20%Ge
Molecular Weight 36.93

TEMPERATURE	SEEBECK COEFFICIENT	ELECTRICAL RESISTIVITY	THERMAL DIFFUSIVITY	HEAT CAPACITY	DENSITY	THERMAL CONDUCTIVITY	ELECTRICAL POWER FACTOR	FIGURE OF MERIT	DIMENSIONLESS FIGURE OF MERIT
	Seebeck and Resistivity Measured Simultaneously GE-SCO		Laser Flash Diffusivity GE-RSO	Drop Calorimetry Ames Lab. MHPS-077P	Immersion Density Thermal Expansion GE-RSO	Calculated	Calculated	Calculated	Calculated
# Points in Fit	77	77	11	11					
Temp. Range of D	300 C	300 C	100 C	375 K					
	968 C	968 C	1089 C	1375 K					
RMSD (%)	0.57	1.96	0.75	0.93	0.33	2.01	3.10	5.11	5.11
A	1.12677E+02	1.48953E+00	2.42050E-02	4.66300E+00	2.94			Z	ZT
B	2.52624E-01	4.23344E-06	1.35354E-05	1.62220E-03	4.300E-06				
C	-1.12818E-04	4.60422E-06	-6.12341E-08	6.31000E+04					
D		-2.48532E-09	4.50206E-11	0.113					
E									
F									
G									
H									

Units for Temp:	C	C	C	K	C				K
Equation	A+BT+...HT^7	A+BT+...HT^7	A+BT+...ET^4	D*(A+BT+C/T^2)	A/(1+B(T-27))^3	a*Cp*d	S^2/r	S^2/rk	ZT
(K)	(C)	(microV/K)	(milliohm-cm)	(cm2/sec)	(J/g-K)	(g/cm3)	(W/cm-K)	(microW/cm-K2)	(1000/K)	
275	2				0.6734	2.941				
300	27				0.6629	2.940				
325	52				0.6557	2.939				
350	77				0.6510	2.938				
375	102			0.0250	0.6481	2.937	0.0476			
400	127			0.0250	0.6465	2.936	0.0475			
425	152			0.0250	0.6460	2.935	0.0474			
450	177			0.0249	0.6463	2.934	0.0473			
475	202			0.0248	0.6473	2.933	0.0471			
500	227			0.0246	0.6488	2.932	0.0469			
525	252			0.0244	0.6507	2.931	0.0466			
550	277			0.0242	0.6530	2.931	0.0463			
575	302	178.65	1.842	0.0239	0.6556	2.930	0.0460	17.33	0.3787	0.2166
600	327	183.19	1.896	0.0237	0.6584	2.929	0.0456	17.70	0.3880	0.2328
625	352	187.60	1.953	0.0233	0.6615	2.928	0.0452	18.02	0.3986	0.2491
650	377	191.86	2.012	0.0230	0.6647	2.927	0.0448	18.29	0.4085	0.2656
675	402	195.96	2.073	0.0227	0.6680	2.926	0.0443	18.52	0.4179	0.2821
700	427	199.95	2.137	0.0223	0.6715	2.925	0.0439	18.71	0.4266	0.2986
725	452	203.79	2.202	0.0220	0.6751	2.924	0.0434	18.86	0.4348	0.3152
750	477	207.49	2.269	0.0216	0.6788	2.923	0.0429	18.97	0.4423	0.3317
775	502	211.04	2.337	0.0213	0.6826	2.922	0.0424	19.06	0.4493	0.3481
800	527	214.46	2.406	0.0209	0.6865	2.921	0.0420	19.11	0.4555	0.3644
825	552	217.73	2.476	0.0206	0.6904	2.920	0.0415	19.14	0.4611	0.3804
850	577	220.86	2.547	0.0203	0.6944	2.919	0.0411	19.15	0.4659	0.3960
875	602	223.85	2.618	0.0200	0.6984	2.918	0.0407	19.14	0.4699	0.4111
900	627	226.70	2.689	0.0197	0.7025	2.917	0.0404	19.11	0.4729	0.4256
925	652	229.41	2.760	0.0195	0.7067	2.916	0.0401	19.07	0.4750	0.4393
950	677	231.98	2.831	0.0193	0.7108	2.915	0.0399	19.01	0.4759	0.4521
975	702	234.41	2.901	0.0191	0.7150	2.915	0.0398	18.94	0.4757	0.4638
1000	727	236.69	2.971	0.0190	0.7192	2.914	0.0398	18.86	0.4741	0.4741
1025	752	238.84	3.039	0.0189	0.7235	2.913	0.0398	18.77	0.4712	0.4830
1050	777	240.84	3.106	0.0189	0.7278	2.912	0.0400	18.67	0.4669	0.4909
1075	802	242.71	3.172	0.0189	0.7321	2.911	0.0403	18.57	0.4612	0.4956
1100	827	244.43	3.236	0.0190	0.7364	2.910	0.0407	18.46	0.4539	0.4993
1125	852	246.01	3.298	0.0191	0.7407	2.909	0.0412	18.35	0.4452	0.5009
1150	877	247.45	3.358	0.0193	0.7451	2.908	0.0419	18.24	0.4351	0.5004
1175	902	248.75	3.415	0.0196	0.7494	2.907	0.0428	18.12	0.4236	0.4979
1200	927	249.90	3.470	0.0200	0.7538	2.906	0.0438	18.00	0.4109	0.4931
1225	952	250.92	3.522	0.0204	0.7582	2.905	0.0450	17.88	0.3972	0.4865
1250	977			0.0210	0.7626	2.904	0.0464	ERR	ERR	ERR
1275	1002			0.0216	0.7670	2.903	0.0480	ERR	ERR	ERR
1300	1027			0.0223	0.7715	2.902	0.0499			
INTEGRATED AVERAGE 302 C TO 952 C		222.72	2.687	0.0205	0.7039	2.92	0.0421	18.63	0.4441	0.4016

Carnot Efficiency from 300 C to 1000 C 54.39
Material Conversion Efficiency from 300 C to 1000 C 6.50

SAMPLE: ITM-75
DESCRIPTION: 80%Si-20%Ge
Molecular Weight 36.93

TEMPERATURE	SEEBECK COEFFICIENT	ELECTRICAL RESISTIVITY	THERMAL DIFFUSIVITY	HEAT CAPACITY	DENSITY	THERMAL CONDUCTIVITY	ELECTRICAL POWER FACTOR	FIGURE OF MERIT	DIMENSIONLESS FIGURE OF MERIT
	Seebeck and Resistivity Measured Simultaneously GE-SCO		Laser Flash Diffusivity GE-RSD	Drop Calorimetry Ames Lab. MHPS-077P	Immersion Density Thermal Expansion GE-RSD	Calculated	Calculated	Calculated	Calculated
# Points in Fit	98	93	11	11					
Temp. Range of D	24 C	24 C	99 C	375 K					
	986 C	986 C	1093 C	1375 K					
RMSD (%)	0.77	1.27	0.80	0.93	0.33	2.06	2.81	4.87	4.87
								Z	ZT
A	1.19771E+02	1.24999E+00	1.97681E-02	4.66300E+00	2.96				
B	2.61756E-01	2.04192E-03	1.68452E-05	1.62220E-03	4.300E-06				
C	-1.16765E-04	-1.02935E-06	-5.88140E-08	6.31000E+04					
D		3.70260E-09	4.16115E-11	0.113					
E		-2.43136E-12							
F									
G									
H									
Units for Temp:	C	C	C	K	C		S^2/r	S^2/rk	K
Equation	A+BT+...HT^7	A+BT+...HT^7	A+BT+...ET^4	D*(A+BT+C/T^2)	A/(1+B(T-27))^3	a*Cp*d			ZT
(K)	(C)	(microV/K)	(milliohm-cm)	(cm2/sec)	(J/g-K)	(g/cm3)	(W/cm-K)	(microW/cm-K2	(1000/K)	
275	2				0.6734	2.961				
300	27	126.72	1.304		0.6529	2.960		12.31		
325	52	133.03	1.354		0.6557	2.959		13.07		
350	77	139.20	1.402		0.6510	2.958		13.82		
375	102	145.22	1.451	0.0209	0.6481	2.957	0.0401	14.53	0.3626	0.1360
400	127	151.10	1.499	0.0210	0.6465	2.956	0.0402	15.23	0.3786	0.1514
425	152	156.83	1.548	0.0211	0.6460	2.955	0.0403	15.88	0.3941	0.1675
450	177	162.41	1.597	0.0211	0.6463	2.954	0.0404	16.52	0.4092	0.1842
475	202	167.85	1.647	0.0211	0.6473	2.953	0.0404	17.11	0.4239	0.2014
500	227	173.14	1.697	0.0210	0.6488	2.952	0.0403	17.67	0.4381	0.2191
525	252	178.29	1.748	0.0209	0.6507	2.951	0.0402	18.18	0.4520	0.2373
550	277	183.29	1.801	0.0208	0.6530	2.950	0.0401	18.66	0.4654	0.2560
575	302	188.14	1.854	0.0206	0.6556	2.950	0.0399	19.09	0.4784	0.2751
600	327	192.85	1.909	0.0204	0.6584	2.949	0.0397	19.48	0.4909	0.2945
625	352	197.41	1.965	0.0202	0.6615	2.948	0.0394	19.83	0.5029	0.3141
650	377	201.83	2.022	0.0200	0.6647	2.947	0.0392	20.14	0.5144	0.3344
675	402	206.10	2.081	0.0197	0.6680	2.946	0.0388	20.41	0.5254	0.3547
700	427	210.23	2.141	0.0195	0.6715	2.945	0.0385	20.64	0.5358	0.3751
725	452	214.21	2.203	0.0192	0.6751	2.944	0.0382	20.83	0.5456	0.3955
750	477	218.04	2.265	0.0189	0.6788	2.943	0.0378	20.98	0.5547	0.4160
775	502	221.73	2.329	0.0187	0.6826	2.942	0.0375	21.11	0.5630	0.436
800	527	225.27	2.394	0.0184	0.6865	2.941	0.0372	21.20	0.5704	0.456
825	552	228.66	2.460	0.0181	0.6904	2.940	0.0368	21.25	0.5770	0.476
850	577	231.91	2.527	0.0179	0.6944	2.939	0.0365	21.28	0.5828	0.495
875	602	235.01	2.594	0.0177	0.6984	2.938	0.0363	21.29	0.5870	0.513
900	627	237.97	2.662	0.0175	0.7025	2.937	0.0360	21.27	0.5902	0.531
925	652	240.78	2.730	0.0173	0.7067	2.936	0.0359	21.24	0.5921	0.547
950	677	243.45	2.798	0.0171	0.7108	2.935	0.0357	21.18	0.5926	0.563
975	702	245.97	2.866	0.0170	0.7150	2.934	0.0357	21.11	0.5918	0.578
1000	727	248.34	2.934	0.0169	0.7192	2.933	0.0357	21.02	0.5890	0.593
1025	752	250.57	3.000	0.0169	0.7235	2.932	0.0358	20.93	0.5846	0.599
1050	777	252.65	3.065	0.0169	0.7278	2.932	0.0360	20.82	0.5786	0.607
1075	802	254.58	3.129	0.0169	0.7321	2.931	0.0363	20.71	0.5708	0.613
1100	827	256.37	3.191	0.0170	0.7364	2.930	0.0367	20.60	0.5613	0.617
1125	852	258.02	3.251	0.0172	0.7407	2.929	0.0372	20.48	0.5501	0.618
1150	877	259.52	3.308	0.0174	0.7451	2.928	0.0379	20.36	0.5373	0.617
1175	902	260.87	3.362	0.0176	0.7494	2.927	0.0387	20.24	0.5230	0.614
1200	927	262.07	3.412	0.0180	0.7538	2.926	0.0397	20.13	0.5074	0.608
1225	952	263.13	3.458	0.0184	0.7582	2.925	0.0408	20.02	0.4906	0.601
1250	977	264.05	3.500	0.0189	0.7626	2.924	0.0421	19.92	0.4730	0.591
1275	1002	264.81	3.536	0.0195	0.7670	2.923	0.0436	19.83	0.4546	0.579
1300	1027			0.0201	0.7715	2.922	0.0453			
INTEGRATED AVERAGE 302 C TO 952 C		233.85	2.664	0.0182	0.7039	2.94	0.0374	20.70	0.5539	0.500

Carnot Efficiency from 300 C to 1000 C 54.9
Material Conversion Efficiency from 300 C to 1000 C 7.7

SAMPLE: ITM-78B
DESCRIPTION: 80%Si-20%Ge
Molecular Weight 36.93

TEMPERATURE	SEEBECK COEFFICIENT	ELECTRICAL RESISTIVITY	THERMAL DIFFUSIVITY	HEAT CAPACITY	DENSITY	THERMAL CONDUCTIVITY	ELECTRICAL POWER FACTOR	FIGURE OF MERIT	DIMENSIONLESS FIGURE OF MERIT
	Seebeck and Resistivity Measured Simultaneously GE-SCO		Laser Flash Diffusivity GE-RSO	Drop Calorimetry Ames Lab. MHPS-077P	Immersion Density Thermal Expansion GE-RSO	Calculated	Calculated	Calculated	Calculated
# Points in Fit	102	96	11	11					
Temp. Range of D	27 C	27 C	96 C	375 K					
	1037 C	1037 C	1083 C	1375 K					
RMSD (%)	0.70	0.17	1.56	0.93	0.33	2.82	1.57	4.39	4.39
A	1.15590E+02	1.29684E+00	2.27903E-02	4.66300E+00	2.98			Z	ZT
B	3.23673E-01	1.80361E-03	1.43503E-05	1.62220E-03	4.300E-06				
C	-5.57873E-04	-2.11818E-07	-6.13620E-08	6.31000E+04					
D	8.81007E-07	6.72786E-09	4.54359E-11	0.113					
E	-5.04316E-10	-1.63582E-11							
F		2.20787E-14							
G		-9.72879E-18							
H									
Units for Temp:	C	C	C	K	C				K
Equation	A+BT+...HT^7	A+BT+...HT^7	A+BT+...ET^4	D*(A+BT+C/T^2)	A/(1+B(T-27))^3 a*Cp*d		S^2/r	S^2/rk	ZT
(K)	(C)	(microV/K)	(milliohm-cm)	(cm2/sec)	(J/g-K)	(g/cm3)	(W/cm-K)	(microW/cm-K2)	(1000/K)	
275	2				0.6734	2.981				
300	27	123.90	1.345		0.6629	2.980		11.41		
325	52	130.99	1.391		0.6557	2.979		12.34		
350	77	137.55	1.437		0.6510	2.978		13.17		
375	102	143.65	1.484	0.0237	0.6481	2.977	0.0457	13.91	0.3046	0.1142
400	127	149.34	1.532	0.0237	0.6465	2.976	0.0456	14.56	0.3190	0.1276
425	152	154.69	1.581	0.0237	0.6460	2.975	0.0456	15.13	0.3320	0.1411
450	177	159.76	1.632	0.0237	0.6463	2.974	0.0455	15.64	0.3439	0.1547
475	202	164.60	1.684	0.0236	0.6473	2.973	0.0453	16.08	0.3548	0.1683
500	227	169.26	1.737	0.0234	0.6488	2.972	0.0452	16.49	0.3652	0.1826
525	252	173.77	1.791	0.0232	0.6507	2.971	0.0449	16.86	0.3752	0.1970
550	277	178.17	1.846	0.0230	0.6530	2.970	0.0447	17.19	0.3850	0.2117
575	302	182.50	1.903	0.0228	0.6556	2.969	0.0443	17.51	0.3948	0.2270
600	327	186.79	1.960	0.0225	0.6584	2.969	0.0440	17.80	0.4047	0.2428
625	352	191.06	2.018	0.0222	0.6615	2.968	0.0436	18.09	0.4148	0.2592
650	377	195.32	2.076	0.0219	0.6647	2.967	0.0432	18.37	0.4252	0.2764
675	402	199.59	2.136	0.0216	0.6680	2.966	0.0428	18.65	0.4360	0.2943
700	427	203.88	2.196	0.0213	0.6715	2.965	0.0423	18.93	0.4470	0.3133
725	452	208.19	2.257	0.0209	0.6751	2.964	0.0419	19.20	0.4584	0.3328
750	477	212.53	2.319	0.0206	0.6788	2.963	0.0414	19.48	0.4700	0.3535
775	502	216.89	2.382	0.0203	0.6826	2.962	0.0410	19.75	0.4816	0.3733
800	527	221.25	2.446	0.0200	0.6865	2.961	0.0406	20.01	0.4932	0.3949
825	552	225.60	2.511	0.0197	0.6904	2.960	0.0402	20.27	0.5048	0.4163
850	577	229.93	2.577	0.0194	0.6944	2.959	0.0398	20.51	0.5154	0.4391
875	602	234.21	2.645	0.0191	0.6984	2.958	0.0395	20.74	0.5255	0.4593
900	627	238.41	2.714	0.0189	0.7025	2.957	0.0392	20.95	0.5345	0.4810
925	652	242.50	2.784	0.0187	0.7067	2.956	0.0390	21.13	0.5421	0.5019
950	677	246.43	2.855	0.0185	0.7108	2.955	0.0388	21.27	0.5480	0.5206
975	702	250.17	2.927	0.0183	0.7150	2.954	0.0387	21.38	0.5518	0.5360
1000	727	253.67	3.000	0.0183	0.7192	2.953	0.0388	21.45	0.5533	0.5503
1025	752	256.87	3.000	0.0169	0.7235	2.932	0.0358	20.93	0.5846	0.5999
1050	777	252.65	3.065	0.0169	0.7278	2.932	0.0360	20.82	0.5786	0.6075
1075	802	254.58	3.129	0.0169	0.7321	2.931	0.0363	20.71	0.5708	0.6138
1100	827	256.37	3.191	0.0170	0.7364	2.930	0.0367	20.60	0.5613	0.6174
1125	852	258.02	3.251	0.0172	0.7407	2.929	0.0372	20.48	0.5501	0.6186
1150	877	259.52	3.308	0.0174	0.7451	2.928	0.0379	20.36	0.5373	0.6173
1175	902	260.87	3.362	0.0176	0.7494	2.927	0.0387	20.24	0.5230	0.6145
1200	927	262.07	3.412	0.0180	0.7538	2.926	0.0397	20.13	0.5074	0.6098
1225	952	263.13	3.458	0.0184	0.7582	2.925	0.0408	20.02	0.4906	0.6010
1250	977	264.05	3.500	0.0189	0.7626	2.924	0.0421	19.92	0.4730	0.5881
1275	1002	264.81	3.536	0.0195	0.7670	2.923	0.0436	19.83	0.4546	0.5736
1300	1027			0.0201	0.7715	2.922	0.0453			
INTEGRATED AVERAGE 302 C TO 952 C		233.85	2.664	0.0182	0.7039	2.94	0.0374	20.70	0.5539	0.5003

Carnot Efficiency from 300 C to 1000 C 54.96
Material Conversion Efficiency from 300 C to 1000 C 7.78

SAMPLE: ITM-83
DESCRIPTION: P-TYPE, MILLED IN WATER
Molecular Weight 36.93

TEMPERATURE	SEEBECK COEFFICIENT	ELECTRICAL RESISTIVITY	THERMAL DIFFUSIVITY	HEAT CAPACITY	DENSITY	THERMAL CONDUCTIVITY	ELECTRICAL POWER FACTOR	FIGURE OF MERIT	DIMENSIONLESS FIGURE OF MERIT
	Seebeck and Resistivity Measured Simultaneously 0E-SC0		Laser Flash Diffusivity 0E-RS0	Drop Calorimetry Ames Lab. MHPS-077P	Immersion Density Thermal Expansion 0E-RS0	Calculated	Calculated	Calculated	Calculated
# Points in Fit	105	106	11	11					
Temp. Range of D	24 C	24 C	100 C	375 K					
	1008 C	1008 C	1102 C	1375 K					
RMSD (%)	0.40	0.21	0.79	0.93	0.33	2.05	1.00	3.05	3.05
								Z	ZT
A	1.23963E+02	1.55229E+00	1.92361E-02	4.66300E+00	2.95				
B	2.44905E-01	2.05536E-03	8.70986E-06	1.62220E-03	4.300E-06				
C	1.25125E-04	-3.17115E-07	-4.30160E-08	6.31000E+04					
D	-1.12080E-06	7.54768E-09	3.45013E-11	0.113					
E	1.73847E-09	-2.26173E-11							
F	-8.63747E-13	3.04497E-14							
G		-1.46024E-17							
H									
Units for Temp:	C	C	C	K	C		S^2/r	S^2/rk	K ZT
Equation	A+BT+...HT^7	A+BT+...HT^7	A+BT+...ET^4	D=(A+BT+C/T^2)	A/(1+B(T-27))^3 a=Cp=d				

(K)	(C)	(microV/K)	(milliohm-cm)	(cm2/sec)	(J/g-K)	(g/cm3)	(W/cm-K)	(microW/cm-K	(1000/K)	
275	2				0.6734	2.951				
300	27	130.61	1.6074		0.6629	2.950				
325	52	136.85	1.6589		0.6557	2.949				
350	77	143.07	1.7111		0.6510	2.948				
375	102	149.20	1.7642	0.0197	0.6481	2.947	0.0377	12.62	0.3351	0.1257
400	127	155.18	1.8184	0.0197	0.6465	2.946	0.0376	13.24	0.3526	0.1410
425	152	160.97	1.8738	0.0197	0.6460	2.945	0.0375	13.83	0.3692	0.1569
450	177	166.54	1.9303	0.0196	0.6463	2.944	0.0373	14.37	0.3848	0.1732
475	202	171.87	1.9880	0.0195	0.6473	2.943	0.0372	14.86	0.3995	0.1897
500	227	176.96	2.0467	0.0194	0.6488	2.942	0.0370	15.30	0.4131	0.2065
525	252	181.79	2.1065	0.0193	0.6507	2.941	0.0369	15.69	0.4257	0.2235
550	277	186.38	2.1673	0.0191	0.6530	2.941	0.0366	16.03	0.4374	0.2406
575	302	190.73	2.2289	0.0189	0.6556	2.940	0.0364	16.32	0.4482	0.2577
600	327	194.86	2.2914	0.0187	0.6584	2.939	0.0362	16.57	0.4582	0.2749
625	352	198.79	2.3548	0.0185	0.6615	2.938	0.0359	16.78	0.4674	0.2921
650	377	202.54	2.4192	0.0183	0.6647	2.937	0.0356	16.96	0.4758	0.3093
675	402	206.14	2.4846	0.0180	0.6680	2.936	0.0354	17.10	0.4837	0.3265
700	427	209.60	2.5512	0.0178	0.6715	2.935	0.0351	17.22	0.4909	0.3436
725	452	212.97	2.6190	0.0176	0.6751	2.934	0.0348	17.32	0.4976	0.3607
750	477	216.26	2.6883	0.0173	0.6788	2.933	0.0345	17.40	0.5036	0.3777
775	502	219.50	2.7593	0.0171	0.6826	2.932	0.0343	17.46	0.5092	0.3946
800	527	222.70	2.8321	0.0169	0.6865	2.931	0.0341	17.51	0.5141	0.4112
825	552	225.88	2.9068	0.0167	0.6904	2.930	0.0339	17.55	0.5183	0.4276
850	577	229.06	2.9837	0.0166	0.6944	2.929	0.0337	17.58	0.5218	0.4435
875	602	232.23	3.0629	0.0164	0.6984	2.928	0.0336	17.61	0.5244	0.4588
900	627	235.40	3.1442	0.0163	0.7025	2.927	0.0335	17.62	0.5260	0.4734
925	652	238.56	3.2278	0.0162	0.7067	2.926	0.0335	17.63	0.5266	0.4871
950	677	241.68	3.3132	0.0161	0.7108	2.925	0.0335	17.63	0.5258	0.4995
975	702	244.73	3.4003	0.0161	0.7150	2.924	0.0336	17.61	0.5236	0.5105
1000	727	247.69	3.4884	0.0161	0.7192	2.924	0.0338	17.59	0.5198	0.5198
1025	752	250.48	3.5769	0.0161	0.7235	2.923	0.0341	17.54	0.5142	0.5271
1050	777	253.05	3.6645	0.0162	0.7278	2.922	0.0345	17.47	0.5068	0.5321
1075	802	255.32	3.7501	0.0163	0.7321	2.921	0.0350	17.38	0.4973	0.5346
1100	827	257.19	3.8319	0.0165	0.7364	2.920	0.0355	17.26	0.4856	0.5342
1125	852	258.55	3.9079	0.0168	0.7407	2.919	0.0363	17.11	0.4719	0.5308
1150	877	259.27	3.9756	0.0171	0.7451	2.918	0.0371	16.91	0.4559	0.5243
1175	902	259.21	4.0320	0.0174	0.7494	2.917	0.0381	16.66	0.4378	0.5144
1200	927	258.20	4.0736	0.0178	0.7538	2.916	0.0392	16.37	0.4177	0.5012
1225	952	256.05	4.0962	0.0183	0.7582	2.915	0.0405	16.01	0.3956	0.4846
1250	977	252.56	4.0952	0.0189	0.7626	2.914	0.0419	15.58	0.3717	0.4646
1275	1002	247.49	4.0649	0.0195	0.7670	2.913	0.0435	15.07	0.3462	0.4414
1300	1027			0.0202	0.7715	2.912	0.0453			
INTEGRATED AVERAGE 302 C TO 1002 C		234.20	3.239	0.0172	0.7081	2.926	0.0356	17.11	0.4835	0.4432

Carnot Efficiency from 300 C to 1000 C 54.98
Material Conversion Efficiency from 300 C to 100 7.04

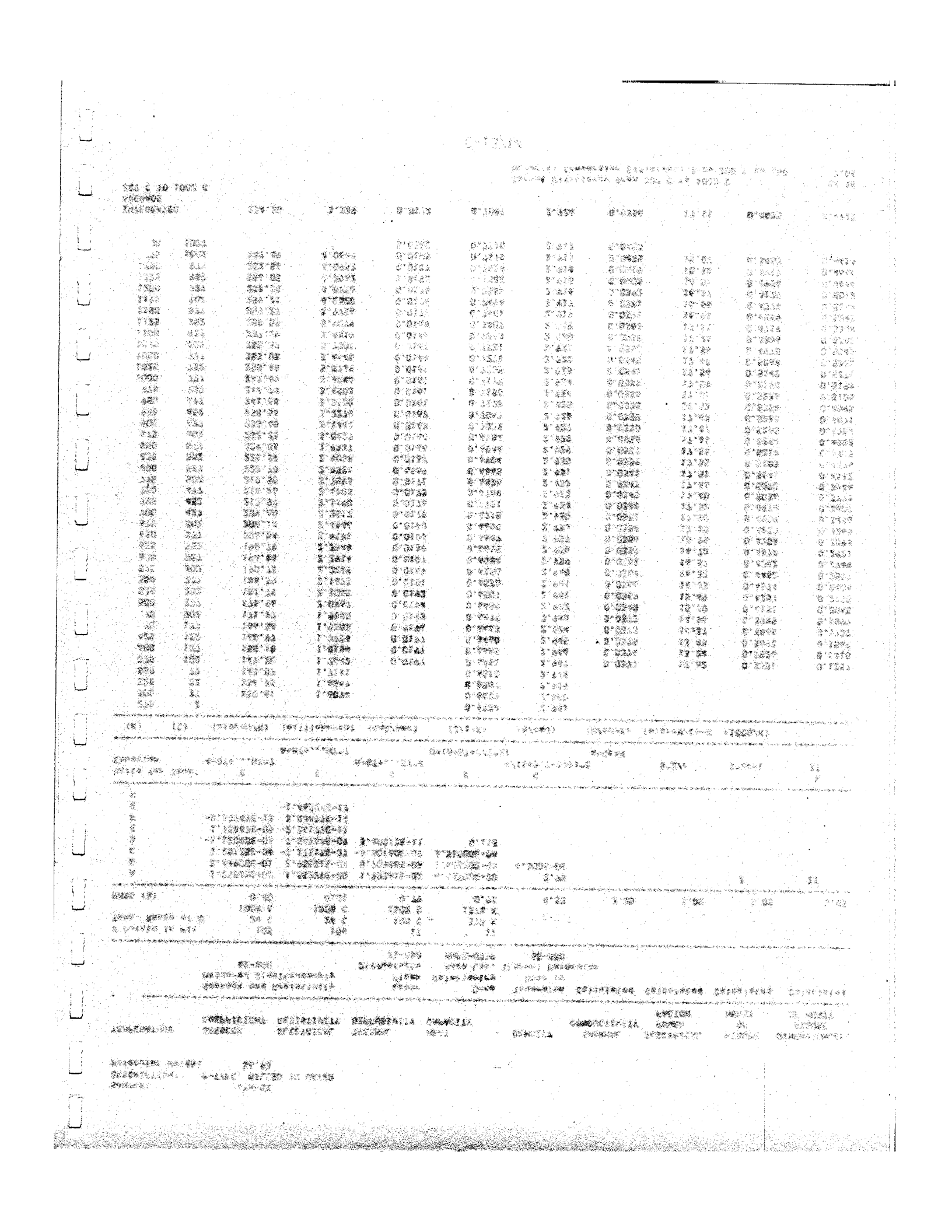

APPENDIX D

DETAILED DESCRIPTION OF PROCEDURES* FOR FABRICATING COMPACTS OF ITM ALLOY 234

* In general these procedures are variations of those employed for manufacture of standard Si-Ge alloys and MOD-RTG SiGe-GaP material.

DESCRIPTION OF ITM-234 COMPACT FABRICATION PROCEDURES

(REFER TO FIGURE D-1 FOR PROCESS FLOW)

1. Prepare vacuum casting with nominal composition $(SiGe)_{0.85}(GaP)_{0.07}P_{0.07}$ by melting Si and Ge chunks in a fused silica crucible and adding GaP and P from test tube to melt.

   100.20 grams Si chunks
   258.96 grams Ge chunks
   31.24 grams GaP flakes
   9.61 grams red P lumps

2. Determine density and measure room temperature Seebeck coefficient on casting.

3. Shatterbox and planetary ball mill vacuum casting to ~5 micron median particle diameter.

4. Vacuum hot press powder blend into a 3" diameter compact according to the following schedule:

   Cold press powder blend to 2800 psi
   30 min outgas at 300°C
   40 min rise to 1000°C
   45 min soak at 1000°C and 11,00 psi
   10 min rise to 1050°C
   45 min soak at 1050°C and 11,000 psi
   Increase load to 28,000 psi
   10 min rise to 1100°C
   45 min soak at 1100°C and 28,000 psi
   10 min rise to 1150°C
   60 min soak at 1150°C and 28,000 psi
   Extrude at 1150°C
   10 min cool to 900°C and He backfill to 1 psig
   Cool to room temperature

5. Determine density and measure room temperature Seebeck coefficient on top and bottom surfaces and from center to edge on hot pressed compact.

6. Shatterbox and planetary ball mill compact to ~5 micron median particle diameter. The nominal composition of this powder blend is $(SiGe)_{0.85}(GaP)_{0.07}P_{0.07}$.

7. Prepare a vacuum casting with a nominal composition of 3 atomic percent phosphorus in silicon. Add red phosphorus lumps from test tube to melt.

   500.00 grams Si chunks
   17.05 grams red P lumps

8. Shatterbox and planetary ball mill to ~5 micron median particle diameter. The nominal composition of this powder blend is $Si_{0.97}P_{0.03}$.

9. Prepare a mixed powder blend consisting of 225.1 grams of the SiGe-GaP powder from Item 6 and 174.9 grams of the P-doped Si powder blend from Item 8. The nominal composition is $Si_{0.747}Ge_{0.187}Ga_{0.016}P_{0.050}$.

10. Vacuum hot press into a 3" diameter compact according to the following schedule:

    Cold press powder blend to 2800 psi
    30 min outgas at 300°C
    Increase load to 28,000 psi
    60 min rise to 1100°C
    45 min soak at 1100°C and 28,000 psi
    120 min rise to 1240°C
    90 min soak at 1240°C and 28,000 psi
    Raise to 1265°C
    5 min soak at 1265°C
    Extrude at 1265°C
    14 min cool to 900°C and He backfill to 1 psig
    Cool to room temperature

11. Determine density and measure room temperature Seebeck coefficient on top and bottom surfaces and from center to edge of the finished compact.

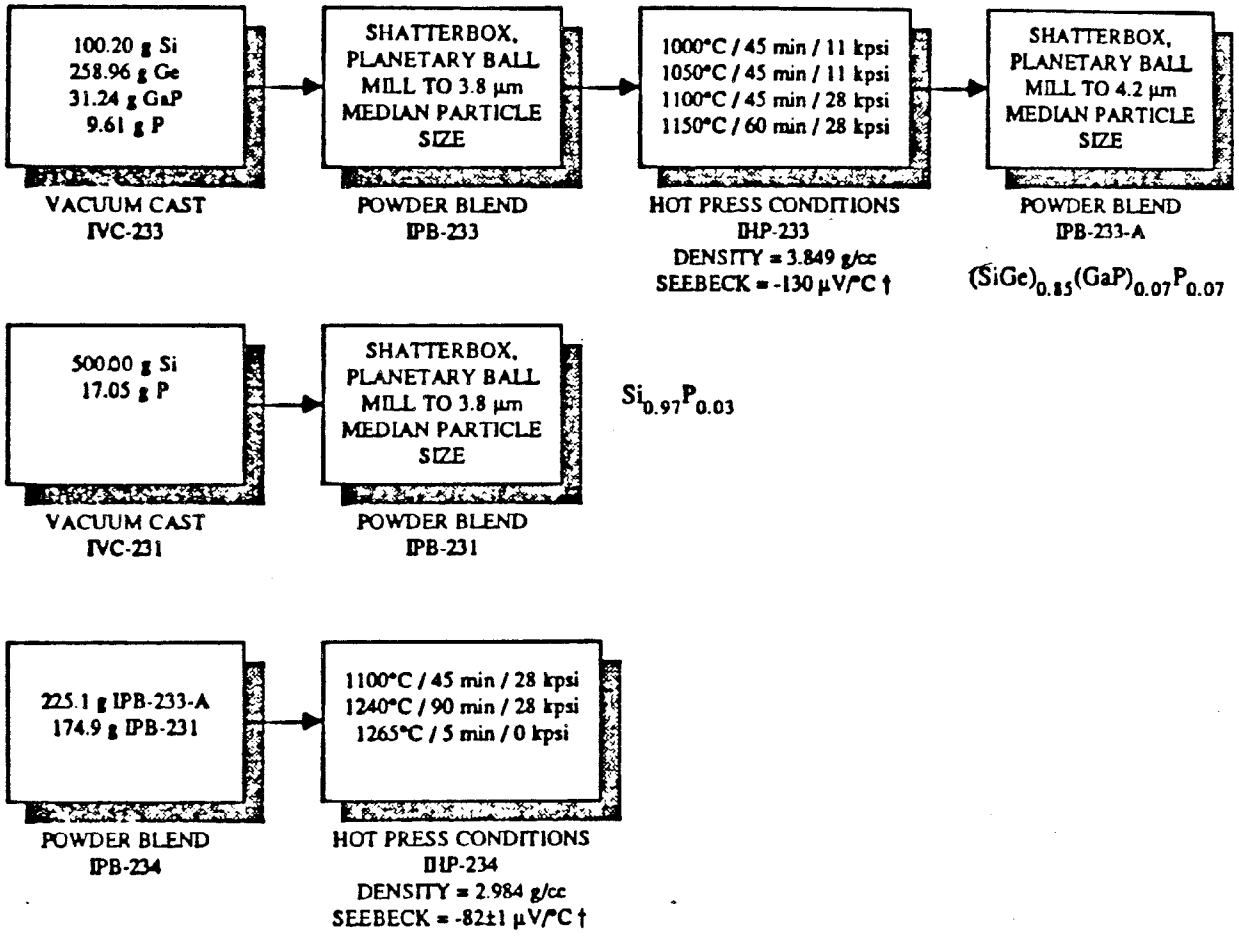

† AVERAGE SEEBECK MEASURED ON TOP AND BOTTOM SURFACES OF COMPACT

Figure D-1. Fabrication Process for ITM 234
$Si_{0.747}Ge_{0.187}Ga_{0.016}P_{0.050}$